UNIVERSITY OF LIVERPOOL

Department of Molecular & Clinical Cancer Medicine

Epigenetic Sensitisation of Chemotherapeutic Compounds in Non- Small Cell Lung Cancer

Thesis submitted in accordance with the requirements of the University of Liverpool for the degree of Doctor in Philosophy by

Ghaliah Obaid F Alnefaie

January 2020

Supervisors: Dr. Triantafillos Liloglou, Dr. Jason Parsons & Prof. John K Field

Dedication

This thesis is the culmination of my journey of Ph. D which was just like climbing a mountain step by step accompanied with encouragement, hardship, trust, disappointmetn and frustration. But I found the Feeling of fulfilment when I saw my name appears on the cover of this dissertation. This would have not happened without my family members, well-wishers, my friends, colleagues and various institutions have contributed to accomplish this huge task. At this moment of accomplishment, I am greatly indebted to my family, friends and supervisors. A special feeling of gratitude to my loving father Obaid whose words of wisdom, encouragement and push for tenacity ring in my ears. I still remember the day he called me doctor Ghaliah when I was a kid, his dream made me resilient and ignited the compassion and thirst for knowledge within. To my beloved mother Khadija, whom this work would not have been possible, without her guidance and involvement, her support and encouragement on daily basis from the start of the project till date. Under her guidance I successfully overcame many obstacles and learnt a lot. I sincerely thank her from bottom of my heart and will be truly indebted to her throughout my lifetime. Special thanks to my little sister Ghaida who truly believed in me in every step of the way. To my aunts Zenab and Hanan for their continuous encouragement, to my brothers, Bandar, Turki and Fahel who never left my side and their robust attitude to keep me persistence. To my dearest friends Dr. Asma Almuhanna and Bushra Al-Derbi for their abundance love and support, for an amazing time we shared in Liverpool that I will take with me and cherish them forever. To my guide Sasonia, she was the best guide in the fourth year who helped in my spiritual knowledge.

Acknowledgements

An enormous gratitude to the primary supervisor, Dr. Triantafillos Liloglou, who has been the greatest mentor during the four years in his lab, his incredible knowledge guiding me to build my own experience in who to be a researcher. He was constantly there, supporting and encouraging me since the first year. As he inspired me with his humility, I learned from him how to teach the students in a humble way.

Many thanks are also due to my secondary supervisors Dr. Jason Parsons in leading and guiding me in his lab and Prof. John K Field, for his significant comments on my writing. I am highly thankful to Dr. Amelia Acha-Sagredo for her support, teaching and guidance, especially when I needed help to perform a new experiment, imparting her knowledge and expertise in this study. Also, Dr. Ahmed Al-Khafaji, with whom it was a pleasure to work in publishing a scientific paper.

I would also like to express thanks and gratitude to my colleagues Dr. Israa Al-Humairi, Dr. Bubaraye Uko, Dr. Xiaolei Yang, Dr. Caroline McCarthy, and all the members of the Liverpool Lung Project team for their help and support throughout these years, allowing me to be surrounded by a fantastic work environment, a strong familial bond.

Special thanks to Emma Dowdall for taking care of all the administrative issues involved. Particular thanks must also be recorded to the International Support Team (IST) at the university. Finally, my thanks and appreciations also go to Taif University and the Saudi Embassy. This study would not have been possible without their financial and moral support.

Disclaimer

All of the work presented in this thesis, unless otherwise stated, is the work of the author.

Table of Contents

Abstract

Lung cancer is currently the highest cancer-related cause of death worldwide, accounting for 1.7 million deaths in 2018. Non-small cell carcinoma (NSCLC) is the most frequent type, accounting for approximately 80% of all lung cancer cases. Chemotherapy is still the first-line therapy offered to NSCLC patients in most countries. While new therapies (targeted compounds, immunotherapy) are evolving, chemotherapy is considered to be used for at least two more decades. Resistance to chemotherapy is among the major factors contributing to lung cancer mortality and has been well established to date through multiple preclinical studies and clinical trials. Currently, there are very few biomarkers, mostly clinical, for predicting chemotherapy efficiency. In addition, sensitization of cancer cells to those compounds is largely ineffective clinically. ***This study explores new avenues of lung cancer cell sensitization to four common chemotherapeutics (cisplatin, carboplatin, gemcitabine, and vinorelbine), with a particular focus in epigenetics and the role of extracellular vesicles***. Using a wide spectrum of molecular and cell biology methods (cloning, inducible transgene expression, shRNA-based silencing, proliferation and apoptosis assays, the neutral comet assay, RT-qPCR, pyrosequencing-based DNA methylation analysis, western blots, EV isolation and characterisation etc.), I analysed a large number of parameters in relation to drug resistance in NSCLC cell lines. Following establishment of the IC50 of each four drugs in eight NSCLC cell lines, resistant cell lines were chosen for sensitization with epigenetic drugs (VPA and DAC), Aminomethylphosphonic acid (AMPA) and fendiline.

VPA demonstrated a significant sensitization potential for all the four chemotherapeutics and this is a novel finding for lung cancer cells. Both VPA and DAC triggered a significant increase in apoptosis activity in cells treated with cisplatin or carboplatin. Double strand DNA breaks

were caused by gemcitabine in A549, CALU-6 and COR-L23 the NSCLC cell lines and pre-treatment with VPA increased this effect, this also being a novel finding in this study.

I also looked into the role of *LANCL1-AS1*; a long-noncoding RNA, which our research group found to be diminished in NSCLC tissues. After establishing an inducible expression model in the SK-MES-1 cell line, it was shown, contrary to the original hypothesis, that *LANCL1-AS1* triggered an increase in proliferation rate, migration invasion, sensitivity to gemcitabine and vinorelbine, increased resistance to platin compounds and, interestingly, expression of its coding counterpart gene, *LANCL1.* LANCL1 shRNA-based silencing led to a decrease in proliferation, migration and sensitivity to oxidative stress. However, sensitivity to all four drugs followed the same pattern as for overexpression of *LANCL1-AS1*, raising thus questions on whether these two functions are related or independent, without being able at this point to exclude the off-target effects of the shRNA approach.

Relatively recently, the role of extracellular vesicles (EVs)' in cancer development and drug resistance has come under investigation. I thus decided to test whether the *LANCL1-AS1* dependent sensitivity to gemcitabine can be transferred through EVs. Increased *LANCL1-AS1* expression led to an increase in the EVs release in a dose-dependent manner. Unfortunately, a number of technical issues related to the toxicity of the EV isolation reagent did not allow establishing knowledge of how *LANCL1-AS1* induced EVs affect gemcitabine resistance when transferred to a recipient cell line. In conclusion, this study has provided a number of novel insights into sensitizing NSCLC cells in a preclinical setting. Further research is required to establish whether these results have clinical value and how they might affect clinical management of lung cancer.

Abbreviations

AB	Antibody
AD	Activation domain
ADC	Adenocarcinoma
AdenoCa	Adenocarcinoma
ADT	Adenosine diphosphate
Ago-1	Argonaute 1
ALK	Anaplastic lymphoma
AMPA	Aminomethylphosphonic acid
APP	Amyloid precursor protein
ATP	Adenosine triphosphate
BCA	Bicinchoricacid
bp	Base pair
C	Unmethylated cytosine
^{m}C	Methylated cytosine
Carb	Carboplatin
CBS	Cystathionine β-synthase
CCD	Charge coupled device
CD74	Cluster of Differentiation 74
CDKs	Cyclin depend kinase
CDKN2A	Cyclin-dependent kinase inhibitor 2A
cDNA	Complementary DNA
CDS	Coding sequence
Cis	Cisplatin
DAC	Decitabine
ddH2O	double-distilled water
DDR2	Discoidin Domain Receptor tyrosine kinase
DEVD	Double-distilled water
DMEM	Dulbecco's modified eagle medium
DNA	Deoxyribonucleic acid
DNMT	DNA methyltransferase
DNMt3a	DNA methyltransferase 3a
dNTP	Deoxy nucleoside triphosphate
DSBs	Double strand breaks
EGFR	Epidermal growth factor receptor

EML4	Echinoderm microtubule associated protein like 4
ErK	Extracellular regulated kinases
ESCRT	Endosomal sorting complex required for transport
ETS	Electronic transport system
EVs	Extracellular vesicles
EZH2	Enhancer of zeste homolog 2
FBS	Fetal bovine serum
5Fu	Fluorouracil
G/A	Guanin transfer to adenine
G/T	Tyrosine transfer to guanin
GM	Gemcitabine
G1 phase	Gap 1 phase
GSH	Glutathione
HAT	Histone acetyl transferases
HCL	Hydrochloric acid
HDAC	Histone deacetylases
HDACi	Histone deacetylace inhibitor
HER2	Human epidermal growth factor receptor 2
HIV	Human immunodeficiency virus
H_2O_2	Hydrogen peroxide
HR	Homologous recombination
HRP	Horseradish peroxidase
HSP	Heat shock protein
IC50	The half maximal inhibitory concentration
ILV	Describe intraluminal vesicle
JAK3	Janus kinase 3
LANCL1	Lanthionine-synthetase component C-like 1
LANCL1-AS1	*LANCL1* antisense RNA 1
LB	Luria-bertani
LCD	Liquid-crystal display
LDS	Lithium dodecyl sulfate
LncRNA	Long non-coding RNA
LOH	Losing heterozygosity
MAPK	Mitogen-activated protein kinase
MDS	Myelodysplastic syndrome
MEG3	Maternity express gene 3
MHC I&II	Major histocompatibility complex class I&II
miRNA	Micro RNA

mTOR	Mechanistic target of rapamycin
MVB	Multivesicular body
NAV3	neuron navigator 3
NEB	New england biolabs
NSCLC	Non-small cell lung cancer
nt	Nucleotides
NTP	Nucleoside triphosphate
O.D.	The option density
ORF	Open-reading frame
OS	Overall survival
PBS	Phosphate buffered saline
PCR	Polymerase chain reaction
PCG	Protein-coding gene
PI3K	Phosphatidylinositol-4,5-bisphosphate 3-kinase
PIP2	Plasma membrane intrinsic protein 2
PIP3	Plasma membrane intrinsic protein 3
piRNA	Piwi interacting-RNA
pN	Pathological nodal status
PPi	Pyrophosphate
PRC2	Polycomb repressive complex2
pT	Pathological T status
PTEN	Phosphatidylinositol 3,4,5-trisphosphate 3-phosphatase
qPCR	*Quantitative polymerase chain reaction*
RB	Retinoblastoma
RBP	RNA binding protein
RIPA	Radioimmunoprecipitation assay
RNA	Ribonucleic acid
RNP	Ribonucleoprotein
ROS	Reactive oxygen species
RP	Random primer
RQ	Relative quantification
rRNA	Ribosome RNA
RT	Reverse transcript
RT	Room temperature
RT-qPCR	Reverse transcription-quantitative polymerase chain reaction
SAM	S-adenosylmethionine
SCC	Squamous cell carcinoma
SCGE	Single-cell gel electrophoresis

SDC4	Syndecan-4
SDS	Sodium dodecyl sulfate
SHMT1	Hydroxymethyltransferase 1
shRNA	Small hairpin RNA
SNAREs	Soluble NSF attachment protein receptors
S phase	Synthesis phase
SqCC	Squamous cell carcinoma
SRNA	Small RNA
SSBs	Single strand breaks
STAT3	Signal transducer and activator of transcription 3
STK11	Serine tyrosine kinase 11
SYTL4	Synaptotagmin-Like Protein 4
T	Thymine
TFs	Transcription factors
TKI	Tyrosine-kinase inhibitors
TLR3	Toll-like receptor 3
TNM	Tumour, node, and metastases system
TP53	Tumor protein p53
tRNA	Transfer RNA
TSG101	Tumor susceptibility gene 101
TSGs	Tumor suppressor genes
U	Uracil
UTR	Untranslated region
V1	Variant1
V2	Variant2
V3	Variant3
VATS	Video-assisted thoracoscopic surgery
VEGF	Vascular endothelial growth factor
VPA	Valproic acid
VPS 4	Vascular protein sorting–associated protein 4
VRL	Vinorelbine

Table

Figures

5.11	The effect of autologous and heterologous EV supplementation comparing cell sources with high and low *LANCL1-AS1* expression
5.12	The exosomes were exchanged with 0.06 μM of gemcitabine in overexpressed *LANCL1-AS1* clone

Chapter 1: Introduction

1.1 Lung Cancer

Lung cancer is one of the most common cancers in the world, occupying in fact the third position, with 1,825,000 new cases diagnosed in 2012 only (Naseer et al. 2018). The highest incidence rate was in North America while the lowest is in middle Africa, substantially depending on the different range of risk factors but also on available means of diagnosis (Alberg et al. 2013).

In 2016, around 47,235 new cases were recorded in the UK, accounting for almost 13% of the entire cancer cases. Overall, it has been concluded that both genders generally have the same incidence rate, while the rate for females is higher in Northern Ireland (CancerResearchUK 2019).

Lung cancer is currently one of the most severe public health problems, caused by a mosaic of risk factors which contribute to contracting the disease in both genders. The most important factor is smoking tobacco, which demonstrates dose-dependence taking into account the length of time and the number of cigarettes per day, generally expressed as "pack-years". Moreover, smoking has been noted to be a greater risk factor for squamous cell carcinomas (SCC) than for adenocarcinoma (ADC) (Molina et al. 2008). Furthermore, inhaling radon gas, which can be found in uranium rocks or 'nuclear waste', can also cause lung cancer, as recorded in the south-west region of the UK. Meanwhile, exposure to a specific type of chemical such as asbestos found in diesel or silica produced in glass making are also mentioned among potential risk factors (Molina et al. 2008).

Moreover, air pollution is considered to be a significant risk factor when it comes to lung cancer (Raaschou-Nielsen et al. 2013). A family history of lung cancer can also increase the risk (Matakidou, Eisen, and Houlston 2005). A past history of other cancers e.g. breast, head and neck or oesophageal cancer as well as pulmonary disease (TB, chlamydia, pneumonia, COPD etc) can also increase the risk (Biesalski et al. 1998).

Other risk factors are immunocompromisation (e.g. HIV patients) and immunosuppression (e.g. for organ transplantation). These can increase the risk threefold, while this can be twofold in the case of lupus (Schulz 2009; Cadranel et al. 1999). As a result, having recognised some of the most important risk factors, many campaigns have attempted to raise awareness around the world (Molina et al. 2008; Biesalski et al. 1998). However, one of the most important problems in lung cancer is late detection. Several symptoms can lead the physician to suspect lung cancer, such as haemoptysis, prolonged chest pain, hoarseness, bone pain, a wheezing sound with short breathing, unsuspected weight loss, feeling tired most of the time and losing energy, among others (Biesalski et al. 1998).

1.1.1 Classification

Most lung cancers have an epithelial origin, more particularly the World Health Organisation (WHO) has classified lung cancer into many different types (Figure 1.1). The primary two categories are small cell carcinoma and non-small cell carcinoma, with the majority of cases being classified under these categories. In fact, approximately 80% of cases are non-small cell lung cancer (NSCLC) (Heighway and Betticher 2004).

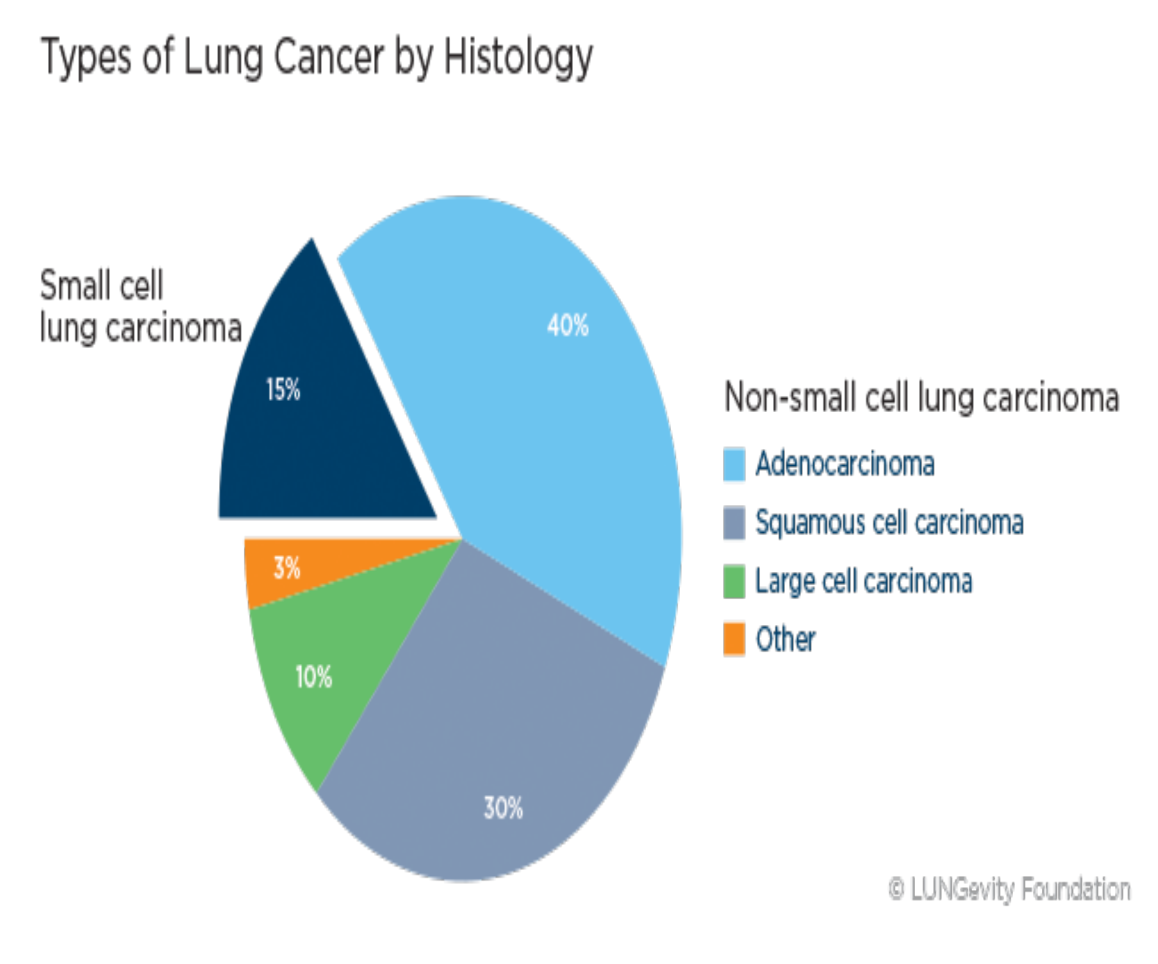

Figure 1.1: *Classification of Lung Cancer.*

There are three subtypes of NSCLC, namely squamous cell carcinoma (SCC), adenocarcinoma (ADC), and large lung cancer, each specified with unique characteristics.

Squamous cell carcinoma is recognised through the keratinised and intercellular edge coming from the bronchial epithelium (Table 1.1), the most severe risk factor for this type of carcinoma being smoking, with around 90% of the squamous cases (Molina et al. 2008).

Adenocarcinoma is characterised by a granular or mucin appearance as ‘acinar, papillary and bronchiolar alveolar’ with a mucin growth pattern, its diagnosis depending on a combination of cytomorphology and architectural features of the cluster. It is characterised by a ‘single-ring cell' shape. A large single cell filled with mucin and disabled cytoplasm leads to compressing the nucleolus to the margins (Heighway and Betticher 2004).

Despite the fact that large cell lung cancer is rarely differentiated from non-small cell lung cancer, it can be recognised through the lack of the cytological and architectural shape of small cell cancer, while it is not glandular or squamous (Heighway and Betticher 2004).

Small cell carcinoma, also known as epithelium malignant tumour, is recognised through a small cell scattered within the cytoplasm, with inexistent or ill-defined cell borders and a high mitotic rate, while necrosis is typical and can be found as a cluster arranged in a linear pattern. Sheet growth without a neuroendocrine morphology pattern is generally the cause (Heighway and Betticher 2004).

Table 1.1: *Lung cancer classification* (Heighway and Betticher 2004; Travis et al. 2012).

SQUAMOUS	**Beaching** **Cell** **Nuclei** **Cytoplasm** **Shape** **Aggregation** **Differentiation** **Metastases**	Necrosis and cellular debris Large display cell in the central Hyper-chromatin, irregular, one or more nuclei, small, bundle Keratinized cytoplasm appears robin's egg blue with Romanowski Bazar "spindle-tadpole" shape May aggregate Stain gets an orange yellow colour Less frequent metastases to distance area	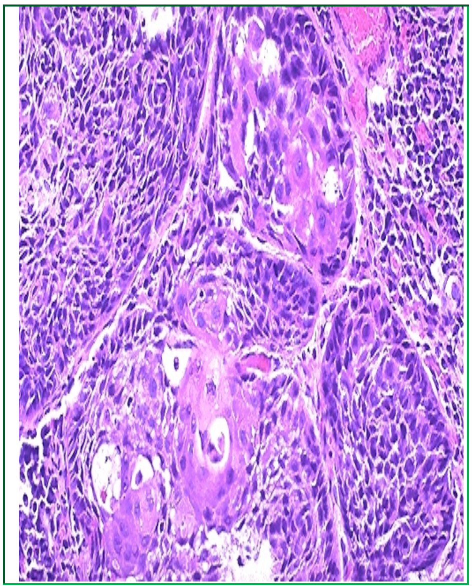
ADENOCARCINOMA	**Shape** **Border cell** **Cytoplasm**	It is most likely single or three-dimension morula acini, pseudo papillae, true papillae, covered with sheet or fibrovascular cores Typical, sharp line bounded Usually single-round or oval eccentric Finely granular	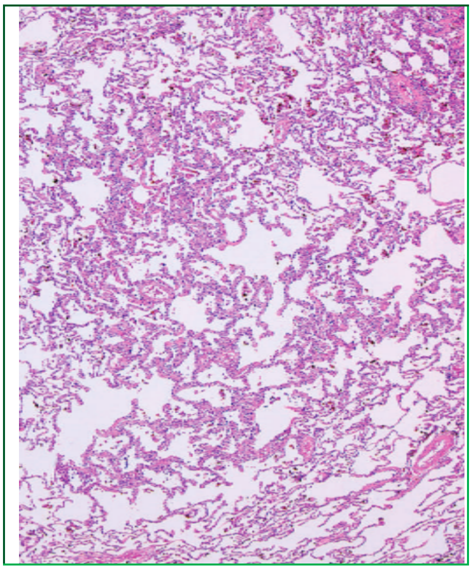
SMALL	**Shape** **Size** **Cytoplasm** **Nuclei** **Chromatin**	Oval, spindle, round Small, less than three cells lymphocyte Scattered cytoplasm A bundle of an inconspicuous nucleus Finely granulated neural chromatin	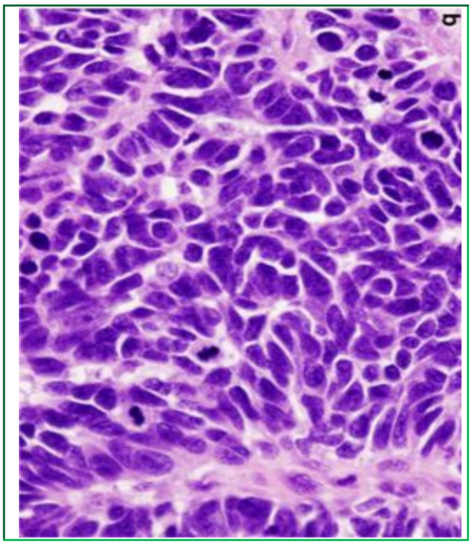

1.1.2 Lung Cancer Stages

Appropriate lung cancer staging is key in deciding which treatment is suitable for the patient. However, the stage is often not definite until the surgery has been carried out. Many systems have been used to categorise the lung cancer stages, such as the UK official system called the TNM (tumour, node, and metastases) system. Here, 'tumour' is related to the size and position of the tumour, 'while node' to whether the cancer is related to the surrounding lymph nodes or not and 'metastasis' relates to whether the cancer has spread to another part of the body (Lardinois et al. 2003).

There are four main stages of lung cancer which have been identified. While in the first stage, the cancer is small and is localised in one area of the lung, in the second and third stages, the size of the cancer increases, most likely having invaded the adjacent or surrounding tissues, most probably locally. Finally, in the fourth stage, advanced cancer is found in the lymph nodes and has begun to spread to other parts of the body through metastasis. The TNM system has sub-categories, which are illustrated in (Figure 1.2) (Molina et al. 2008).

TNM has different stages, namely that in cases such as tumours (T): a, b, 2, 3, 4), most stages are in the main description (Table 1.2), while, nodes have three stages: N0, no lymph invasion; N1, cancer is in the lymph nodes near the mediastinum, but on the same side of the affected lung; N2, lymph in the branches, wind pipe; N3, lymph nodes in the opposite lung or the collarbone or the top of the lung are invaded; M0, cancer has not spread anywhere or to any part; M1, tumour spread in both lungs and the fluid surrounding the lungs involves malignant pleural effusion and pericardial effusion; M2, cancer invades distant organs or bones (Lardinois et al. 2003).

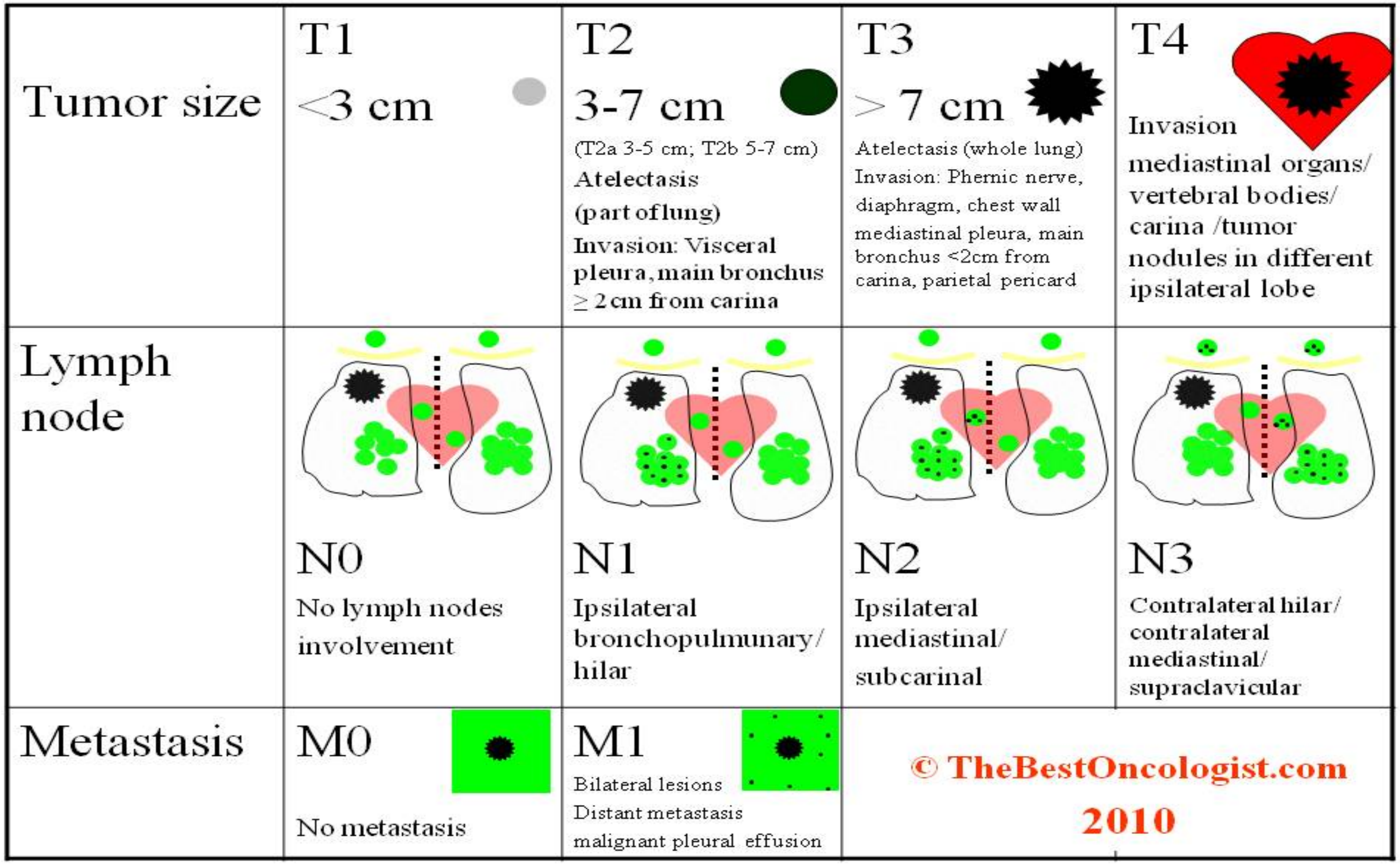

Figure 1.2: *TNM system adapt from.* Adopted from (Nasser 2010).

Table 1.2: *Lung cancer tumour (T) stages* (Lardinois et al. 2003).

Stage		
1	***1a***	At this stage the tumour is small up to 3cm
	1b	The tumour size is between 3 to 5cm May invade the near tissue “main airway of the lung (bronchus) or the membrane covers the lung (pleura) or lung collapsed”
2	***2a***	Two states: • Cancer size between 5 to 7 cm and no lymph nodes infected • Size is 5cm or less and cancer in near lymph nodes In both states, cancer may spread to adjacent tissues (bronchus, pleura) collapse
	2b	Different scenarios: • Size between 5 to 7cm and there is cancer in the lymph nodes near the affected lung • Larger than 7cm, there are no cancer cells in the lymph nodes • Not in the lymph nodes but it spread to the diaphragm, mediastinal pleura, and parietal pericardium • In branches near each lung • Any size but there is more than one tumour in the same lobe of the lung tumour
3	***3a***	Characters: • Size is larger than 7cm there are cancer cells in the near lymph nodes • Spread in near tissues (diaphragm, pleura and pericardium) or lymph nodes • Any size and it grows in the other adjacent tissues (trachea, oesophagus and larynx), bones • More than one lobe of the same lung and lymph nodes close.
	3b	Cancer in the lymph nodes in the mediastinum and diaphragm, trachea major stream tune esophageal and main blood vessels
4		It may be: • Both lungs • Other parts of the body, liver, and bones Fluid around lungs has cancer cells, malignant pleural effusion or pericardial effusion

1.1.3 Molecular Biology of Lung Cancer

In the last 20 years, an enormous amount of information has been produced with regard to gene alterations in lung cancer on multiple molecular levels (genetic, epigenetic and protein expression); in certain cases, such information has promoted the progress in diagnosis, prognosis, and treatment. Molecular alterations involved in aggravating cell proliferation or reducing cell death. In fact, many mutations have been recorded in a lung cancer cell, mutations such as duplication, point mutation, amplification and structure rearrangement in multiple oncogenes such as *ALK, AKT, BRAF, EGFR, HER2, KRAS, c-MET, NRAS, PI3K, RET*, and *ROS1* causing uncontrolled signalling that leads to increased cell growth rates. Also, mutations as a deletion and point mutation in tumour suppressors' genes such as *PTEN, TP53 RB, STK11 CDKN2A, FH1T, RASFIA,* may cause reduction in cell death (Figure 1.3) (Larsen and Minna 2011; Massion and Carbone 2003). The revolution brought by next generation sequencing has also increased the range of mutations detected. Indeed, one study detected 727 new mutations in NSCLC patients by using a complex genome approach (Larsen and Minna 2011).

Gene alteration is noticed in the early and late stage of NSCLC, more particularly losses of chromosomal regions in 3p and 9p are recognised in early stage, while point mutations in p53 and KRAS have been reported in the late stage of NSCLC. Molecular alteration that promotes cell growth such as the amplification or overexpression of growth factors, an oncogene or hormonal receptor, can lead to NSCLC (Brady et al. 2015; Takenaka et al. 2007).

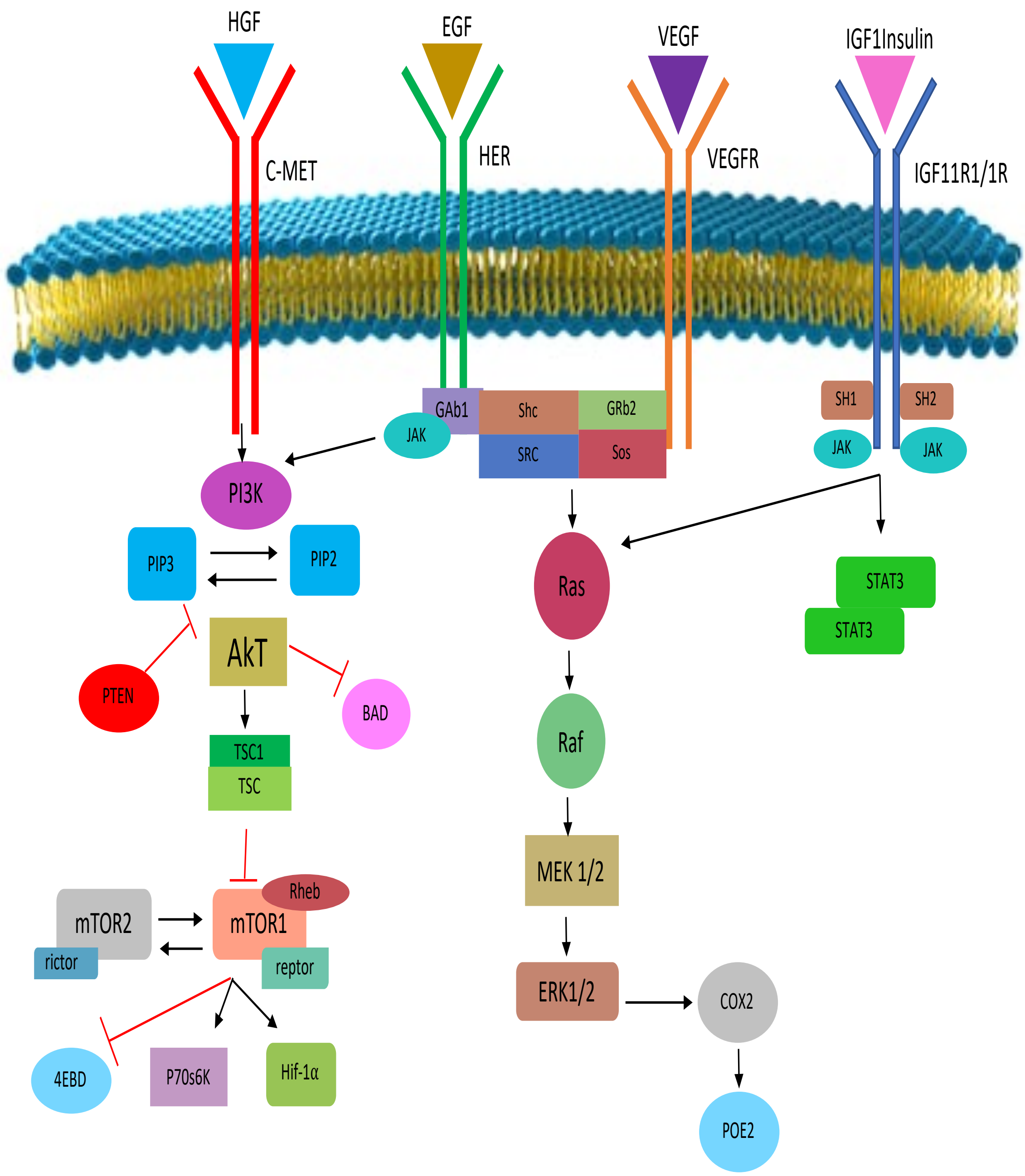

Figure 1.3: *Oncology pathways*: *EGFR, c-MET, VEGF and ROS1* are signalling downstream pathways, such as RAS-RAF pathway, MEK-ERK pathway, PI3K-AKT-mTOR pathway and JAK-STAT3 pathway, which play a role in cell survival, proliferation, invention, differentiation and anti-apoptotic that control cell growth. Any pathogenic molecular alteration leads to uncontrolled cell growth that can cause cancer (original).

Molecular alteration that occurs in *EGFR VEGF, c-MET, ROS1* leads to uncontrolled signalling to PI3K-mTOR, RAS-RAF-MAPK pathways that increase cell proliferation, survival, invasion, angiogenesis, while metastasis also has an anti-apoptotic effect (Table 1.3) (Larsen and Minna 2011; Massion and Carbone 2003).

On the other hand, the molecular alterations in the tumour suppressor genes (TSG) is carcinogenic; in other words, TSGs such as p53, retinoblastoma *RB* and serine tyrosine kinase *STK11, CDKN2A, FH1T, RASFIA, PTEN* work as a negative regulator for cell proliferation (Cooper et al. 2013). The loss of TSGs occurs in many types of cancer, including lung cancer, in which case alleles are usually inactivated either epigenetically through methylation, deacetylation, and DNA adduct, or by another type of alteration (Massion and Carbone 2003). Meanwhile, the inactivation of the secondary allele occurs by losing the heterozygosity LOH region of the chromosome by deletion, non-reciprocal translocation or mitotic recombination (Cooper et al. 2013).

Table 1.3: *Genes involved in lung cancer*

Genes	Gene Alteration
Epidermal growth factor receptor EGFR	EGFR mutations appear in intracellular tyrosine kinase domain in four exons (18, 19, 20 and 21), 45% of the EGFR mutation in NSCLC is deletion {del E746 – A750] in the exons19, 40%-point mutation L858R in exon 21, 14% mutation in exon 18 and 5-10% duplication in exon 20 (Raparia et al. 2013).
Vascular endothelial growth factor VEGF	Four polymorphisms in VEGF regulate the expression. Meanwhile, 2578 C/C, 634 G/G, 1154 A/A alleles lead to under-expressed VEGF, while 2578 C/A 634 G/C, 1154 C/A alleles lead to over-expressed VEGF in 36 NSCLC patient pathway (Koukourakis et al. 2004).
C-MET	The amplification of c-MET causes over-expression that leads to increased cell survival through PI3K-mTOR.
ROS1	ROS1 rearrangement occurs in lung cancer with a F16 gene in 2% of NSCLC cases. In addition, some infusion is noted with KDEIR2, SDC4, LR1G3, EZR, SLC34AZ, CD74 (Cooper et al. 2013).
KRAS	Gene alteration of ATP leads to increasing the RAS signalling. 30% of NSCLC cases have RAS mutation. Approximately 25-40% of ADC cases are caused by KRAS point mutation in codon 12, while this rarely occurs in codon 13 and 16 (Cooper et al. 2013).
BRAF	The mutation occurs in NSCLC located in kinase domain-like V600E, D594G, and L596R or G-loop-like G465V and G468A. V600E accounts for 50% of BRAF mutation in NSCLC (Cooper et al. 2013).
MEK	Somatic mutation in MEK in exon 2 has been reported in two cases of ADC in NSCLC (Cooper et al. 2013).
Anaplastic lymphoma ALK	Intron 19 of ALK is infused with intron 13 of EML4 [ALK(inv(p21;p23)] or exon 1-3 of EML4 joined exon 20-29 of ALK (Raparia et al. 2013).

P13K-AKT-mTOR pathway	Around 50-70% of NSCLC cases involve molecular alterations in the P13K-AKT-mTOR pathway, while this more likely occurs in SCC (47%) (Cooper et al. 2013). Uncontrolled activation of the P13K pathway occurs through amplification of P13K or loss of PTEN, which usually occurs to stop P13K working. Around 5% of NSCLC cases involve amplification of P13K. AKT mutations occur in 0.5%-2% of NSCLC cases (Raparia et al. 2013).
Fibroblast growth factor receptors FGFR	FGFR amplification most likely occurs in 20% of SCC cases (Larsen and Minna 2011; Cooper et al. 2013).
Discoidin Domain Receptor DDR2	c.2304T>A (S768R) mutation (Cooper et al. 2013).
RET	RET-KIF5B rearrangement occurs in 1-2% of ADC cases, the translocation is fused between exon 12-20 of the RET tyrosine kinase domain with the first 15 exons of the KIF5B (kinase family B gene).
Phosphatidylinositol-4,5-bisphosphate 3-kinase TP53	Homozygous deletion of TP5 has occurred in 90% of small lung cancer cases, 65% of NSCLC cases and around 60-100% of lung cancer cases (84% SCC and 45% ADC) (Cooper et al. 2013). G/T transversion occurs more than G/A transversion in cancer patients who have never smoked. G/T transversion that has occurred in smoking patients causes the bulking of the DNA adduct, which involves 'covenant modification of DNA. TP53 mutation is common with KRAs and EGFR mutations (Gajra et al. 2002).
Phosphatidylinositol 3,4,5-trisphosphate 3-phosphatase PTEN	c.697C>T (R233) mutation results in the introduction of a premature stop codon into the PTEN gene (Cooper et al. 2013).
LKB1 (STK11)	LKB1 mutation as deletion occurs in ADC cases, with a with 10-11%rate (Cooper et al. 2013).
P16INK4-cyclinD1-CDK4-RB pathway	80% of ADC NSCLC cases involve inactivated P16INK4 due to the methylation that prevents the G1 passing through the checkpoint, while it occurs in 75% of SCC cases. 40% of NSCLC cases involve overexpression of D1 Inactivate RB occurs in 90% of SCC cases and 10-15% of ADC (Cooper et al. 2013).

1.2 Therapy

The tumour type and location, the diagnosis clinical phase and the general health status are considered vital elements required to treat non-small cell lung cancer (NSCLC) (Table 1.4). Once the position of the tumour has been established and based on the patient's good health status, the best treatment option is surgery, followed by additional chemotherapy and radiotherapy. Nevertheless, neither surgery nor radiotherapy are viable options in metastasized cancer cases; such cases can only be treated with various courses of chemotherapy if not showing resistance, otherwise target therapy would be suggested (Howington et al. 2013).

Table 1.4: *Therapies applicable depend on the cancer stage* (Howington et al. 2013).

<table>
<tr><th></th><th>Surgery</th><th>Radiotherapy</th><th>Chemotherapy</th></tr>
<tr><td>Stage 0</td><td rowspan="4">Applicable depending on the health state</td><td>Depending on the health state</td><td>Depending on the health state</td></tr>
<tr><td>Stage I</td><td rowspan="4">Applicable</td><td rowspan="4">Applicable</td></tr>
<tr><td>Stage II</td></tr>
<tr><td>Stage IIIA</td></tr>
<tr><td>Stage IIIB</td><td>Not Applicable</td></tr>
<tr><td>Stage IV</td><td>Not Applicable</td><td>Not Applicable</td><td>Applicable with target or immune therapy</td></tr>
</table>

1.2.1 Surgery

Commonly, the first treatment choice for NSCLC patients who are in stable health at stages 1 or 2 is video-assisted thoracic surgery (VATS), which involves a tiny camera attached to a light injected inside the lung (scope) with a monitoring video that allows the surgeon to cut the malignant part without the need for a major operation. Two systematic reviews conducted by (Soldà et al. 2013; Vansteenkiste et al. 2013) reveal the outcomes of thoracoscopic surgery compared to those of VATS in NSCLC's case, more particularly the wider benefits including short duration of the chest tube insertion, a shorter stay in hospital, a longer overall survival (OS) rate and lower mortality rates in early stage NSCLC (Soldà et al. 2013; Vansteenkiste et al. 2013).

Three types of lung cancer surgery can be performed to treat NSCLC, depending on the size and position of the tumour. While in the early stages of NSCLC, the tumour is generally located in a single small area of the lung and in this case, 'wedge resection or segmentectomy surgery' is the best choice`, if a tumour is located in one lung lobe, a 'lobectomy' surgery is usually performed. Moreover, in some cases, the tumour could have spread across the middle lobes of one lung or even the entire lung; as a result, in such a case a 'pneumonectomy' surgery involving the removal of the whole lung is recommended; moreover, generally, the surgeon will also remove the affected lymph nodes during the surgery (Vansteenkiste et al. 2013). A recent review also shows a significant result in terms of increasing the overall survival rate in NSCLC cases when the surgeon dissects the lymph nodes during the lung surgery (Davies 2014).

Meanwhile, additional support following lung surgery via further chemotherapy or radiotherapy is recommended to avoid any regrowth of the remaining tumour cells that were not removed during the surgery. A systemic review also reveals a notable increase in the survival rate for NSCLC patients when they receive post-surgical chemotherapy (Vansteenkiste et al. 2013).

1.2.2 Radiotherapy

Several types of radiotherapy can be used to treat NSCLC, depending on the evolution of the disease; more specifically, in the early stage. Radiotherapy is generally the preferred option in the first, second and the third stages of NSCLC, when the patient suffers from heart disease or the cancer reaches the edge of the heart or has spread out too much to be solved through surgery (Vansteenkiste et al. 2013; Soldà et al. 2013).

First, external beam radiation therapy (EBRT) involves radiation focused on the exterior of the body from different angles and aimed at the cancer cells, the measurement and the direction of the beam being generally determined in the simulation stage. Meanwhile, 3D-CRT, IMRT, SBRT, SRS are different types of radiotherapy that are used for various purposes, depending on availability (Soldà et al. 2013).

1.2.3 Chemotherapy

The process of chemotherapy supposes the use of an anti-cancer agent to eliminate tumour cells and reduce cancer symptoms, most frequently after the surgery (adjuvant chemotherapy) (Vansteenkiste et al. 2013). However, when surgery is not applicable, due to either the patient's poor health or the cancer having spread to essential organs, chemotherapy can also be administered in the late stage to reduce the symptoms. Chemotherapy is usually conducted in cycles, the number of which depending on the stage and the severity of the disease (Vansteenkiste et al. 2013). In neoadjuvant settings, chemotherapy is given before surgery to reduce the tumour size, a technique that, in turn, increases the chance of removing all tumour cells during the surgery. However, combined chemotherapy is generally recommended for NSCLC patients who cannot undergo surgery due to their poor health state. In such case, platinum is generally the primary drug that is combined with a form of chemo, while in the late stage, target therapy is generally used along with chemo (Scheff and Schneider 2013; Burdett, Stewart, and Rydzewska 2006); chemotherapy treatments include platinum "cisplatin, carboplatin", vinorelbine, gemcitabine, paclitaxel (taxol), docetaxel (taxotere), pemetrexed, albumin-bound paclitaxel (reb-paclitaxel, abraxane), irinotecan (camptosar), vinblastine, etoposide (VP-16), pemetrexed (alimta) (see Table 1.5) (Scheff and Schneider 2013; Bunn and Kelly 1998).

Different antineoplastic categories have been used to treat NSCLC. For example, alkylating agents such as platinum (cisplatin-carboplatin) are generally a non-specific cell cycle, usually active in the resting phase of the cell. In fact, this is the first non-hormonal drug to have been approved (Baxevanos and Mountzios 2018). Platinum stops cancer cell proliferation through the process of adding an alkyl group to the guanine base of the DNA molecule, at the number

7 nitrogen atom of the purine ring, preventing the strands of the double helix from joining and causing DNA damage that interferes with the cell replication (Scheff and Schneider 2013; Bunn and Kelly 1998).

Plant alkaloids originate from plants, including the Vinca alkaloid, which comes from the periwinkle plant (vinorelbine and vinblastine), while other drugs, such as podophyllotoxin (etoposide), are generated from the mayapple plant.

Antimetabolites, which normally are small molecules that replace the natural substance without performing its function, interfere with the cancer cell's metabolism, which leads to stopping the cell cycle in a specific phase. For example, antifolate pemetrexed can inhibit thymidylate synthase that stops the methylation of C5 of deoxyuridine monophosphate (dUMP), thereby preventing the synthesis of deoxythymidine monophosphate (dTMP). Another example is a pyrimidine antagonist such as gemcitabine, where fluorine atoms replace the hydrogen atoms on the 2' carbon of deoxycytidine incorporated into DNA strands, therefore leading to stopping further DNA synthesis and to cell death (Scheff and Schneider 2013; Cullen 2003).

Antitumour antibiotics work in nonspecific cell cycle phases. Antibiotics are extracted from microorganisms and affect DNA synthesis, while antihormones such as oestrogens generate an unsuitable environment for cancer cell growth.

In order to increase the efficiency of the drug, combined chemotherapies are used, including platinum therapy, which has been combined in four regimens (Baxevanos and Mountzios 2018), namely cisplatin plus paclitaxel or docetaxel and Cisplatin plus gemcitabine. Patients who received carboplatin plus paclitaxel show less toxicity compared to patients receiving a cisplatin-based treatment. Other types of non-platinum combined therapy including gemcitabine plus taxanes or vinorelbine have been used to treat IV NSCLC.

Histology can help make decisions regarding the combined chemotherapies that can be used. For example, cisplatin plus pemetrexed shows higher overall survival (OS) in adenocarcinoma, while cisplatin plus gemcitabine showed a better response in OS in squamous cell carcinoma (Scheff and Schneider 2013). The most common combined chemotherapies with cisplatin are etoposide and vinorelbine, which are widely recommended among the clinics (Vansteenkiste et al. 2013).

Table 1.5: *Drugs to treat NSCLC* (NationalCancerInstitute 2019).

DRUG	Description
Navelbine (Vinorelbine), Taxol (Paclitaxel) Taxotere (Docetaxel)	It stabilizes microtubules, preventing their depolymerization so inhibiting cellular motility, mitosis, and replication. **Results** in cell- cycle arrest at the G2/M phase and cell death hereby resulting in the inhibition of cell division with antineoplastic activity. **Taxol:** blocking the function of the apoptosis inhibitor protein Bcl-2 (B-cell Leukaemia 2. induces apoptosis. **Taxotere:** This agent also inhibits pro-angiogenic factors such as vascular endothelial growth factor (VEGF).
Alunbrig (Brigatinib), Xalkori (Crizotinib), Alecensa (Alectinib), Lorbrena (Lorlatinib)	Aminopyridine-based an ATP-competitive manner. It inhibits ALK kinase and ALK fusion proteins with antineoplastic activity. **Alunbrig:** inhibits the epidermal growth factor receptor (EGFR). **Xalkori:** inhibitsthe c-Met/hepatocyte growth factor receptor (HGFR). **Alecensa:** inhibits the gatekeeper mutation ALKL1196M. **Lorbrena:** ROS oncogene 1 (Ros1).
Everolimus (Afinitor)	A derivative of the natural macrocyclic lactone sirolimus. It binds to the immunophilin FK Binding Protein-12 (FKBP-12) to generate an immunosuppressive complex that binds to and inhibits the activation of the mammalian Target of Rapamycin (mTOR), a key regulatory kinase with immunosuppressant and anti-angiogenic properties.
Trexall (Methotrexate)	The disodium salt of a synthetic pyrimidine-based an antimetabolite and antifolate agent with antineoplastic and immunosuppressant activities. It inhibits the enzyme dihydrofolate reductase. **Result** in inhibition of purine nucleotide and thymidylate synthesis and, subsequently, inhibition of DNA and RNA synthesis.
Imfinzi (Durvalumab), Keytruda (Pembrolizumab), Tecentriq (Atezolizumab), Opdivo (Nivolumab)	Monoclonal immunoglobulin (Ig) G4 antibody directed against programmed cell death-1 ligand 1 (PD-L1; B7 homolog 1; B7H1), with potential immune checkpoint inhibitory and antineoplastic activities. **Opdivo:** works against the negative immunoregulatory human cell surface receptor programmed death-1 (PD-1, PCD-1,)
Avastin (Bevacizumab), Cyramza (Ramucirumab)	Monoclonal antibody directed against the vascular endothelial growth factor (VEGF), a pro-angiogenic cytokine.

Paraplat (Carboplatin)	This agent is activated intracellularly to form reactive platinum complexes that bind to nucleophilic groups such as GC-rich sites in DNA, thereby inducing intrastrand and interstrand DNA cross-links, as well as DNA-protein cross-links with antineoplastic properties. These carboplatin-induced DNA and protein effects. **Result** in apoptosis and cell growth inhibition
Mustargen (Mechlorethamine Hydrochloride)	The hydrochloride salt of mechlorethamine, a nitrogen mustard and an analogue of sulphur mustard, with antineoplastic and immunosuppressive activities. Mechlorethamine is metabolized to an unstable, highly reactive ethyleniminium intermediate that alkylates DNA, particularly the 7 nitrogen of guanine residues, resulting in DNA base pair mismatching, DNA interstrand crosslinking, the inhibition of DNA repair and synthesis, cell-cycle arrest, and apoptosis.
Tafinlar (Dabrafenib)	It is inhibitor of B-raf (BRAF) protein with potential antineoplastic activity. Activity of B-raf, which may inhibit the proliferation of tumour cells which contain a mutated BRAF gene.
Portrazza (Necitumumab)	A fully human IgG1 monoclonal antibody directed against the (EGFR) with potential antineoplastic activity.
Gilotrif (Afatinib Dimaleate), Vizimpro (Dacomitinib), Tagrisso (Osimertinib)	The dimaleate salt anilinoquinazoline derivative and inhibitor of the receptor tyrosine kinase (RTK) epidermal growth factor receptor (ErbB; EGFR) family, with antineoplastic activity. **Gilotrif:** EGFR mutants, **Vizimpro:** exon 19 deletion, **Tagrisso:** exon 21 (L858R) the EGFR T790M gatekeeper mutation
Mekinist (Trametinib)	It is an inhibitor of the mitogen-activated protein kinase (MEK MAPK/ERK kinase) with potential antineoplastic activity.

1.2.4 Targeted therapy

Thus far, chemotherapy has provided moderate to poor efficiency for treatment of lung cancer, as demonstrated by the very high mortality, but also the usually high toxicity of classical chemotherapy, which creates morbidity problems. In the last two decades, targeted therapy has started being implemented to eliminate cancer cells carrying specific aberrations. More specifically, Targeted therapy is a drug aimed to attack a certain molecular agent or pathway involved in the development of cancer such as erlotinib and gefitinib which work as inhibitors for cancer cell growth and are administered in NSCLC cases when surgery and radiotherapy are no longer applicable. On the other hand, target therapy is usually used instead of chemotherapy in the late stage (Ulivi et al. 2013), due to the fact that, in the advanced stage of NSCLC, cancer cells spread out and cannot be reached through surgery, while chemotherapy with radiotherapy involve some resistance. The first target for the doctor is stopping the spreading of tumour cells (Baxevanos and Mountzios 2018), which need new blood vessels to continue growing, therefore, inhibiting angiogenesis is required. A mono-antibody such as 'bevacizumab (avastin) and ramucirumab (cyramza)' is the first target, while the other therapy goal involves the receptor of the vascular endothelial growth factor VEGF stopping the growth of new blood vessels. This targeted therapy is usually used in combination with chemotherapy (Baxevanos and Mountzios 2018; Rolfo et al. 2017). Moreover, most common tumours have a mutation in *EGFR, ALK, ROS1 and BRAF* genes (Rolfo et al. 2017; Vansteenkiste et al. 2013; Ulivi et al. 2013).

Furthermore, EGFR plays a critical role in dividing and proliferation. Therefore, targeted therapy such as [erlotinib (tarceva), afatinib (gilotrif) gefitinib (iressa) osimertinib (tagrisso) dacomitinib (vizimpro) responsible for blocking EGFR signalling in NSCLC patients who have an EGFR mutation is recommended. In some cases, NSCLC patients developed secondary mutations such as T790M showing resistance against specific targeted therapy; as a result, in this case osimertinib is recommended because it works against the T790M mutation (Ulivi et al. 2013; Rolfo et al. 2017).

Furthermore, *ALK* rearrangement most commonly appears in adenocarcinoma in NSCLC, at a rate of approximately 50%. *ALK* rearrangement leads to an increase in cell growth and spreading. Target therapy such as crizotinib (xalkori), ceritinib (zykadia), alectinib (alecensa), brigatinib (alunbrig) and iorlatinib (iorbrena) is used for both ALK rearrangement and also for *ROS1* mutation. *BRAF* gene alteration also leads to the spreading of cancer cells, therefore, target therapy such as dabrafenib (tafinlar) has been used to inhibit BRAF, with trametinib (mekinist) used to block *MET* (Golding et al. 2018; Hallberg and Palmer 2011; Ulivi et al. 2013).

Crizotinib, ceritinib, and alectinib are ATP competitive molecules which function as *ALK* inhibitors. Two studies compared crizotinib with platinum target therapy and chemotherapy, the first showing an increase in progression-free survival PFS of 7.7 months for 347 NSCLC patients who had ALK rearmament and who were treated through chemotherapy, followed by crizotinib. This was compared with other NSCLC patients who still take chemotherapy with PFS (3 months) (Golding et al. 2018). Meanwhile, the other study involved 343 NSCLC patients who had ALK rearrangement and who received systemic treatment for advanced cancer, receiving either crizotinib orally or platinum through intervenors. The study shows better PFS results with crizotinib compared with platinum (10.9 vs. 7.0 months) (Golding et al. 2018). Resistance appears following treatment with crizotinib after two years because secondary mutations most likely develop in the *ALK* gene (Hallberg and Palmer 2011). Many mutations have been recorded in the *ALK* tyrosine kinase domain, such as 1151 Tins, which leads to promoting ATP binding stability, while with active ALK, C1156Y does the same. Meanwhile, L1196M leads to inactivating sites that prevent crizotinib from binding, while G1269A impairs the affinity of crizotinib for the ATP binding site. In addition, D1203N located in ATP binding in ALK also plays a role in the resistance (Golding et al. 2018; Hallberg and Palmer 2011).

1.2.5 Immunotherapy

The main problem with classical chemotherapy is its low efficiency and high toxicity. However, targeted therapies used to overcome this obstacle are not problem free either, as in the case of lung cancers which are heterogeneous, exhibiting a mosaic of the targeted aberrations. For example, abnormalities have been shown in 10%-15% of EGFR and 2-7% of ALK rearrangement. Therefore, a new modality has been devised to treat human cancer, including lung, by targeting cancer cells through the patient's own immune cells (Davies 2014).

Immunotherapy, aimed at using the immune cells to recognise and target cancer cells, has begun to be used to treat NSCLC by using immune checkpoint inhibitors, while usually the immune system uses these checkpoints to protect the normal cells attacked by the immune cells. These checkpoint inhibitors are aimed at turning off the checkpoints, which leads to recognising the cancer cells (Rolfo et al. 2017).

Blood tests used to detect specific protein (PD-1) are usually requested because increasing the level of PD-1 leads to a better response with immune and target therapy cells (Rolfo et al. 2017). Immunotherapy such as nivolumab (opdivo) and pembrolizumab (keytruda) targets programmed cell death PD-1.

NSCLC cases commonly involve the PD-1/PD-L1. More specifically, using anti-PD-1/PD-L1 antibodies shows a significant increase in overall survival rate. NSCLC patients who have increased expression of PD-1 show a better survival rate when treated with one of the checkpoint inhibitors as well as less toxicity.

Many studies have shown that the use of a combination of chemotherapy and immunotherapy as a first line treatment for NSCLC patients is highly beneficial (Baxevanos and Mountzios 2018; Iwai et al. 2002) as immunotherapy assists the immune system finding and destroying tumor cells (Lazzari et al. 2018).

1.3 Drug Resistance

It is now well established that drug resistance in cancer cells is caused by different levels of molecular alterations leading to increased drug efflux, drug inactivation, and sequestration by enzymes, DNA repair, target modification, and evasion of apoptosis (Wangari-Talbot and Hopper-Borge 2013). The usual late detection of lung cancer presents with a complication regarding drug sensitivity: the long natural history of tumour is normally associated with high molecular heterogeneity; therefore, an increased chance of acquired mutations that may cause drug resistance.

When treated with chemotherapy agents, NSCLC patients may develop a second mutation (Wangari-Talbot and Hopper-Borge 2013) with diverse phenotypic outcome affecting drug response: increased DNA repair, high expression of oncogenes, or reduced expression/activity of tumour suppressor genes, reduced apoptotic potential the apoptosis pathway etc. (d'Amato et al. 2007).

1.4 Selected chemotherapeutics in this study

In this study, I selected to put the spotlight on four chemotherapeutic agents, i.e. gemcitabine, vinorelbine, cisplatin, and carboplatin.

1.4.1 Platinum

Platinum is a chemotherapeutic agent approved to treat cancers such as NSCLC, lipomas, and germ cell tumours. It is one of the oldest drugs still widely used and prescribed until present, especially in the third world where targeted therapy has not reached yet. Therefore, Cisplatin and Carboplatin have been chosen for this research. Both Cisplatin (Cis) and Carboplatin (Carb) lead to miscoding by adding alkyl agents where they do not belong, stopping the correct bases from combining. Platinum forms cross-linked bonds with DNA, both interstrand and intrastrand, therefore stopping cell proliferation.

1.4.1.1 Platinum action

Platinum is an antineoplastic which works through three different mechanisms. First, by adding an alkyl group to the DNA base, it stops both DNA synthesis and RNA transcription due to the fact that repairing enzymes start fragmenting the DNA to replace the alkyl group. Second, platinum leads to DNA damage by forming cross-like bonds between atoms and DNA, which also prevents DNA synthesis and transcription. Third, mutation occurs through the mispairing of nucleotides (Drugbanck 2019a) (Figure 1.4).

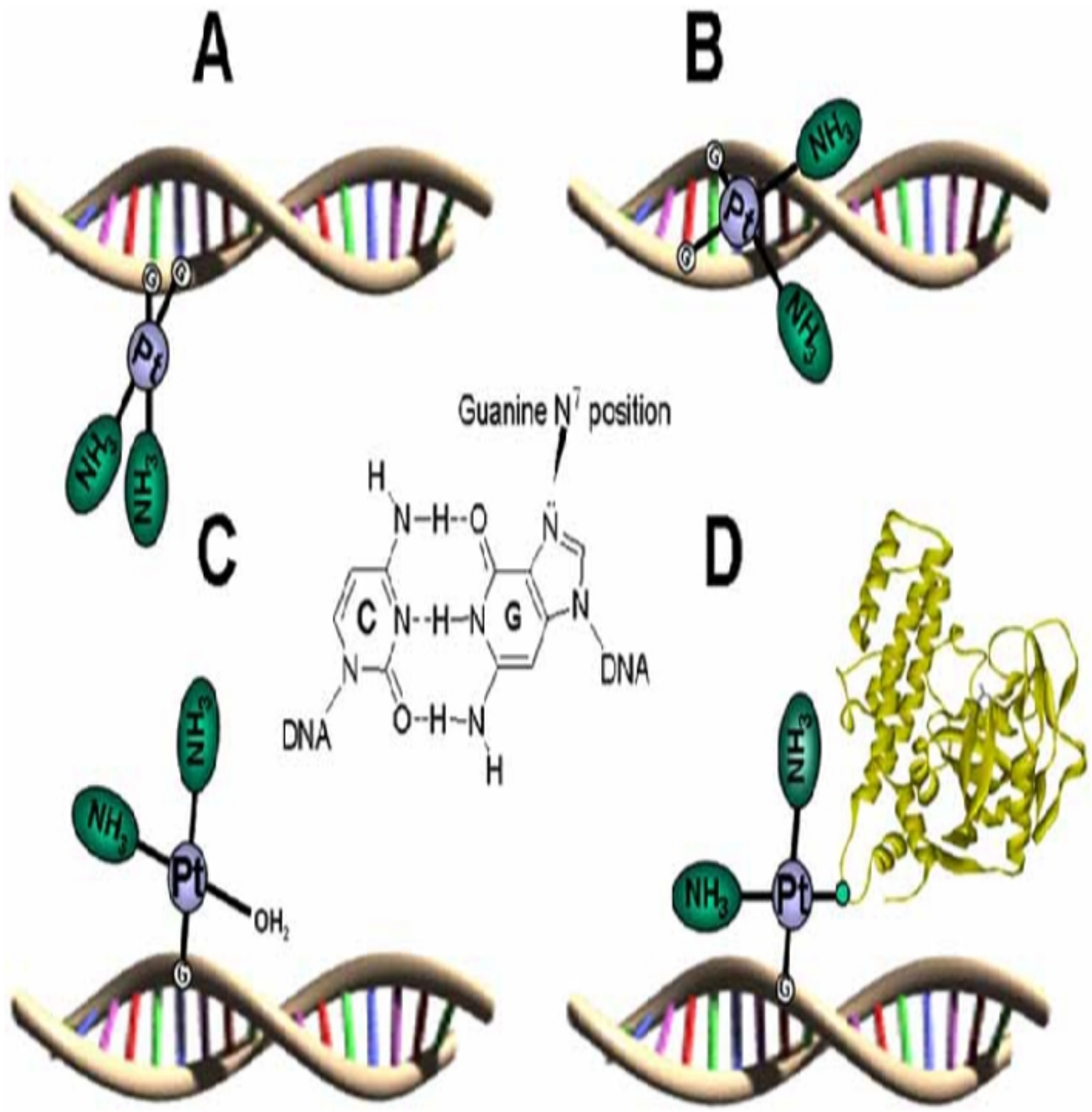

Figure 1.4: *Cisplatin DNA adducts*: Cisplatin is an alkylating agent that can add an alkyl group to the electronegative group under specific conditions inside the cell. Cisplatin directly targets the DNA by forming a cross-link. A: Cisplatin forms intrastrand (within the same strand) cross-links with DNA. B: interstrand cisplatin cross-links that occur between the two opposite strands of double-stranded DNA. C: Monoadducts form with DNA. D: DNA-Cisplatin-protein adducts. Adopted from (Fahmy and Gharib 2014).

1.4.1.2 Platinum resistance

Resistance to platinum develops through multiple factors and on either the external or internal pathways. Platinum adds an alkyl group to the DNA to form DNA adducts, resulting in cross-linking interstrands or intrastrands. Resistance can aggravate by recognising the defect and fixing it with one of these five DNA repair pathways: nucleotide excision repair NER, mismatch repair MMR, double-strand break repair, base excision repair BER, and direct repair (Martin, Hamilton, and Schilder 2008).

1.4.2 Gemcitabine

Gemcitabine is an antineoplastic antimetabolite, is a nucleoside analog used to treat NSCLC and many other cancers. Gemcitabine masks purine or pyrimidine in order to replace one of the nucleic acid building blocks, as well as replacing cytidine in nucleic acid during DNA replication, which stops cell division as new nucleosides cannot add to the affected nucleoside, arresting the cell in S phase and causing cell death. It can both inhibit the enzyme responsible for altering the cytosine nucleotide into the deoxy derivative (Conroy et al. 2011).

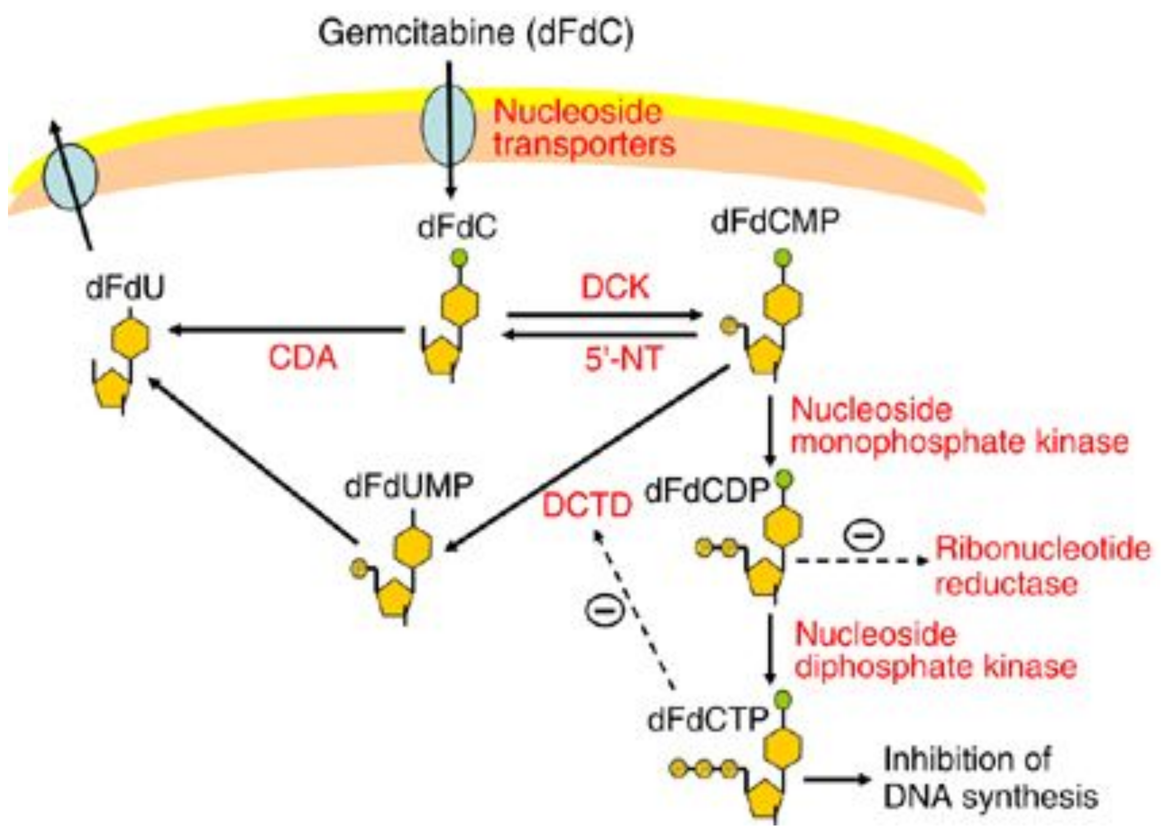

Figure 1.5: *Gemcitabine mechanism of action*: gemcitabine dFdC is carried into the cell by nucleoside transporters. First, deoxycytidine kinase (DCK) phosphorylates dFdC to gemcitabine monophosphate dFdCMP. Subsequently, dFdCMP phosphorylates to gemcitabine diphosphate dFdCDP by nucleoside monophosphate kinase. Gemcitabine diphosphate can effectively inhibit ribonucleotide reductase. Then, it phosphorylates to gemcitabine triphosphate dFdCTP by nucleoside diphosphate kinase. dFdCTP inhibits deoxycytidine monophosphate deaminase DCTD, which suppresses inactivation of dFdCMP. In contrast, most of the gemcitabine is inactivated by converting into2′-deoxy-2′,2′-difluorouridine (dFdU) by CDA. dFdCMP can also be inactivated by converting into 2′-deoxy-2′,2′-difluorouridine monophosphate dFdUMP by DCTD. (Ueno, Kiyosawa, and Kaniwa 2007).

1.4.2.1 Gemcitabine Action

Gemcitabine causes cell death by inhibiting thymidylate synthesis, resulting in the arrest of cell synthesis. It is a pro-drug activated after intracellular conversion by deoxycytidine kinase DCK into two active metabolites: gemcitabine-diphosphate and gemcitabine triphosphate. Gemcitabine-diphosphate inhibits ribonucleotide reductase, which is the enzyme responsible for catalysing the synthesis of deoxy nucleoside, triphosphates required for DNA synthesis. Gemcitabine triphosphate competes with endogenous deoxy nucleoside triphosphates for incorporation into DNA. Phosphorylated metabolites of gemcitabine can reduce cellular 5′-nucleotidase (5′-NT), and dFdCMP is also converted and deactivated, by deoxycytidine monophosphate deaminase DCTD into (dFdUMP) (Figure 1.5) (Plunkett et al. 1996).

1.4.2.2 Gemcitabine Resistance

Resistance against Gemtcitabine (GM) has been a setback, being mainly caused through defects in the activation enzyme involved in the metabolism of GM or the proteins involved in programmed cell death (Baxevanos and Mountzios 2018). GM resistance is caused by either d-cyc deaminase (dCDA) or decreased d-cyc kinase (dCK), which plays a role in activation of GM through transfer dFdC to dFdCMP by RRM 1/2 which inhibit dCK (Figure 1.5) (Ueno, Kiyosawa, and Kaniwa 2007). Ribonucleotide reductase contains RRM 1/2 and is involved in DNA synthesis by working a critical role in converting ribonucleotides to deoxy-ribonucleotides through DNA polymerisation and repair (Davidson et al. 2004). NSCLC patients were treated with GM advanced: the patients with RRM 1 +ve had worse OS and disease control than the patients with RRM 1 -ve tumours. Many studies have recognised RRM 2 is the reason behind GM resistance. One of the studies has indicated that RRM 2 expression was high in resistance cells. Also, it was found that the resistance was reversed through used GM8510 as an inhibitor for RRM 2 (Chen et al. 2018). GW8510 plus GM leads to autophagy induction parallel with the impairment of DNA DSB repair, increasing apoptosis and autophagy (Chen et al. 2018).

1.4.3 Vinorelbine

Vinorelbine (VRL) is an antitumour chemotherapy used to treat NSCLC and other cancers counting as the third generation of Vinca alkaloids. It combines with platinum or gemcitabine to treat NSCLC, the toxicity of a combined treatment was studied, and the combination increased the survival rate in lung cancer patients. Vinca alkaloids act as a poison for spindles and work through the depolymerisation of tubulin, which is necessary to make the microtubules that play a critical role in cell division (Wangari-Talbot and Hopper-Borge 2013) (Figure 1.6).

1.4.3.1 Vinorelbine Action

Vinorelbine is antimitotic and interacts with tubulin, leading to stop mitosis in metaphase. In cell division, VRL poisons the spindle (which plays a role in chromosome segregation), ending the cell in the G2/M phase. It has been hypothesised that just as VRL targets microtubulin, it can also target chromatin components. VRL can target chromatin, DNA, and histones (Figure 1.7) (Drugbanck 2019b).

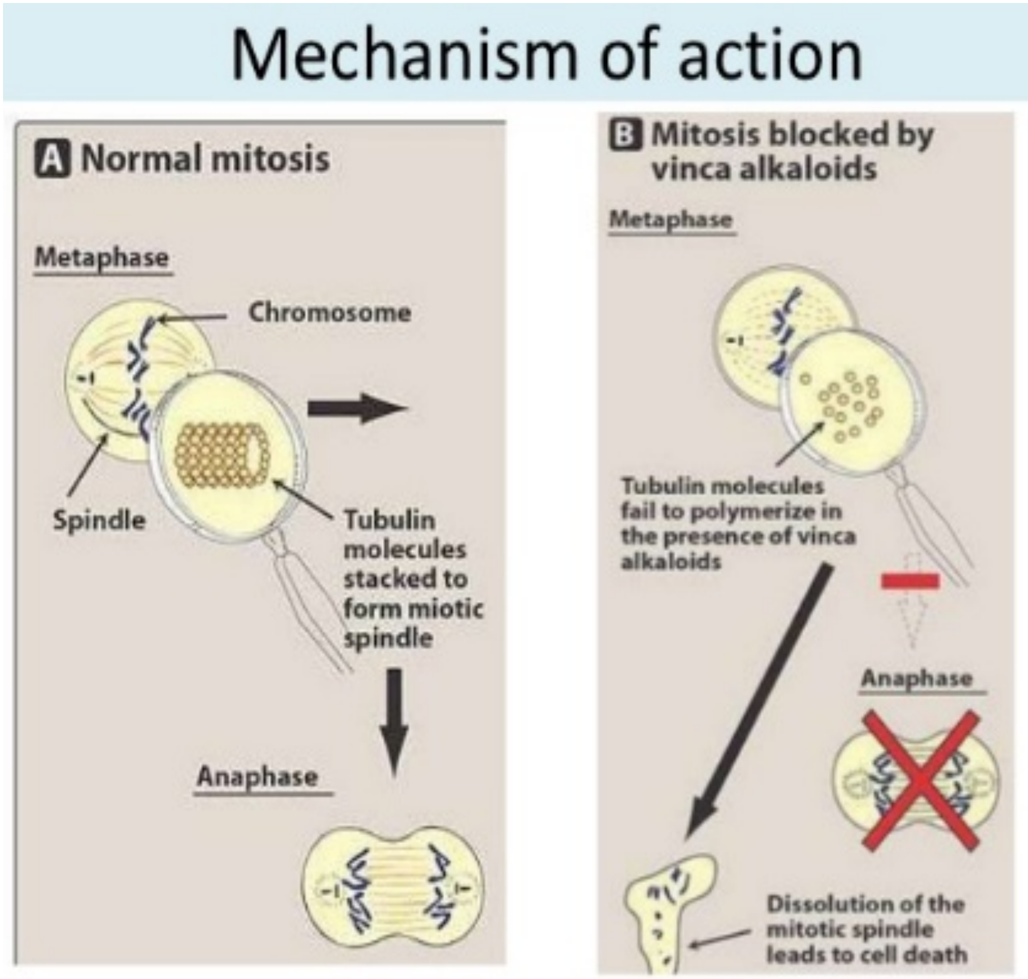

Figure 1.6*: Vinca alkaloid mechanism*: In normal metaphase, the micro-tubulin complex polymerase consists of tubulin dimers stacked to form the spindle. However, in the presence of Vinca alkaloids, microtubules depolymerise and cannot stack together to form the spindle as in normal mitosis, leading to cell death (Kim et al. 2011).

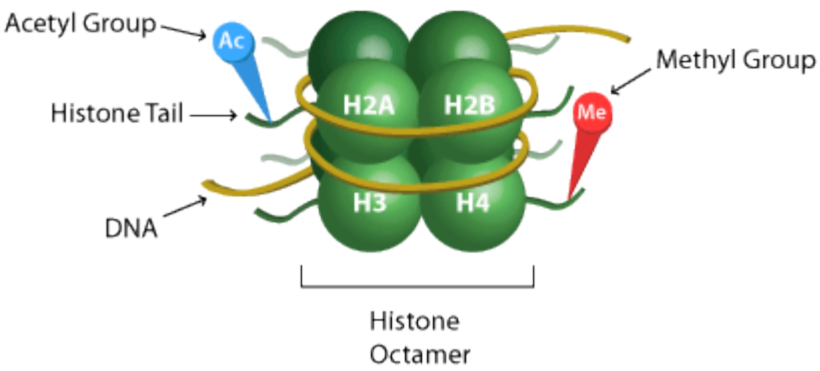

Figure 1.7: *Histone octamer:* inside the cell, DNA combines with specific proteins, and histones make nucleosomes. Usually, a histone includes an 'H1 family and four core histone nucleosomes H2A, H2B, H3, H4', set in an octamer shape. DNA is infolded within nucleosomes, which are chromatin units adding methyl and acetyl groups to regulate gene expression by controlling the opening and closing of the chromatin (Rastogi et al. 2010).

1.4.3.2 Vinorelbine Resistance

Resistance against VRL has been identified in NSCLC patients, the mechanism behind the resistance possibly coming from micro-tubulin components. Micro-tubulin complex polymerase consists of tubulin dimers (one a-tubulin and one b-tubulin). Tubulin polymerisation and function can be regulated by micro-tubulin polypeptide proteins, such as t protein, micro-tubulin associate protein 4, and stable tubule only polypeptide protein (Sève et al. 2005).

It has been noted that a high level of class III b-tubulin is associated with poor progression and short OS in NSCLC patients exposed to VRL, as it causes resistance (Sève et al. 2005). Moreover, it has been determined that the expression of the tubulin isotype is associated with resistance against anti-tubulin agents. Ninety-three NSCLC patients in stages III and IV treated with VRL-based chemotherapy showed the high levels of class III b tubulin expression associated with resistance against VRL. The increase of class III-tubulin isotype correlates with shortening progression-free survival and overall survival P=0.002. High p2-a tubulin was associated with short OS P=0.018 (Sève et al. 2005). Additionally, immunohistochemistry assays performed for 2665 patients in the NCIC JBR.10 trial demonstrated that high expression of III b-tubulin levels is related to promotion of the response to adjuvant chemotherapy Vinorelbine/Cisplatin (Sève et al. 2007).

The ABC family, which binds to ATP, is one of the drug transporter proteins that plays a role in drug resistance. It has been recorded that increased expression of ABC leads to an increase in drug efflux and a decrease in the drug accumulation that causes resistance to Cisplatin and Vinca alkaloids. P-glycoprotein (P-gp) from the ABC family of proteins works as a drug efflux pump and is found to be overexpressed in drug resistance to NSCLC. One study conducted by (Wangari-Talbot and Hopper-Borge 2013) found that increased expression of ABC transporter proteins (ABCC10/MRP7) in 12 lung cancer cell lines was related to VRL resistance.

Moreover, RLIP76 non-ATP binding cassette transport proteins, has having a role in mediating VRL transport and resistance. The ATP catalysis depends on the efflux of unconjugated VRL, (Stuckler et al. 2005) finding that the augmented expression of RL1P76 increases efflux, which subsequently increases resistance. Anti 1P76 can sesitize lung cancer cells to VRL by inhibiting efflux.

1.5 Selected sensitising agents

In this study, I selected two epigenetic drugs (sodium valproate and decitabine) and two other approved drugs (aminomethylphosphonic acid and fendiline) to increase chemosensitivity. The basis of selection was literature based. Epigenetic sensitisation has been previously shown (Lin et al. 2008) while AMPA and fendiline have also been shown to sensitise cells to certain chemotherapy agents (Woods et al. 2015), therefore I wanted to validate previous observations.

1.5.1 Sodium valproate (VPA)

Due to its anticonvulsant properties, sodium valproate (VPA) is used to treat epilepsy and functions as a histone deacetylase inhibitor (HDACi). HDACis are small molecules or compounds that can inhibit the activity of HDACs, activate the expression of a large number of genes and subsequently alter various phenotypic characteristics such as cell proliferation or apoptosis (Figure 1.8) (Eggert et al. 2001).

Valproic acid, in addition to selectively inhibiting the catalytic activity of class I HDACs, stimulates proteasomal degradation of HDAC2. Valproic acid induced HDAC2 turnover critically depend on the E2 ubiquitin conjugase Ubc8 and the E3 ubiquitin ligase RLIM. Ubc8 gene expression is induced by VP. Thus, poly-ubiquitination and proteasomal degradation provide an isoenzyme-selective mechanism for downregulation of HDAC2 (Krämer et al. 2003).

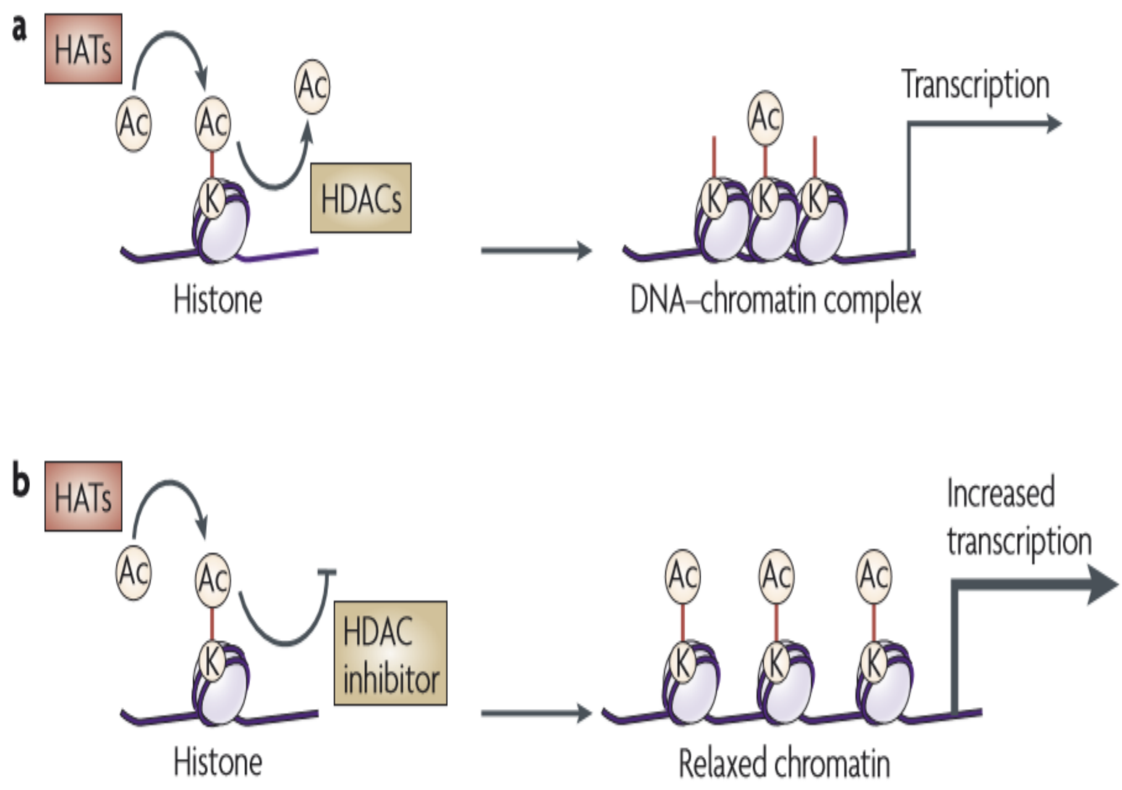

Figure 1.8: *Mechanism of histone deacetylation inhibitor.* Normally, cells control the coiling and uncoiling of DNA around histones. a- In the transcription gene, opening of the chromatin by histone acetyl transferases (HAT) can acetylate the lysine residues in core histones. In contrast, silenced genes to control the transcriptional amount by histone deacetylases (HDAC) can remove the acetyl groups from the lysine residues formation of a condensed chromatin. b- Histone deacetylation inhibitor (HDACi) can reverse the closing of the chromatin by blocking the HDAC that leads to the hyperacetylation of histones which opens the chromatin and increases the transcription. In cancer, most of TSGs are silenced, therefore, HDACi is targeted to re-express the silenced genes. Adapted from (Kazantsev and Thompson 2008).

It has been reported that VPA induces differentiation of tumour cells through acetylation of histone H3 as well as to induce acetylation of α-tubulin (Khan et al. 2008; Gurvich et al. 2004). Moreover, sodium valproate stimulates alterations in the expression of other cell cycle-related proteins, for example (p27 and cyclin D1) (Johnson and Walker 1999).

Corresponding to the results of pre-clinical studies and early clinical trials, HDACi in combination therapy with chemotherapeutics may be very useful (Nolan et al. 2008) both for small cell lung cancer (Hubaux et al. 2010) and NSCLC (Schiffmann et al. 2016). More particularly, in pre-clinical studies, HDACi has been revealed to be synergistic with various chemotherapeutics agents, therefore it is expected to be most effective therapeutically when used in combination with other anti-cancer agents (Nolan et al. 2008).

1.5.2 aza-2’-deoxycytidine (Decitabine)

Decitabine DAC was used to treat the myelodysplastic syndrome (MDS). More particularly, DAC can incorporate into DNA and RNA during replication and transcription. 5-aza-20 -deoxycytidine (decitabine) contains nucleoside analogues, which are phosphorylated by cellular kinases. When incorporated into DNA, they form a covalent bond with the DNMT trapping the enzyme and making it unavailable for additional methylation, thus subsequent in demethylation of replicating nascent DNA (Szyf 2009).

The incorporation of decitabine in the nascent DNA leads to the formation of an irreversible covalent bond between the nitrogen in the fifth position of the modified pyrimidine and the catalytic site of the DNMT1 (Raynal and Issa 2016). DAC works as an inhibitor of methyltransferase, which results in demethylation in the endogenous sequence. Demethylation of DNA leads to an increase in the hypomethylation of the DNA responsible for differentiation or apoptosis, leading to renovate the gene functions that may be responsible for cell proliferation and differentiation (Figure 1.9).

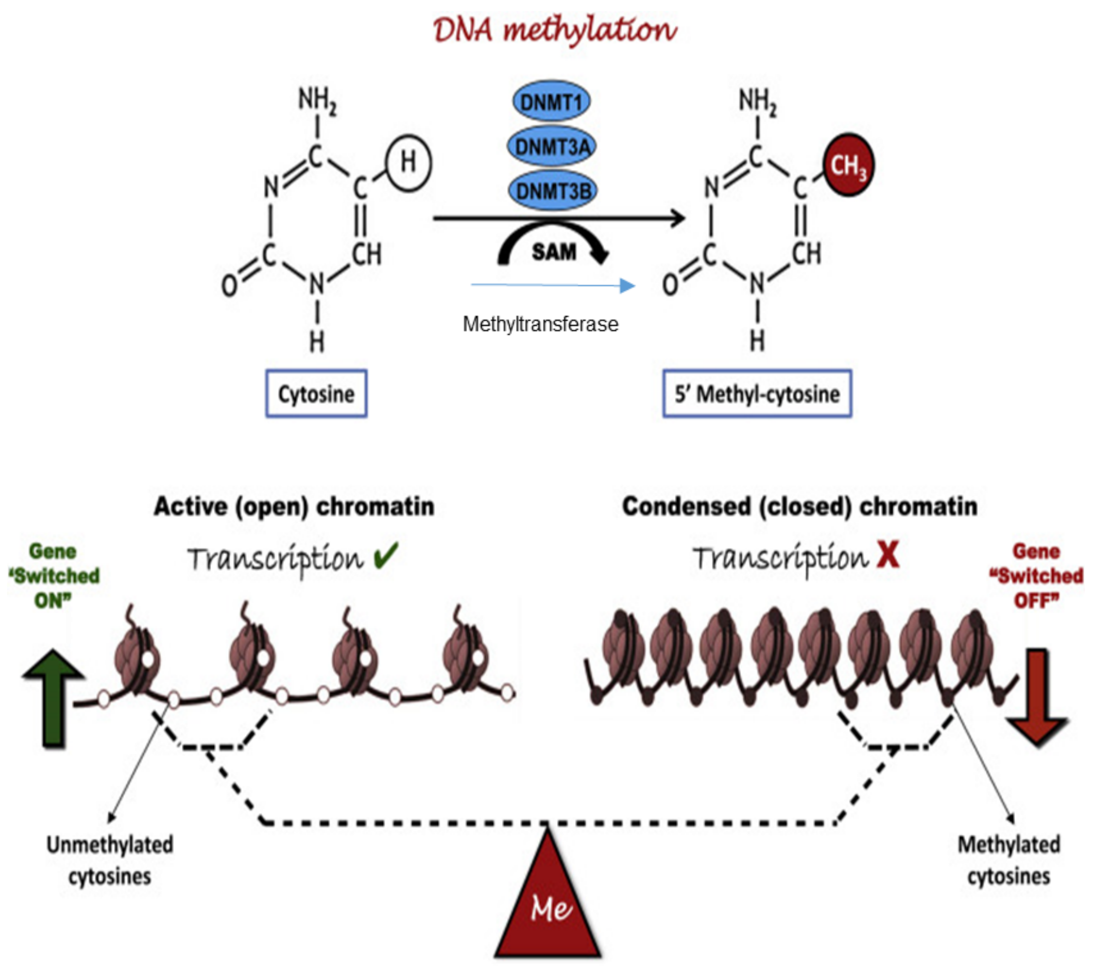

Figure 1.9: *Methyltransferase DNMTs*: DNA methylation controls gene expression by working as an epigenetic switch to open and close the chromatin by altering the interactions between DNA and proteins. Unmethylated cytosines open the chromatin and increase the transcription. DNA methylation performed by transfer of methyl groups from S-adenosylmethionine (SAM) to the C-5 position of cytosine can be catalysed by methyltransferases (DNMTs). Adopted from (Agrawal et al. 2018).

Moreover, DAC does not cause a major suppression of DNA synthesis. Furthermore, DAC can create a covalent adduct between DNA and DNA methyltransferase that increases the cytotoxicity in rapidly dividing cancer cells. DAC works in S phase of the cell cycle, so the non-proliferating cells are not sensitive (Goffin and Eisenhauer 2002). Decitabine has been tested in several trials (Šorm et al. 1964; Goffin and Eisenhauer 2002) in head and neck squamous cell carcinoma (Viet et al. 2014) and NSCLC (Momparler and Ayoub 2001).

1.5.3 Aminomethylphosphonic acid (AMPA)

Aminomethylphosphonic acid (AMPA) is an approved drug, which functions as a Serine hydroxymethyltransferase1 (SHMT1) inhibitor (Anderson and Stover 2009). SHMT is the major source of one-carbon units required for nucleotide synthesis. Humans have cytosolic (SHMT1) and mitochondrial (SHMT2) isoforms, which are up-regulated in lung cancers (Wang et al. 2007), making the enzyme an attractive drug target (Scaletti et al. 2019).

Serine hydroxymethyltransferase plays an important role in cellular one-carbon pathways by catalysing the reversible, simultaneous conversions of L-serine to glycine and tetrahydrofolate (THF) to 5,10-Methylenetetrahydrofolate. In addition to folate, changes in amino acid metabolism can also affect cofactor levels. For instance, glycine and serine provide methyl groups to SAM via the activities of serine hydroxymethyltransferase (SHMT) and the glycine cleavage system. SHMT plays a role in epigenetic changes (Meier 2013).

In addition, AMPA has been determined to be a proliferation inhibitor and increases the apoptosis activity in pancreatic cancer (Parajuli et al. 2016).

One of the PhD students as a previous study in the lung group studied examined the effect of SHMT1 expression when PE/CA-PJIS cell line is treated with AMPA combined with a 5-Fu chemotherapy agent. The study demonstrated that AMPA increased the sensitivity of the 5-Fu (Li et al. 2013).

1.5.4 Fendiline

Fendiline acts as a calcium channel blocker. A study has reported that targeting calcium signalling can reverse epigenetic silencing of tumour suppressor genes (Raynal et al. 2016).

Another study has demonstrated that calcium-mediated splicing monitoring mechanism depends on the changes of histone modifications. Especially, the regulation that appears across changes in calcium-responsive kinase activities results in alterations of that histone modifications and subsequent changes in the transcriptional elongation rate and exon skipping. Also, the study determined that increased intracellular calcium levels result in histone hyperacetylation along the body of the genes containing calcium-responsive alternative exons by disrupting the histone deacetylase-to-histone acetyltransferase balance in the nucleus. Accordingly, the RNA polymerase II elongation level increases remarkably in those genes, leading to in the skipping of the alternative exons (Sharma et al. 2014).

Changes in sarcoplasmic reticulum Ca2+ release caused changes in the expression of the developmental phase specific genes, which may be the result of changes in class IIa HDAC-localisation (Karppinen et al. 2018).

Finally, Fendiline was chosen in this research to re-sensitize chemotherapies due to the fact that a paper published in 2015 on evidence in pancreatic cancer which showed that Fendiline inhibits proliferation and invasion by interfering with β-catenin signalling in the Wnt pathway, which is often deregulated in pancreatic cancer (Woods et al. 2015).

1.6 LANCL1 and LANCL1-AS1 role in chemosensitivity

Despite the fact that the long noncoding RNA (LncRNA) revolution has impacted on all levels of gene transcription, the functions of LncRNA still remain unclear, with many studies having been conducted to investigate the basic attributes. As a result, a part of the current work identifies LncRNA markers in cancer management.

The lung group at the University of Liverpool has recently evaluated LncRNA deregulation in non-small-cell lung cancer (NSCLC) to support the existing data. More specifically, they achieved a major discovery with 44 tissue pairs (normal and tumour), besides employing both 29 technical pairs (normal and tumour) and 38 independent biological pairs (normal and tumour) to validate the target. This research determined that the 14 LncRNA profile remarkably discriminated NSCLC tissue from normal lung tissue, one of them being *LANCL1-AS1*, which is absent in NSCLC (Acha-Sagredo et al. 2020) (Figure 1.10).

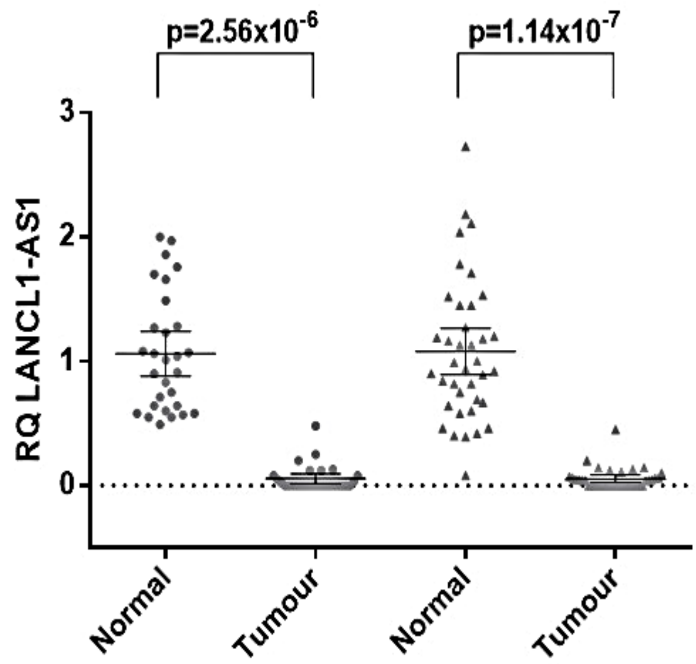

Figure 1.10: *LANCL1-AS1 is absent in NSCLC tissue in comparison with normal lung tissue.* The ideal threshold was a 2> fold change and they chose a $p < 0.01$ value as a validation goal. The p-value and fold change values were used to gain a descriptive estimation of the microarray analysis validity. Adapted from (Acha-Sagredo et al. 2020).

1.6.1 LANCL1-AS1

1.6.1.1 LncRNA

Recent improvements in sequencing technology have led to the understanding of a transcriptional profile of the entire human genome. This work has also led to the transcription of 70% to 90% of the mammalian genes (Fang and Fullwood 2016; Kashi et al. 2016; Lu et al. 2013; Spizzo et al. 2012).

Around 2% of the transcribed genome is composed of proteins, specifically coding RNA. However, the majority of the transcribed genes, around 70% to 90%, are noncoding RNA, which is either short or long in nature. Short noncoding RNA usually has less than 200 nucleotides and includes ribosome RNA (rRNA), transfer RNA (tRNA), micro RNA (miRNA), small RNA (SRNA) with between 21 and 24 nucleotides (nt), and piwi interacting-RNA (piRNA) (Fang and Fullwood 2016; Lu et al. 2013; Sun et al. 2014; Villegas and Zaphiropoulos 2015). In contrast, LncRNA contains more than 200 nucleotides that produce coding with a low expression level and low conservation. The definition of LncRNA is insufficient and arbitrary with the 200-nt cut-off, depending on the RNA purification method and according to the RNA binding to the cilice column during the RNA isolation process. LncRNA has an essential role not only in cell differentiation, proliferation and angiogenesis, but also the reduction of the apoptosis and the expression of tumour suppresser genes (Fang and Fullwood 2016; Lu et al. 2013; Sun et al. 2014; Spizzo et al. 2012; Ponting, Oliver, and Reik 2009).

Therefore, a better understanding of LncRNA's biological functions and molecular mechanisms is necessary to study cancer development and prognosis. One of the characteristics of the protein-coding gene (PCG) is open-reading frame (ORF), which requires less than 100nt to synthesize proteins. LncRNA has a non-functional ORF with more than 100nt without a synthesis protein, however, bifunctional RNA has been recognised as having the ability to either code or non-code the protein. LncRNA is variable, ranging between unstable (29%) with two-hour half-life and extra stable (70%) with a 12-hour half-life (Fang and Fullwood 2016). Moreover, LncRNA, located in the cellular cytoplasm and the nucleus (Lu et al. 2013) is involved in various diseases, especially glioblastoma and leukaemia, breast, colon, liver, prostatic, and bladder cancers. LncRNA can work as a proto-oncogene LncRNA

(AnRNA) or present as a tumour suppressor genes (TSG) such as maternity express gene 3 (MEG3), which was found to be downregulated in relation with NSCLC.

Research has found that the (MEG3) is regulated normally in glioblastoma cell lines, working as a TSG to reduce proliferation and increase apoptosis. MEG3 has been recognised to be lost in the early stage of tumour formation because of MEG3 hypermethylation in either the promoter or the intergenic sequence. Also, SPRY4-IT1 LncRNA was found to be downregulated in NSCLC patients with short-term survival, therefore both SPRY4-IT1 and MEG3 can be used as markers for the poor prognosis of NSCLC patients. Moreover, circulating LncRNA PR11-397D12-4, AC007403-1, and -ERICHI-AS1 plays a role in cancer prognosis and development, therefore it is used as markers to predict tumour genesis in NSCLC patients (Lu et al. 2013; Tang et al. 2015; Villegas and Zaphiropoulos 2015).

LncRNA has a unique role as a histone marker in the promoter region such as trimethylation in lysine 4 and lysine 36 of histone 3 (H3K4m3 and H3K36m3, respectively) with the presence of a polymerase II (pol II) binding site, which can transcribe both PCGs and LncRNA (Figure 1.11). Furthermore, LncRNA shows mono-methylation of lysin4 of histone 3 (H3K4m1) as marker distinguishing between LncRNA and mRNA (Fang and Fullwood 2016; Kashi et al. 2016).

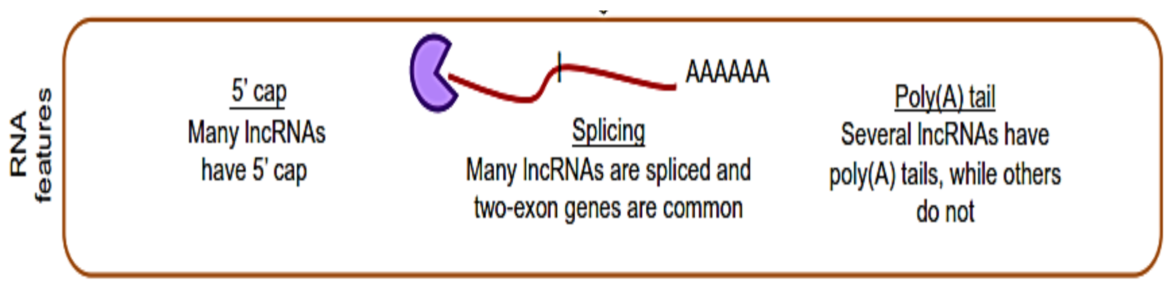

Figure 1.11*: LncRNA characteristics* (Adapted from (Fang and Fullwood 2016).

HOTAIR and MALAT were the first LncRNA distinguished before reviling the epigenetic markers. These LncRNAs act to suppress gene transcription by interacting with polycomb group proteins, around 20% interacting with polycomb repressive complex2 (PRC2) (Spizzo et al. 2012). LncRNA regulates gene expression through altering histone markers and changing chromatin structures by directing the polycomb protein to the target region in DNA, e.g. enhancer of Zeste homolog 2 (EZH2), which is a histone-lysine N-methyltransferase enzyme catalase subunit member in PRC2. The overexpression of EZH2 has been reported in NSCLC (Sun et al. 2014). LncRNA regulate transcription and translation mRNA, including through gene expressing, silencing and imprinting (Batista and Chang 2013) (Figure 1.12).

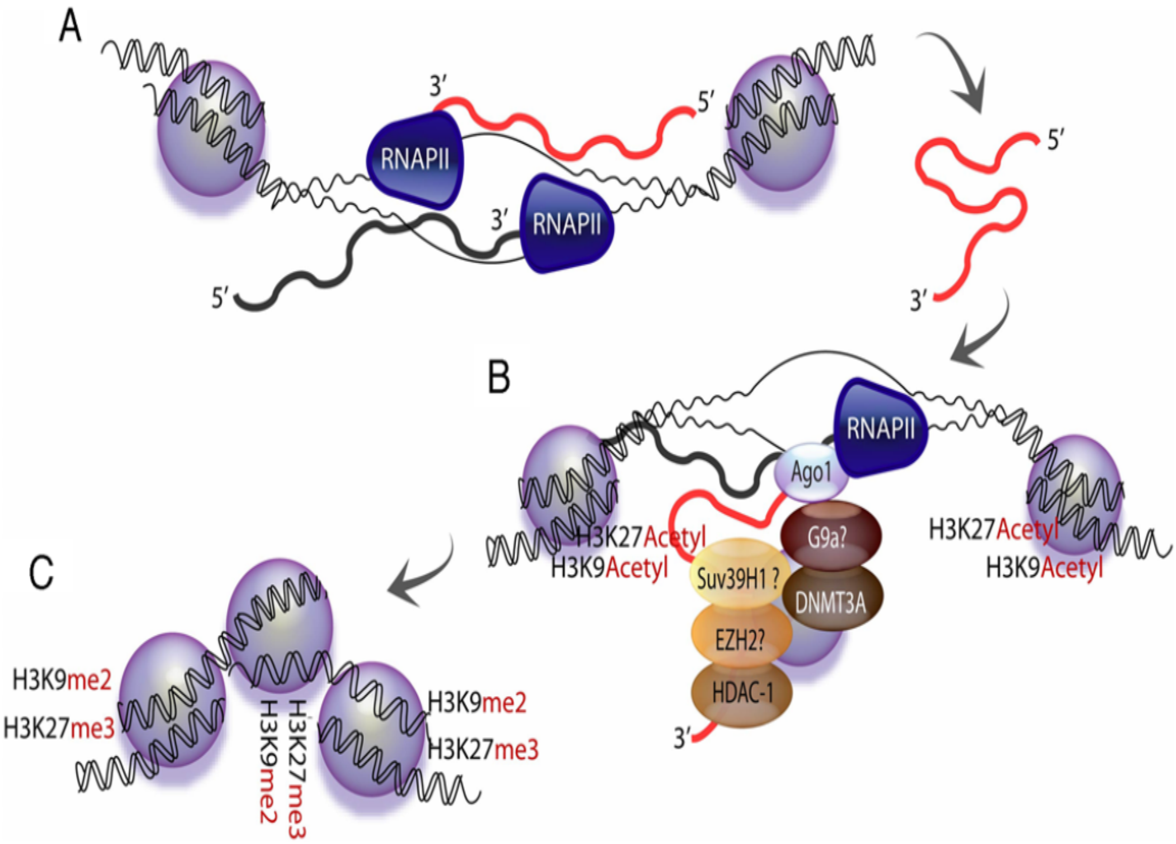

Figure 1.12: *Transcriptional regulation mediated by long antisense noncoding RNA*: (A) Antisense LncRNA is created at bidirectionally transcribed loci; (B) LncRNA is expected to co-operate "with regions of homology in a sense promoter-associated transcript". Otherwise, LncRNA can work with the desirable strand. For example, interfaces are assumed to generate the recruitment of chromatin-remodelling proteins DNA methyltransferase 3a (DNMt3a), Argonaute 1 (Ago-1), enhancer of Zeste (ezh2), suv39 h1, histone deacetylase 1 (HDAC-1), and G9a. (C) Local chromatin construction is altered by chromatin-remodelling complexes counting methylation of DNA, particularly at loci directed by the LncRNA. **Antisense strand**; **sense strand** in black. Adapted from (Saayman et al. 2014).

1.6.1.2 Antisense RNA

LANCL1-AS1 is an antisense RNA, which is one of the LncRNA members. Antisense is a transcript frame, an opposite strain to the PCG ‘sense’. Around 63% of the transcriptional strain has an antisense pair with low expression level. Antisense can operate in a cis or trans way, depending on where they are active. Operating through the cis means that antisense RNA will interact with sense gene transcript frame in the same DNA region. Moreover, trans means the antisense RNA will interact with transcript gene in distance loci or on other chromosomes (Villegas and Zaphiropoulos 2015) (Figure 4.13). LncRNA application function of action are based on the molecular interaction with nucleic acids DNA-RNA, RNA-RNA and Protein-RNA.

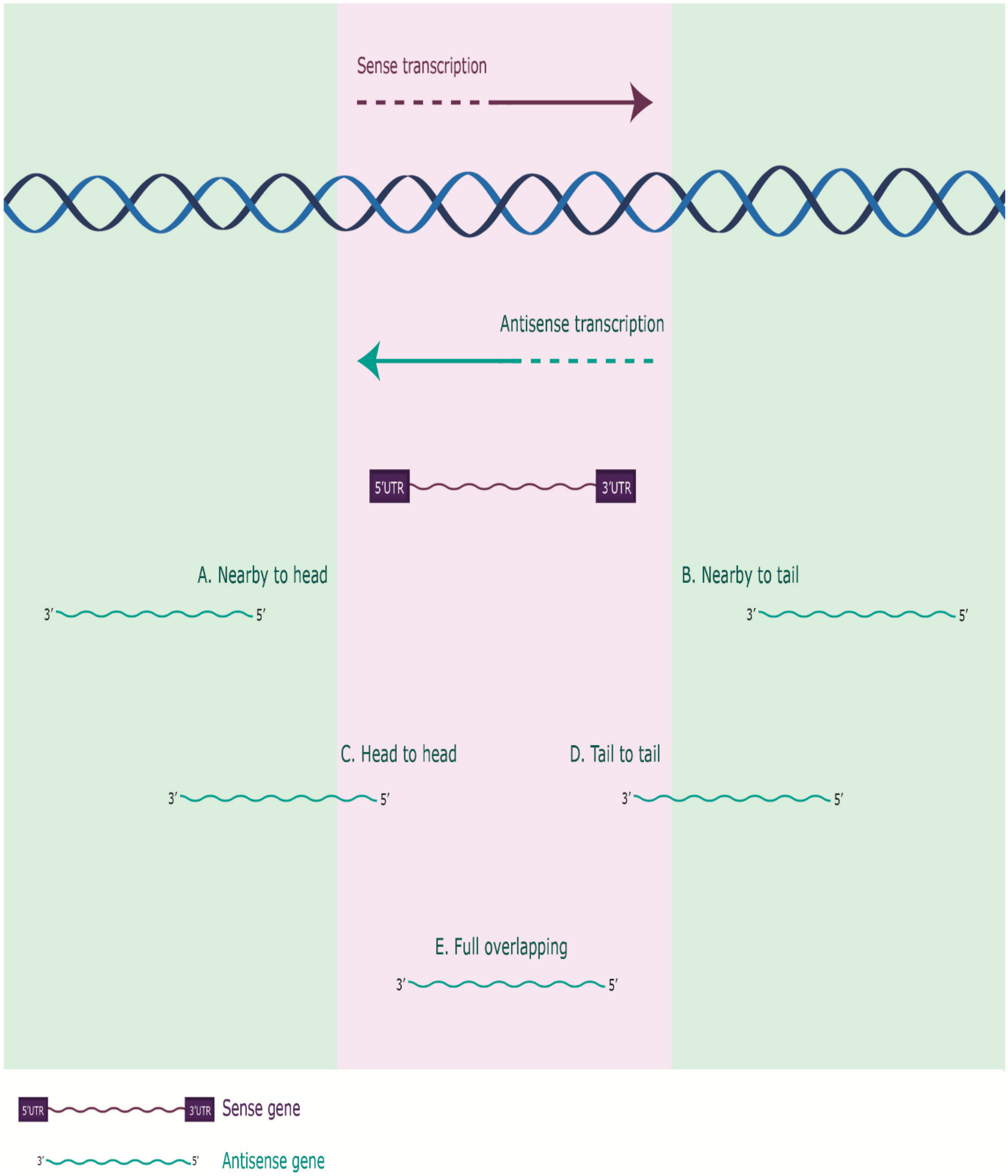

Figure 1.13: *Antisense LncRNA classification scheme.* **Intergenic**: when the sense and antisense near the head or the tail 3' end of the sense near 3' of antisense or 5' end of the sense near the 5' of the antisense. **Divergent**: when the head to the head of the sense and antisense. Convergent when tail to tail of the sense and antisense. **Overlap**: when the sense and antisense completely overlap. Adapted from (Villegas and Zaphiropoulos 2015).

1.6.3 LANCL1

Lanthionine synthetase-like protein 1 *LANCL1* is also known under alternative names, such as P40 or GRP69A. *LANCL*-like proteins are part of a big family containing groups of peptides that modify enzymes found in plants and bacteria. *LANCL1* is the mammalian member in the *LANCL*-like protein (Huang et al. 2014), with *LANCL1*, *LANCL2*, and *LANCL3* in humans. *LANCL1*3 is still under investigation, while *LANCL2* has a role in diabetes. *LANCL1*, which will be studied in this research, has 399 amino acids. Initially, research indicated *LANCL1* as a factor of stomatocytosis due to the combination with the erythrocyte protein stomatin (Zhang et al. 2009).

Due to the fact that the *LANCL1*, gene overlaps with *LANCL1-AS1* and in order to learn more about *LANCL1-AS1* (Figure 1.14) we chose to proceed with our investigation and inquire whether *LANCL1-AS1* plays a specific role in the regulation of the *LANCL1* gene. Furthermore, based on the study conducted by Zhang *et al* (2009), *LANCL1* is known to establish a direct effect to protect the brain cell against oxidative stress, which plays a major role in chemotherapy resistance (Zhang et al. 2009).

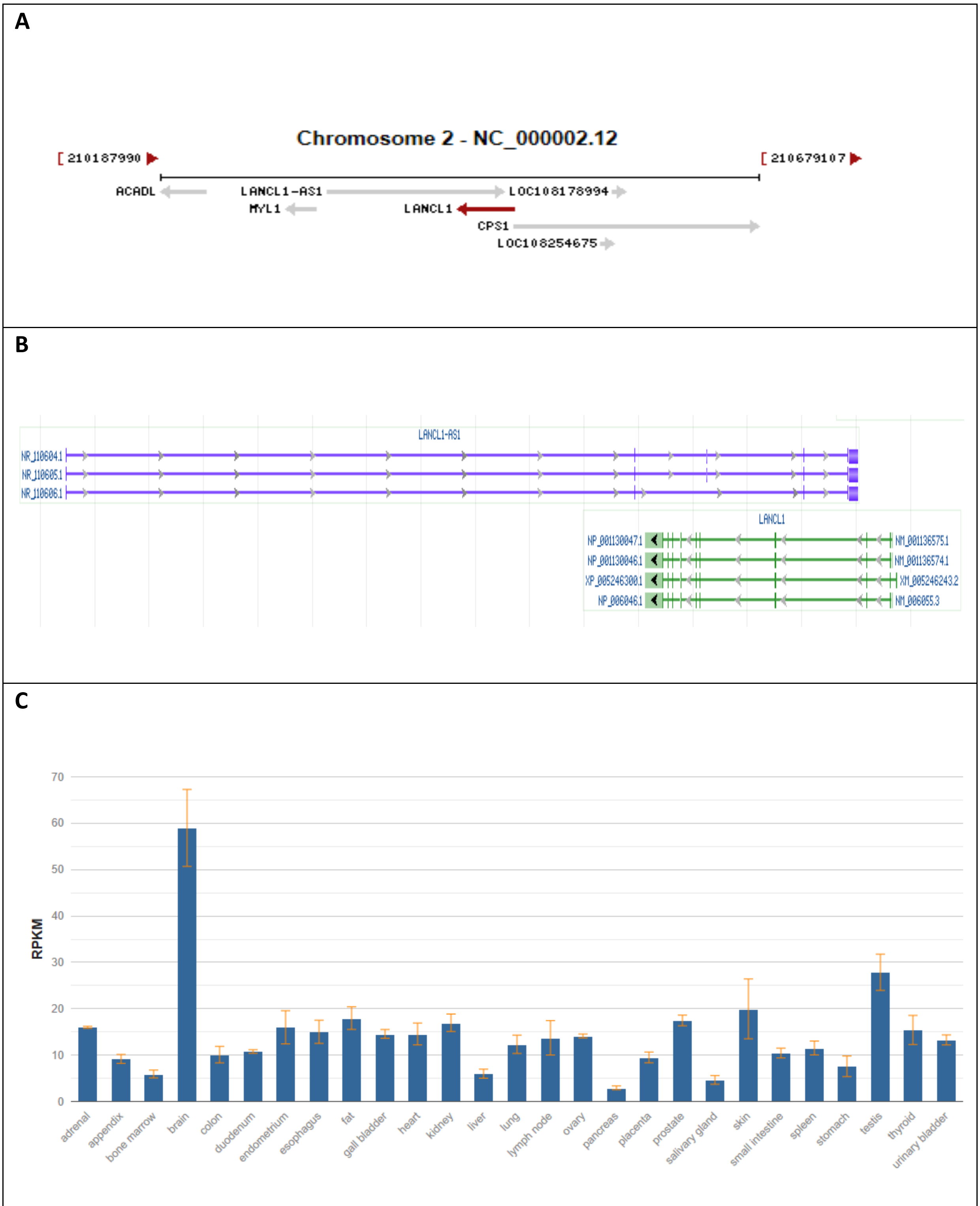

Figure 1.14: (A) *LANCL1(Chr.2: 210431249-210477618)* and antisense LncRNA *LANCL1-AS1 (Chr. 2: 210324712 – 210470333)*, *LANCL1-AS1* transcription occurs in the reverse direction from *LANCL1.* Carbamoyl phosphate synthase 1 (CPS1), that is localized in mitochondria and plays a role in regulatory the pyrimidine/purine balance to control the integrity of nuclear

DNAs. Silencing of the CPS1 gene expression result to an incomplete S-phase or apoptotic cell death due to increased DNA damage. The duplicated GGAA present in the CPS1/LANCL1 bidirectional promoter region, is indicative of genes expressing mitochondria localised proteins and DNA repair related protein encoding genes (Uchiumi et al. 2017). (B) Despite their co-localisation, the two genes have no overlap at all in their exonic areas. However, the overlap of the preRNA forms in nucleus may affect splicing. Antisense transcription has been shown to control sense gene splicing. (Alló et al. 2009). At this locus, co-expressed sense and antisense transcripts can form double-stranded RNA (dsRNA) over the region of sense–antisense overlap, leading to splice site masking and a following shift in mRNA isoform production (Garcia-Blanco, Baraniak, and Lasda 2004). (C) LANCL1 is highly expressed in the brain and testes while demonstrating moderate expression in lung. It has been chosen for investigation being the coding counterpart gene for LANCL1-AS1. – Figures adapted from https://www.ncbi.nlm.nih.gov/gene/10314 .

However, little data have been published about *LANCL1* function and characterisation in cancer development. *LANCL1* was found to have a role in the development of breast cancer (Mayer et al. 2001; Althubiti et al. 2014) and prostate cancer (Wang et al. 2018).

LANCL1 is highly expressed in the brain, testes, kidneys, and other organs (Mayer et al. 2001; Zhang et al. 2009) which display the crystal structure of *LANCL1* in both free and complex forms with glutathione (GSH) showing a double-seven helix barrel fold; *LANCL1* also contains many GxxG sequence motifs (Figure 1.15) its structure also allowing binding with the SH3 domain of the EP58 signalling protein. Correspondingly, research shows that *LANCL1* plays a role in signalling and differentiation, as *LANCL1* mutation in PC12 cells (neuronal cell) may result in defects in EP58, which lead to the inhibition of the neural growth factor (NGF), inducing neural outgrowth in the PC12 cell line (Zhang et al. 2009).

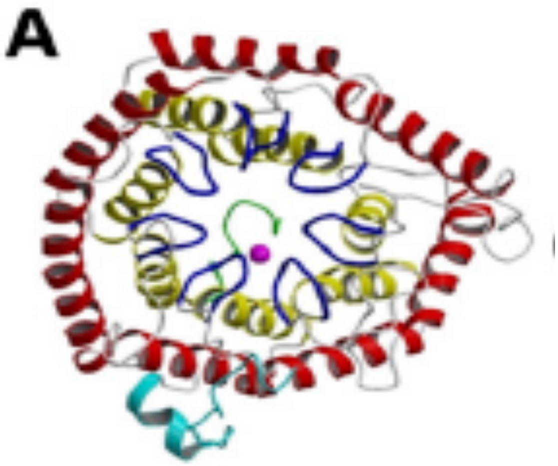

Figure 1.15: *LANCL1* structure. The inner helix barrel is represented in yellow, while the outer helix barrel is shown in red. The seven GxxG-containing bulges are presented in blue, the cyan colour indicating the N-terminal, while the green colour showing C-terminal regions. The Zn2+ ion is represented with a magenta sphere. Adapted from (Rao's 2009).

LANCL1 is essential for neural development, due to its role in protecting neural cells from oxidative stress damage (Huang et al. 2014), as deletion of *LANCL1* in neural cells can lead to neural damage, caused by accumulating reactive oxygen species (ROS) in the brain and related protein, lipid, and DNA damage as well as mitochondrial dysfunction (Zhong et al. 2012). As mentioned before, *LANCL1* protects neural cells from oxidative stress (Huang et al. 2014), in other words *LANCL1* has a responsibility in reducing oxidative stress by binding with cystathionine β-synthase (CBS) and regulating CBS activity., the suppression of *LANCL1* expression increasing the CBS activity (Zhong et al. 2012). More particularly, CBS plays an important role in regulating oxidative stress by reducing GSH; that is, under oxidative stress, CBS dissociates from *LANCL1* and CBS activity begins to maintain the ratio between GSH and GSSG, this is reduced and oxidised glutathione (Zhong et al. 2012).

Therefore, this research suggests that *LANCL1* is an antioxidative gene. In addition, high *LANCL1* expression was observed in prostate cancer (Wang et al. 2018). The latter study also highlights the role played by *LANCL1* in cell proliferation and that suppression of LANCL1 by siRNA in prostatic cells leads to cell death, being associated with apoptosis through inhibition of the JNK pathway (Wang et al. 2018). The high expression of *LANCL1* is related with cancer cells, with a role in cell survival, especially in breast cancer (Althubiti et al. 2014).

1.6.4 Reactive oxygen species (ROS)

Reactive oxygen species (ROS) play a critical role within the cell through signalling transduction and modulate phagocytosis. Multicellular function can induce ROS, involving carefully regulated free radicals (e.g. superoxide, hydrogen peroxide). An essential production of free radicals can form a free electronic transport system (ETS) that manages oxidative stress inside the inner mitochondria membrane. During the ETS, two electrons are transported via oxidative phosphorylation involving adenosine triphosphate (ATP) (Figure 1.16). 2% of the electrolyte escape electronic transport system produces ROS, which can interfere with various cellular micro-components, molecules such as proteins, lipids, DNA, and interact with essential functions inside the cell. Moreover, alterations caused by ROS can cause cancer (Conklin 2004).

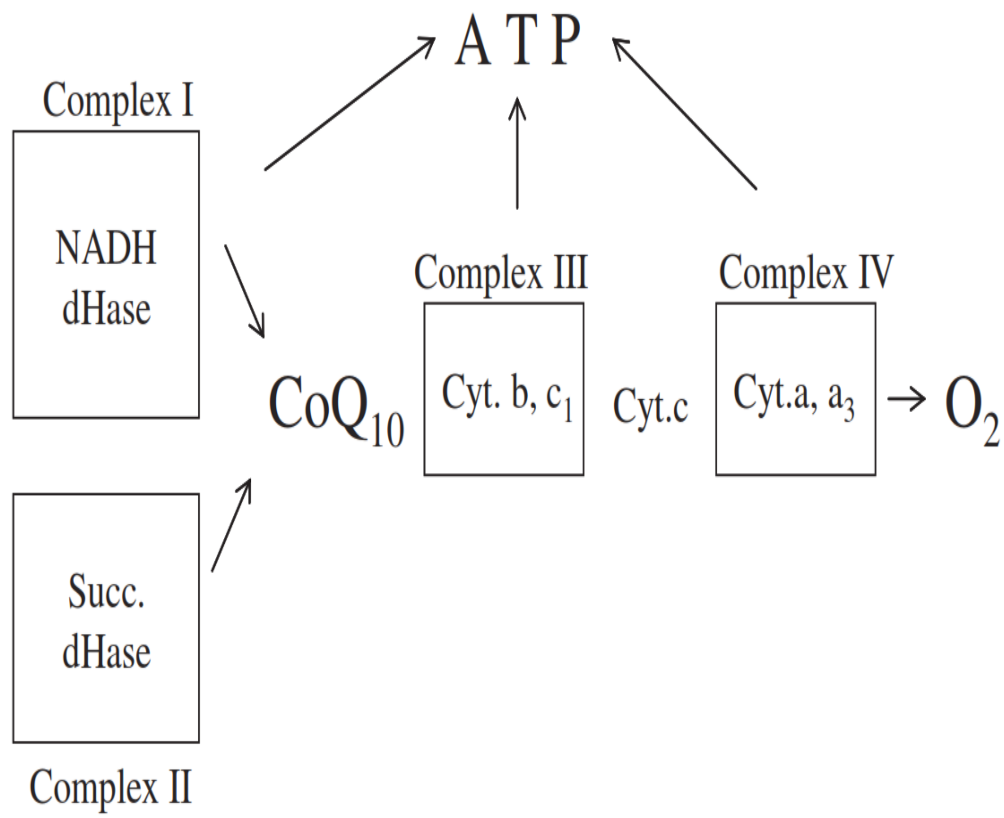

Figure 1.16*: ETS electronic transport system.* Free radical superoxide anions (O_2^-) are produced when electrons are given from complex I 'NADH dehydrogenase' and II 'succinate dehydrogenase' of ETS to O_2 instead of the suitable ETS subunit. Generally, it transports electrons to the CQ10 co-enzyme to end up with 4 electrons with subsequent transferal to oxygen. 2_4% of the total O_2 consumption may go toward the production of ROS instead of energy as ATP. Adapted from (Conklin 2004).

1.6.4.1 Oxidative stress mediate cell cycle and apoptosis

Oxidative stress targets many cellular molecular components such as cellular lipids that generate electrophilic aldehyde, the electrophilic proportion which allows aldehyde to interact with the nucleophilic group, e.g. amino acids cysteine, and serine. These are essential compared with the enzyme active site and are also important to maintaining the protein structure. The interaction of the aldehyde with protein leads to the inhibition of the enzyme and changes in the cellular receptor structure, which can interfere with cytotoxicity (Conklin 2004).

In the stimulation of oxidative stress, natural antioxidative molecules are not enough to prevent the damage caused by ROS. Chemotherapeutic agents generate reactive oxygen species (ROS) in patients undergoing chemotherapy, in whom toxically oxidative stress is an important contributor in the response to anticancer therapies (Conklin 2004).

Prolonged exposure to chemotherapy-induced ROS has been reported to induce drug resistance. Chemotherapy may even cause cancer cells to have increased genetic instability due to mutations caused by ROS. (Sallmyr et al. 2008).

Platinum coordination complexes and alkylating agents induce higher levels of ROS (Wang et al. 2013), while vinca alkaloids, nucleotide analogues and antimetabolites, including nucleoside, generate lower levels of ROS (Conklin 2004).

There are two main reasons for increased cellular ROS production during chemotherapy. The first is the mitochondria ROS initiation and inhibition of the cellular antioxidant system. Chemotherapy has been identified to induce a loss of mitochondrial membrane potential and stop complexes I and II, resulting in disruption of mitochondrial electron transport chain (ETC) and electronic leakage, as platinum also targets mitochondria and induces cellular ROS generation (Marullo et al. 2013). The second reason for elevated cellular ROS production during chemotherapy is the inhibition of the antioxidant system, which includes low molecular mass antioxidants such as GSH and ascorbic acid. (Apel and Hirt 2004).

1.7 Extracellular vesicles role in chemosensitivity

Exosomes work as cargo transporters by carrying multiple components from cells to other cells to facilitate communication (Simons and Raposo 2009). Recently, researchers have found that exosomes play a role in drug resistance and cancer progression (Giallombardo et al. 2016).

1.7.1 Exosomes

Studies have reported that exosomes remain attached to the cell surface and may work as a signalling platform. Therefore, exosomes are more than a method to collect contents from the cells, working as cargo transportation to send information between cells (Bebelman et al. 2018).

Communication between cells is essential for development. More specifically, cells can communicate intracellularly with either neighbours or distance cells, local communication being facilitated by gap junctions that allow the signalling molecules pass through the cytoplasm. Communication over long distances by sending signals through hormones ca be achieved via the circulation. Extracellular vesicles (EVs) were found to play an essential role in either local or distant intercellular communication between the cells, an interaction which can alter the behaviour of the target cells. Exosomes play an essential role in cell communication by delivering information between cells following the release into the extracellular space (Bebelman et al. 2018).

In 1983, exosomes discovered during maturation of sheep reticulocytes, small vesicles released in the extracellular space experience a generation of an “intracellular sac filled with small membrane-enclosed structures of nearly uniform size" (Pan and Johnstone 1983). In 1989, Rose Johnstone proposed the name 'exosomes,' when it was first mentioned as a term (Pan and Johnstone 1983). EVs work as cargo transporters carrying survival components like protein, RNA, and DNA to other cells (Bebelman et al. 2018).

1.7.1.1 Structure, Formation, and Regulation

Exosomes have a small cell size of 30 to 150nm and originate from endosomes that are released from all cell types and present cell fluids similar to saliva (Gallo et al. 2012), urine, (Lv et al. 2013) and blood (Hu et al. 2010). Exosomes, one of the EV subgroups generated directly from the plasma membrane, are spherically shaped and nanometers in size, containing bilayers consisting of multiple proteins and lipids derived from the parental cell (Bebelman et al. 2018). Moreover, when stained with negative staining under transmission microscopy, they are cup-shaped cells which (Simons and Raposo 2009) can be identified by specific proteins, such as tetraspanin proteins CD63, CD9, and CD81 (Simons and Raposo 2009). To understand exosomes' biogenesis, the following will describe intraluminal vesicle (ILV) budding and multivesicular body (MVB) formation (Figure 1.17) (Bebelman et al. 2018). The development of endocytic vesicles occurs from the plasma membrane by internalizing, through invagination, a part of the endosome small vesicles created inside endosomes, followed by the inward budding of the endosomes. Creating vesicles inside the lumen "intraluminal vesicles" leads to the accumulation of ILVs which could promote MVB formation. Ceramide is one of the lipid types that can regulate the formation of curvature of limiting membranes to form MVBs and ILVs (Heijnen et al. 1999). Ceramide forms the membrane's curved shape created by sphingomyelin which can be hydrolysed by neutral sphingomyelinase (ns Masch), leading to budding ILV conversion into MVBs. Furthermore, endosomal sorting complex required for transport (ESCRT) is responsible for sorting and ubiquitinating proteins in ILVs (Trajkovic et al. 2008). An infusion of MVB with plasma membrane causes the release of the vesicles' content, i.e. exosomes. The release mechanism of these intracellular vesicles outside the cells is opposite from the mechanism of eternalization of extracellular molecules to inside a cell (Henne, Buchkovich, and Emr 2011).

MVBs transport to plasma membrane along the microtubules through molecular motor kinesins, which regulated by ArI8 and RAB7-dependent protein complexes and docking MVBs to plasma membrane controlled by RAB27 and RAB35. Also, this process is assisted by stabilizing branched actin filaments that generate the docking site (Bebelman et al. 2018).

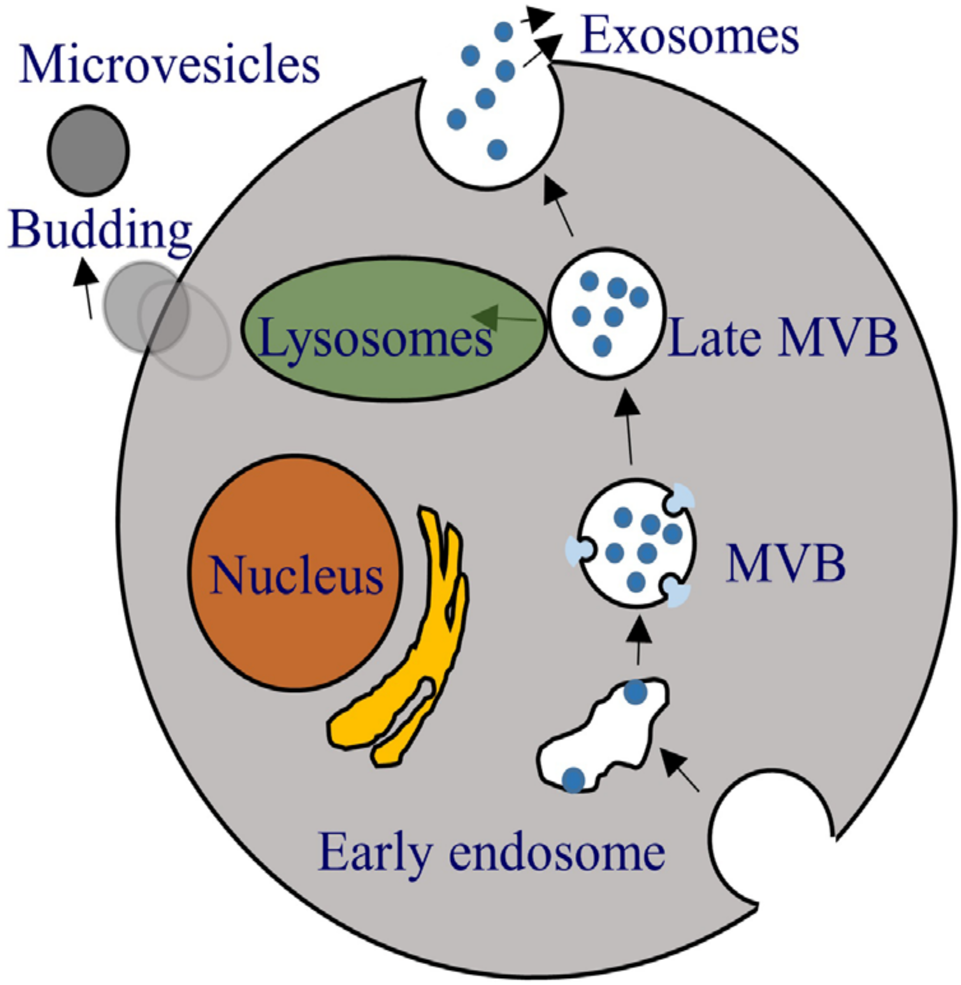

Figure 1.17: *Exosome Formation:* The exosome originates from the endosome, formed from the plasma membrane. Early endosomes become mature later and the inward budding appears to create numerous ILV. The accumulation of ILVs could lead to MVBs. There are two ways that MVB can present, either by degradation by lysosomes or fusing with the plasma membrane to release exosomes. Moreover, microvesicles can also form the budding of the plasma membrane (Ha, Yang, and Nadithe 2016).

After transport and docking, MVBs bind with soluble N-ethylmaleimide-sensitive factor attachment protein receptors (SNAREs) to infuse with the plasma membrane. SNARE has been reported to have a role in releasing exosomes in cancer cells such as SNAP23, syntaxin-4, and vesicle-associated membrane protein (Verweij et al. 2018), therefore suggesting the ability of a multifaceted mechanism to control SNARE by phosphorylation or other different residues that regulate exosomes release (Snyder, Kelly, and Woodbury 2006). At the end of MVBs' infusion with plasma membrane, the release of the exosomes in the extracellular environment leads to the interaction with and influence of the extracellular matrix; it can also enter the circulation through lymphocytes or blood. Ras-related protein (*Rab27a and Rab27b*) are responsible for regulating exosome secretion, with researchers finding that downregulating Rab27 affects Synaptotagmin-Like Protein 4 (*SYTL4*), which blocks exosomes' secretion (Ostrowski et al. 2010).

The endosomal sorting complex required for transport (*ESCRT)* family includes ESCRT 0, ESCRT I, ESCRT II, ESCRT III, which are essential for sorting special proteins into ILV (Katzmann, Odorizzi, and Emr 2002). Regarding factors blocking ESCRT that lead to the inhibition of exosome secretion, studies have found that the inhibition of Hrs (hepatocyte growth factor-regulated tyrosine kinase substrate), which is one component of ESCRT-0 membranes, may result in a reduction of exosomes released in HeLa cells (Hoshino et al. 2013). Moreover, diminished tumor susceptibility gene 101 (*TSG101*) leads to a reduction in exosomes release among tumour cells, immobilizing in human retinal pigmented epithelial 1 (RPE1) cells (Figure 1.18) (Abrami et al. 2013).

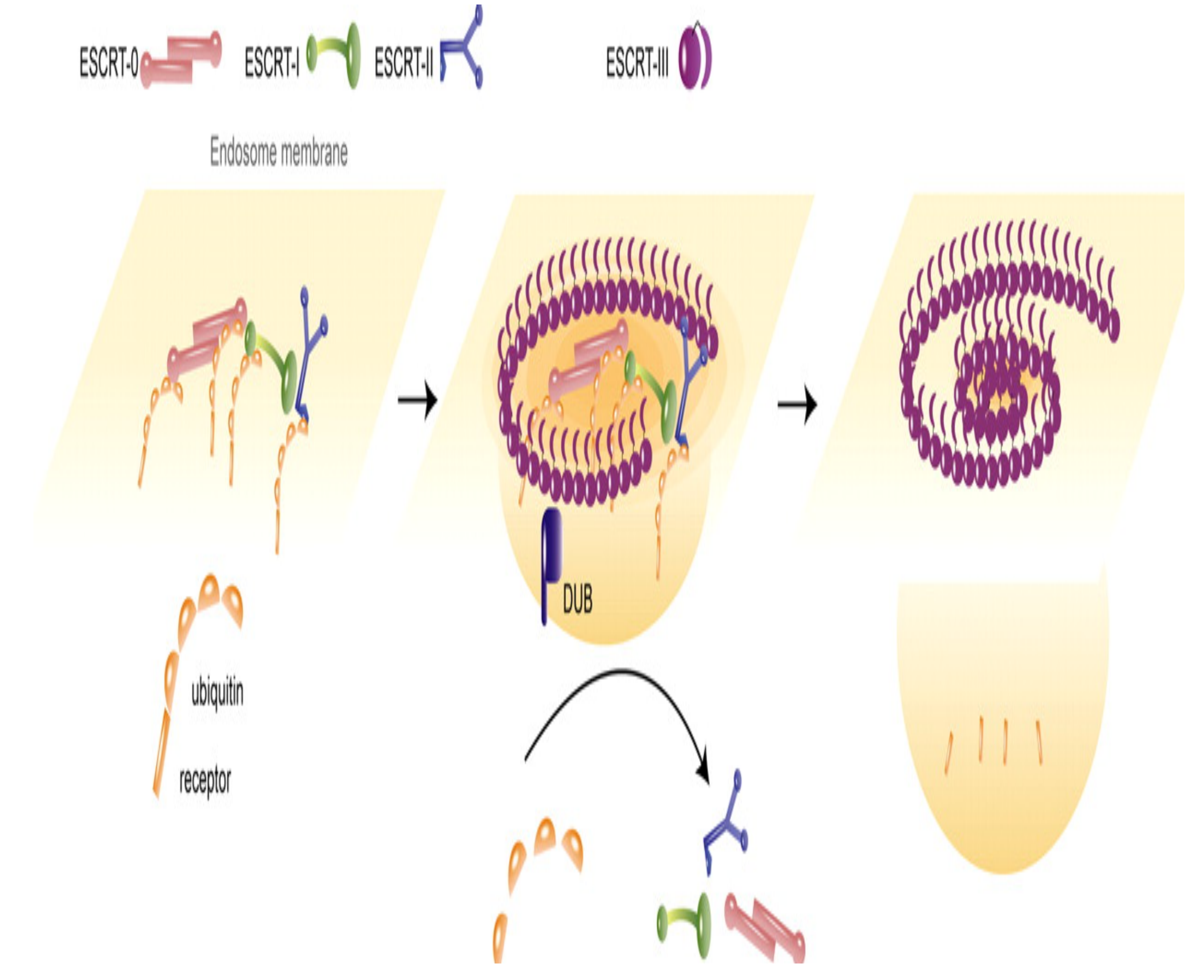

Figure 1.18: *ESCRT family*. ESCRT-0 plays a fundamental role in the creation of multivesicular bodies by binding and cargo clustering ubiquitinated proteins and/or receptors on endocytosed receptors. This cargo protein will join with ILV and become part of exosomes. ESCRT I helps in the generation of multivesicular bodies by clustering ubiquitinated proteins and operating as a bridge between the ESCRT-0 and ESCRT-II complexes, including tumour susceptibility gene 101 (*TSG101*), which incorporate with ubiquitinated cargo protein and lead to the activation of ESCRT II. ESCRT II has multifaceted functions primarily observed during the biogenesis of MVBs and the delivery of ubiquitin-tagged proteins to the endosome. Once active, the budding can start, generating MVB proteins. Ubiquitin-tagged proteins are passed from ESCRT-0 to ESCRT-I and then to ESCRT-II. ESCRT III, which pinches the cargo containing closed vesicles, “forms long filaments that coil around the site of membrane constriction just prior to membrane cleavage” and is disassembled by vascular protein sorting–associated protein 4 (*VPS 4*), Vta1, and ATPase. Adapted from (Février and Raposo 2004).

1.7.1.2 Contents

Exosomes can carry different components, such as proteins, lipids, RNA and DNA, which make it a potential tool for genetic therapy to control gene expression (Figure 1.19) (Bebelman et al. 2018).

Exosome membranes involve many proteins and lipids, having the ability to carry a large molecule such as a protein (Clayton et al. 2007).

Many studies have reported that EVs collected from alternate media or plasma were found to include genomic DNA (Balaj et al. 2011), mitochondrial DNA, (Sansone et al. 2017).

The RNA, which is transported by exosomes to target cells, has the ability to transform horizontally from the donor cell to the recipient cell, which was first demonstrated by Ratajczak in 2006. Messenger RNA (mRNA) and microRNA (miRNA) have been found in exosomes (Villarroya-Beltri et al. 2013; Gibbings et al. 2009). Short-noncoding RNA is abundant in eukaryotic cells. Exosomes contain more noncoding RNA, which can modify gene expression in recipient cells (Png et al. 2012).

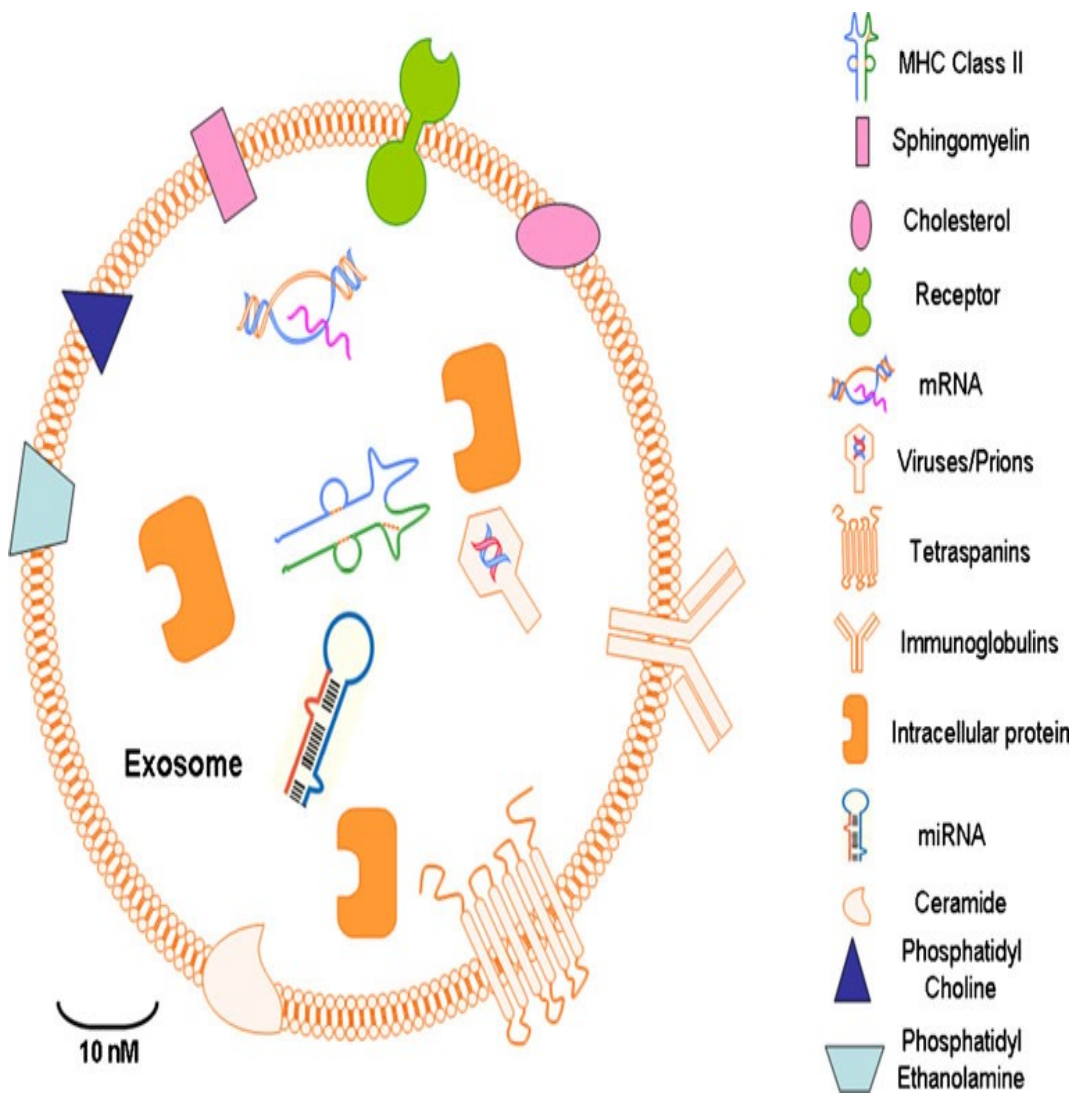

Figure 1.19*:* *Exosomes structure*: exosomes have the ability to involve a wide range of molecules including viruses, nucleic acids (RNAs and DNA), and microRNAs depending on a variety of factors, including cell type or origin. Many factors inducing exosomes content contain pathological states of the host organism. Adapted from (Azmi, Bao, and Sarkar 2013).

1.7.2.3 Trafficking Exosomes

Different means of exosome interaction with recipients include delivering interactions between transmembrane protein exosomes with signalling receptors of target cells or infusing the exosomes with the plasma membrane. Once exosomes are engulfed by recipient cells, they merge with endosomal components in order to undergo another stage of transcytosis and be released to the neighbouring cells (Zhang et al. 2015).

1.7.3 Exosomes Function

Communication is facilitated between the cell and transport components to show physiological response, as the old function of exosomes was assumed to be that of a carrier for all the unwanted protein during cell maturation. Exosomes can play a role in the biological process, such as removing all unrequired protein and RNA, as well as antigen presentation in the immune response, coagulation, inflammation, and angiogenesis and transferring miRNA horizontally (Bebelman et al. 2018). Exosomes are often associated with many diseases. For instance, in cancer, exosomes play an essential progression role in preparing the protumour microenvironment by transferring proteins and miRNA to remote areas to induce angiogenesis, thrombosis, and proliferation. Exosomes carry the misfolded protein derived from the unhealthy neural cells to distant healthy cells to spread the disease (Zhang et al. 2015).

1.7.4 Exosomes and Cancer

Mature MVBs can operate in two ways, either fusing through the plasma membrane to release exosomes, or degrade their cargo by fusing with lysosome (Riches et al. 2014). The rate between these two pathways is recognised to be imbalanced or shifted in cancer cells, which was reported to cause exosome release in cancer cells more so than normal cells (Riches et al. 2014; Muntasell, Berger, and Roche 2007).

The properties of exosomes in the cancer microenvironment are recognised by their cargo and the dynamic of the release and uptake. It has been shown that cancer cells release EVs more than normal cells and that overexpression of ESCRT syntenin and heparan has been reported in tumour cells (Koliopanos et al. 2001).

1.7.5 Exosome-Induced Chemoresistance

Drug resistance can spread between cells by molecular changes carried by exosomes which, engulfed by recipient cells, receive drug resistance information from the resistant cells (Giallombardo et al. 2016). There are three methods for exosomes to mediate drug resistance: drug export to the exosome pathway, neutralization of an antibody-based drug, and exosomes mediation of the miRNA transfer (Figure 1.20) (Giallombardo et al. 2016). Firstly, the drug export via the exosome pathway includes the biological reaction for regulation by an influx and efflux of the biological matrix through the nuclear and plasma membrane (Azmi, Bao, and Sarkar 2013), for example, in ovarian cancer cells (Giallombardo et al. 2016). In this case, researchers have found that the resistance against cisplatin in ovarian cancer was related with abnormality in protein trafficking and secretion. Lysosomes have decreased by 40% in resistance cell lines as compared to sensitive cell lines. Also, exosomes released from resistance cells contained 2.6-fold more cisplatin than those released from sensitive cells. Besides, it has been concluded that a significant increase in gene expression may produce function in membrane fusion and vesicle trafficking (Safaei et al. 2005). Resistant cells have reduced in size remarkably due to abnormality in lysosome proteins and partially transport cisplatin to exosomes. (Safaei et al. 2005).

1.7.6 Exosome in therapy

Exosomes are used for both diagnosis and therapy, for example the diagnosis of cancers such as prostate and breast cancers.

Although small interference RNA (siRNA) is used in genetic therapy to disrupt the gene of interest, siRNA has a low stability and fast degradation in the systemic circulation. Using exosomes to deliver siRNA can act as a protector for siRNA to deliver it to the target (Alvarez-Erviti et al. 2011). Researchers have attempted to find a way to deliver the vector in gene therapy, believing that exosomes can deliver siRNA to T-cells and monocytes in a safe way (Tian et al. 2014).

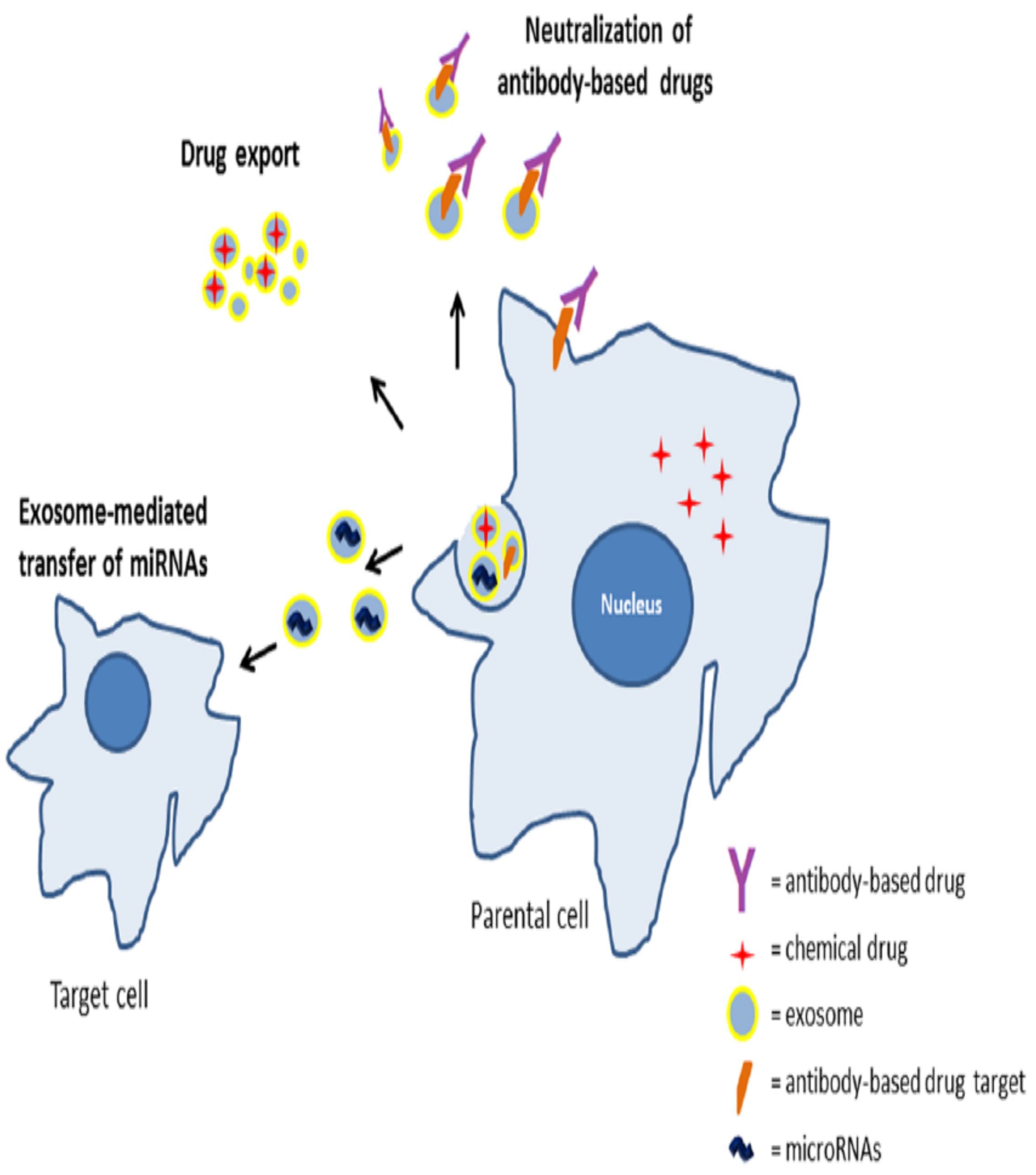

Figure 1.20: *Outline of three exosome-mediated drug-resistance mechanisms.* Adapted from (Giallombardo et al. 2016).

1.7.6.1 Delivering Drugs

Exosomes are involved in many biological and pathological processes. More specifically, the fact that exosomes work as a transporter allows scientists to identify new approaches to delivering drugs and other nanoparticles (Azmi, Bao, and Sarkar 2013). Recently, researchers have been hoping to use exosomes as a drug delivery system based on exosomes properties (Ingato et al. 2016; Boelens et al. 2014).

However, a later study isolated exosomes or EVs from prostatic cancer cells, followed by loading the exosomes with paclitaxel and found that paclitaxel delivered to recipient cells led to an increase in cytotoxic effects (Armstrong, Holme, and Stevens 2017).

Last but not least, exosomes were determined to be a new approach to deliver drug therapy. It offers a survival advantage, such as avoiding build-up or turnover in the liver as well as preventing the first-pass metabolic effect that reduces the concentration of drug at the target (Katzmann, Odorizzi, and Emr 2002).

1.8 Aims and Objectives

The main aim of this study is to expand the current knowledge in sensitizing non-small cell lung cancer (NSCLC) cells to four chemotherapeutic agents (cisplatin, carboplatin, gemcitabine and Vinorelbine).

The specific objectives are:

1- To investigate the efficiency of two epigenetic (Decitabine, valproic acid) and two non-epigenetic (aminomethylphosphonic acid and fendiline) compounds in modifying the sensitivity of NSCLC cells to the four above mentioned chemotherapeutic agents.

2- To explore the role of *LANC1* and *LANCL1-AS1* genes in chemosensitivity to the four drugs.

3- To investigate the changes that extracellular vesicles (EVs) undergo following drug treatment and look for any involvement of EV in chemosensitivity.

Chapter 2: Materials and Methods

2.1 Non-small cell lung cancer cell lines and growth condition

Eight non-small cell lung cancer (NSCLC) cell lines have been used in this study, namely (A549, CALU-3, CALU-6, COR-L23, H358, LUDLU, SK-LU-1, and SK-MES-1 (seeTable 2.1). Prior to any experimentation, cell authentication has been performed using the GenePrint® 10 system (cat no. B9510, Promega, UK; see Table 2.2). In addition, the mycoplasma-free condition was verified using an e-Myco™ plus Mycoplasma PCR Detection Kit (cat no. 17341). We amplified 10 ng of DNA from each NSCLC cell line using an Applied Biosystems® 3130 Genetic Analyzer (Thermo Fisher Scientific, UK). Also, amplification products were mixed with an Internal Lane Standard 600 and allelic ladder using the GeneMapper® ID-X software (Applied Biosystems).

The allelic profiles found (Table 2.2.) where verified against the data in ATCC database. Eight NSCLC cell lines (A549, CALU-3, CALU-6, COR-L23, H358, LUDLU, SK-LU-1, and SK-MES-11) were grown and maintained in Dulbecco's modified Eagle medium (DMEM/F-12 medium supplement [1:1]) with L-glutamine LOT1737510 and 5% foetal bovine serum Fetal bovine serum (FBS; Sigma-Aldrich, St. Louis, Missouri, UK); cell lines were incubated in a 37°C, 5% CO2 incubator.

Table 2.1: *NSCLC cell lines used in this study and their associated histological types*

NSCLC cell line	*Histological type*
A549	Adenocarcinoma
CALU-3	Adenocarcinoma
CALU-6	Anaplastic carcinoma
COR-L23	Large cell carcinoma
H358	Bronchioloalveolar adenocarcinoma
LUDLU-1	Squamous cell carcinoma
SK-LU-1	Adenocarcinoma
SK-MES-1	Squamous cell carcinoma

Table 2.2: *STR profiles of NSCLC cell lines*

	A549	CALU-3	CALU-6	COR-L23	H358	LUDLU1	SK-LU-1	SK-MES-1
Amelogenin	X, Y	X	X	X,Y	X, Y	X	X	X, Y
CSF1PO	10, 12	19	12	11	11, 12	11	10	12
D13S317	11	12	11	10, 11	8, 12	12	10	11
D16S539	11, 12	12, 14	13	11, 13	12, 13	13, 14	8	13
D5S818	11	11	11	10, 12	10, 12	12	11	11
D7S820	8, 11	10, 11	10	9	10, 11	10, 12	9	8
TH01	8, 9.3	6, 9, 3	9	9	6	6	7	6, 9.3
TPOX	8,11	8	8	8, 11	8, 9	8, 11	8, 10	8
vWA	14	16, 17	17	19	17	17, 19	16, 17	14

2.2 Cell exposure to chemotherapeutic agents

2.2.1 Cell growth curve

A cell growth curve was generated to determine the characteristics of each cell line. Therefore, in order to maximize growth, 103 cells were seeded in flat-bottomed, 24-well plates in six replicates and cultured in 1 ml of DMEM + 5% FBS. In order to count living cells, MTT assay was then performed for six replicates every 24 h over 4 days. The average of the cell counts was calculated for six replicates on a daily basis. A pilot test was implemented before the actual cell growth to establish sitting protocol.

2.2.2 Examination of cellular phenotypic characteristics

We used an Eclipse TS100 inverted microscope (Nikon) to examine the cell line phenotype and to monitor cell growth rungs, confluence, and the formation of colonies.

2.2.3 NSCLC cell lines treated with chemotherapeutic agents

Depending on the proliferation rate of NSCLC cell lines, 103 cells of A549, CALU-6, COR-L23, H358, SK-LU-1, and SK-MES-1 and 104 cells of CALU-3 and LUDLU-1 were seeded in each well of flat-bottomed, 48-well plates in six replicates, cultured in 500 μl growth medium + 5% FBS, and incubated overnight. The next day, confluence reached 40% and the medium was replaced with fresh medium containing a range of concentrations of 0–4 μM gemcitabine (cat no. G6423, Sigma-Aldrich), 0–0.5 μM vinorelbine (VRL; cat no. V2264, Sigma-Aldrich), 0–0.1 mM cisplatin (cat no. P4394, Sigma-Aldrich), 0–0.1 mM carboplatin (cat no. C2538, Sigma-Aldrich) cell lines were incubated for 48 h in a 37°C, 5% CO2 incubator.

2.2.4 NSCLC cell lines treated with H2O2

The eight NSCLC cell lines were each seeded in 25-cm^2 flasks with medium + 5% FBS, left until confluence reached 70%, then treated with two different doses of 25 μM/ 50 μM H_2O_2 for two different periods, namely 3h and 6h to extract RNA. In order to confirm the results, SK-MES-1 was seeded in a flat-bottomed, 12-well plate until reaching 70%, and six replicates were control untreated while the other six replicates treated with 25μM H2O2 for 6h.

Furthermore, parental cell line SK-MES-1, scrambled and overexpressed LANCL1-AS1 clones were grown in coumermycin or novobiocin. Also, knocked down LANCL1 clones A6/26, A9/10 were treated with seven different doses of H2O2 range between (100μM-0) and incubated in 37°C, 5% CO2 for 48 h after MTT assay was performed.

2.2.5 Drugs sensitization experiments

For the epigenetic sensitization such as DNA methylation/histone acetylation inhibition, the two most resistant cell lines to the (cisplatin, carboplatin, gemcitabine and vinorelbine) drugs were treated, once combined, with the same range of concentrations once combined epigenetic agent 100 nM of decitabine (5-Aza-2'deoxcytidine [DAC]; cat no. A3656, Sigma-Aldrich) or 1 mM valproic acid (VPA; cat no. P4543, Sigma-Aldrich) with chemotherapeutic for 48h or pre-exposed epigenetic agents for 48 h. Then, refresh the medium with the range of chemotherapeutics concentrations alone or plus the epigenetic drugs mix, while incubation continued for another 48h.

Additionally, we attempted to sensitize the same two resistant cell lines for each chemotherapeutics combined with 25 mM of aminoimethyl phosphonic acid (AMPA; cat no. 324817, Sigma-Aldrich) or 10 nM fendiline (cat no. 6407, Tocris Bioscience, Minneapolis, Minnesota, UK), followed by incubation for 48 h.

2.3 Proliferation (MTT) assay

The cell viability of NSCLC cell lines, overexpressed LANCL1 AS1 and knocked down LANCL1 clone, and drug toxicity were measured by using an MTT proliferation assay. MTT assay can assess metabolic activity inside a cell by determining the purple-coloured formazan product of reducing tetrazolium dye MTT 3-(4, 5-dimethylthiazol dimethylthiazol-2-YL)-2, 5-diphenyl tetrazolium bromide, with absorption of the purple colour product occurring at ~570 nm. However, as dead cells lose the ability to reduce MTT into insoluble formazan, this makes MTT becomes a useful marker for cell viability (Berridge, Herst, and Tan 2005).

Cells seeded in flat-bottomed, 48-well plates to measure cell viability or treated with chemotherapeutic agents for a suitable duration to measure drug toxicity were washed with PBS and incubated with MTT (cat no. 45655, Sigma-Aldrich) and made up in fresh DMEM medium to a final concentration 0.75 mg/ml of MTT reagent; also, the incubation was for a period of 2.5–3.0 h at 37°C and 5% CO2. During this time, formazan crystal lysis with 200 µl of 0.04 HCL in isopropanol alcohol was completed. In the minutes thereafter, the developed purple colour became observable, its intensity being related to cell viability. To measure colour absorbance, a GENios plate reader (Tecan Austria GmBH) was used to record the optical density (O.D.) at 590 nm with a 630 nm reference absorbance (Figure 2.1).

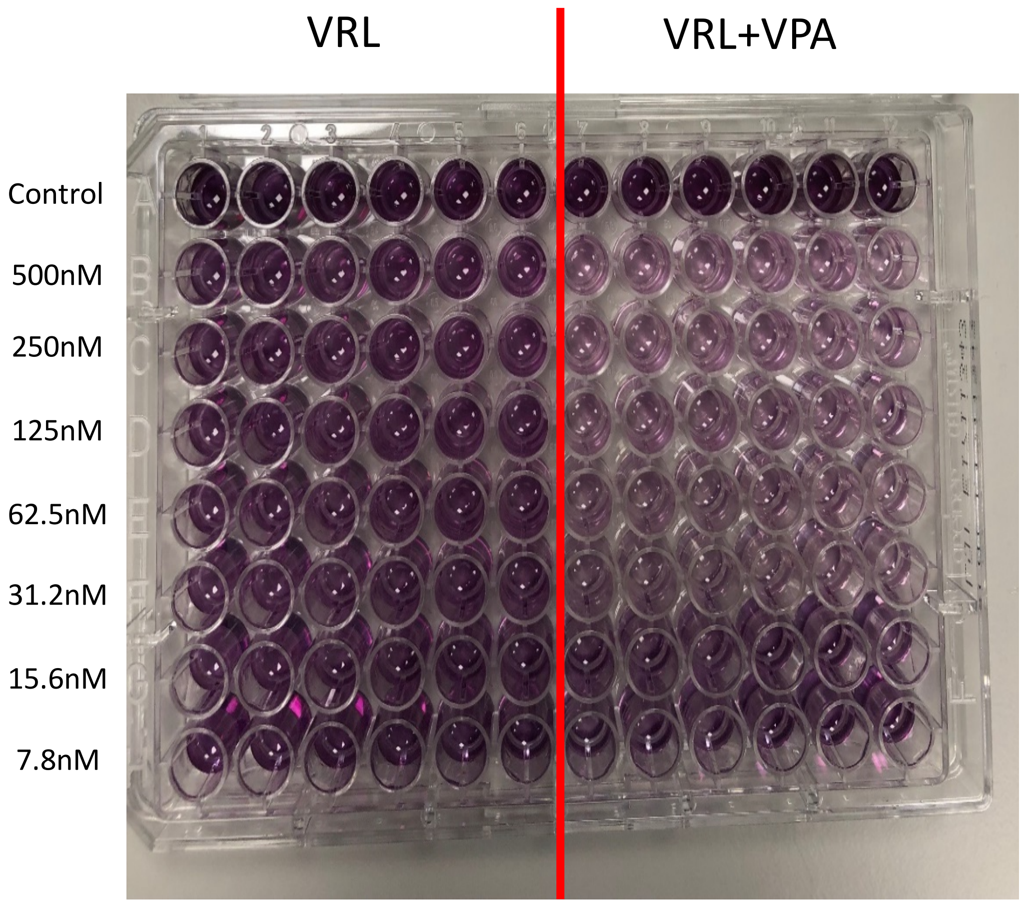

Figure 2.1: *MTT assay for SK-LU-1 NSCLC cell line treated with VRL.* The first six columns from the left were treated with VRL different doses for 48h, and the remaining six columns were treated with VRL different doses + VPA (1mM) for 48h; the first row is the control. Concentration of cell viability was seen more in the columns treated with VRL depending on colour intensity, which means that combined drugs worked better in killing the cancer cells.

2.4 Apoptosis Caspase-Glo3/7 assay 8/9

The Caspase-Glo® 3/7 assay (Promega) is a homogeneous, luminescent assay that can measure the activity of caspase 3/7. The assay contains a luminogenic caspase-Glo® 3/7 substrate is cleaved to liberation aminoluciferin, a substrate of luciferase used in the production of light, substrate involves the tetrapeptide sequence DEVD. Caspase-Glo® 3/7 reagent is optimised for determining the caspase activity, luciferase activity, and cell lysis. The addition of Caspase-Glo® 3/7 reagent in the mixture lead to cell lysis, followed by caspase cleavage of the substrate and production of a glow-type luminescent signal. The Caspase-Glo® 3/7 assay is aimed at practising with multi-well plate formats, making it perfect for automated high-throughput screening of caspase activity or apoptosis. The experiment was performed on resistant NSCLC cell lines seeded in white well, 96-well plates (LUMITRAC™ 200 Lot E14030M5; Greiner Bio-One) for the stated chemotherapeutics alone and chemotherapeutics combined with the epigenetic agents or pre-exposed with epigenetic agents.

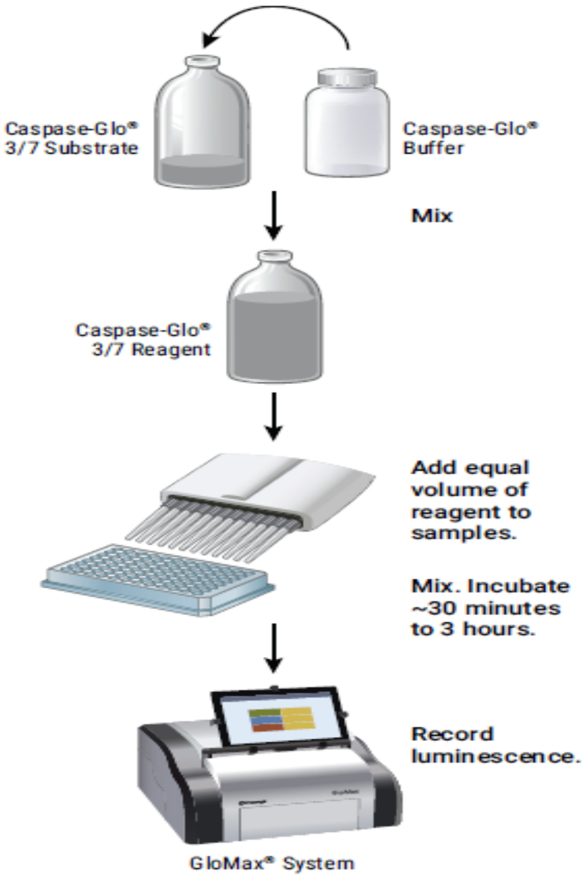

Figure 2.2: *Apoptosis Caspase-Glo3/7 assay*. Resistant NSCLC cell lines for the chemotherapeutics were seeded in a white 96-wells plate after treatment with desirable drug alone or combined with sensitizers for a suitable time period in 37°C, 5% CO_2 condition. To prepare the reagent, the Caspase-Glo 3/7 substrate was mixed with Caspase-Glo buffer. Next, the plate was removed from the incubator, and reagent was added to the treated or control medium (1:1 ratio). The plate was incubated in RT for 1.5–2.h in darkness; this protocol results in cell lysis, followed by caspase cleavage of the substrate and generation of a glow-type luminescent signal measured by a luminometer gene plate reader (Tecan Austria GmbH). Image taken from (Promega 2019a).

2.5 The neutral Comet assay

Also known as the single-cell gel electrophoresis assay (SCGE), the neutral comet assay is used to evaluate DNA strand break or damage in eukaryotic cells. Cells were treated with desirable chemotherapeutics combined with epigenetic agents for a suitable period in 37°C, 5% CO_2. Cells were encapsulated in a low-melting point agarose suspension and embedded in high salt, resulting in the formation of nucleoids involving a supercoiled loop of DNA linked to the nuclear matrix. Electrophoresis was performed to the lysed cells at high pH that led to the 'structures resembling comets', which were then stained with fluorescent stain SYBR® Safe DNA Gel Stain (cat no. P/N S33102, Thermo Fisher Scientific); as seen in Figure 2.3, the comet tail is the result of the amount of DNA damage.

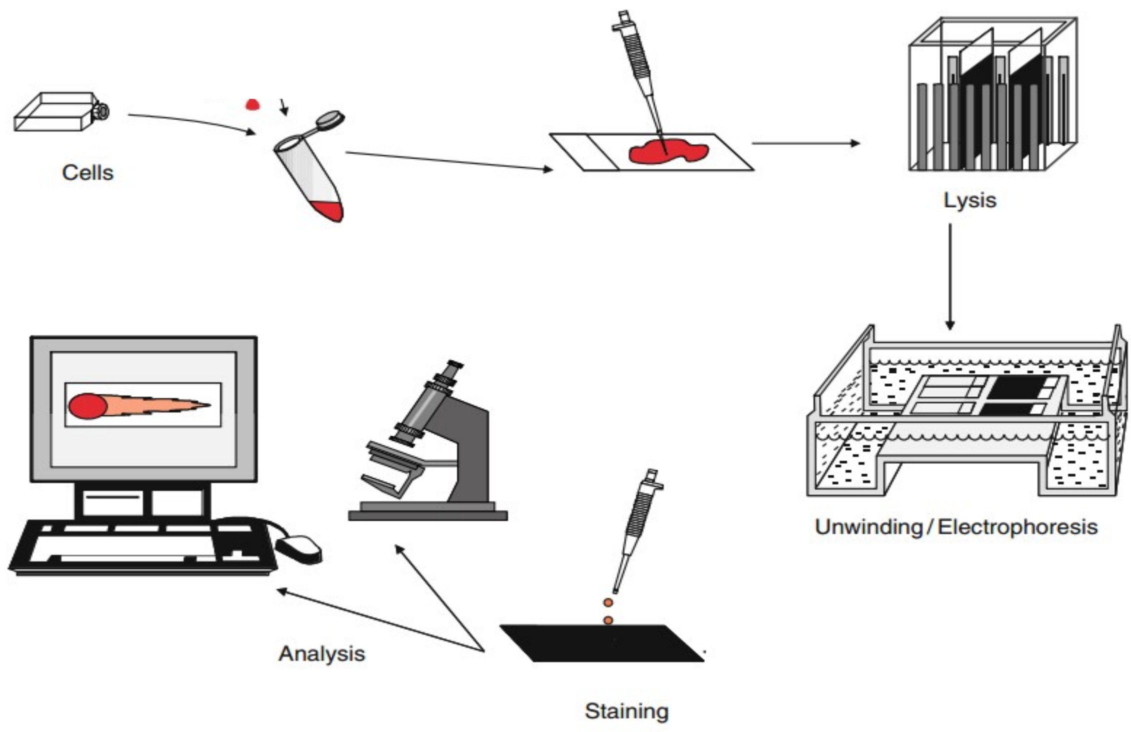

Figure 2.3: The neutral *comet assay procedure.* Adapted from (BiotechAdvisers 2019)

2.6 mRNA expression analysis

2.6.1 RNA extraction

We used a Direct-zol™ RNA MiniPrep Kit (Zymo Research, Irvine, California, UK) to extract RNA, with a centrifuge set at 16,000 ×g for 1 minute. Total cell line RNA extraction was preceded by cell lysis once confluence had reached 80%–85% in the culture flask. First, the liquid medium was discarded, and cells were washed with Dulbecco Phosphate-Buffered Saline (PBS); 600 µl of TRIzol® Reagent (Thermo Fisher Scientific) was then used for cell lysis. Cells were scraped with a plastic cell scraper and collected into 1.5-ml Eppendorf tubes and vortexed. An equal amount of ethanol 100% was added to homogenised lysate and mixed well by vortex for 1 minute. The whole mixture was transferred by micropipette to a Zymo-Spin II column (Zymo Research) with a collection tube and then centrifuged. The collection tube containing the flow-through was discarded and replaced with a new one. Next, the DNase I treatment was conducted, followed by washing the column matrix 400 µl RNA Wash Buffer, and centrifugation. Also, the flow-through that followed the incubated DNase I treatment and contained 5µl DNase 1 with 75µl DNA digestion buffer was discarded. The DNase I treatment mix was prepared in an RNA-free tube, while the incubation was extended by 15 minutes at room temperature. 400 µl of the pre-wash buffer was added to the column after the incubation buffer, then centrifuged at this time for 2 minutes. To ensure that all the buffer had been removed, dry spin was performed for, a 4 minute. After transferring the column to the RNA-free tube, 40 µl of DNase/RNase-free water was warmed and then added directly to the column and incubated for 2 minutes; the at room temperature mixture was centrifuged for 2 minutes to elute the RNA. All RNA was stored in –80°C for future study, except for a small amount of DNA that was taken to perform quality and quantity checking using a NanoDrop 2000 spectrophotometer (Thermo Fisher Scientific). A UV-Vis spectrophotometer was used to identify RNA purity and quantity at 280/260 nm wavelength.

2.6.2 Reverse transcription

We created a single-strand cDNA using a high-capacity cDNA reverse transcription kit (Applied Biosystems). The manufacturer's protocol, briefly explained below, was followed. the preparation of the master mix of reverse transcript (RT) included 2 μl of 10X RT buffer, 2 μl of Random Primer (RP), 0.8 μl of NTP mix (100 mM), 1 μl of MultiScribe™ Reverse Transcriptase (Invitrogen, Thermo Fisher Scientific), and 4.2 μl of RNAse free H2O. Thermal cycling was then used to perform transcript reaction under the following conditions: 10 minutes at 25°C, 120 minutes at 37°C, and 5 sec at 85°C; the product cDNA was then diluted with ddH2O five times, and 3 μl of cDNA was used for the subsequent quantitative PCR reactions.

2.6.3 Quantitative real-time PCR expression assay

LANCL1 and *LANCL1-AS1* were selected based on existing data taken from the lung group, who performed the investigation of the long non-coding RNA (LncRNA) dysregulated in NSCLC. The LncRNA profiles were carried out with the use of 44 pairs (normal, tumour) and completed both technical (29 pairs) and independent biological (38 pairs) validation of aims, with the intention of identifying LncRNA profiles significantly discriminating NSCLC tissue from paired normal lung tissue. Based on lung group findings, *LANCL1* and *LANCL1-AS1* were targeted to identify the state of expression on lung cancer by using qPCR-based expression to minimize optimisation time; also, a predesigned FAM-MGB-labelled TaqMan expression assay was used to determine the expression level of both *LANCL1* and *LANCL1-AS1* in NSCLC cell lines and lung cancer tissue (Table 2.3).

Table 2.3: *Assay IDs and reporter dye of predesigned (Life Technologies) FAM-MGB-labelled TaqMan expression assays for the LANCL1 and LANCL1-AS1 genes*

Gene	Assay ID	Reporter dye	Quencher
LANCL1	H498-42-1438	FAM[1]	MGB-NFQ[2]
LANCL1-AS1	H23-19-4440	FAM	MGB-NFQ

[1]FAM: Fluorescein amidite, [2]MGB-NFQ: minor groove binding- non fluorescent quencher

Endogenous controls ACTβ and TBP were selected as reference genes based on data from a microarray experiment (ALMAC Platform 2009) that clearly showed similar levels of ACTβ and TBP transcripts among lung normal and tumour samples (Table 2.4, Figure 2.4).

Table 2.4: *Endogenous controls primers*

Endogenous controls	Forward Primer (5’ 3’)	Reverse Primer (3’ 5’)	Probe
ACTB	CCAGCACAATGAAGAT CAAGATCA	CATACTCCTGCTTGCTG ATCCA	CTCCTCCTGAGCGCAA GTACTCCGTG
TBP	GGGGAGCTGTGATGTG AAGTTT	AAACCAGGAAATAACT CTGGCTCA	AAGGCCTTGTGCTCAC CCACCAAC

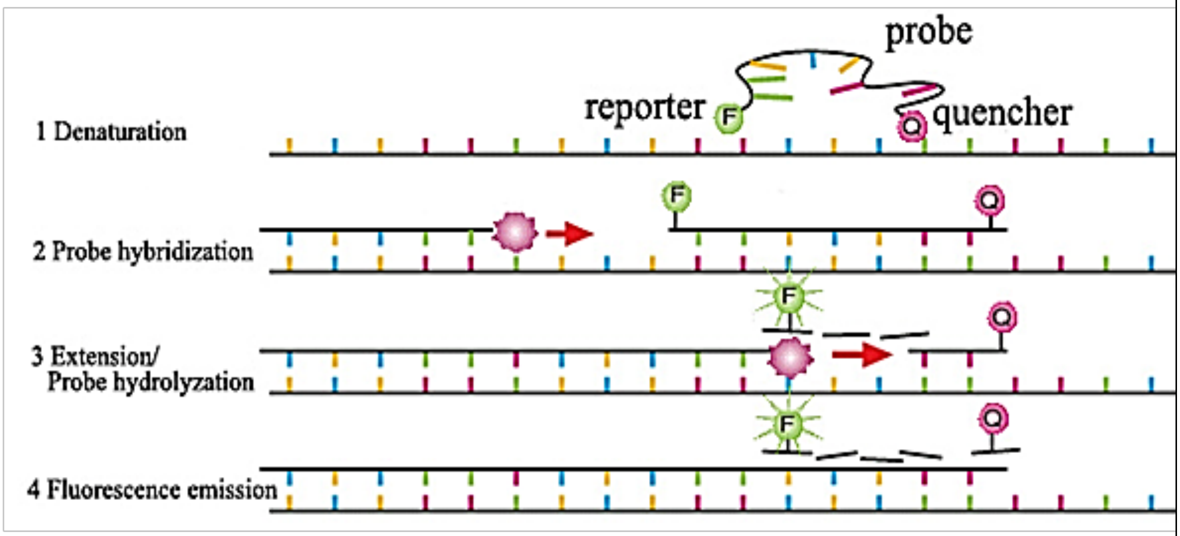

Figure 2.4: *TaqMan Probe qPCR Method.* Regarding the closeness of the reporter to the quencher stopping its fluorescence emission, the hydrolysation of the probe by 5' to 3' exonuclease activity of the *Taq* polymerase liberates the reporter and thus allows the emission of fluorescence. Subsequently, an increase in the product targeted by the reporter probe at each PCR cycle leads to a proportional increase in fluorescence. Fluorescence is exposed and measured in a qPCR. Adapted from (SinoBiological 2019).

qPCR reaction (20µl total) were run in duplicate and contained 10µl of 2X QuantiTect Probe PCR Master Mix (Qiagen), 900nM of each F and R primer and 250nM probe (for both target and endogenous control) and 3µl of cDNA. Reactions were run on a 7500 Fast Real-Time PCR system (applied Bosystems. Cycling conditions are given in Tables 2.5 and 2.6); the Applied Biosystems 7500 software v.2.3 was used to analyse the data. Relative quantification value (RQ) expressed the mRNA level, calculated as RQ=2 $^{(-\Delta\Delta CT)}$. A calibrator sample (that automatically takes RQ value=1) was used in all plates to serve as basis to compare expression results.

Table 2.5: *Thermal profiles of LANCL1 quantitative fluorescence PCR*

Step	Temperature	Time	No. of Cycles
Taq Activation	95°C	15 minutes	45
Denaturation	94°C	15 Sec.	
Annealing	55°C	15 Sec.	
Extension	60°C	50 Sec.	

Table 2.6: *Thermal profiles of LANCL1-AS1 quantitative fluorescence PCR*

Step	Temperature	Time	No. of Cycles
Taq Activation	95°C	15 minutes	50
Denaturation	94°C	15 Sec.	
Annealing	55°C	20 Sec.	
Extension	60°C	45 Sec.	

2.7. Detection of LANCL1 splice variation in NSCLC

The *LANCL1* gene schematic is shown in (Figure 2.5). The splice variant PCR assay was designed by using the oligo 7.0 primer (Molecular Biology Insights, Inc., UK). An endpoint PCR reaction was utilized with a final volume of 20 µl that contained 10 µl of 2X HotStarTaq Master mix (Qiagen), 0.8 µl of end primer mixture (stock solution, 100 mM), 5 µl of reverse primer RP (stock solution, 100 mM), and added 3 µl of reverse transcript RT product (cDNA diluted five times); this added up to 6.2 µl ddH_2O with primer vortex and spin to react in endpoint thermal cycle (Table 2.8) annealing temperature (Table 2.7). That product is then used to determine the quality and quantity of the umbilical sample by performing 2% agarose gel electrophoresis and UV visualisation on a UVP VisionWorks™ LS instrument.

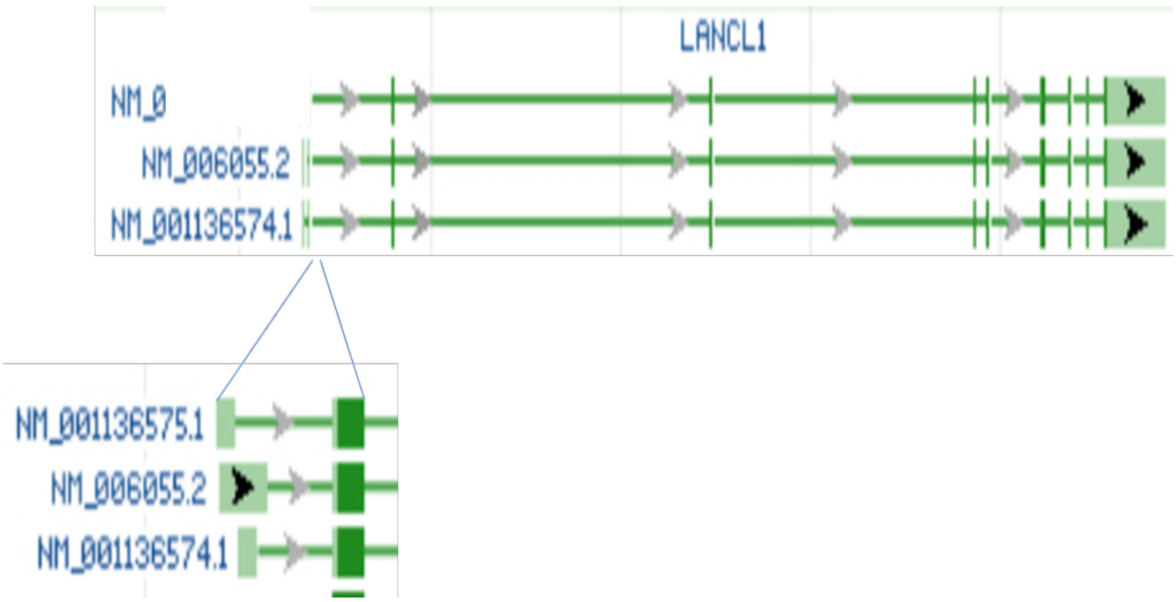

Figure 2.5: *LANCL1* splice variation

Table 2.7: *LANCL1 transcript variants assay designed assays for endpoint PCR*

Assay	Forward Primer (5' 3')	Reverse Primer (3' 5')	Annealing Temperature (X°C)	PCR Product
V1-2	AAG GGC TTC AGG ACG CGC (Exon)	GCA GCA TCA AAG TAG CCT TCG G (Exon)	65°C	V1=173 bp V2=146 bp
V3F	CCT GGC AGG AAC TGG GC (Exon)	GCA GCA TCA AAG TAG CCT TCG (Exon)	61°C	V3=247 bp

Table 2.8: *Thermal profile of LANCL1 splice variants endpoint PCR reaction*

Step	Temperature	Time	No. of Cycles
Taq Activation	95°C	15 minutes	40
Denaturation	95°C	30 Sec.	
Annealing	X*°C	30 Sec.	
Extension	72°C	30 Sec.	
Final Extension	72°C	10 minutes	

X* Table 2.7 (Annealing Temperature X°C)

2.8 DNA methylation analysis

2.8.1 DNA extraction

DNeasy® Blood & Tissue Kit (spin column protocol; Qiagen) was used to isolate DNA from the NSCLC cell lines. The manufacturer's protocol was followed and is briefly described below. All centrifuge settings were 16,000 × *g*, and NSCLC cell lines were seeded in 75 cm^2 until confluence reached 80%–85%. The medium was then aspirated, and cells washed with PBS. Next, 500 µl ATL lysis buffer with 10 µl Proteinase K (Qiagen) was added. Cells were scraped by plastic scraper, followed by the addition to the mixture 500 µl of AL lysis buffer and mixed, the cell lysates were transferred to a 2 ml centrifuge tube; the tube was incubated in at 56°C for 15-30 minutes. After finishing the incubation period, 500 µl of Ethanol (100%) was added and the resultant mixed well via vortex. The entire mixture was then transferred to the DNeasy Mini Spin column (containing a silica-based membrane), which was placed in a 2 ml collection tube. Centrifuge followed for 1 minute, 700 µl of AW1 buffer was then added to the column, followed by another centrifuge for 1 minute. Next, 680 µl of AW2 buffer was added and centrifuged for 1 minute, followed by the repetition of the AW2 buffer wash. Furthermore, a dry spin centrifuge was conducted for 4 minutes to ensure that the entire DNeasy membrane was dry. The DNAeasy column was then transferred to a new 1.5 ml Eppendorf tube and 50 μl warm AE buffer added, with incubation at room temperature for 5 minutes. The sample was eluted by centrifuge for 1 minute, and a NanoDrop 2000 Spectrophotometer was used to assess the quality and quantity of the DNA sample at wavelength 260/280 nm.

2.8.2 Sodium bisulphite treatment of DNA

To determine *LANCL1* methylation status in 60 samples containing 40 NSCLC tumour samples and 20 normal samples (control), the EZ DNA Methylation-Gold™ Kit (cat no. D5005 & D5006, Zymo Research) was utilized to perform bisulphite genomic sequencing. In the bisulphite conversion reaction, the methylated cytosine (^{m}C) does not change, while the unmethylated cytosine (C) is converted to Uracil (U). The manufacturer's protocol was followed. First, CT conversion reagent was prepared by adding (in order) 900 μl of water, 300 μl of M-Dilution, and 50 μl M-Dissolving buffer mixture with vortex for 2 minutes, then left for 8 minutes in the rotor that will prepare the reaction and ensure preparation of the M-wash buffer by adding 24 ml of Ethanol (100%) to 6 ml M-wash buffer concentration (D5006) or 96 ml of Ethanol 100% to 24ml of M-wash buffer concentration (D5006) before use. To start the conversion reaction in the PCR tube strip, mix 130 μl of CT conversion reagent were mixed with 20 μl of each DNA sample (1.6 μg of the sample), mix by pipetting upside down or by flicking the tubes, followed by the centrifuge of the tubes, replacement of the tubes in the thermal cycler, and the next step of 98°C for 10 minutes, 64°C for 2.5 h.

2.8.3 Reaction clean-up

Following the conversion reaction, samples were transferred to a 1.5 ml Eppendorf tube. The pipetting of 600 μl of M-binding buffer in a 1.5 ml Eppendorf tube was conducted successfully. The entire mixture was then transferred into a Zymo-spin™ IC column placed into a collection tube, centrifuged at >10,000 × *g* for 1 minute, followed by the discarding of the flow. Subsequently, 200 μl of M-Desulphonation buffer was added to the tube and left at room temperature (20°C–30°C) for 15–20 minutes; after the incubation period was then followed by high-speed centrifuge for 30 sec, and flow-through discarding. Then, 300 μl of M-wash was added to the tube and centrifuged at high speed for 30 sec; this step was repeated, followed by 4 minutes of dry spin to ensure removal of all traces of alcohol. Next, the Zymo-Spin™ IC column was transferred to a new 1.5 ml tube, and 35 μl of warm M-Elution buffer was added, followed by 5-minute incubation at the new temperature; a 1-minute high-speed spin eluted the sample DNA.

2.8.4 Preparation of pyrosequencing samples

The method of this technology comprises two parts: the first part is done manually, preparing the sample to be sequenced; while second is done automatically, taking place in a 96 MA pyrosequencing (Qiagen) instrument.

The first step of *LANCL1* pyrosequencing is to prepare the DNA samples to be sequenced through amplification of the target DNA sequence by PCR with *LANCL1* assay (GenBank accession no. M80343); both primers were designed using PyroMark Assay Design 20 Software (Qiagen), in which one of the primers biotinylated and the other did not (Table 2.9).

Table 2.9: *Designed primers for LANCL1 pyrosequencing assays. BIO: biotinylated end*

Promotor	Forward Primer (5’ 3’)	Reverse Primer (3’ 5’)	Sequencing Primer (5’ 3’)
LANCL1	BIOTTAATAAATTGTAAGAGAGAAGGG	CCCCCCAATTCCTACCAA	AACCAATCAAAACCTT

PCR amplification for the target sequence was performed using Qiagen HotStarTaq plus Master Mix Kit, 5μM biotinylated primer, 10μM non-biotinylated primer, and 4μl (approximately 80ng) of bisulphite-treatment DNA; the thermal profile is shown in (Table 2.10). The quality of the amplification reaction product was assessed by 20% agarose gel and visualised on a UVP VisionWorks LS instrument. The result of the amplification reaction was that methylated cytosine (^{m}C) transferred to cytosine (C), while uracil (U) transferred to thymine (T). We thereby were able to show cytosine C as a C/T SNP (Figure 2.6).

Table 2.10: *Thermal profile of LANCL1 endpoint PCR reaction for the production of pyrosequencing template*

Step	Temperature	Time	No. of Cycles
Taq Activation	95°C	15 minutes	
Denaturation	94°C	30 Sec.	
Annealing	53°C	30 Sec.	42
Extension	72°C	20 Sec.	
Final Extension	72°C	10 minutes	

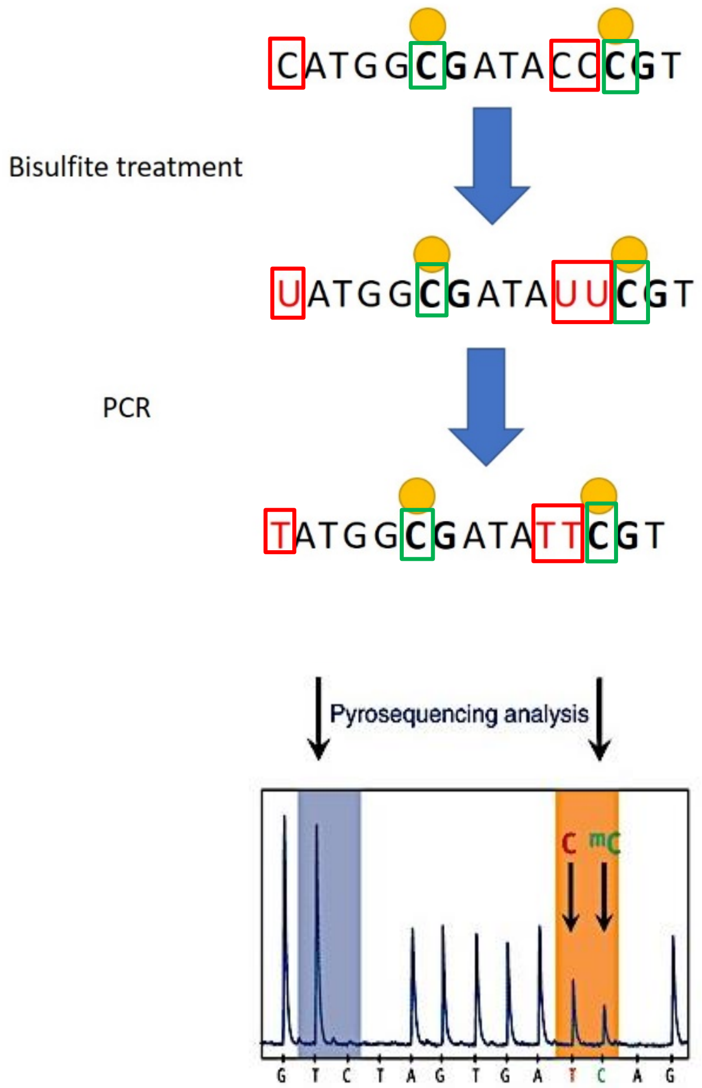

Figure 2.6: P*rinciple of pyrosequencings-based methylation analysis.* The methylated C (green) and unmethylated C (red) are differentiated by bisulphite conversion and PCR During pyrosequencing, DNA methylation at each individual site is determined by the relative incorporation of T (for unmethylated) and C (for methylated) (England and Pettersson 2005).

2.8.5 Pyrosequencing analysis

The *LANCL1* DNA methylation status was examined in 60 samples (40 NSCLC tumour and 20 normal lung samples) using the Pyromark SQA kit (Qiagen) following the manufacturer's protocol. The reaction took place in a 96 MA Pyrosequencer (Qiagen). Briefly, 75µl of the pyrosequencing binding mix included 50µl of PyroMark binding buffer, 23µl of ddH2O, and 2ml of streptavidin-coated sepharose beads mixed with PCR product; the mixture was then transferred to a pyrosequencing plate, with the assistance of a vacuum preparation tool, and the beads, in which the desired PCR product was bound, were then held over the filter, through a capture step in purification. The tip of the vacuum was then immersed in the second out of three baths (first, 70% ethanol, then NaOH for the determination and separation of the DNA strand). Finally, a wash buffer was used to neutralize the immobilised strand. This process only results in the PCR product containing streptavidin beads, with the biotinylated strand remaining attached to the tool. Subsequently, the beads were released in a new 96-well pyrosequencing plate, which included 45µl of annealing mix per well. This mix was prepared in advance with 43.5µl PyroMark annealing buffer and 1.5µl of *LANCL1* pyrosequencing primer. At this point, the plate was incubated at 80°C for 2 minutes, then cooled for 2 minutes at room temperature, as incubation period is the time required to prepare the pyrosequencing cartridge by dispensing the nucleotide, substrates, and enzyme reagents out of the proper well. The pyrosequencing plate and cartridge are then placed into the pyrosequencing instrument, while the DNA template, with annealing sequencing primer, were being incubated with enzyme DNA polymerase, ATP sulfurylase, luciferase, and apyrase, and additionally, enzyme substrates adenosine phosphosulfate (APS) and luciferin.

In a systematic manner, triphosphates (dNTP) were injected into the reaction one by one, respectively. In the DNA strand, if the first dNTP creates a U base pair with a template strand, the DNA polymerase will catalyse the incorporation, as each incorporation is finished by the release of inorganic pyrophosphate (PPi) with an equal amount to incorporate the nucleotide. PPi converts to ATP in present APS by ATP sulfurylase (PPi works as a substrate for ATP sulfurylase). The amount of the ATP released equals oxyluciferin ATP that helps drive luciferin, and this generates a visible light signal wherein the amount of the signal is equal to the amount of the ATP. The charge coupled device (CCD) captures the light produced as a result of the luciferase-catalysed reaction and displays it as a peak in the diagram. The number of nucleotides incorporated was proportionate to the height of each peak (light signal) (Figure 2.7). The unincorporated nucleotides were removed by apyrase along with ATP, and nucleotide degradation in-between base addition by apyrase is important in the coordinated DNA synthesis. Subsequently, the complementary DNA strand is built up and the nucleotide sequence is identified from the signal peaks in the program (Figure 2.7).

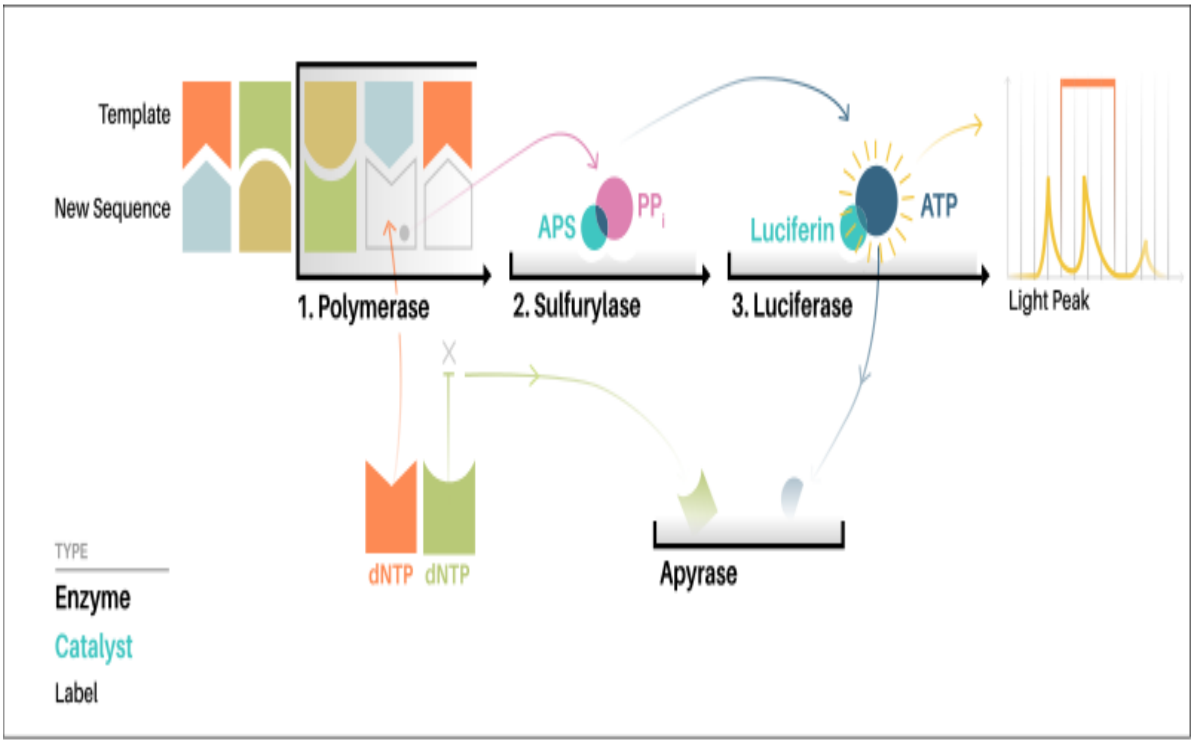

Figure 2.7: *Graphical illustration of pyrosequencing technology principles.* Adapted from (Studio 2014).

2.9 Transfection

2.9.1 LANCL1 knockdown by shRNA

Five different constructs were utilised to target *LANCL1* mRNA expression: four in the CDS region and one in 3'-UTR (Table 2.11) which belongs to type PLKO-hPGK-Puro vector, along with the scrambled control MISSION PLKO-hPGK-Puro non-mammalian shRNA Control Plasmid DNA (Sigma-Aldrich; Figure 2.8).

Table 2.11: *LANCL1 gene knockdown constructs from the MISSION shRNA library* (Sigma-Aldrich)

	Region	Clones ID		Sequence	Legacy NO.
LANCL1 shRNA	**3'-UTR**	TRCN00000011687	A6	CCGGCCAAGGAAACAAAGAGTCAAACTCGAGTTTGACTCTTTGTTTCCTTGGTTTTT	NM_006055.1-1384s1c1
	CDS	TRCN00000011688	A7	CCGGGCTCCAAATGAAATGCTCTATCTCGAGATAGAGCATTTCATTTGGAGCTTTTT	NM_006055.1-543s1c1
		TRCN00000011689	A8	CCGGGTACCTGTATAGGGCCTGTAACTCGAGTTACAGGCCCTATACAGGTACTTTTT	NM_006055.1-1133s1c1
		TRCN00000011690	A9	CCGGGCTGTGCTTTACTTACATCTTCTCGAGAAGATGTAAGTAAAGCACAGCTTTTT	NM_006055.1-309s1c1
		TRCN00000011691	A10	CCGGCACGGCTAATTCACCTAAATACTCGAGTATTTAGGTGAATTAGCCGTGTTTTT	NM_006055.1-508s1c1

2.9.1.1 Propagation of MISSION short-hairpin (shRNA) constructs

All the MISSION shRNA constructs (Figure 2.8) used in this research were propagated in a Luria-Bertani (LB) broth medium. 100 µl of the constructs was added to 150 ml LB medium supplement in 100 µg/ml of ampicillin and were left on the shaker overnight at 37°C and 150 rpm. The next day, plasmid extraction was performed.

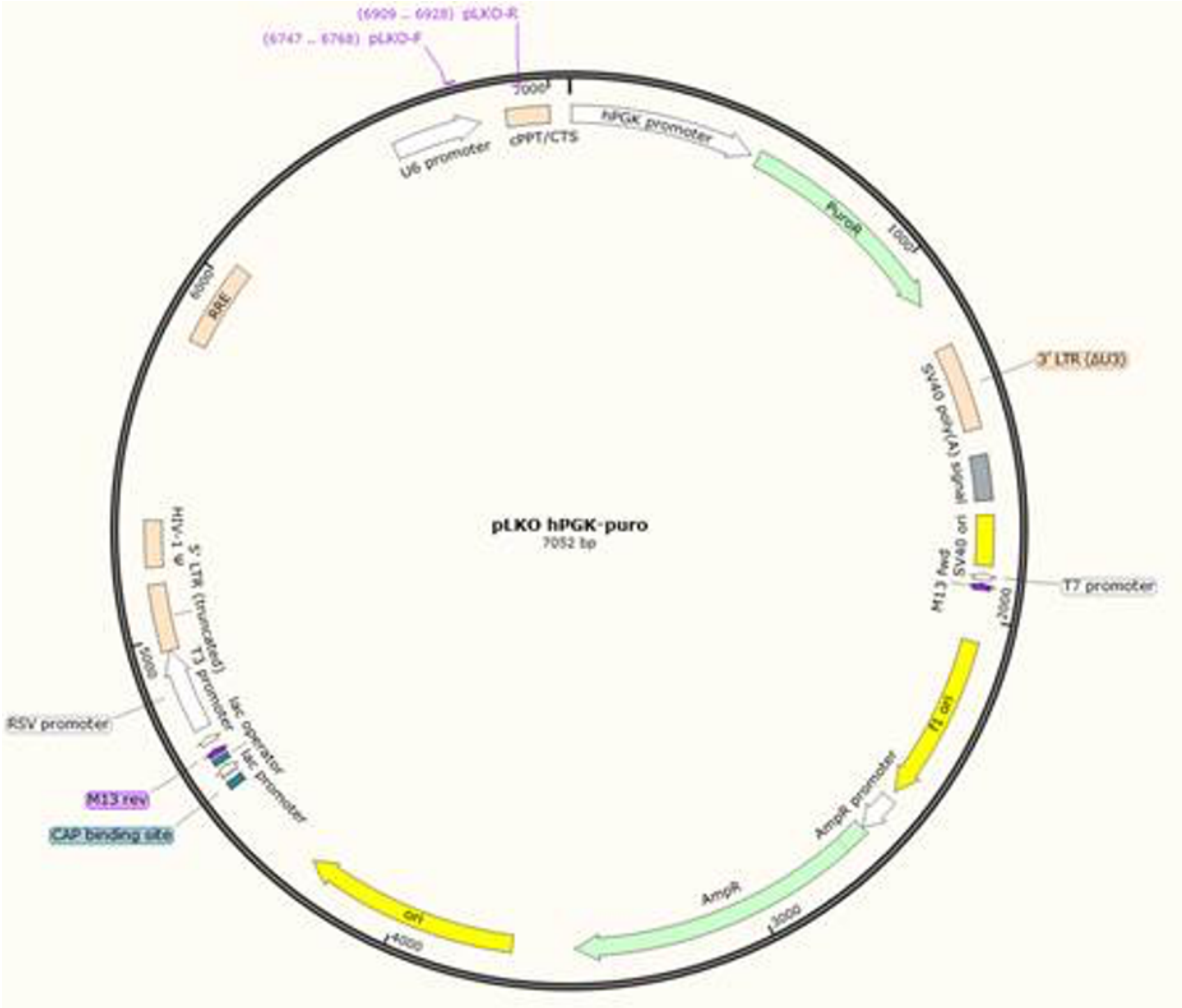

Figure 2.8: *Graphic maps of MISSION PLKO-hPGK-Puro non-mammalian shRNA Control Plasmid DNA* (Sigma-Aldrich).

2.9.1.2 shRNA construct DNA isolation

We used a ZymoPURE™ plasmid Maxiprep Kit (cat no. D4202&D4203) to extract the plasmids of the shRNA constructs, following the manufacturer's protocol. Briefly, after the propagation step, 150 ml of fresh bacterial culture was divided in 3X 50 ml falcon tubes and centrifuged at 3,400 × *g* for 10 minutes, followed by the supernatant being discarded in a beaker containing Chemgene. 14 ml of ZymoPURE PI buffer (red colour) was added to the pellet (~4.6 ml in each tube), re-suspended carefully via vortex, and then combined within one falcon tube. 14 ml of

ZymoPURE P2 buffer (green) was added and mixed by inverting the tube four to six times; for ensuring complete lysis, the tube was left standing for 1 minute. Next, 14 ml of ZymoPURE P3 (yellow) was added and completely mixed until the entire tube mixture became yellow in colour, which meant that neutralization was complete; the tube was left standing for 5–8 minutes to give the precipitate time to float to the top; then, ensuring that the bottom of the ZymoPURE syringe filter was plugged, followed by transferring the mixture to a ZymoPURE Syringe Filter with Luer Lock, the plug was removed from the bottom of the syringe filter and placed into a 50-ml conical tube. The solution was then pushed through the syringe filter by placing the plugs in the syringe, the result recovering around 35–33 ml of clean lysate. 14 ml of ZymoPURE binding buffer was added and mixed by inverting the tube 10 times. The Zymo spin™ V-P column assembly was then placed into the vacuum and the connections were ensured to be tight. The entire mixture was transferred to the column and the vacuum turned on until all of the mixture had passed through. After turning off the vacuum, the 50 ml reservoir from the loop of the column was discarded, followed by 5 ml of ZymoPURE wash 2 added to the V-P column. Turning on the vacuum allowed all the liquid to pass through, therefore 5 ml of ZymoPURE wash 2 was added and the vacuum was turned on until all the liquid passed through, a step further repeated. To ensure removing all remaining wash buffer, the V-P column was placed in a collection tube and centrifuged at >10,000 × *g* for 4 minutes (dry spin). After transferring the V-P column in a new 1.5 ml Eppendorf tube, 400 µl of warm ZymoPURE elution buffer was added to the column and incubated for 2 minutes at room temperature, then centrifuged at >10,000 × *g* for 1 minute to elute the plasmid. A NanoDrop 2000 spectrophotometer was used to assess the quality and quantity of the DNA at wavelength 260/280 nm.

2.9.1.3 Transfection of the cell line

As SK-MES-1 shows the highest *LANCL1* expression compared with the other NSCLC cell lines, it was chosen to be transfected with the *LANCL1* constructs. TRCN0000011687, TRCN0000011690 were used with FuGENE® HD Transfection reagent (Promega), following the manufacturer's protocol. Briefly, 5×10^5 cells/1 ml of SK-MES-1 cell line was seeded in a 10 cm tissue culture dish and cultured in 8 ml of DMEM culture medium containing 5% FBS serum and antibiotic, incubated in 37°C and 5% CO_2, and maintained until confluence reached 50%. As transfection was now possible, 5 μg of plasmid DNA was added to 15 μl FUGENE® HD reagent to reach a final volume of up to 400 μl diluted with fresh medium containing FBS and mixed by vortex for 5 sec, followed by a brief spin. Incubation was at room temperature for 7–15 minutes, during which the medium in the dish was aspirated and the dish washed with 10 ml PBS after the addition of 8 ml of medium + 2.5% FBS and antibiotic selected marker puromycin 3 μg/ml (the short hairpin construct has the puromycin resistance gene); after the incubation period, the mixture was then added dropwise carefully into the dish in the cell culture medium while rotating the dish then incubate in 37°C, 5% CO_2 for 24–48 h; after incubation, the transfected mixture was removed by aspiration and the dish was washed with PBS, then 8 ml of the medium was added with 2.5% FBS + puromycin. Incubation of the dish under the same conditions followed.

2.9.1.4 Generation of SK-MES-1 down-regulated stable cell line clones

The SK-MES-1 cell line was transfected with shRNA constructs in order to down-regulate the expression of the *LANCL1* gene. The short hairpin construct carries the puromycin resistance gene. To optimise the suitable concentration of puromycin to kill cells from SK-MES-1, the presence of puromycin was applied in different concentrations. The optimal low puromycin concentration that can stimulate complete SK-MES-1 death was identified as 3 μg/ml; after the incubation period of 24–48 h of transfection, *LANCL1* shRNA and scrambled plasmid to SK-MES-1 cells were growing in a growth medium containing puromycin. The growth medium with antibody refreshed as needed. Therefore, after approximately 10 days of selection, colonies were isolated by using cloning cylinders, trypsin, and flask transfer to develop under normal growth condition 37°C, 5% CO_2 and in the presence of puromycin as the selected marker. *LANCL1* down-regulation was checked both at mRNA and protein level. The selected colonies with >50% knockdown efficiency were grown for the use in the further functional analysis.

2.9.2 Construction of a LANCL1-AS1 inducible expression plasmid system

This commercially available (Promega) expression system is composed by two plasmids (Figure 2.9) and allows for the inducible expression of the target transgene using coumermycin and novobiocin that do not affect the host mammalian genes.

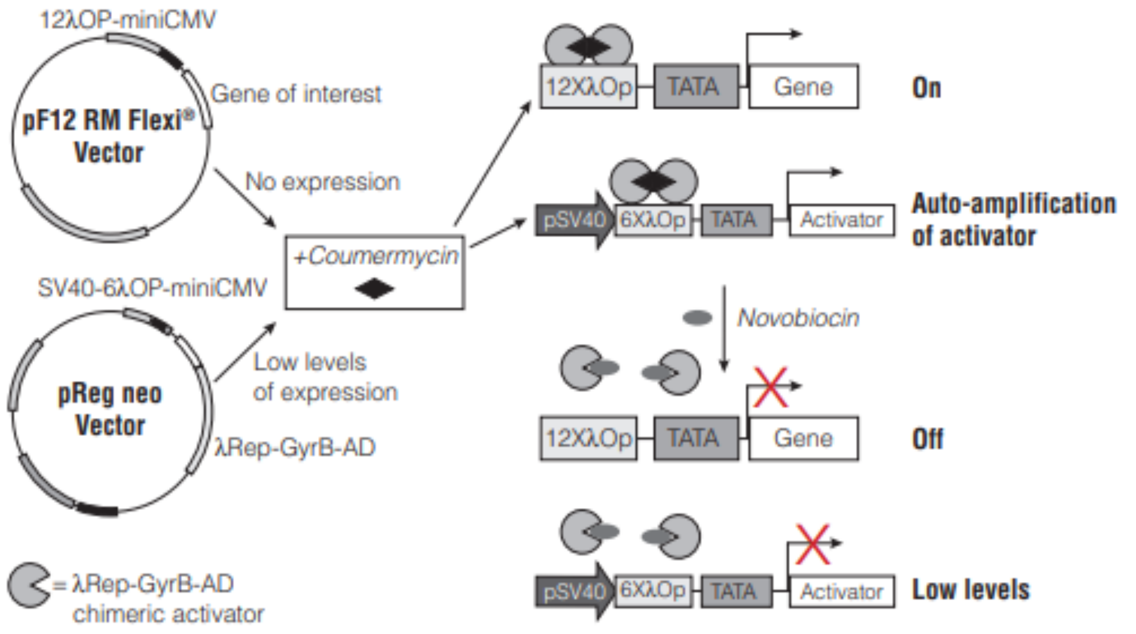

Figure 2.9: *Coumermycin switch on/off system*. The pReg neo Vector is designed to express a chimeric transactivator protein that interacts with the promoter region in pF12 RM Flexi® Vector in response to coumermycin and novobiocin. The pReg neo vector expressed the chimeric transactivator, which consisted of three parts: a λ repressor DNA binding domain (λRep), a bacterial gyrase B subunit domain (GyrB), and a NF-kB p65 transcriptional activation domain (AD). To activate the transcription, it needs coumermycin-dependent binding the bacterial GyrB domain and following dimerization of the chimeric transactivator protein. One molecule of coumermycin can dimerize two subunits of the GyrB domain, permitting the λ repressor domain to bind λ operator sequences to turn it on. That brings the NF-kB p65 transcriptional activation domain of the chimeric transactivator protein in adjacent proximity of the minimal promoter and induce transcription of the sequence of interest. In the present, of novobiocin in cells cause dissociation of the dimerized trans activator to switch OFF the trans-gene and render the constitutive expression of the trans activator. Adapted from (Promega 2019b).

2.9.2.1 Pf12ARM vector preparation

Pf12ARM plasmid (cat no. C9470, Promega; Figure 2.10) carried human *LANCL1-AS1* mRNA in mammalian cells and the G418 resistance gene as a selective marker to ensure the success of the transfection.

One shot TOP10 chemically competent E.coli (cat no. C4040-03, Life Technologies). The manufacturer's protocol (Life Technologies) was followed. Briefly, 1μl (50μg/μl) of the DNA was added to a vial of one shot cells (E.coli) and incubated on ice for 30 minutes, followed by exposure to a heat shock for 45 sec at 42°C to ensure the bacterial cell was open to engulf the plasmid, then placing the vial on ice for 2 minutes. Subsequently, 900μl of pre-warmed Super Optimal Broth S.O.C medium was added to the mixture and incubated in a shaking incubator at 37°C for 1h at 225rpm. After incubation, 200μl of mixture was spread on a selective plate (Luria-Bertani-medium [LB] containing ~50–100μg/ml ampicillin) and incubated overnight at 37°C. After the incubation, some of the bacteria was picked and transferred to a flask already containing (150ml of LB + 150μl ampicillin), followed by incubation in a shaker incubator at 37°C overnight, 80rpm. Plasmid was then isolated using ZymoPURE™ Plasmid Maxiprep that is explained in 2.9.1.2.

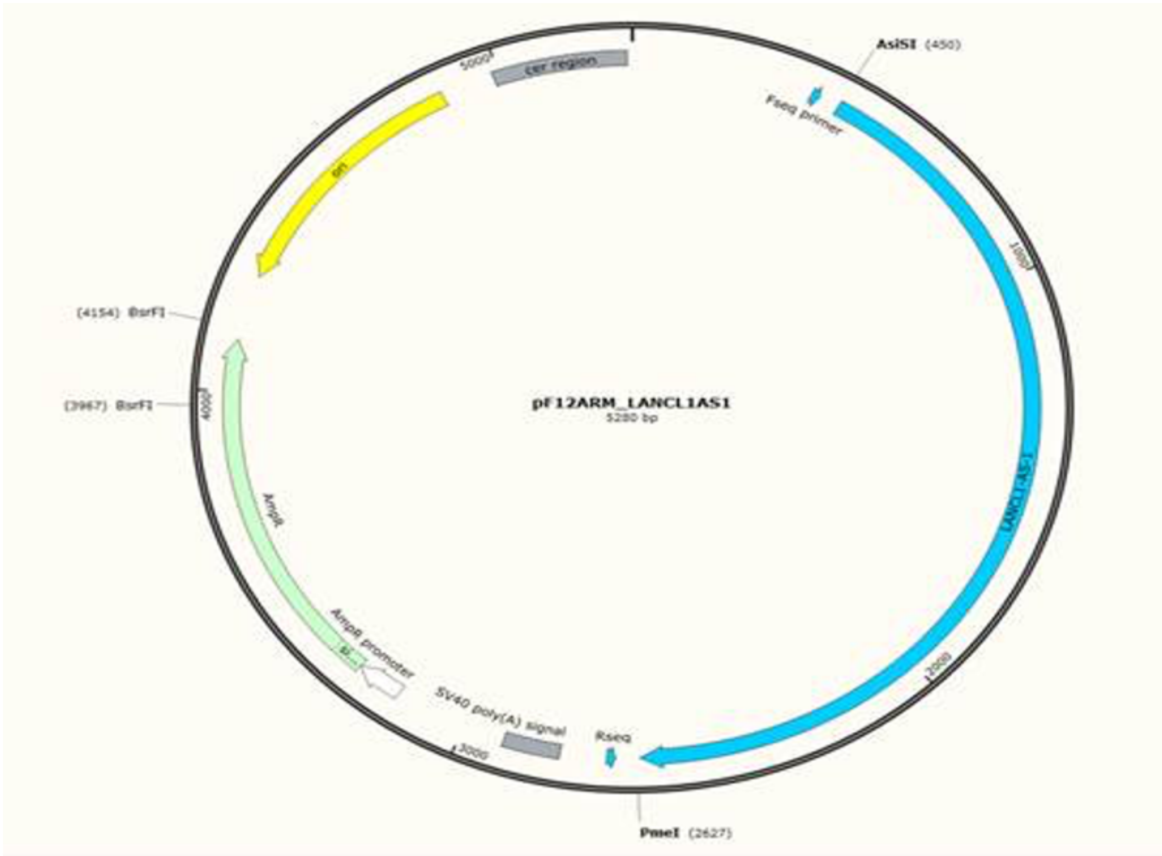

Figure 2.10: *Graphic maps of Pf12ARM_LANCL1-AS1 plasmid digested using AsiSI, PmeI, and Bsrfα1 enzymes* (Sigma-Aldrich).

2.9.2.2 Pf12ARM vector digestion

12µl of 10µg pf12-968 vector DNA was digested with 4µl of 10 unit/µl AsiSI (cat no. R0603L, New England Biolabs [NEB]), 4µl of 10 units/µl PmeI (cat no. R0560L, NEB), and 4µl of 10 units/µl Bsrfα1 (cat no. R06825, NEB) in 12µl NEB buffer and incubated at 37°C in the PCR overnight. After the incubation period, the product was run in a 0.8% low-melting-point agarose gel. The DNA fragments were then cut from the agarose gel by scalpel and transferred in a colourless tube.

2.9.2.3 Gel clean up

QIAquick® Gel Extraction Kit (cat no. 28704&28706, Qiagen) was used to clean up the gel. First, the gel, which was first weighed, then a three-time column of QG gel buffer was added to one-time volume gel; the following ftep includes the incubation for 10 minutes in S.O.C, then vortex for 2–3 minutes to ensure the gel dissolved completely and that the pH < 7.5 by shaking, and the colour was yellow. An equal amount of isopropanol to the gel volume was then added and mixed, the mixture was transferred to a QIAquick spin column and vacuum was used to discard the flow, after adding 500 μl buffer QG, vacuum was then applied. At that time, 750 μl buffer PE was added and left for 2–3 minutes, followed by vacuuming. Dry spin was then applied by transferring the column in a collection tube and centrifuging it for 4 minutes at 17,000 × *g*. The column was placed in a new collection tube, and 30 μl of pre-warm buffer EB was added to elute the DNA. NanoDrop 2000 Spectrophotometer was used to assess the quantity and the quality of the DNA at 260/280 nm, and 2% agarose gel was applied to ensure the success of digestion through the band size of the digestion and clean up.

2.9.2.4 Alkaline phosphatase calf intestinal CIP treatment

The alkaline phosphatase calf intestinal (cat no. M02905, NEB) treatment was performed to prevent re-ligation of linearized plasmid DNA. CIP is usually used to eliminate 5'-phosphate groups from DNA, and the elimination of 5'-phosphates is very valuable in preventing self-ligation of cleaved DNA vectors. This property significantly decreases background (plasmids without insert) in cloning procedures. Briefly, from the previous step gel clean up, the DNA eluted was 30μl, added to 2μl of 10 units/μl of alkaline phosphatase calf intestinal (C/P) plus and 11μl cut smart buffer (10X) mix, followed by incubation for 1h at 37°C in PCR, then 65°C for 20 minutes and placed on ice; PCR purification was then performed.

2.9.2.5 PCR purification

Moreover, the alkaline phosphate treatment QIAquick PCR Purification Kit (cat no. 28104, QIAGene) was used to clean up the product DNA following the manufacturer's protocol. After adding five times the volume of buffer PB to a one-time volume of DNA, mixing was done and pH < 7.5 was ensured by checking that the colour was yellow. The mixture was transferred in a QIAquick column, then the vacuum was applied to discard the flow. The wash step was performed by adding 750μl buffer PE, left for 2 minutes at room temperature, and vacuum applied as well. Dry spin was performed to ensure all wash buffer residue was removed by placing the column in the collection tube, followed by a 4-minute centrifuge at 17,900 × *g*. The column was placed in a new tube, 30μl of pre-warmed buffer EB was added and left for 2 minutes at room temperature, followed by a 1-minute centrifuge at 17,900 × *g* to check the purification DNA quality, and 2% agarose gel was applied.

2.9.2.6 Ligation

The ligation reaction set up according the 1:3 molar ratio of vector: insert. (64.5ng) 1.5μl of vector (Pf12ARM) DNA (183ng) and 1.5μl of *LANCL1-AS1* insert DNA mix by inverting the tube and incubating at 65°C for 5 minutes, then 2 minutes on ice. After that, 2μl buffer T4 and 1μl ligase T4 was added to the mix, then incubated at 4°C overnight; ligase was mixed in 25μl ligation reaction.

2.9.2.7 Transfection of E. coli with Pf12ARM-LANCL1-AS1 plasmid

Transformation was performed to propagate the genetically engineered plasmid Pf12ARM-*LANCL1-AS1* One Shot TOP10 chemically competent E.coli cells. The procedure was manufactured on a 2.9.2.1 section at the final step after incubating with S.O.C for 1h. A serial dilution was performed, then plated on TOP10 chemically competent E.coli cells (50µg/µl) ampicillin, followed by incubation overnight at 37°C. The next day, the clones picked from the plate and each clone will mixed in 4mL LB+Ampicillin and incubate for 7h then 2 ml from each tube incubated at 4°C and the other 2ml was centrifuged at high speed for 2 minutes; supernatant was discarded in a beaker containing Chemgene, followed by the pellet then mixed in 120µl TET. Next, 5-minute boiling at 95°C was conducted, then centrifuging at 12,000 × *g* for 5 minutes; from the supernatant, 60µl of this DNA was taken in a new tube to perform 2% agarose gel. Determination of the quality and quantity of the sample was done by performing 2% agarose gel, electrophoresis, and UV visualisation on a UVP VisionWorks LS instrument. All the tubes or samples showed success transfection of the plasmid. Then, three samples were chosen for proceeding with sequencing (Figure 2.11).

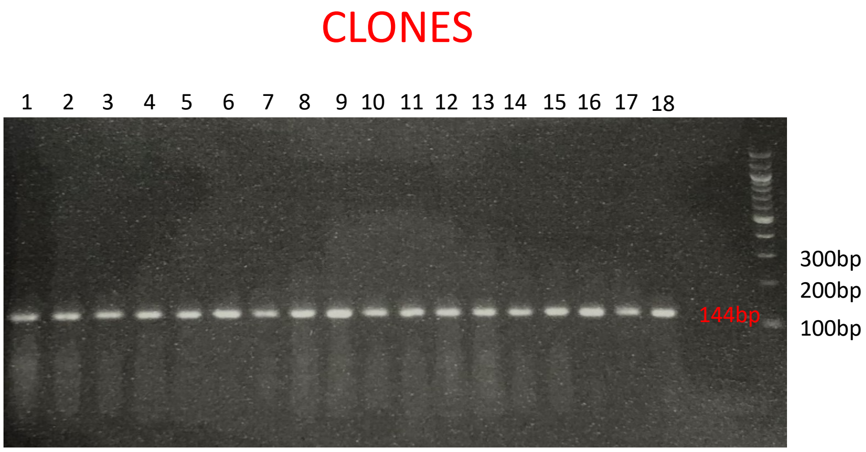

Figure 2.11: *2% agarose gel for the successful transfect of the Pf12ARM-LANCL1-AS1 plasmid*

2.9.2.8 Plasmid Miniprep isolation

To extract the plasmid from the three successfully chosen samples, growth in LB + ampicillin overnight was needed; the following day, ZymoPure™ Plasmid Miniprep Kit (cat no. D4208, D4209, D4210, D4211, D4212, Zymo Research) was used to isolate the plasmid. First, 6ml of bacterial was transferred in a falcon tube and centrifuged full speed for 10 minutes, followed by flow discard, then 250µl of P1 (red) added to re-suspend the pellet with vortex. Subsequently, 250µl P2 (green) was added, then the tube was mixed by inverting left for 3 minutes to ensure complete lysis; next, 250µl P3 (yellow) was added, followed by mixing via inversion until the mixture was yellow to ensure complete neutralization, incubation of the mixture on ice for 5 minutes, and centrifugation at 16,000 × *g* for 5 minutes. 600µl from the supernatant was then transferred to a new Eppendorf tube, followed by the addition of 275µl ZymoPURE binding buffer and mixing by inverting the tube. The Zymo-spin 11-P column was then placed into the vacuum and the mixture was transferred to the column; the vacuum was applied until all the mixture passed through, then 800μl of ZymoPure wash 1 was added to the column, followed by opening the vacuum to pass the wash buffer and then turning it off, adding 800μl wash 2, then turning the vacuum on until the wash buffer passes through. This step was repeated with 2,000μl wash buffer 2, followed by dry spin centrifugation at 10,000 × *g* for 4 minutes. The column was then placed into a new collection tube, 25μl of warmed ZymoPure elution buffer was added, and the tube was left standing for 2 minutes, followed by centrifugation for 2 minutes at 10,000 × *g*. A NanoStep 2000 Spectrophotometer was used to assess the quality and quantity of the DNA. Then, for each sample 550ng in two tubes was needed to perform the sequencing assay—one for the forward primer, and one for the reverse primer.

2.9.2.9 Sequencing of Pf12ARM-LANCL1-AS1 plasmid

Sequencing reactions were prepared in two tubes containing Pf12ARM-*LANCL1-AS1* DNA plasmid and the forward and reverse sequencing primers in respect (Table 2.12). Primers were designed using Primer Express Software V3.0—3μl of the sequencing buffer, 6μl BigDye sequencing, 3μl sequencing primer, and 6μl DNA template (recombine plasmid, then the tube is placed on a thermal cycler; Table 2.13).

Table 2.12: *Pf12ARM sequencing primers*

Pf12A-RM-SeqR	5’-TCC TTT CGG GCT TTG TTA-3’
Pf12A-RM-SeqF	5’-GTT TAG TGA ACC GTC AGA TCC-3’

Table 2.13: *Thermal profile amplification PCR reactions*

Step	Temperature	Time	No. of Cycles
Taq Activation	96°C	1 minutes	27
Denaturation	95°C	20 Sec.	
Annealing	50°C	15 Sec.	
Extension	60°C	3 minutes	
Final Extension	60°C	10 minutes	

2.9.2.10 Sequencing Analysis

Samples were dried by vacuum and then re-suspended in 1 µl Hi-Di formamide (cat no. 4311320, Life Technologies). Afterwards, the suspension was heated at 95°C for 2 minutes then placed on 2 minutes, and samples were analysed by 3130 Genetic analysers (cat no. 3130-01R, Applied Biosystems). The sequence Pf12ARM-*LANCL1-AS1* plasmid was confirmed.

2.9.2.11 Transfection of SK-MES-1 cell lines with Pf12ARM-LanCL-AS1 plasmid

SK-MES-1 cell line was transformed with Pf12ARM-*LANCL1-AS1* plasmid following the procedure mentioned in 2.9.1.3 and confirming *LANCL1-AS1* mRNA overexpression was performed by qPCR. Following the procedure in section 2.6.3, the successful clone LS3 was then picked for sub selective analysis.

2.9.2.12 Using coumermycin and novobiocin to regulate expression of transgene

To measure transgene expression, coumermycin and novobiocin were used to regulate the expression. While coumermycin increased the expression of the transgene, novobiocin worked in an opposite manner. During the experiment, to maintain the expression, clone LS3 will be seeding in 10nM coumermycin called (LS3C) and 10 µM Novobiocin called (LS3N).

2.10 Western blot

2.10.1 Bicinchoricacid BCA assay for qualification of the protein

2.10.1.1 Protein extraction

The eight NCLCS cell lines plus the knockdown *LANCL1* and overexpressed *LANCL1-AS1* clones were seeded in 75cm^2 flask until confluence reached 75%–80%. The medium was aspirated, and the flask washed twice with PBS, then was placed immediately on ice. Cells were then lysed with 800µl (RIBA) buffer (cat no. 89900, Thermo Fisher Scientific) plus 8µl proteinase inhibitor; all adhesion cells were scraped off with a plastic scraper, a step processed on ice). A Bioruptor sonication system (cat no. B01010001 [UCD200TM], Diagenode) was used as an extra lysis step to sonicate the cells following the manufacturer's instructions. Briefly, we ensured that the bioruptor sonicator was kept at 4°C, a tempersture reached by adding ice-chilled water; the cell lysis tube holder was then placed and sonicated in cycle condition 15 sec ON and 15 sec OFF for 3 minutes, and the tube was centrifuged at 12,000 × *g* for 15 minutes at 4°C to remove the remaining insoluble material. Supernatant was then transferred to a new Eppendorf tube; the rest was stored at -20°C for use in future analyses.

2.10.1.2 Preparation bovine serum albumin BSA standard curve

In order to create the standard curve, serial dilution or different concentration of BSA (0.125, 0.25, 0.5, 1, 2, 4, and 8) mg/ml was prepared from 20 mg/ml main stock calculated from BSA (cat no. A7906, Sigma-Aldrich) by using the serial dilution RIBA buffer. Following the manufacturer's procedure, BCA working reagents were prepared. Briefly, 5 units of reagent A were mixed with 1 unit of reagent B (cat no. 23224, Thermo Fisher Scientific). 4µl of BSA was diluted, and the samples were added to 80µl of BCA working reagents and mixed by vortex. The mixture was incubated at 37°C for 30 minutes, left to stand at room temperature for 5 minutes with a brief vortex; the BSA curve was plotted, and the unknown samples were measured using the NanoDrop 2000 Spectrophotometer (Thermo Fisher Scientific) following the user manual V1.0.

2.10.3 Electrophoresis immunoblotting and detection

2.10.3.1 Electrophoresis preparation

Preparing the samples for Sodium dodecyl sulfate SDS polyacrylamide gel electrophoresis, 20 µg of total protein from eight NSCLC cell lines, knocked down *LANCL1*, and overexpressed *LANCL1-AS1* clones were mixed with 2.5 µg of (4X)-6.25µl NuPAGE® LDS sample buffer (cat no. NP0008, Life Technologies), 2.5 µl of (XOX) NuPAGE® reducing agent (cat no. NP0004, Life Technologies), and adding H2O up to the total reduction of the volume 25 µl gel capacity volume mix, followed by being, briefly determined by incubating the mixture in 70°C for 10 min.

2.10.3.2 NUPAGE® cells electrophoresis for protein

NUPAGE® Novex Bis-Tris-Acetate (SDS-PAGE) mini gels (cat no. NP0321, PK2-Novex) was used for total protein electrophoresis. After removing the white tape near the bottom, the gel was placed in the X cell sure lock TM mini-cell gel running tank (cat no. EI001, Invitrogen). 200 ml of 1XNUPAGE Tri-Acetate-SDS running buffer mixed with 500μl NUPAGE antioxidant (cat no. NP0005, Invitrogen) was used to fill the lower chamber, while ~700 ml of 1XNUPAGE Tris-Acetate SDS running column was used to fill the upper chamber. Then, the combe was removed from the gel wells, and the well was washed twice with 1XNuPEGE Tris-Acetate SDS running buffer (cat no. LA0041, Invitrogen). After that, all the preparation samples were loaded onto the gel (also, see blue® plus 2 pre-stained standard loaded [cat no. LC5925, Invitrogen]). Finally, run the gel at 200 V (110–125) mA/gel for 90 minutes.

2.10.4 iBlot western blot detection

An iBlot® dry blotting system (cat no. IB1001, Invitrogen) was used for blotting electrophoresis proteins. After electrophoresis, the gel was removed from the cassette plate and washed with ddH2O three times in 5 minutes. The gel was then placed onto a PVDF blotting surface of an anode iBlot gel transfer stack (cat no. IB8010-01, Novex) and covered with pre-soaked iBlot filter paper which was pre-placed in deionised water at the top of the filter paper, and cathode iBlot was placed on with side facing up and aligned along the right edge. A blotting roller was placed to help remove the air bubbles. Finally, a disposable sponge with metal in the corner was placed on the upright curve on the lid. After ensuring that the lid was closed securely, the iBlot dry blotting system was switched on at setup in program P3 for standard (voltage: 20 and time: 9 minutes). After transfer was finished, the gel and membrane were washed three times with PBS-T. The gel was then stained with compass blue (e.g. simple blue safe stain; Invitrogen), distain with (methanol 40% + Acetic acid 10%), and photographed with the aid of UV Prism works instrument; the PVDF blotting membrane was used to complete the iBind by using the iBined western system (Life Technologies). The membrane was kept with 5ml iBind complex (1XBind addictive). iBind was used to apply the Binding primary antibody and secondary contain (1:1000 with same diluent) and washing stop by iBind complex. Rabbit monoclonal primary antibodies to *LANCL1* (cat no. PA5-57107 & PAS-31080, Thermo Fisher Scientific) and actinβ (cat no. 84575) cell signalling technology were used as primary antibody, while, the secondary antibody was antirabbit IgG HRP-linked antibody (cat 70745-cell signalling technology); all antibodies were used following the manufacturer’s protocol, and no further calibrator was required because they worked well. The first chamber was filled with primer antibodies LanCL1 plus Actβ, the second chamber with iBind complex for washing, the third chamber with secondary antibody, and the fourth chamber with iBind for complete washing. The reset of the immune complex was detected by using the chemiluminescence imaging system GENE system (synGENE). After iBind, the membrane was washed with ddH2O, then placed on the nailon; we prepared HRP chemiluminescent substrate reagent (cat no. WP20005, Invitrogen) 1:1 reagent 1 and 2, then added the total to the membrane cover for 3 minutes because of light sensitivity.

2.11 Wound healing assay

The wound healing assay (scratch assay) was chosen to measure cell migration and wound-healing capacity, of SK-MES-1 parental, scramble, overexpress *LANCL1-AS1*, and knocked down *LANCL1* clones. Approximately 5 × 10^4 cells were seeded in flat-bottomed, six-well plates cultured with medium + 5% FBS and antibiotic. Upon confluence, covered the well, the monolayer was scratched by using a tip, plates were washed with PBS, and the medium was refreshed with +5% FBS. Time lap images was digitally captured by microscope (EVOS XL core imaging system, cat no. AMEX1000, Thermo Fisher Scientific) at different time points on 0h, 3h, 12h, 24h, 36h, and 48h with digital camera, precision optics, LCD display, and USB storage. The open wound area was calculated/measured by ImageJ software (Fiji) (Rasband 1997-2018).

2.12 Invasion assay

Cell movement was monitored through extracellular matrices, fundamental function, and cellular processes (e.g. angiogenesis, metastasis). The assay was carried out in flat-bottomed, 24-well plates, where the trans well (ThinCert™ Cell Culture Inserts 24 Well cat no.662638 Greiner Bio-One) was placed in one of the wells, then 100µl of Geltrex™ (cat no. A15696-01, Life Technologies) was added to the trans well and incubated in 37°C; 5% FBS + AB was added under each trans well, adding around 10,000 cells in 200µl medium + 5% FBS with antibiotic added on top of the gel mixture and incubated in 37°C 5% FBS for 24h. After incubation, the medium was discarded in a beaker containing Chemgene; we then washed the well with PBS, transferred the trans well into a new well, added 100µl of cold methanol to the trans well, and incubated it in the freezer for 10 minutes. After discarding the methanol on the beaker, washed twice with PBS, then 100µl of (1:4, 20% methanol + 0.16% crystal violate) was added to the trans well and incubated for 30 minutes. After incubation, the stain was discarded and the well washed twice with PBS. A cotton badge was used to remove the remaining cells on top of the trans well. A microscope (EVOS XL core imaging system, cat no. AMEX1000, Thermo Fisher Scientific) was used to capture the images under different magnifications (4×, 10×, 20×, 40×).

2.13 Statistical analysis

The entire statistical analysis was performed using IBM® SPSS® (statistics precision 2). Continuous variables were checked for normal distribution using the 1 K-S test. As this demonstrated lack of normal distribution the non-parametric Mann–Whitney test was selected to compare continuous variables in two independent categorical groups. The Wilcoxon signed-rank test was used to compare between different expressions of LANCL1 and LANCL1-AS1 between tumour and adjacent non-tumour samples in a paired fashion.

The IC50 values were determined by using Prism 8.0 (graphpad) that can fit the dose responses with log concentration values (on the *X*-axis), while the response plot in *Y*-axis $P < 0.05$ was considered/selected statistically significant. In Prism, the IC50 values were calculated by (inhibitor) vs normalized response variable slope equation. The (also non-parametric) Spearman's rank-order correlation was used to examine associations between continuous variable.

2.14 Preparation of the cell or special feeding for the cell to extract extracellular vesicles EVs

Isolating exosomes from the NSCLC cell lines requires a special medium. Therefore, once confluence had reached 80%, the flask was washed with PBS twice, then the medium DMEM without FBS was added. Serum-free medium is used to minimise the albumin and different other proteins and metabolites in serum contamination in the FBS; the ratio is 1 ml medium: 2μl cocktail, 500X TC (Table 2. 14; e.g. T75:10 ml medium + 20μl cocktail will be added). The cell is left in the incubator at 37°C, 5% CO_2, maximum from 12–16h; the medium is then collected to extract exosomes. The medium was collected with cocktail TC 500X that contains EVs in a universal tube, centrifuged at 300 × *g* for 5 minutes, then filtered through 0.22μM in a falcon tube.

Table 2.14: TC 500X

Substance	1X	500X Stock
Tri-iodothyronine	10 ng/ml	5 ug/ml
EGF	10 ng/ml	5 ug/ml
Insulin	2 ug/ml	1 mg/ml
BSA	2 ug/ml	2 mg/ml
Holo-transferrin	5 ug/ml	2.5 mg/ml
Epinephrine	1 ug/ml	500 ug/ml
Glucose	95 ug/ml	47.5 mg/ml
Hydrocortisone	0.5 ug/ml	0.25 mg/ml

2.15 Count extracellular vesicles EVs using NanoSight

Cells were seeded in Xwell plates or else using serum free medium. At the selected time for each experiment, the supernatant medium was collected, span at 300g for 10 min, filtered through 0.22 µm syringe filters and applied onto Nanosight instrument following the supplier's standard protocol. Three measurements of independent injections on the machine were taken for each specimen. The mean number of EVs and the size distribution was reported for each specimen.

2.16 Protein extraction from EVs

A biolipid affinity spin column (exoEasy Kit. cat no. 77044, Qiagen) was used to efficiently isolate EVs for this purpose. After collecting the serum-free medium plus cocktail containing EVs, XBP to bind the filtered sample to the column, buffer was added in an equal amount to the medium and mixed in a rotator for 3 minutes. The liquid was then transferred onto a filter and collection tube; all the mixture was filtered through the vacuum, XWP buffer was added to the tube and then filtered through the vacuum, centrifuged in 4,000 × *g* for 5 minutes (dry spin), and XE elution buffer added to elute the samples. EV isolates were dialysed twice against PBS (300 ml) using TSlide-A-Lyzer®, (cat no. P00090554, Thermo Fisher Scientific) Then, the dialysis performed (Figure 2.12).

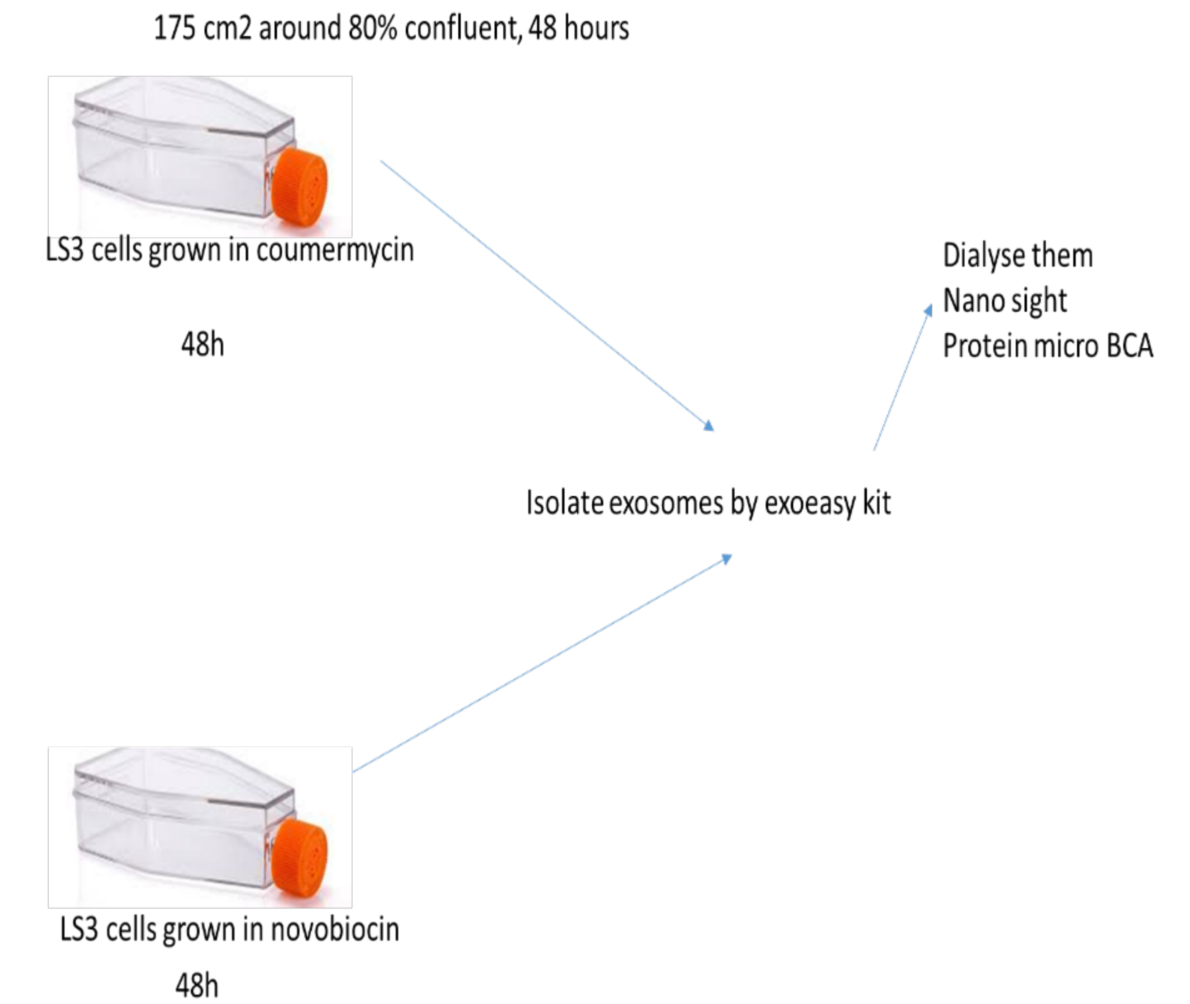

Figure 2.12: *Isolate EVs from overexpressed LANCL1 AS1 clones grown in coumermycin and novobiocin by using an exoEasy Kit.* Most of the exoEasy product dialysed to reduce the toxicity of the elution buffer, and NanoSight was used to count the EVs, small parts of the product used to measure the protein for normalization.

2.17 Exchanging the whole medium between sensitive LS3Cand resistant LS3N cell lines

Seeding overexpressed *LANCL1-AS1* with medium + 5% FBS grown in novobiocin LS3N in flat-bottomed, 48-wells plate until confluence, reached 40%. Then, the medium was changed in half of the plate by serum-free media, conditioned for 48h in overexpressed LANCL1-AS1 cells grown in coumermycin (heterologous) or novobiocin (autologous). The other half of the plate was treated with IC50 gemcitabine 0.6µM added to serum-free media, conditioned for 48h in overexpressed LANCL1-AS1 cells grown in coumermycin (heterologous) or novobiocin (autologous). Following incubation for 48h in 37°C, 5%CO2, the cell viability was measured using an MTT assay (Figure 2.13).

The reduction in replication shown in the autologous medium replacement most probably reflects the partial exhaustion of medium resources as the growth factors in SF-media are being degraded (control receives fresh SF medium with supplements for the corresponding 48h incubation). In contrast, the heterologous replacement with media from cells with high *LANCL1-AS1* expression, causes a significant reduction on the target cells (with low expression of *LANCL1 -AS1*).

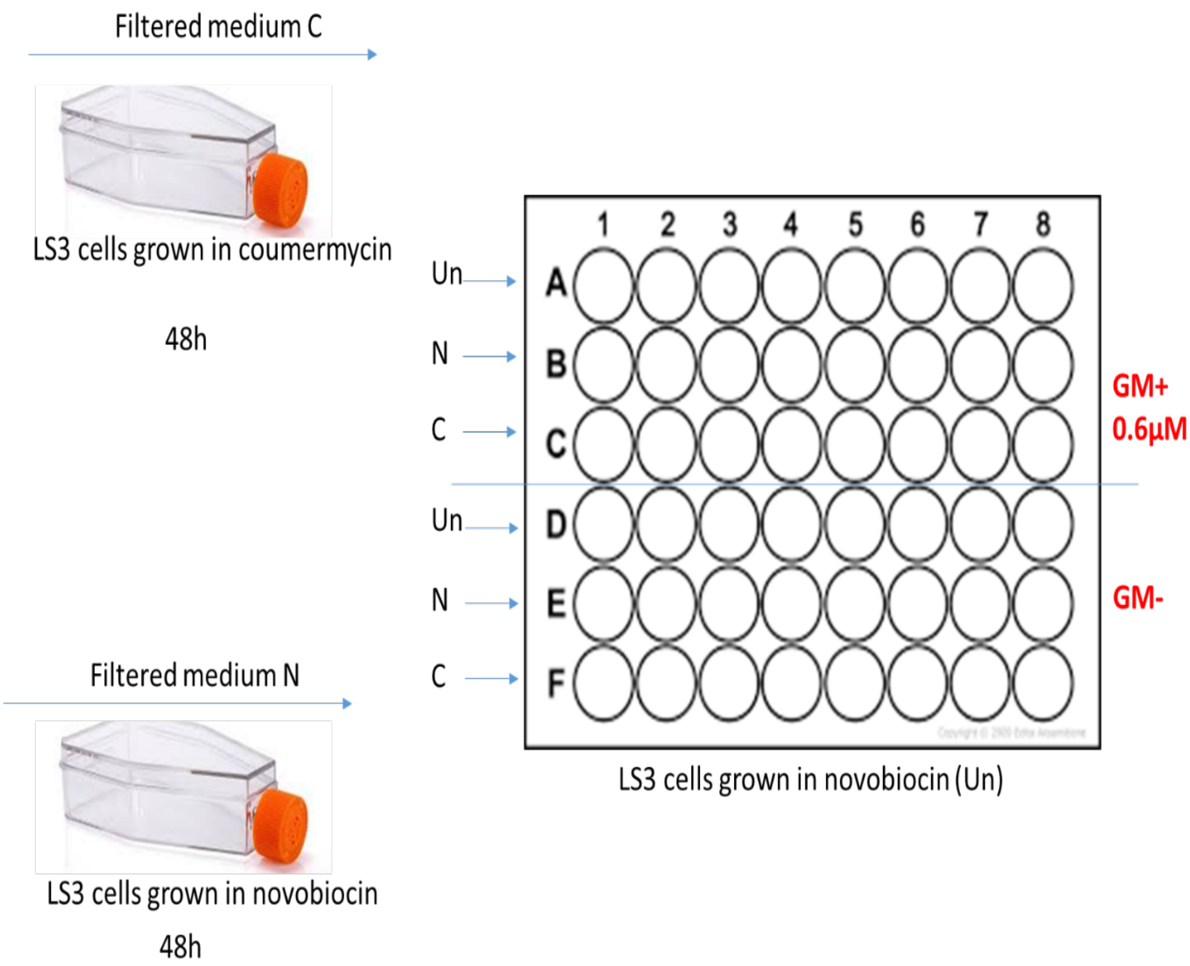

Figure 2.13: *Exchanging medium between low and high LANCL1 AS1 expression*. Low *LANCL1 AS1* expression cell line grown in novobiocin seeded in flat-bottomed, 48-wells plate until confluence reached 40%. Then, half of the plate was treated with 0.6 µM GM. The medium was exchanged with filtered medium collected from (N) low *LANCL1 AS1* expression grown in novobiocin, (C) high *LANCL1 AS1* expression grown in coumermycin, and (UN) medium with 5% FBS. The plate was incubated for 48 h in 37°C, 5% CO_2.

2.18 Exchange EVs between cell lines

We seeded overexpressed *LANCL1-AS1* with medium + 5%FBS grown in novobiocin LS3N in flat-bottomed, 48-wells plates until confluence reached 40%. The medium of half the plate was then replaced with serum-free medium with cocktail and exosome isolated from overexpressed LANCL1-AS1 grown in coumermycin (heterologous) or novobiocin (autologous). The other half of the plate was treated with IC50 gemcitabine 0.6µM added to serum-free medium with cocktail and exosome isolated from overexpressed LANCL1-AS1 grown in coumermycin (heterologous) or novobiocin (autologous). Following incubation for 48 h in 37°C, 5% CO_2, cell viability was measured using an MTT assay (Figure 2.14).

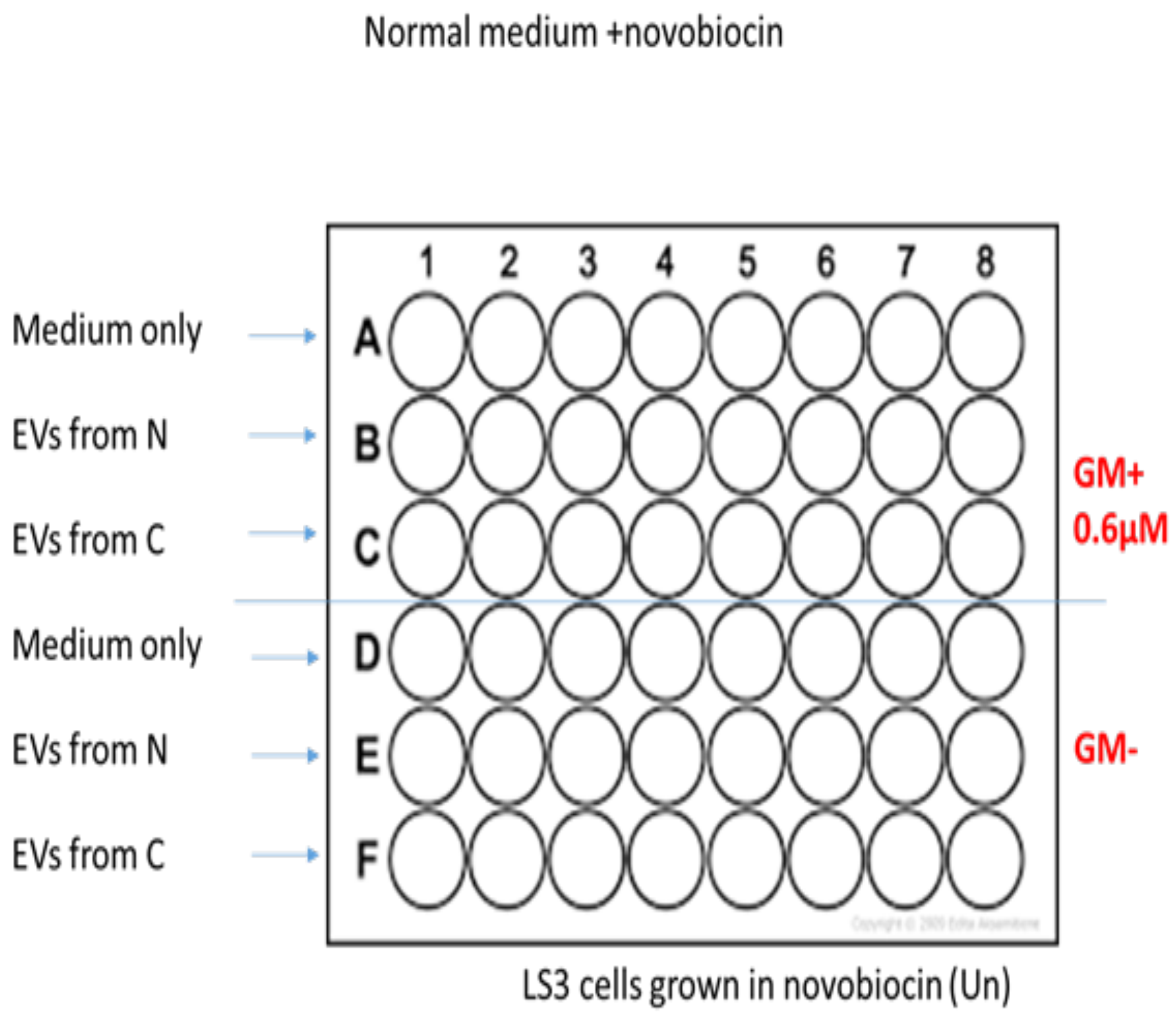

Figure 2.14: *Exchanging EVs low and high LANCL1 AS1 expression.* Low *LANCL1 AS1* expression grown in novobiocin seeded in flat-bottomed, 48-wells plate until confluence reached 40%. Then, half of the plate was treated with 0.6 µM GM. Exchanged EVs isolated from (N) low *LANCL1 AS1* expression grown in novobiocin, (C) high *LANCL1 AS1* grown in coumermycin, and for control exchange with medium with 5% FBS. Incubated the plate for 48 h in 37°C, 5% CO_2.

Chapter 3: Epigenetic sensitization of non-small cell lung cancer (NSCLC) to chemotherapeutic compounds

3.1 Introduction

Sensitising NSCLC by combining chemotherapeutics with other sensitizer drugs that are already approved and available. Chemotherapy is still used to treat either early or late stage NSCLC (Zhou et al. 2011). Four chemotherapeutic agents (cisplatin, carboplatin, gemcitabine, and vinorelbine) were chosen to be re-sensitized in NSCLC cell lines by combining them with sodium valproate (VPA) (Schiffmann et al. 2016), decitabine (DAC) (Szyf 2009), aminomethylphosphonic acid (AMPA) (Li et al. 2013), and fendiline (van der Hoeven et al. 2013).

VPA and DAC have been identified as epigenetic regulation agents. Valproic acid can inhibit histone-deacetylation. It selectively induces proteasomal degradation of HDAC2 (Krämer et al. 2003), while decitabine inhibits methyltransferase and leads to increased demethylation. (Szyf 2009). Decitabine induces selective degradation of DNA methyltransferase 1 by a proteasomal pathway (Ghoshal et al. 2005).

Therefore, the epigenetic drugs (VPA or DAC) can play a role in epigenetic regulation, as both can increase tumor suppressor gene expression or other oncogenes that may improve the chemo-sensitivity.

Moreover, aminomethylphosphonic acid (AMPA) AMPA works as Serine hydroxymethyltransferase1 (SHMT1) inhibitor and SHMT plays a role in epigenetic alteration.

Also, AMPA has been determined as a proliferation inhibitor which also increases the apoptosis activity in pancreatic cancer (Naseer et al. 2018). Fendiline works as a calcium channel blocker and pointing calcium signalling can reverse epigenetic silencing of tumour suppressor genes (Raynal et al. 2016). Fendiline inhibits proliferation and invasion by interfering with β -catenin signalling in the WNT pathway, which is often deregulated in cancer (Alberg et al. 2013).

Therefore, AMPA and fendiline are evidenced to play a role in epigenetics modulation and inhibiting proliferation. Pointing epigenetic pathways is a promising method for cancer therapy. As such, they were chosen to be combined with four chemotherapeutic agents in this research in order to investigate their roles in NSCLC (van der Hoeven et al. 2013; Li et al. 2013).

The aim of this part of the study was to explore and assess sensitization of NSCLC cell lines to the four chosen chemotherapeutic agents. For this purpose, the following objectives were set:

a) Determine the IC50 for the four selected chemotherapeutic agents (cisplatin, carboplatin, gemcitabine, and vinorelbine) in eight NSCLC cell lines.

b) Examine the effect of combined epigenetic drugs (VPA and DAC) with chemotherapeutics in both conditions (synchronous and pre-treatment) Sensitizing NSCLC

c) Investigate the mechanism of cell death in combined chemotherapeutics by using caspase 3/7 activity to determine apoptotic, and the neutral comet assay to determines DSB

d) Explore the effect of co-treatment of anti-proliferation agents (AMPA and fendiline) combined with chemotherapeutics in the cell viability.

3.2 Results

3.2.1 Chemo-sensitivity of non-small lung cancer cell to gemcitabine, vinorelbine, cisplatin, and carboplatin

The sensitivity of the four most commonly chemotherapeutic agents used in lung cancer–gemcitabine (Gemzar), vinorelbine (Navelbine), cisplatin (Platinol®), and carboplatin (Paraplatin®) was determined on eight NSCLC cell lines, namely A549, CALU-3, CALU-6, COR-L23, H358, LUDLU-1, SK-LU-1, and SK-MES-1. Half-maximal inhibitory concentration (IC50) was used to estimate the chemo-sensitivity of the cell lines, following a 48h exposure to the different compounds. The MTT assay was used to measure the cell viability and IC50 values were calculated using Graph Pad Prism version 8.0 software. As expected, sensitivity ranged widely among the eight NSCLC cell lines (Table 3.1, Figure 3.1). All the chemotherapeutic agents reduced the cell growth in a concentration-dependent manner. The effective concentration of each compound was, again not surprisingly, different. Specific information on each of the drugs is shown below.

Evaluation of the IC50 values and the 95% confidence intervals following 48 hours treatment of the NSCLC cell lines with (0-4μM) gemcitabine showed that A549 with IC50 (0.04539μM) and SK-MES with IC50 (0.04582μM) were the most sensitive NSCLC cell lines, while CALU-6 with IC50 (0.3924μM), H358 (0.3286μM), and SK-LU-1 (0.3193μM) were the most resistant cell lines.

Furthermore, after 48h treatment with (0-500nM) vinorelbine, lowest absorption reading detected in both COR-L23 and CALU-6 with IC50 (0.01094nM-0.03036 nM). While, CALU-3, SK-LU-1, and A549 have highest IC50 with (61.79nM-23.99nM-12.26nM) respectively.

In cisplatin, the MTT absorption reading identified CALU-6 (1.103μM) and COR-L23 (1.609μM) with low IC50 values; the most resistance cell lines after 48h treated with (0-100μM) cisplatin with the highest IC50 were in CALU-3 (7.01μM), H358 (6.903μM), and A549 (4.922μM).

Moreover, following 48h treatment of the NSCLC cell lines with (0-100μM) carboplatin, the IC50 were highest in SK-MES (25.53μM), A549 (21.25μM), and COR-L23 (12.4μM), and the lowest IC50 were in the H358 (3.033μM) and SK-LU-1 (4.934μM) cell lines (Figure 3.1).

A

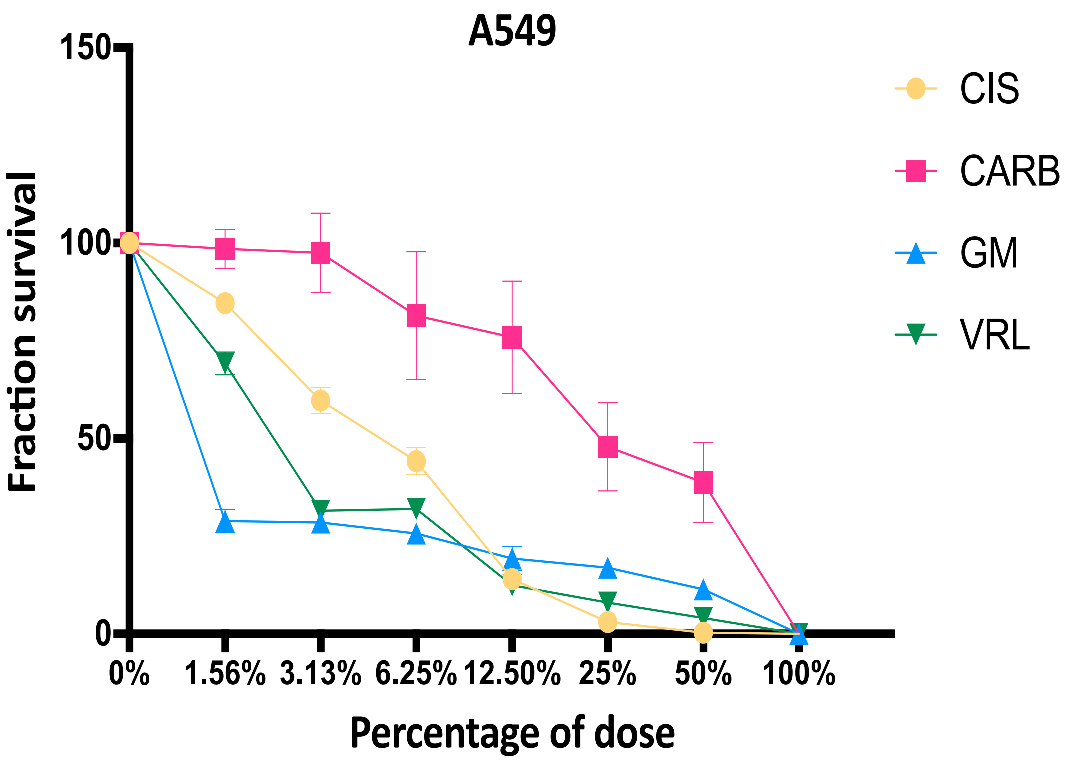
A549
150
100
50
0
Fraction survival
0%
1.56%
3.13%
6.25%
12.50%
25%
50%
100%
Percentage of dose
CIS
CARB
GM
VRL

B

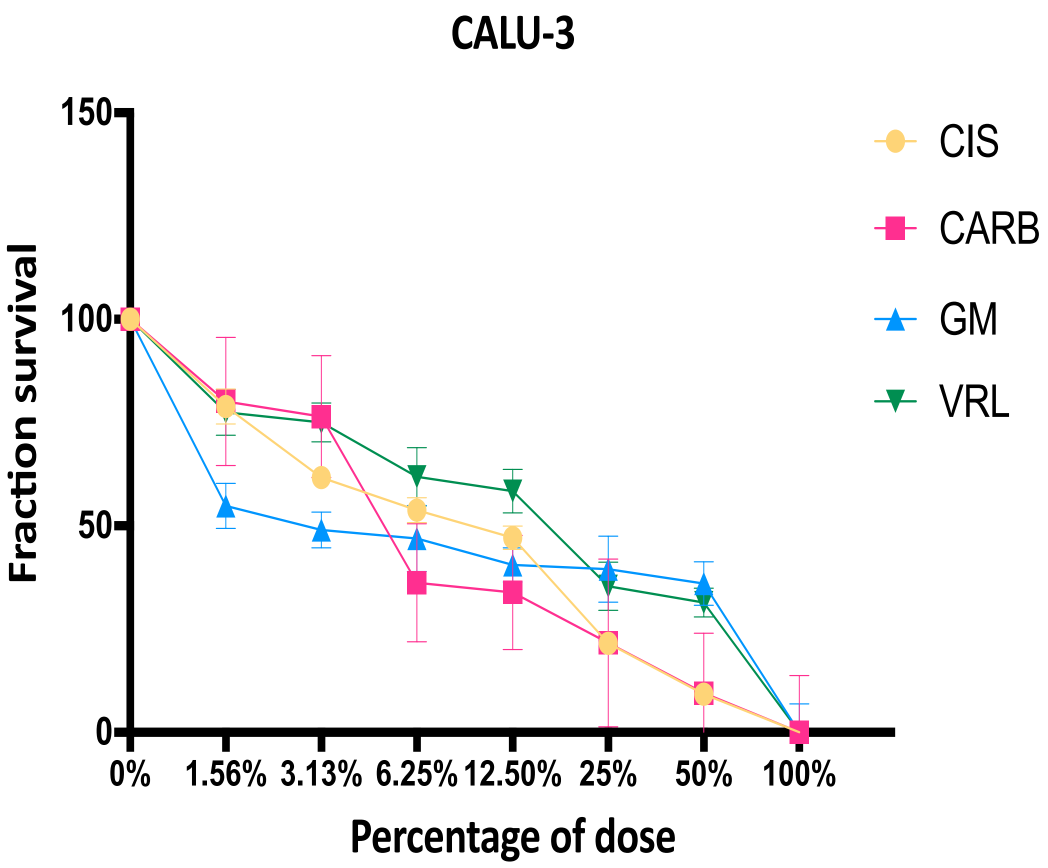
CALU-3
150
100
50
0
Fraction survival
0%
1.56%
3.13%
6.25%
12.50%
25%
50%
100%
Percentage of dose
CIS
CARB
GM
VRL

C

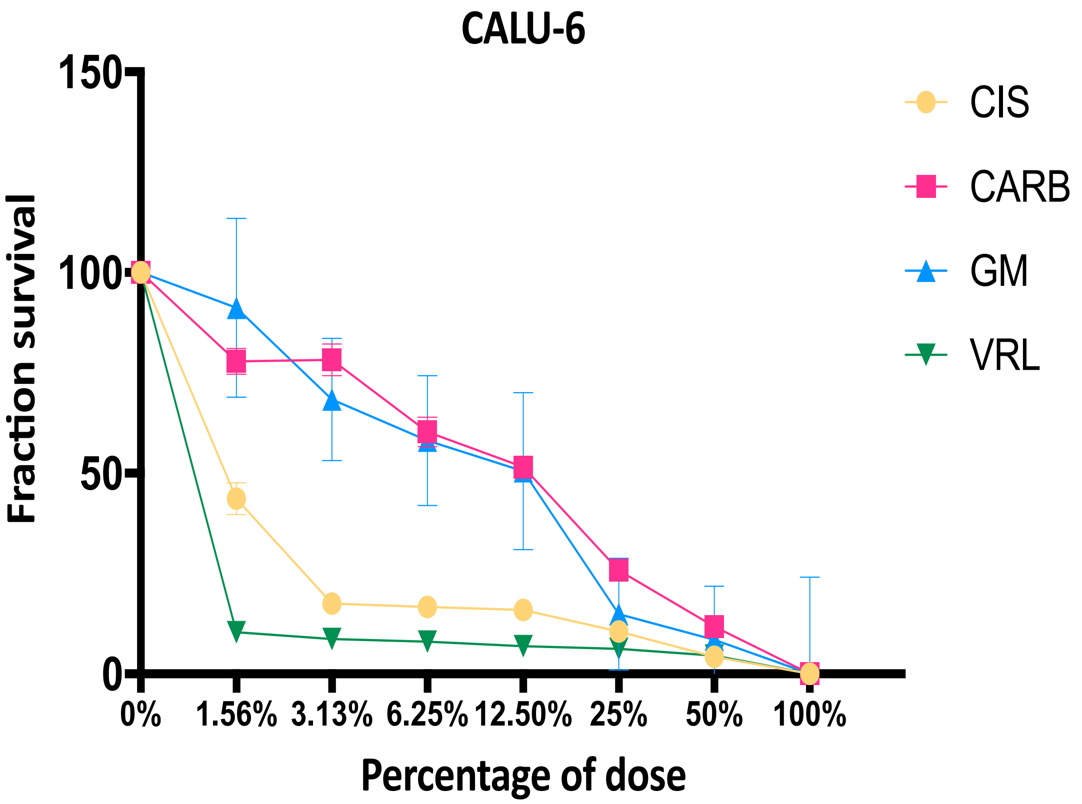
CALU-6
150
100
50
0
Fraction survival
0%
1.56%
3.13%
6.25%
12.50%
25%
50%
100%
Percentage of dose
CIS
CARB
GM
VRL

D

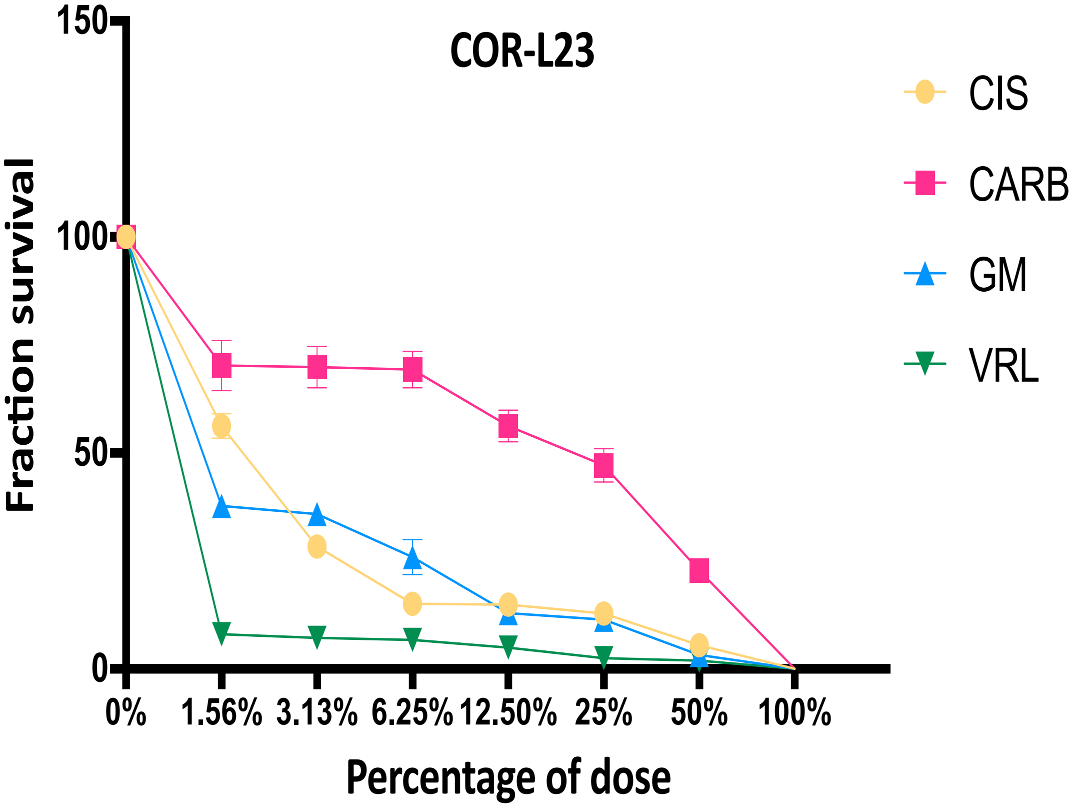
COR-L23
150
100
50
0
Fraction survival
0%
1.56%
3.13%
6.25%
12.50%
25%
50%
100%
Percentage of dose
CIS
CARB
GM
VRL

E

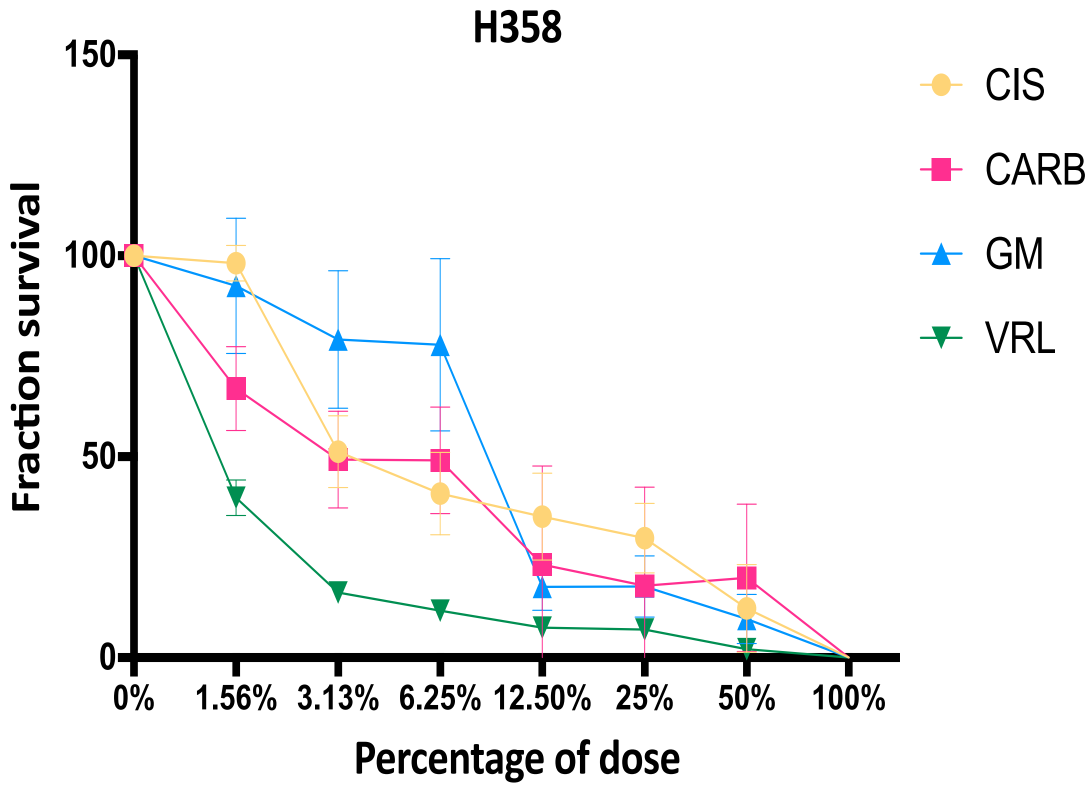
H358
Fraction survival
150
100
50
0
0%
1.56%
3.13%
6.25%
12.50%
25%
50%
100%
Percentage of dose
CIS
CARB
GM
VRL

F

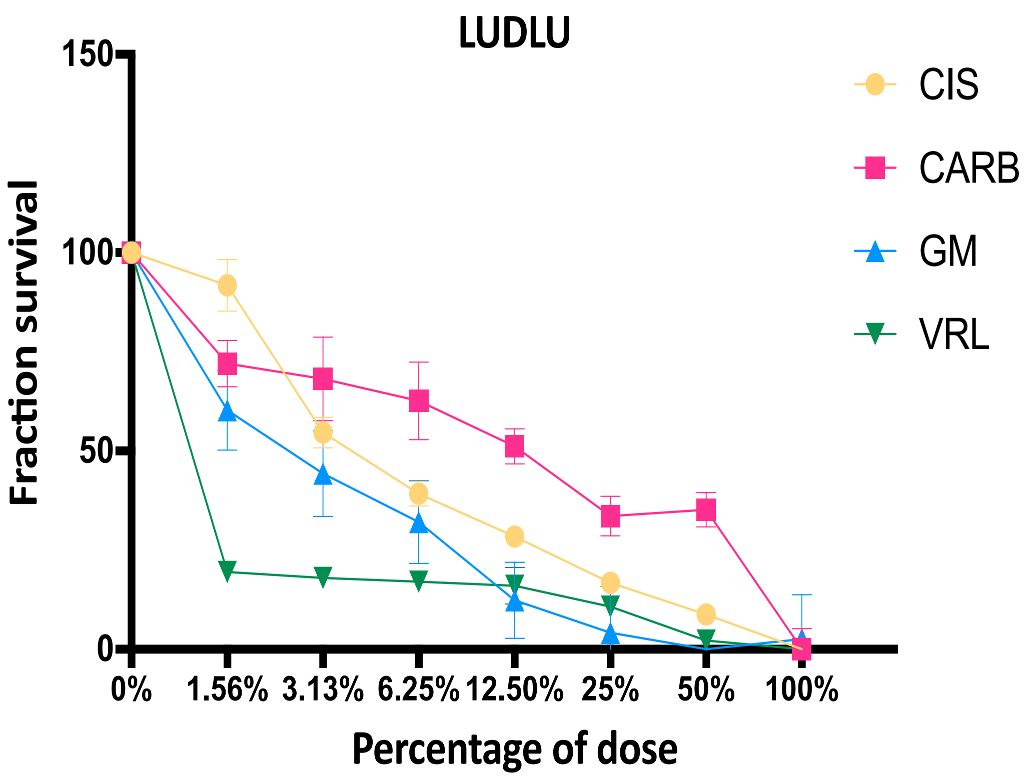
LUDLU
Fraction survival
150
100
50
0
0%
1.56%
3.13%
6.25%
12.50%
25%
50%
100%
Percentage of dose
CIS
CARB
GM
VRL

G

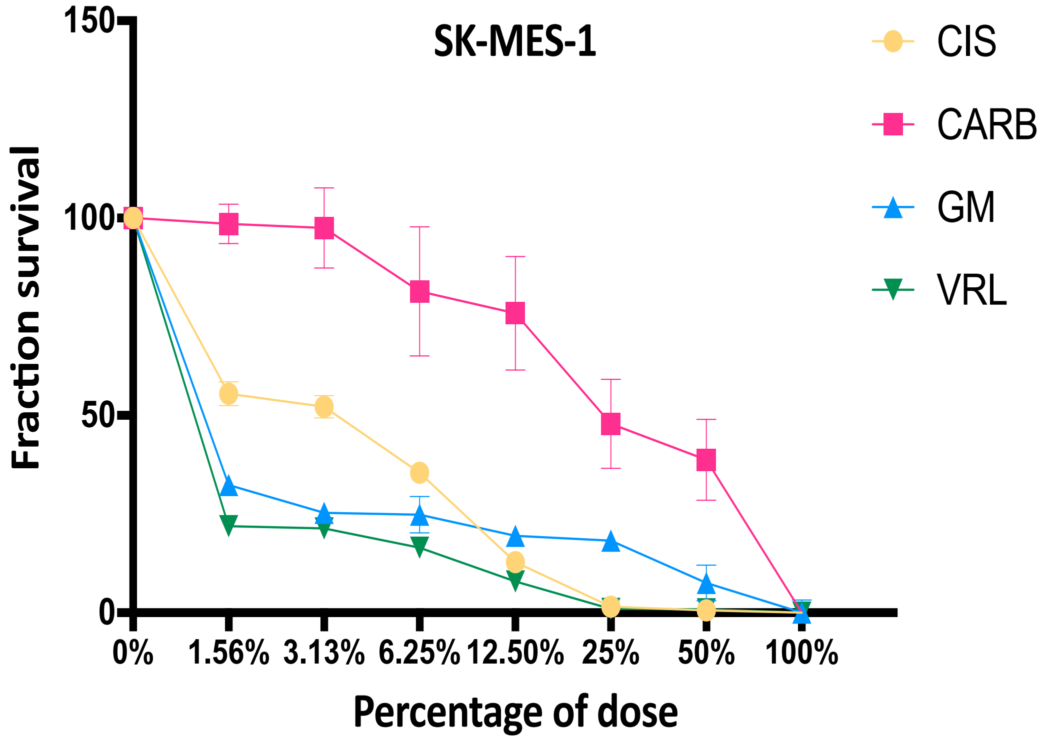
SK-MES-1
CIS
CARB
GM
VRL
Fraction survival
150
100
50
0
0%
1.56%
3.13%
6.25%
12.50%
25%
50%
100%
Percentage of dose

H

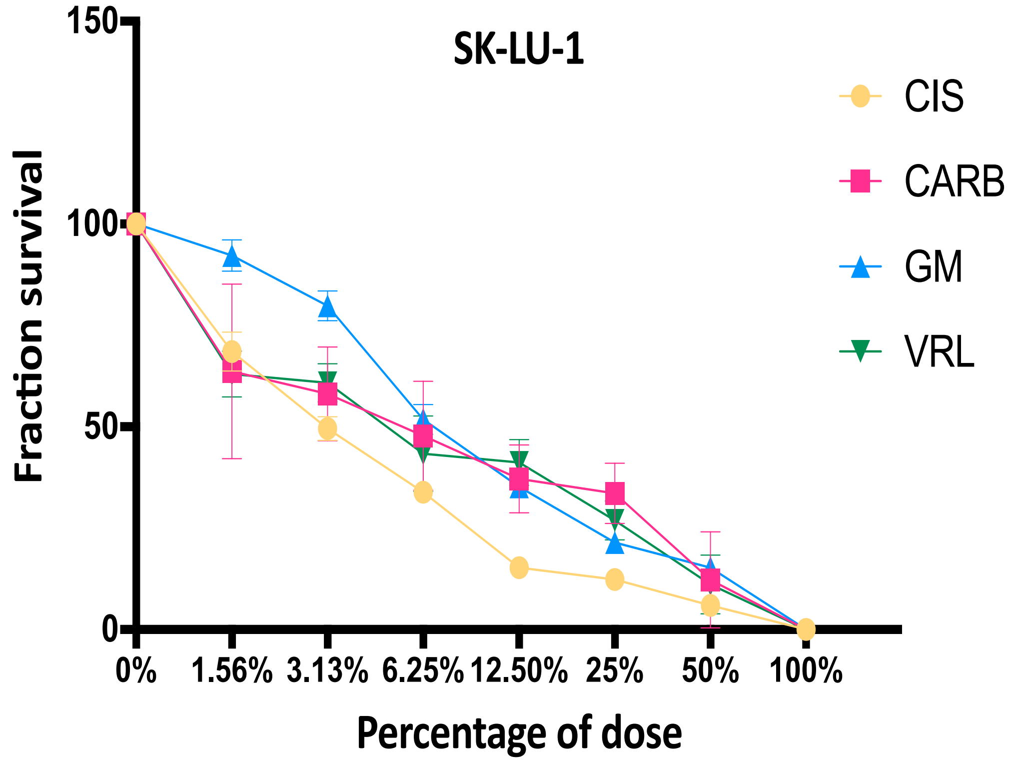
SK-LU-1
CIS
CARB
GM
VRL
Fraction survival
150
100
50
0
0%
1.56%
3.13%
6.25%
12.50%
25%
50%
100%
Percentage of dose

Figure 3.1: *Heterogeneous response of the studied eight non-small cell lung cancer cell lines following 48h hours*: graph represent the MTT absorbance readings for gemcitabine (**GM**), vinorelbine (**VRL**), cisplatin (**CIS**), and carboplatin (**CARB**). 100% dose state in the X axis corspond to the concentation of the drugs (cisplatin (100µM), carboplatin (100µM) gemcitabine (4µM), and vinorelbine (0.5µM). In eight NSCLC cell lines A: **A549**, B: **CALU-3**, C: **CALU-6**, D: **COR-L23**, E: **H358**, F: **LUDLU**, G: **SK-MES-1** and H: **SK-LU-1**. COR-L23 and SK-MES-1 are the most resistant cell lines for carboplatin, while H358 and A549 are the most resistant cell lines for cisplatin. For vinorelbine, both A549 and SK-LU-1 showed the highest resistance. SK-LU-1 and CALU-6 showed resistance for gemcitabine. The mean and error values in all graphs represent six technical replicates, and the error bars symbolise 95% confidence intervals.

Table 3.1: *The IC50 values of the eight NSCLC treated with four chemotherapies*: IC50 values and their respective 95% confidence intervals of eight non-small cell lung cancer cell lines exposed to gemcitabine (0-4µM), vinorelbine (0-0.5µM), cisplatin (0-0.1mM), and carboplatin (0-0.1mM)

	Gemcitabine		**Vinorelbine**		**Cisplatin**		**Carboplatin**	
Cell line	IC50 (µM)	95% CI (µM)	IC50 (nM)	95% CI (nM)	IC50 (µM)	95% CI (µM)	IC50 (µM)	95% CI (µM)
A549	0.045	0.034 - 0.058	12.260	10.65 - 13.91	4.922	4.165 - 5.8 09	21.250	15.02 - 30.06
CALU-3	0.220	0.139 - 0.343	61.790	47.52 - 79.75	7.010	6.096 - 8.052	5.957	3.232 - 10.34
CALU-6	0.392	0.263 - 0.585	0.030	4.2 E-4 - 0.230	1.103	0.932 - 1.292	9.604	8.340 - 11.02
COR-L23	0.057	0.048 - 0.067	0.011	3.179E-6 - 0.183	1.609	1.437 - 1.794	12.400	9.507 - 15.99
H358	0.329	0.169 - 0.626	4.648	3.372 - 5.828	6.903	5.090 - 9.34 1	3.033	0.98 - 5.65
LUDLU	0.096	0.061 - 0.143	0.356	0.0308 - 1.190	4.152	3.574 - 4.813	10.250	7.005 - 14.65
SK-MES-1	0.046	0.034 - 0.059	1.544	0.8326 - 2.387	3.079	2.754 - 3.436	25.530	17.87 - 36.39
SK-LU-1	0.319	0.279 - 0.364	23.990	16.33 - 33.21	2.566	2.248 - 2.919	4.934	1.931 - 9.294

3.2.2 Epigenetic modulation of drug sensitivity by deoxy-azacytidine (DAC) and sodium valproate (VPA).

Epigenetic inactivation of key genes controlling cell growth is a frequent event in human cancer (Schiffmann et al. 2016). Gene silencing can be achieved by a combination of epigenetic events such as DNA methylation, histone modifications and changes in the non-coding RNA patterns. Re-expression of genes epigenetically deactivated may result in disease state suppression or sensitization to specific treatments. Small molecules that reverse epigenetic inactivation, such as valproic acid and decitabine, are currently undergoing clinical trials for tumours (Hubaux et al. 2010; Tan et al. 2010).

Epigenetic deregulation has been identified as one factor leading to chemosensitization (Steinhardt and Gartenhaus 2013). In this study, epigenetic sensitisation of four chemotherapeutic agents was investigated in NSCLC cell lines, using drugs VPA (an HDACi) and DAC (a DNMTi). VPA can induce cell cycle arrest in G1 (Catalano et al. 2005). Since epigenetic drugs can arrest the cell cycle at a specific point, therefore reducing proliferation rates, they could have an opposite to the desired effect on chemotherapeutic agents targeting dividing cells. Therefore, we attempted to examine both the effect of pre-treating the NSCLC cell lines with epigenetic agents before treated with chemotherapeutics, also the effect of synchronous epigenetic agents with chemotherapeutics at the same time.

Our hypothesis was investigated through extensive research that identified the potential efficacy of combining epigenetic agents with chemotherapy in various cancer types (Lin et al. 2008; Kanda et al. 2005; Del Bufalo et al. 2014; Steinhardt and Gartenhaus 2013).

In this study, we examined the influence of epigenetic drugs in re-sensitizing gemcitabine, vinorelbine, cisplatin, and carboplatin in resistant NSCLC cell lines, as identified from our previous experiments (Table 3.1): CALU-6, H358, and SK-LU-1 to gemcitabine, SK-LU-1 and A549 to vinorelbine, H358 and SK-LU-1 to cisplatin, and COR-L23 and SK-MES-1 to carboplatin.

While the DAC and VPA toxicity was tested in this study by the MTT assay to measure cell viability, apoptotic death was determined by caspase 3/7 activity.

3.2.2.1 Toxicity of the two drugs alone

Initially, we determined the toxicity of the two drugs alone. The final concentration of the two compounds was decided to match the clinical dose. The normal prescription for VPA is 1000mg per day, which in an adult with an average 5lt blood volume, corresponds to 1 mM. The DAC dose was decided based on 100nM our results show that DAC and VPA slightly affect cell proliferation. The toxicity result is shown in (Figure 3.2) the rate of cell viability after exposed to VPA and DAC not change comparing with the control which mean the drugs are safe. However, CALU-6 showed a significant decrease in cell viability with P=0.004 under both VPA and DAC that may different genotype showed different effect (Mann Whitney).

A

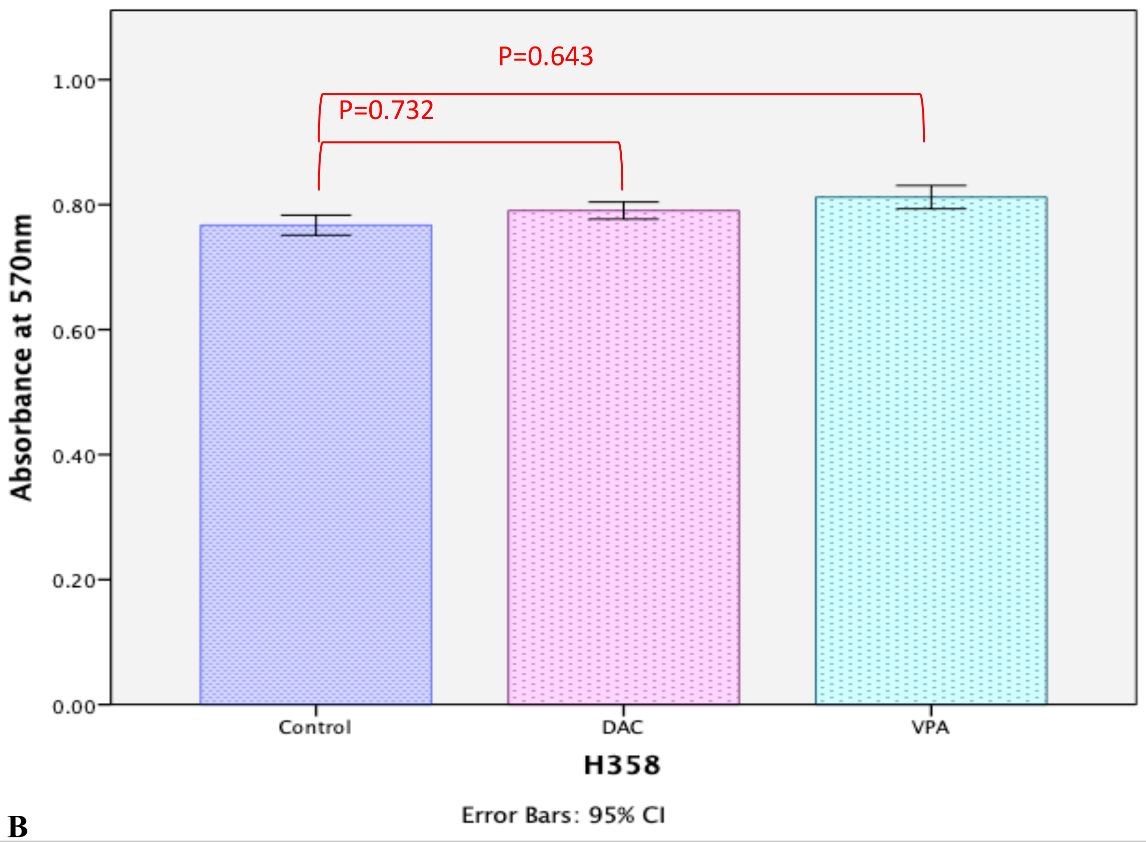
P=0.643
P=0.732
1.00
0.80
0.60
0.40
0.20
0.00
Absorbance at 570nm
Control
DAC
VPA
H358
Error Bars: 95% CI

B

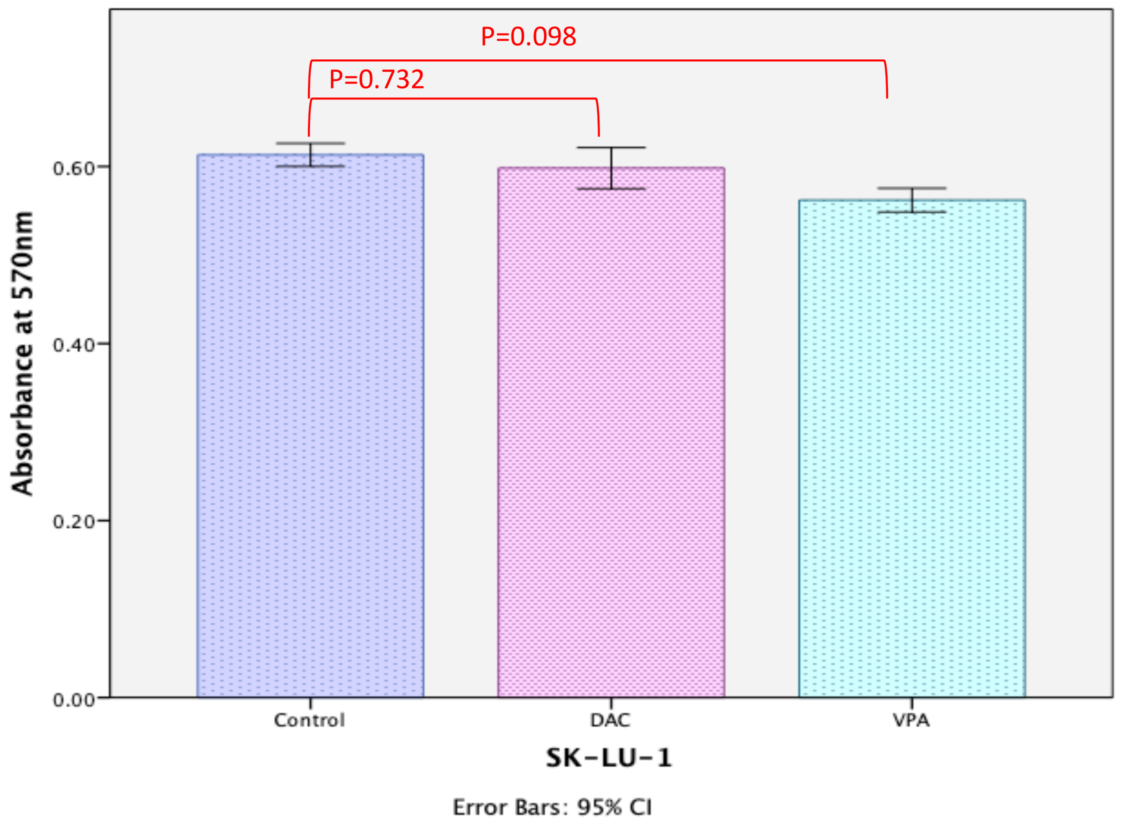
P=0.098
P=0.732
0.60
0.40
0.20
0.00
Absorbance at 570nm
Control
DAC
VPA
SK-LU-1
Error Bars: 95% CI

C

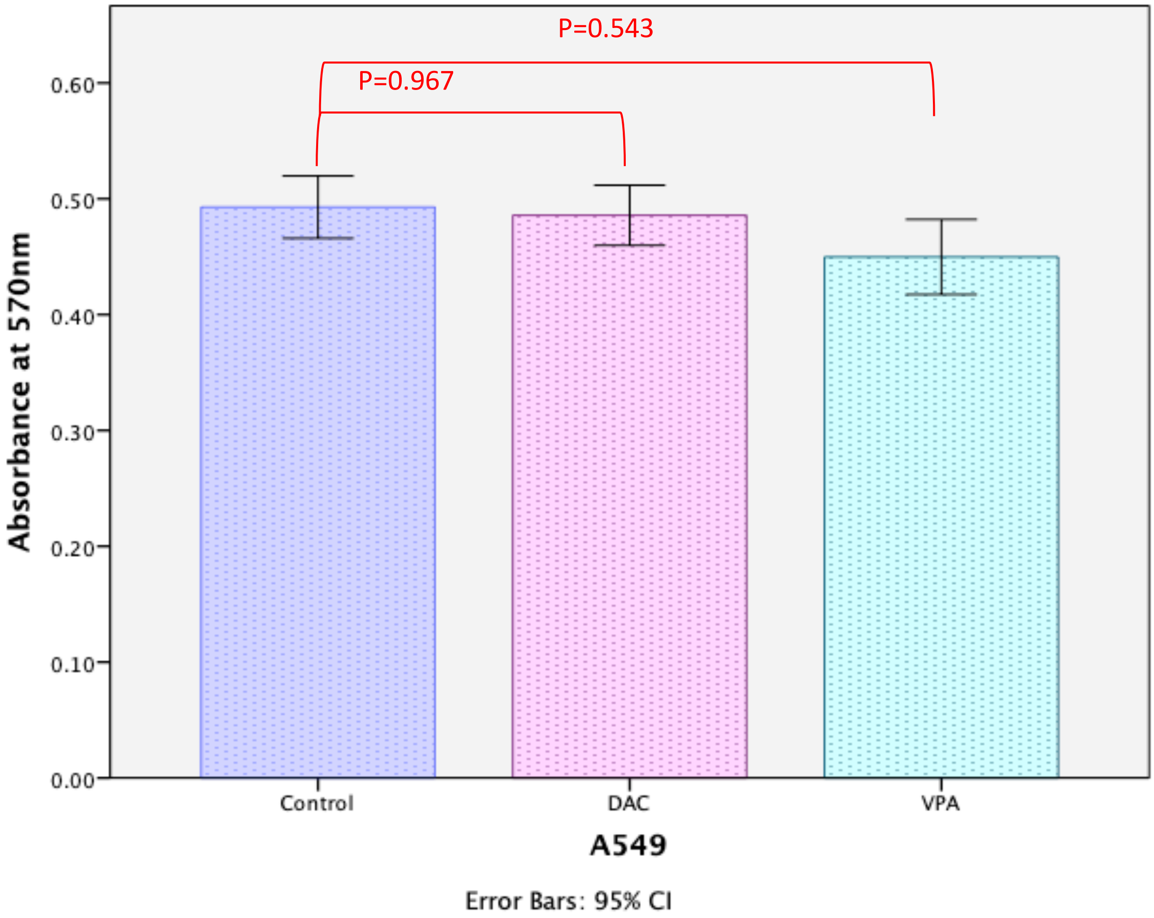
P=0.543
P=0.967
Absorbance at 570nm
0.60
0.50
0.40
0.30
0.20
0.10
0.00
Control
DAC
VPA
A549
Error Bars: 95% CI

D

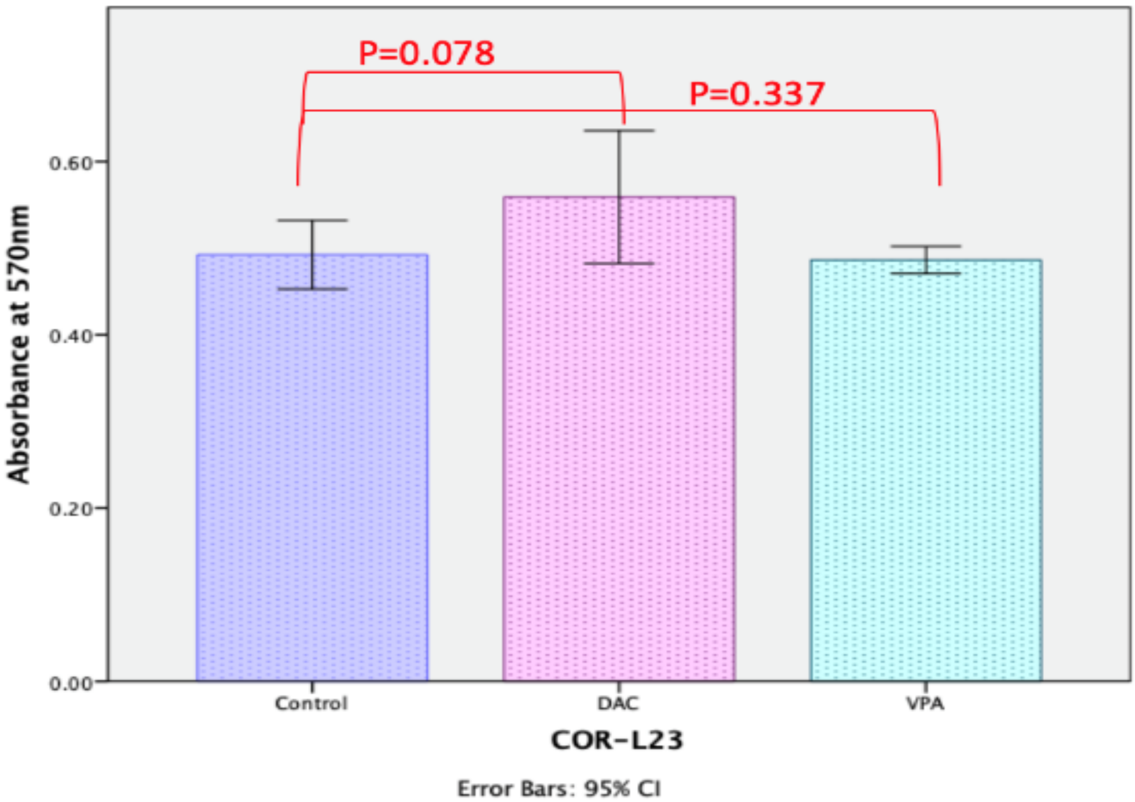
P=0.078
P=0.337
Absorbance at 570nm
0.60
0.40
0.20
0.00
Control
DAC
VPA
COR-L23
Error Bars: 95% CI

E

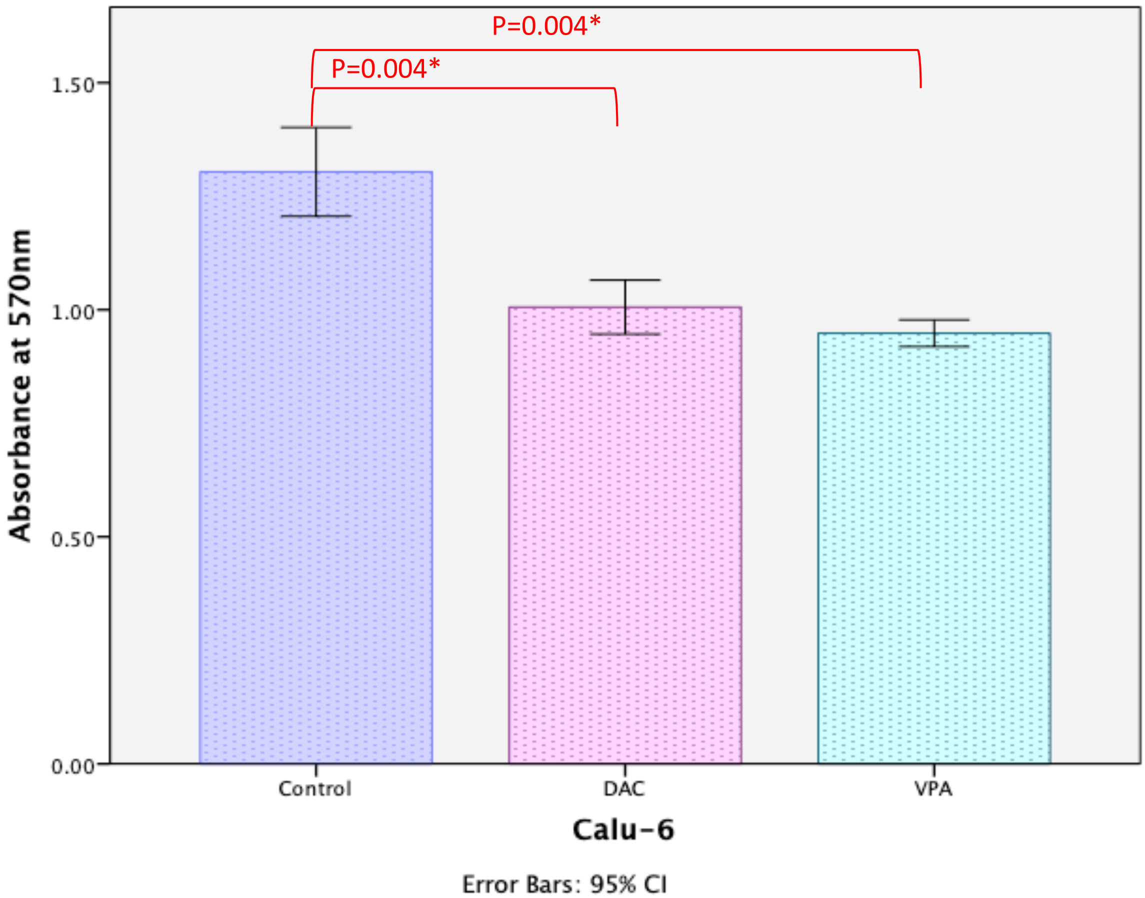

P=0.004*
P=0.004*
1.50
1.00
0.50
0.00
Absorbance at 570nm
Control
DAC
VPA
Calu-6
Error Bars: 95% CI

F

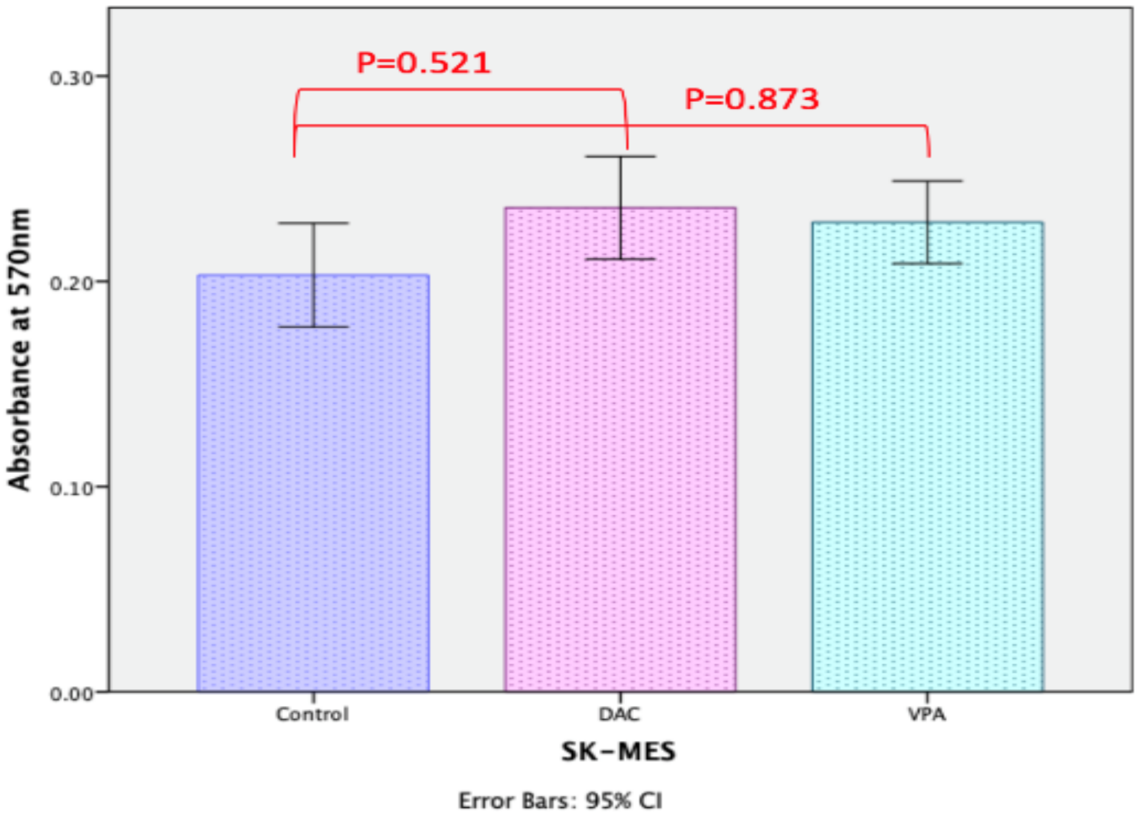

P=0.521
P=0.873
0.30
0.20
0.10
0.00
Absorbance at 570nm
Control
DAC
VPA
SK-MES
Error Bars: 95% CI

Figure 3.2: *Bar charts exhibiting DAC and VPA toxicity NSCLC cell lines.* It displays the MTT absorbance readings for resistant cell lines A: H358, B: SK-LU-1, C: A549, D: COR-L23, E: CALU-6 and F: SK-MES-1 were treated with 1mM VPA and 100nM DAC at 48-hour exposure, in six replicates. Error bars represent 95% confidence intervals. *Indicate the significant differences (Mann Whitney).

3.2.2.2 Apoptotic death induced by DAC and VPA by measuring caspase 3/7 activity

In addition, we measured the apoptotic death induced by DAC and VPA by measuring caspase 3/7 activity (Figure 3.3). DAC did not show a significant increase in the caspase 3/7 activity in A549, H458 and SK-LU-1 while significant reduction in the activity was observed in SK-MES-1 (Mann Whit test). VPA showed a significant decrease in caspase 3/7 activity within A549, SK-LU-1 and SK-MES-1 and a significant increase in the activity within H358.

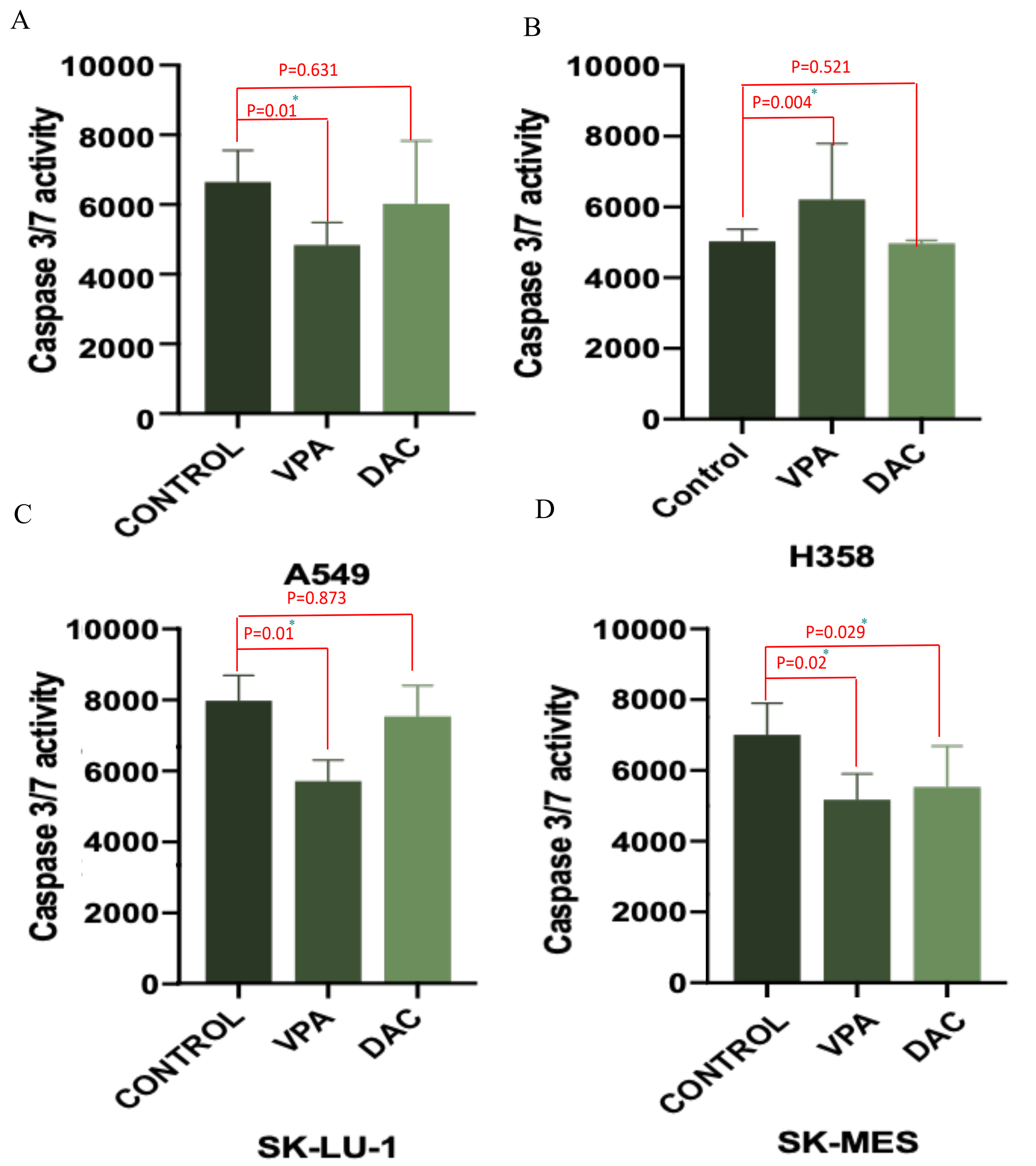

Figure 3.3: *Caspase 3/7 activity assy in NSCLC cell lines treated with DAC and VPA.* The resistant cell lines A: A549, B: H358, C: SK-LU-1 and D: SK-MES-1, were treated with 1mM VPA and 100nM DAC at 48-hour exposure, in six replicates. The caspase 3/7 activity assay used to measure the apoptosis activity. Bar charts represent six technical replicates; the error bars represent 95% confidence intervals. *Indicate the sigificant differences (Mann Whitney).

3.2.2.3 Conditions to sensitizing the NSCLC cell lines by epigenetic drugs

Based on our previous observations, the pre-treatment or synchronous treatment with DAC and VPA may affect the efficiency of each drug differently. As a result of a pilot test (Figure 3.4). The pilot test showed no chang in cell viability when the NSCLC cells treated with either gemcitabine combined with DAC for 48h or when the cells pre-treated with DAC for 48h then gemcitabine added for 48h. While, reduction in cell viability have been noticed when pre-treated with VPA for 48h then gemcitabine was added for the next 48h. It was decided to perform and compare both pre-treatment and synchronous treatment with VPA/DAC for all the cell lines and drugs tested. A final concentration of 100nM DAC and 1mM VPA was used along with the variable doses of GM, VRL, Cis and CARB (Tables 3.2 and 3.7). We also tested whether replenishing VPA and DAC at the time of main drug added had any effect during the pre-treatment experiments, given that after 48 h, the VPA and DAC activity was expected to decrease significantly. However, replenishing VPA and DAC did not demonstrate any difference compared to solely adding the main tested drug (Figure 3.5).

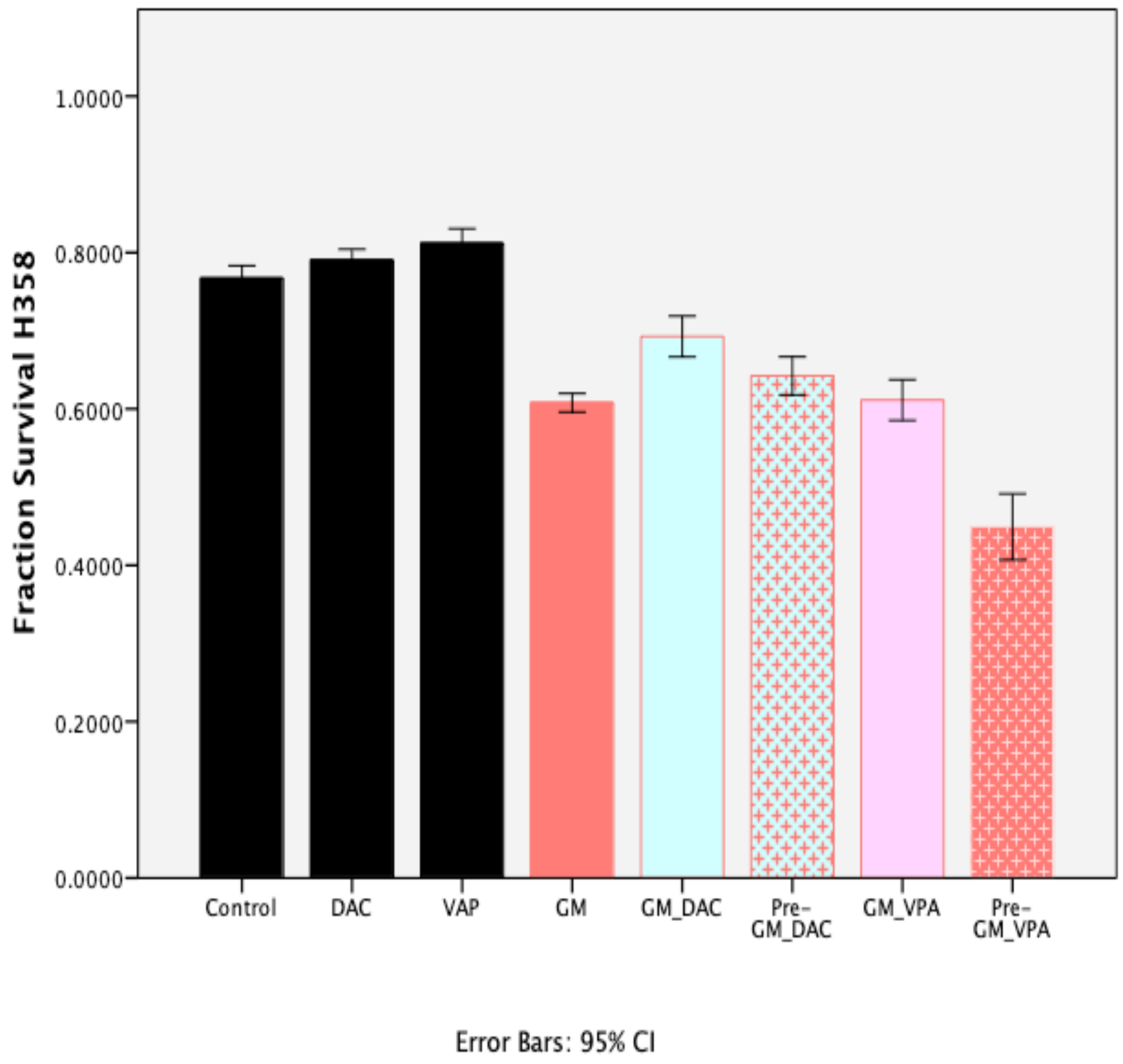

Figure 3.4: *Pilot test for synchronous and pre-treatment for both VPA/DAC combined with GM.* The bar charts present the results of the MTT absorbance readings. H358, one of the resistant NSCLC cell line, was selected to test the effect of combined VPA/DAC to IC50-GM.

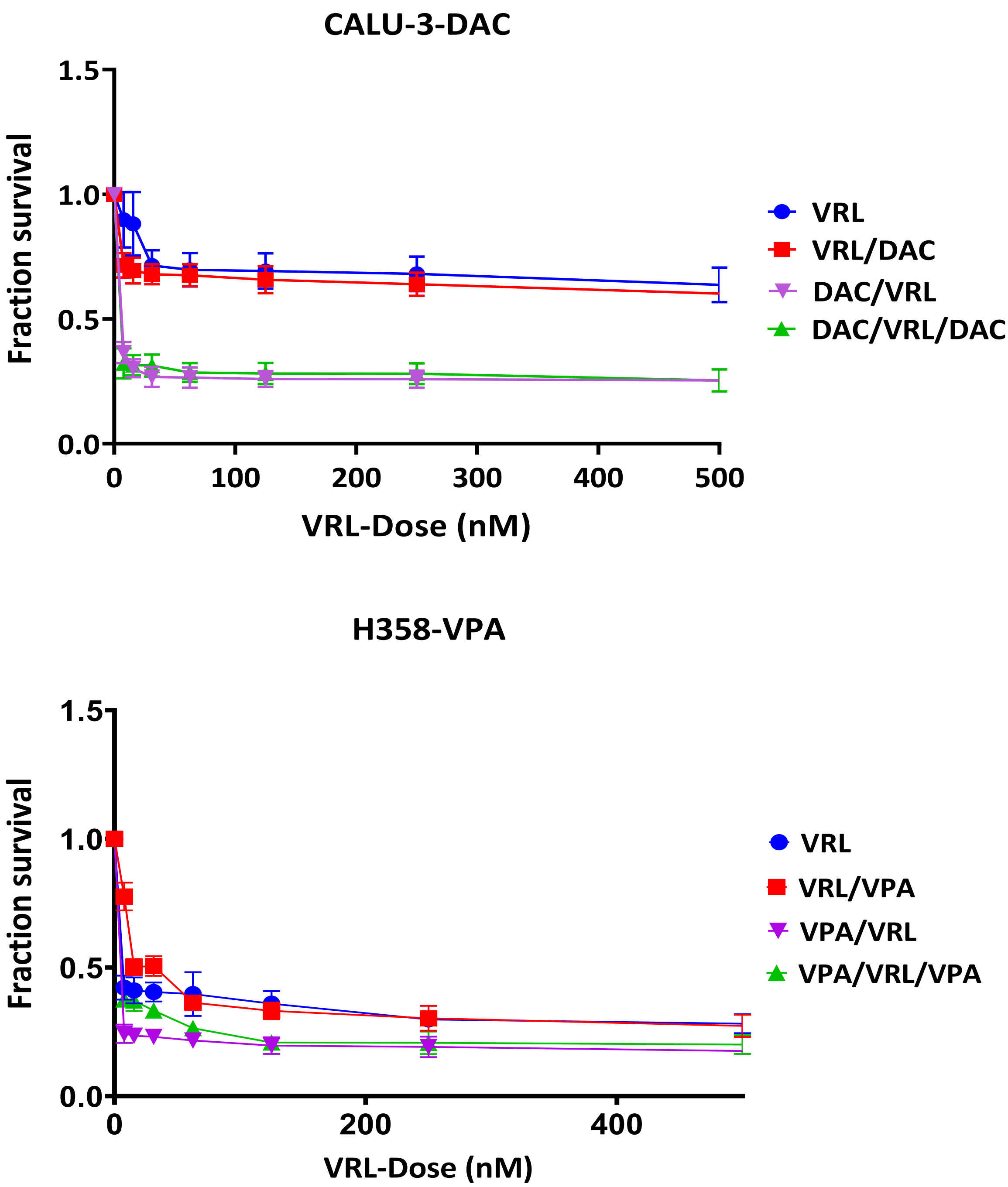

Figure 3.5: *Epigenetic agents (VPA-DAC) combined with VRL.* The Figure display MTT absorbance readings. Blue line: VRL alone 48h and two conditions for combined epigenetic agents with VRL (red line is synchronous and purple and green line pre-treatment). After the pre-treatment with VPA 48h, the cell either exposed to the chemotherapeutic purple line alone 48h or green line chemotherapeutic combine with VPA 48h.

3.2.2.4 Decitabine DAC

Our results (Table 3.2: Figure 3.6) identified that synchronous treatment of DAC with VRL showed a reduction in IC50 values in both SK-LU-1 and A549 cell lines compared to VRL alone. In addition, A549 showed more cell reduction when pre-treated with DAC for 48h than with VRL alone. However, DAC did not sensitize cisplatin, carboplatin, or gemcitabine as shown in (Table 3.2).

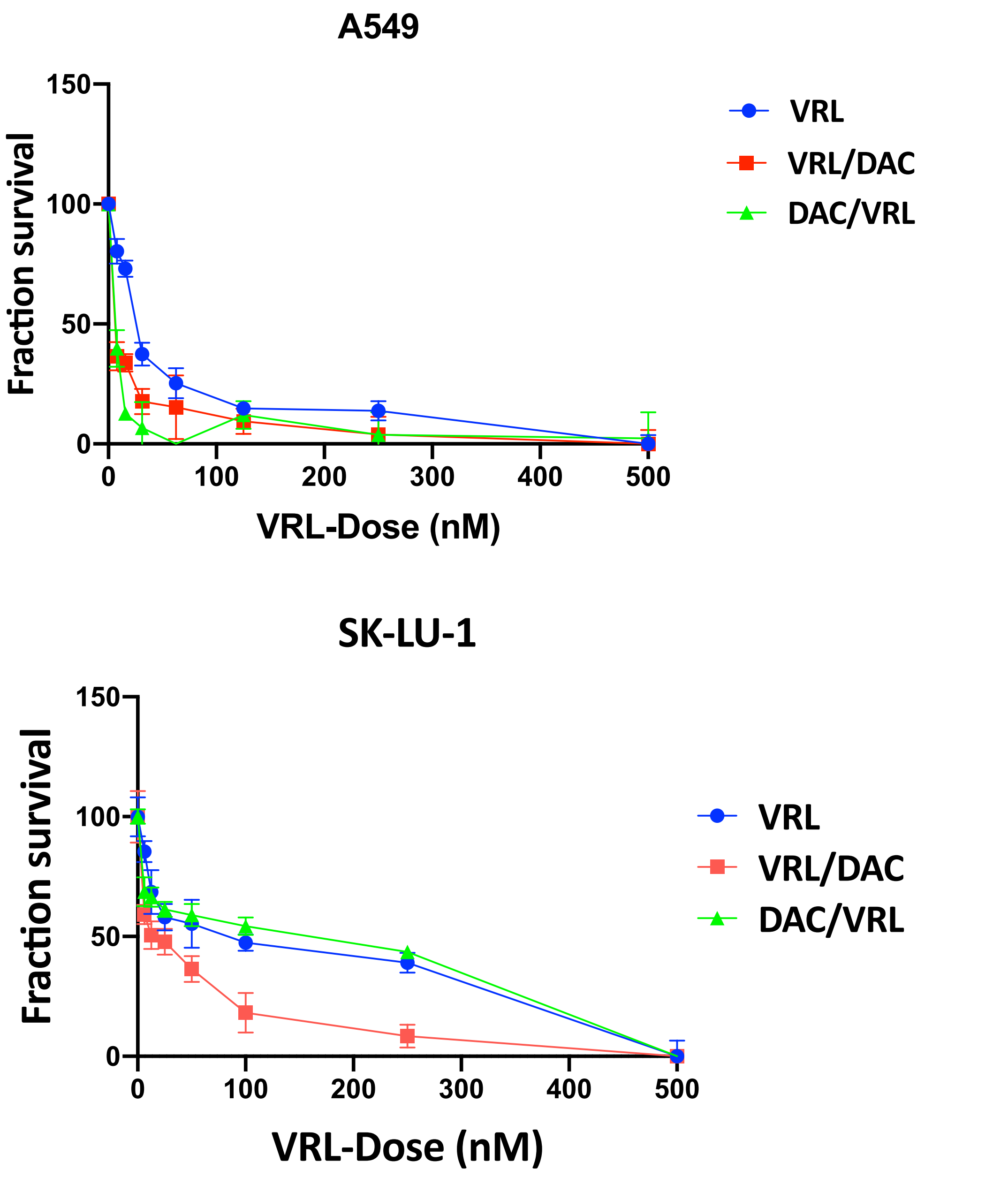

Figure 3.6: *Sensitization of the two most VRL resistant cell lines with DAC*: the graphs represent the response of the MTT absorbance readings of 48h VRL exposure (blue line), synchronous 48h DAC with VRL (red line), and 48h pre-treatment with DAC followed with 48h VRL exposure (green line) in both A549-SK-LU-1 NCSLC cell lines. The mean and error values in all graphs represent six technical replicates, and the error bars represent 95% confidence intervals.

Table 3.2: *Modulation of drug response (IC50 values) following DAC co-treatment.*

Drugs	Cell Lines		Drug alone	Synchronous	Pre-treatment
				Drug + DAC	48h VPA followed with 48h drug
Gemcitabine	CALU-6	IC50 (µM)	0.392	0.525	0.698
		95% CI (µM)	0.118-0.954	0.372-0.758	0.025-1.65
	SK-LU-1	IC50 (µM)	0.319	0.561	1.976
		95% CI (µM)	0.044-0.804	0.07-0.878	0.998-4.885
Vinorelbine	A549	IC50 (nM)	12.260	0.452	0.314
		95% CI(nM)	7.675-17.364	0.249-0.96	0.141-1.396
	SK-LU-1	IC50 (nM)	23.990	19.672	32.542
		95% CI (nM)	11.65-14.286	13.583-29.96	24.985-39.753
Cisplatin	H358	IC50 (µM)	6.903	17.069	12.555
		95% CI (µM)	4.661-12.106	13.946-20.331	8.968-21.0
	SK-LU-1	IC50 (µM)	2.566	8.139	8.864
		95% CI (µM)	1.985-3.217	5.631-9.655	1.745-3.126
Carboplatin	COR-L23	IC50 (µM)	12.400	12.400	22.708
		95% CI (µM)	7.641-19.429	6.98-19.892	21.39-27.543
	SK-MES-1	IC50 (µM)	25.530	25.530	30.943
		95% CI (µM)	18.346-33.9	17.812-30.043	15.627-50.822

3.2.2.5 Sodium valproate VPA

In contrast, our study (Table 3.3) showed significant results in sensitizing platinum with VPA. VPA worked significantly with Cis in all conditions, either synchronous or pre-treated in H358, compared to Cis alone. Synchronous VPA and Cis resulted in a significant reduction cell viability in SK-LU-1 compared to Cis. Moreover, the IC50 reduced and VPA sensitized Carb in both COR-L23 and SK-MES-1. Synchronic treatment reduced COR-L23, while the pre-treatment condition showed more significant reduction in both COR-L23 and SK-MES-1 cell lines compared to Carb alone.

The results revealed a significant reduction in MTT absorption readings and IC50 values when VPA was combined with GM in SK-LU-1 compared to GM alone. However, the pre-treatment of both cell lines (CALU-6, SK-LU-1) with VPA for 48h and exposure to GM for another 48h showed more significant cell reduction.

Pre-treatment of VPA added to VRL 48h showed a reduction with IC50 in SK-LU-1, but more reduction in A549 compared to VRL alone. Additionally, synchronous VPA with VRL showed a IC50 in A549, but more reduction in SK-LU-1 (Figure 3.7).

.

Table 3.3*: Modulation of drug response (IC50 values) following VPA co-treatment.*

Drugs	Cell Lines		Drug alone	Synchronous	Pre-treatment
				Drug+VPA	48h VPA followed with 48h drug
Gemcitabine	CALU-6	IC50 (µM)	0.392	0.334	0.191
		95% CI (µM)	0.267-0.573	0.188-0.581	0.125-0.284
	SK-LU-1	IC50 (µM)	0.319	0.242	0.079
		95% CI (µM)	0.057-1.514	0.0486-0.488	0.027-0.486
Vinorelbine	A549	IC50 (nM)	12.260	8.409	5.158
		95% CI(nM)	9.8-14.795	5.077-10.762	2.119-7.963
	SK-LU-1	IC50 (nM)	23.990	2.904	8.205
		95% CI (nM)	19.582-44.69	0.764-5.603	6.592-9.68
Cisplatin	H358	IC50 (µM)	6.903	0.071	0.051
		95% CI (µM)	3.696-8.836	0.043-0.99	0.024-0.819
	SK-LU-1	IC50 (µM)	2.566	0.891	2.740
		95% CI (µM)	0.85-4.733	0.052-2.576	0.45-4.322
Carboplatin	COR-L23	IC50 (µM)	12.400	1.842	0.969
		95% CI (µM)	7.914-16.321	0.526-3.059	0.171-2.526
	SK-MES-1	IC50 (µM)	25.530	39.563	23.131
		95% CI (µM)	13.479-38.19	27.33-52.313	15.87-27.733

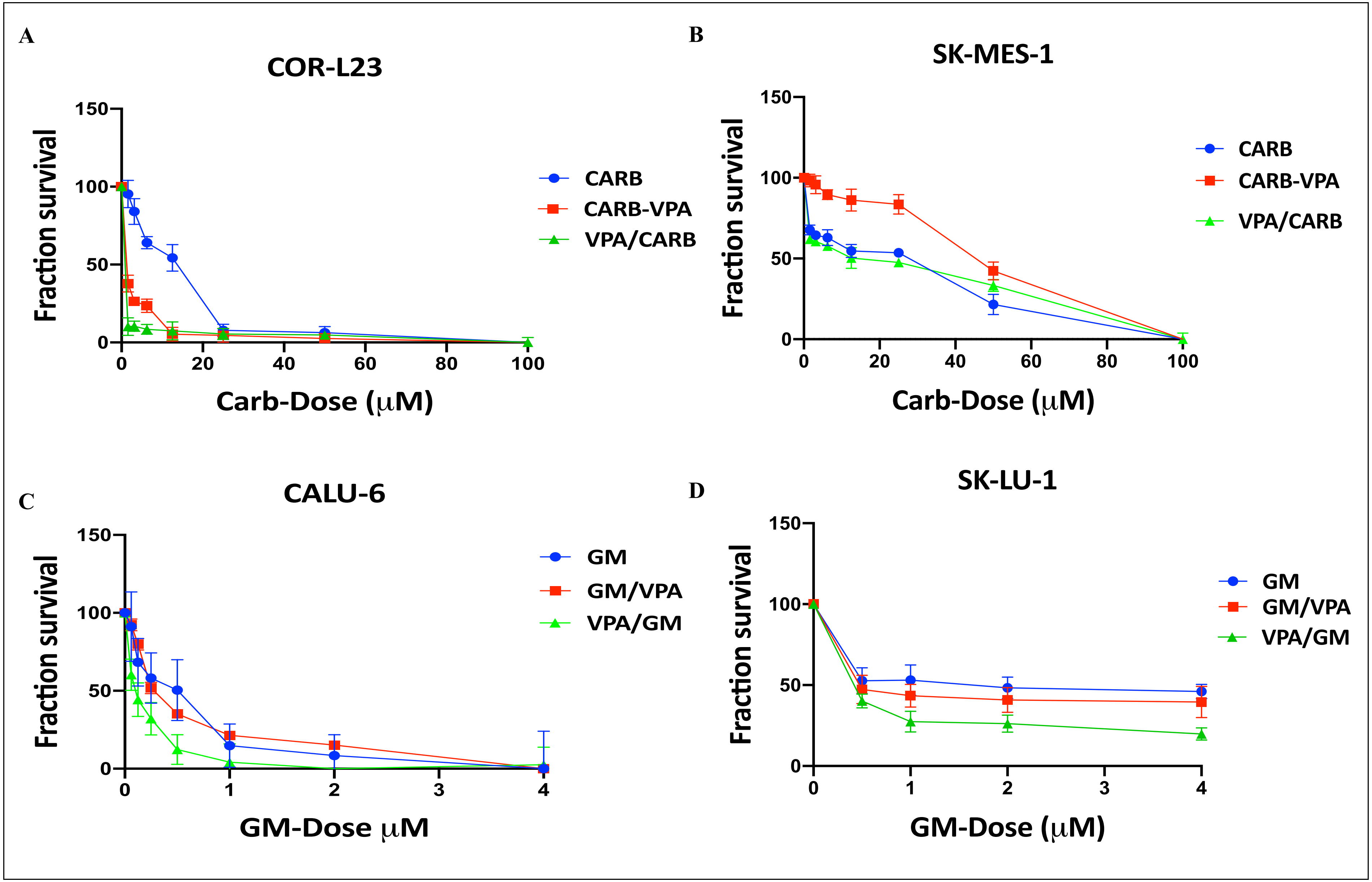
A
COR-L23
Fraction survival
Carb-Dose (μM)
CARB
CARB-VPA
VPA/CARB
B
SK-MES-1
Fraction survival
Carb-Dose (μM)
CARB
CARB-VPA
VPA/CARB
C
CALU-6
Fraction survival
GM-Dose μM
GM
GM/VPA
VPA/GM
D
SK-LU-1
Fraction survival
GM-Dose (μM)
GM
GM/VPA
VPA/GM

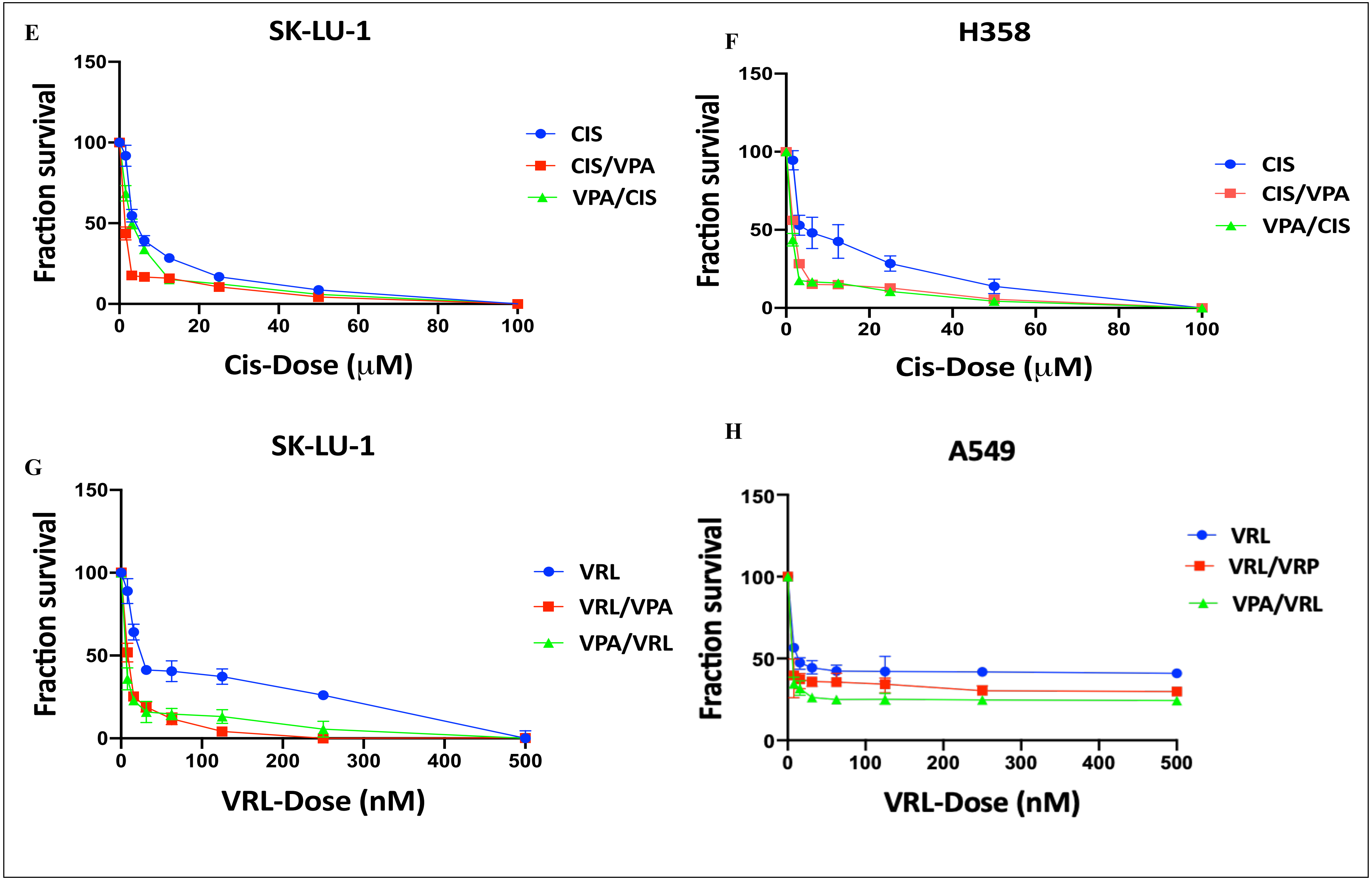
E
SK-LU-1
Fraction survival
150
100
50
0
0
20
40
60
80
100
Cis-Dose (μM)
CIS
CIS/VPA
VPA/CIS
F
H358
Fraction survival
150
100
50
0
0
20
40
60
80
100
Cis-Dose (μM)
CIS
CIS/VPA
VPA/CIS
G
SK-LU-1
Fraction survival
150
100
50
0
0
100
200
300
400
500
VRL-Dose (nM)
VRL
VRL/VPA
VPA/VRL
H
A549
Fraction survival
150
100
50
0
0
100
200
300
400
500
VRL-Dose (nM)
VRL
VRL/VRP
VPA/VRL

Figure 3.7: *The response of sensitizing the two most NSCLC resistance cell lines with VPA:* the graphs represent the result of the MTT absorbance readings: the blue line represents 48h chemo exposure, the red line represents synchronous 48h DAC with chemo, and the green line represents 48h pre-treatment with VPA followed by 48h chemo exposure in the two most resistant cell lines for each drug. A and B represent carboplatin, C and D represent gemcitabine, E and F represent cisplatin and G and H represent vinorelabine. **The X axis is log10,** the mean and error values in all graphs represent the six technical replicates, and the error bars represent 95% confidence intervals.

3.2.3 Caspase-Glo® 3/7 activity assay determines the apoptosis activity

In order to explore the apoptosis activity in the most resistant NSCLC cell lines treated with DAC and VPA in both conditions synchronous and pre-treatment following exposure with four chemotherapies (GM, VRL, Cis, and Carb). Caspase-Glo® 3/7 activity assay has been used (Figure 3.8). The assay was targeted to measure the caspase 3/7 activities, which played an essential role in apoptosis. Therefore, the amount of luminescent signal is associated with the amount of caspase 3/7 activities.

Most of the chemotherapeutic agents showed a significant increase in caspase 3/7 activity in all tested cell lines. Remarkably, carboplatin in SK-MES-1 showed a significant result in synchronous P=0.029 with VPA, while in COR-L23 the results were significant in synchronous P=0.034 with VPA and significant results in both conditions with DAC P=0.01. Moreover, cisplatin showed an increase in 3/7 activity significantly in H358 when pre-treated or synchronous with DAC and only with pre-treatment with VPA with P=0.004, however, synchronous VPA in SK-LU-1 P=0.004 were elevated in 3/7activity. Gemcitabine or vinorelbine in both synchronous and pre-treated with VPA and DAC did not show any caspase 3/7 activity significant result (Mann Whitney).

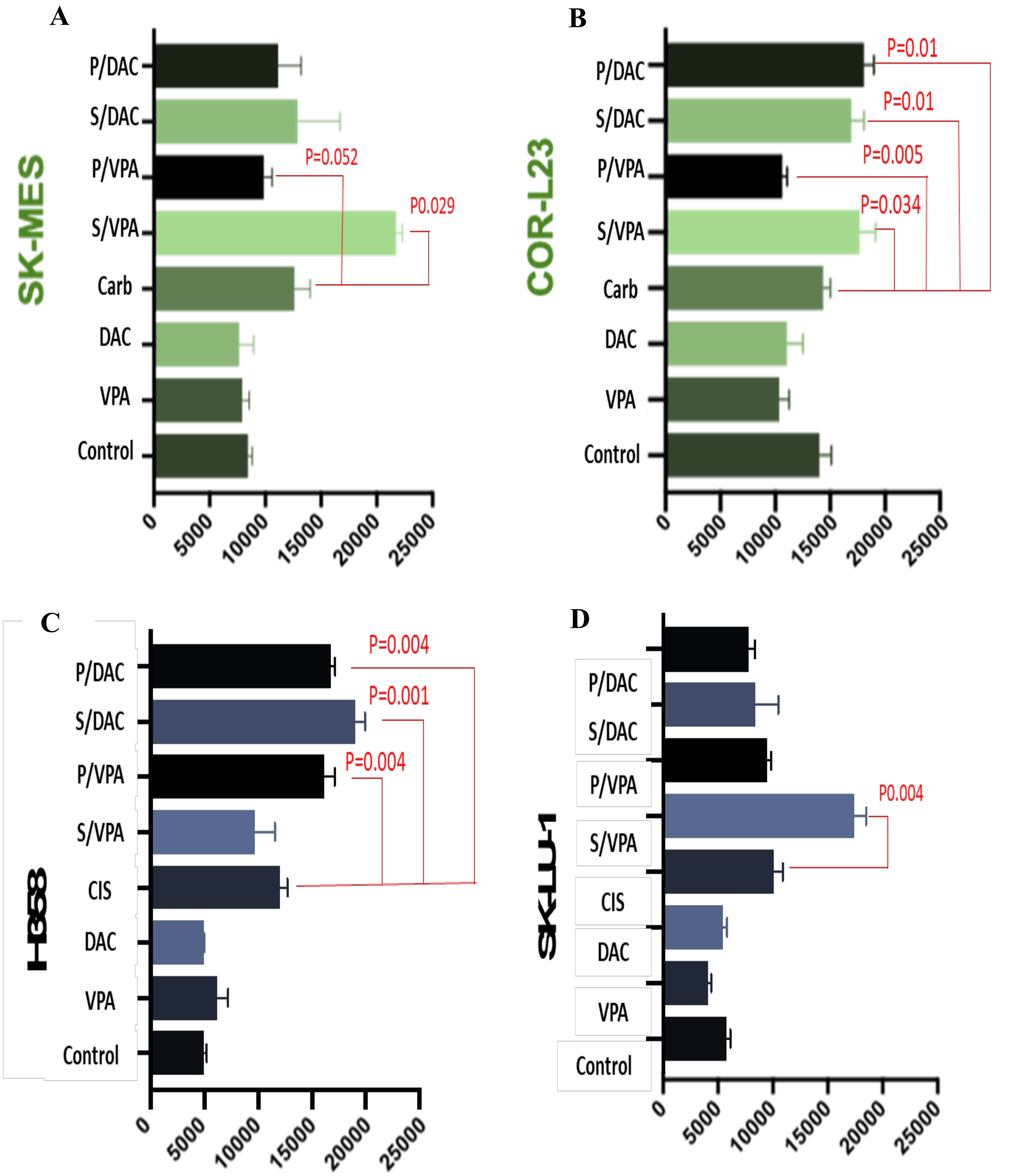

Figure 3.8: *Caspase 3/7 activity in two most resistant NSCLC cell lines treated with platin* (A and B represent carboplatin) (C and D represent cisplatin) agents in the presence/absence of VPA and DAC as synchronous treatment (s) or pre-treatment (p) for 48 hours. (Mann Whitney).

3.2.4 Evaluation of DNA damage

Following the observation of the VPA/DAC effect on the drug efficiency, as seen above (Figure 3.8 and 3.9), we investigated the potential changes that VPA/DAC could confer to DNA damage induced by the chemotherapeutics examined in this study. The neutral comet assay is an established assessment of a fraction of DNA strand breakage by measuring the percentage of DNA in the tail (Figure 3.9). DNA double strand breaks (DSBs) in a single cell leave a tail, which creates the comet shape. Eight NSCLC cell lines treated with drug alone, synchronous VPA and the drug for 48h, and pre-treated 48h with VPA followed by 48h with drug were tested. Only gemcitabine, both alone and with VPA pre-treatment showed increased DNA DSBs in A549, COR-L23 and CALU-6 NSCLC cell lines. Our results showed a significant increase in the percentage of DNA DSBs in A549 P=0.009 CALU-6 P=002, and COR-L23 with p=0.029 when pre-treated with VPA 48h followed by GM 48h, compared to GM alone (Table 3.4, Figure 3.9) (Mann Whitney).

Table 3.4: *Percentage of DNA double strand breaks* in A549, CALU-6 and COR-L23 treated with gemcitabine and pre-treated with VPA followed with gemcitabine

Tail %	A549	CALU-6	COR-L23
GM	16%	23%	31%
Pre-treated with VPA then GM	46%	65%	57%

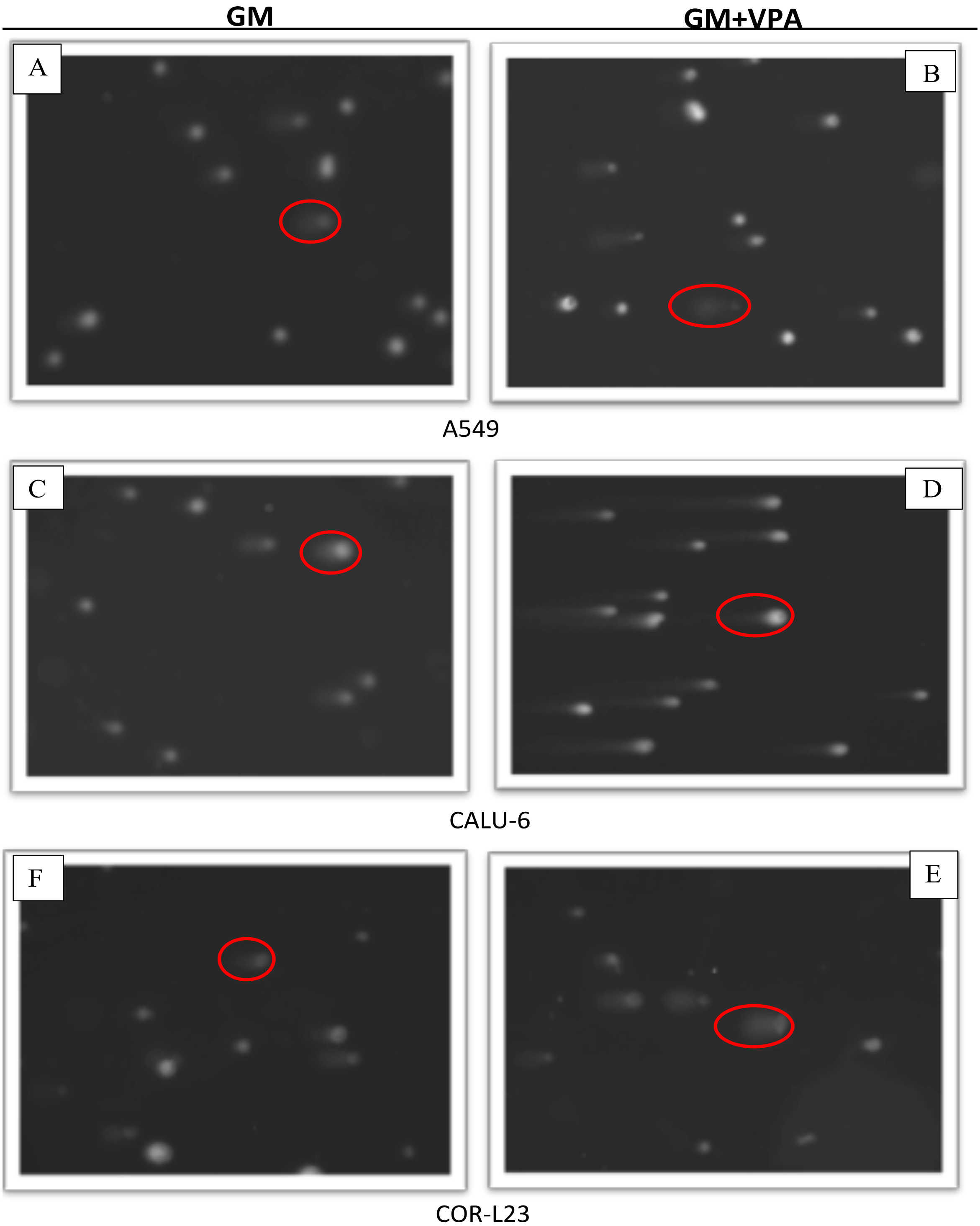

Figure 3.9: The neutral *comet assay for NSCLC cell lines treated with gemcitabine alone or pre-treated with VPA for 48h*: the comet shape present in the NSCLC cells after treatment with gemcitabine for 48h in A-A549, C- CALU-6, and E-COR-L23. Pre-treated VPA for 48h followed by a 48h exposure of the cell with gemcitabine in B-A549, D- CALU-6, and F-COR-L23. The red circles show the difference between the length of the comets.

3.2.5 Other drugs sensitivity NSCLC to the chemotherapeutic agents

3.2.5.1 Fendiline

Fendiline was chosen in this research to re-sensitize chemotherapeutics, based on recent evidence in pancreatic cancer which showed that fendiline inhibits proliferation and invasion (van der Hoeven et al. 2013; Li et al. 2013). The two most resistant cell lines to the four chemotherapies (GM, VRL, Cis, and Carb) were co-treated for 48h with 10nM fendiline (Table 3.5, Figure 3.10). Even though there was a significant reduction in IC50 for SK-LU-1 when treated with fendiline in combination with GM compared to GM alone, however, it did not sensitize CALU-6. The combination also revealed a remarkable decrease in viable cells in SK-MES-1 when treated with fendiline in combination with Carb IC50, compared to IC50 Carb alone, while, without any success when combined with COR-L23. However, the fendiline and Cis combination did not show any reduction in the IC50 in both SK-LU-1 and H358. Also, the fendiline with VRL shows reduction in the IC50 in A549 but not in SK-LU-1.

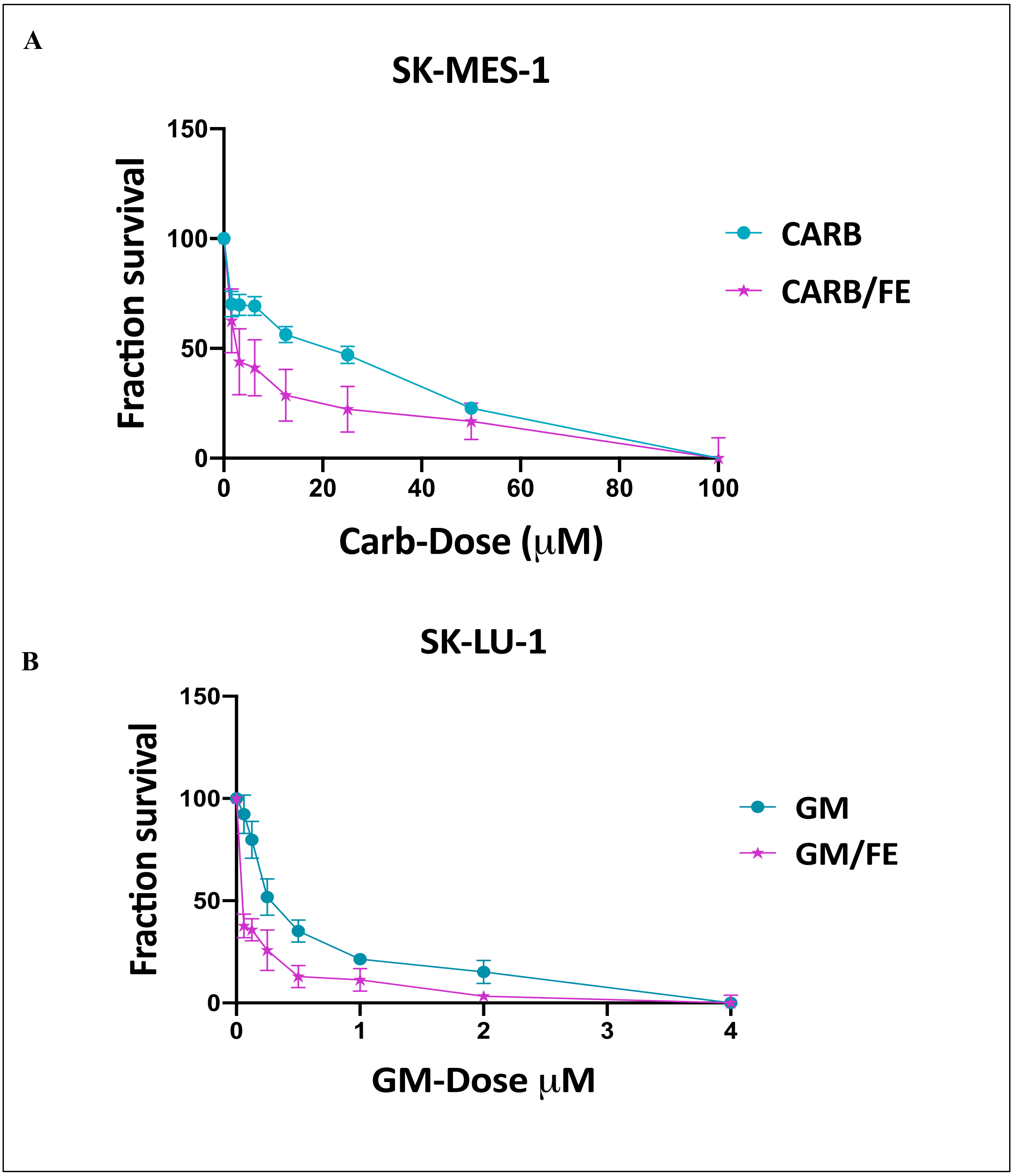

A
SK-MES-1
Fraction survival
150
100
50
0
0
20
40
60
80
100
Carb-Dose (μM)
CARB
CARB/FE
B
SK-LU-1
Fraction survival
150
100
50
0
0
1
2
3
4
GM-Dose μM
GM
GM/FE

C

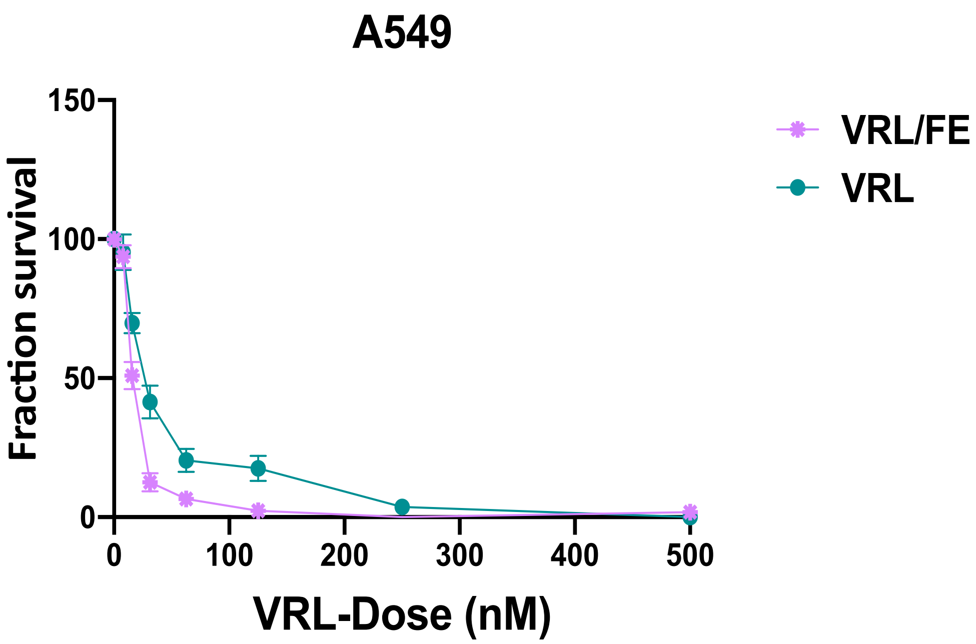

Figure 3.10: *The cell survival rate of NSCLC resistance cell lines treated with fendiline combined with carboplatin or gemcitabine or vinorelbine*: MTT absorbance readings are displayed in the graph. The mean and error values in all graphs are the six technical replicates, and the error bars represent 95% confidence intervals for the NSCLC treated with 48h drug alone (green line) and combined with fendiline for 48h (pink line). A: SK-MES-1 resistance to carboplatin. B: SK-LU-1 resistance to gemcitabine. C: A549 resistance to vinorelbine.

Table 3.5: *IC50 values of sensitizing NSCLC with fendiline*: the IC50 and their respective 95% confidence intervals of the two most resistant cell lines of each drug treated with combined fendiline with one of the four chemotherapies (GM, VRL, Cis, and Carb) for 48h.

Drugs	Cell Lines		Drug	Drug+ Fendiline
Gemcitabine	CALU-6	IC50 (µM)	0.392	0.842
		95% CI (µM)	0.259-0.589	0.466-1.512
	SK-LU-1	IC50 (µM)	0.319	0.079
		95% CI (µM)	0.164-0.497	0.027-0.274
Vinorelbine	SK-LU-1	IC50 (nM)	12.260	21.017
		95% CI (nM)	11.456-13.148	18.272-24.24
	A549	IC50 (nM)	23.990	22.236
		95% CI (nM)	19.915-35.047	14.736-26.178
Cisplatin	SKLU-1	IC50 (µM)	6.903	11.683
		95% CI (µM)	4.612-8.286	6.291-13.757
	H358	IC50 (µM)	2.566	2.587
		95% CI (µM)	1.93-3.341	2.234-2.99
Carboplatin	SK-MES-1	IC50 (µM)	12.400	2.587
		95% CI (µM)	8.87-16.609	0.01-2.139
	COR-L32	IC50 (µM)	25.530	50.996
		95% CI(µM)	16.491-33.325	23.029-57.321

3.2.5.2 Aminomethylphosphonic acid AMPA

Aminomethylphosphonic acid AMPA has been determined to be a proliferation inhibitor and increase the apoptosis activity in pancreatic cancer (Parajuli et al. 2016). MTT assay was used to measure cell viability in the two most resistant NSCLC cell lines, which were treated with IC50 of the compounds (GM, VRL, Cis, and Carb) and 25mM AMPA (Figure 3.11).

AMPA alone had no effect on cell viability in the examined cell lines with the exception of H358; in fact, the results showed significant reduction in viability when AMPA was combined with cisplatin in SK-LU-1 and H358 compared to the cisplatin alone (Figure 3.11). Moreover, the combination of AMPA with Cis showed a significant reduction of viable cells, similar to the IC50 for H358 and SK-LU-1 (4.992μM-12.3μM) compared to the exposure to cisplatin alone (12.5μM-18.18μM).

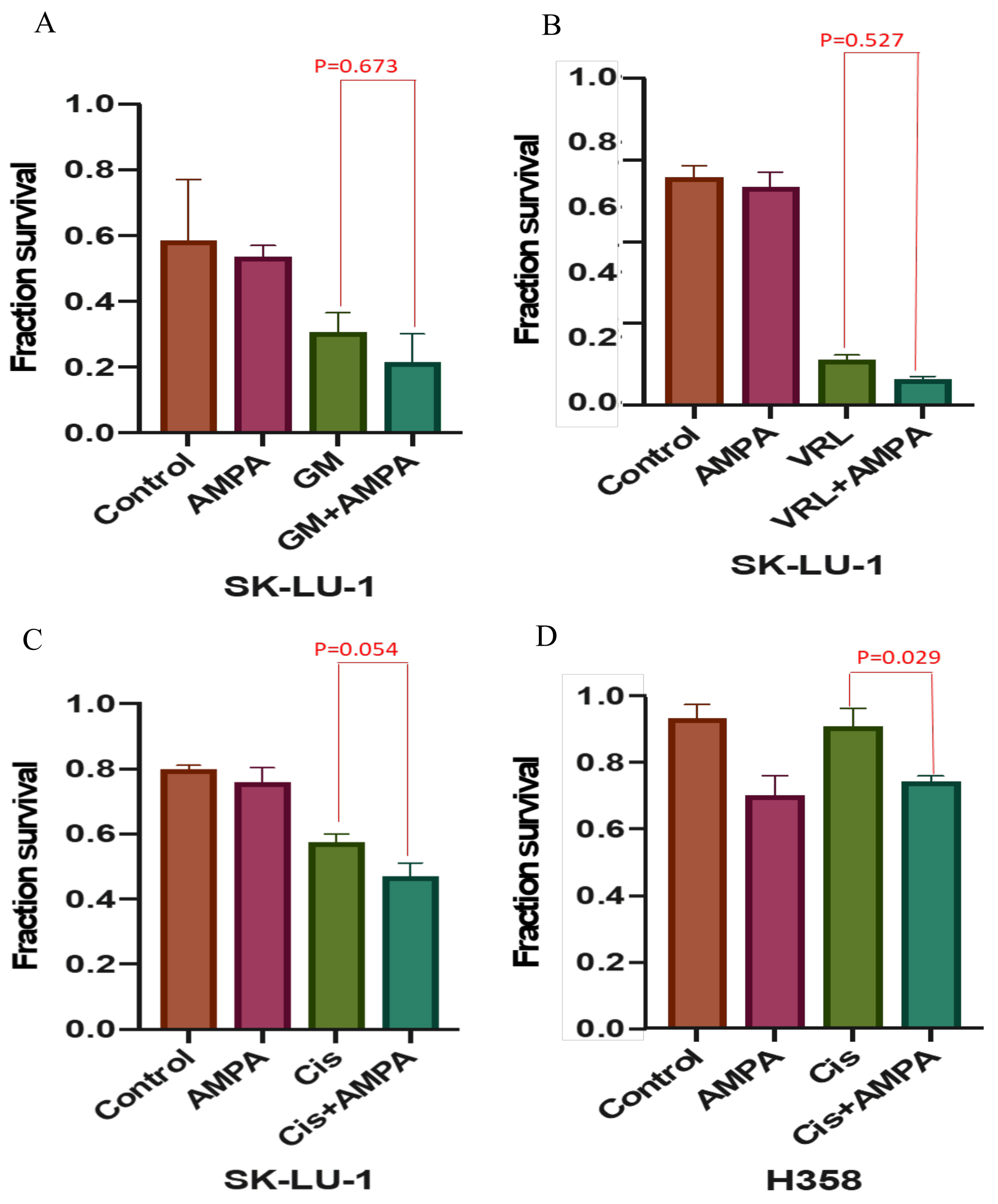

Figure 3.11: *The response of NSCLC resistant cell lines treated with AMPA and chemotherapies*: the bar charts represent the MTT absorbance readings of the resistant NSCLC (SK-LU-1, H358) treated with drug alone for 48h and AMPA combined with one of the chemotherapies (A: gemcitabine, B: vinorelbine, and C&D cisplatin). The mean and error values in all graphs are the six technical replicates, and the error bars represent 95% confidence intervals. (Mann Whitney).

3.3 Discussion

Resistance to chemotherapy is well established to date through multiple preclinical studies and clinical trials. Despite the fact significant research efforts have been allocated to investigate reversing mechanisms of this resistance, the problem still persists (Wangari-Talbot and Hopper-Borge 2013). The chemotherapeutics were chosen in this research are cisplatin, carboplatin, gemcitabine and vinorelbine.

The aim of this part of the project was to re-sensitize NSCLC cell lines against chosen chemotherapies (gemcitabine, vinorelbine, cisplatin, and carboplatin). As expected (Wangari-Talbot and Hopper-Borge 2013), the degree of sensitivity to the different drugs of the examined cell lines varied significantly. The IC50s calculated were different to those found in literature, which are diverse themselves anyway. Besides the difference in laboratory conditions, source, preparation and storage of the chemicals, this is also due to the fact that each lab works with different passages of the cell lines. Nevertheless, it is crucial to highlight that these cell lines have considerably evolved in each lab, depending on the conditions and time grown, therefore, genetic, epigenetic and phenotypic differences are manifested. We selected the two most resistant cell lines for each drug to carry out the downstream sensitization experiments.

In this study, we attempted to sensitize the resistant NSCLC cell lines to GM, VRL, Cis, and Carb by using the epigenetic drugs VPA and DAC. VPA is one of the HDACi, in both synchronous and pre-treatment re-sensitized NSCLC cell lines. The latter was a decision taken based on the reproducible observations that following pre-treatment, keeping the epigenetic drug during chemotherapy treatment did not have a differential effect (example in Figure 3.5).

Significant sensitization of A549 to VRL was observed for both synchronous and pre-treatment with DAC. In contrast, sensitization of SK-LU-1 to VRL was only achieved during the synchronous treatment. This is due to the different genotypes that may give different responses to combined therapy.

In fact, DAC did not deliver any cytotoxicity advantage to any of the remaining drugs tested (GM, Cis, and Carb). DAC shows some clinical activity against metastatic NSCLC in the phase I/II study (Momparler et al. 1997), as well as the loss the pro-apoptotic gene, caspase 8 and expression because the hypermethylation within the neuroblastoma cell lines has been recovered via exposure to decitabine which increases the sensitivity of the chemotherapeutics (Eggert et al. 2001). Moreover, decitabine also recovers the cyclin-dependent kinase inhibitor p21WAF1 (CDKN1A) expression in primary rhabdomyosarcoma tumours which was found to be hypermethylated (Chen et al. 2000).

Published literature (Glasspool et al. 2014; Viet et al. 2014; Momparler et al. 1997) provides a number of examples where DAC shows certain benefits in combination to chemotherapy.

One of the researches points towards the requirement of the design of clinical trials on patients with advanced NSCLC, to focus on understanding the pharmacology of decitabine and its delayed epigenetic action on cancer cells. (Momparler 2013).

Despite the fact that DAC combined with cisplatin showed beneficial results in squamous cell carcinoma of the cervix, the toxicity was significant (Viet et al. 2014; Pohlmann et al. 2002). Combining Cis with DAC increased drug sensitivity in the head and neck squamous cell carcinoma (Viet et al. 2014). However, there are also studies more in line with our results, DAC increased the resistance rather than reversed it when combined with Carb in ovarian cancer (Glasspool et al. 2014). Decitabine has been studied in phase I–II in patients with stage IV NSCLC who survived 81 months (Momparler and Ayoub 2001).

A combined treatment of decitabine with EZH2 inhibitors displayed a synergistic antineoplastic activity on human lung carcinoma cells. The combined drugs have induced signs of senescence and apoptosis, and the combinations increased the expression of several tumour suppressor genes to a greater extent than either agent alone. (Nascimento et al. 2016).

Exposure to epigenetic therapy azacytidine might promote the response of lung tumours to irinotecan. While there is no evidence of enhanced response with epigenetic treated with other chemotherapeutic agents, the effects of epigenetic pre-treatment of NSCLC on response to subsequent chemotherapy appear to be highly context-dependent. (Vendetti et al. 2015).

The novel finding that DAC sensitize s VRL requires further investigation. Moreover, DAC may work by reactivating the transcriptional activity of silenced genes, which may be involved in the chemo resistance pathway, following the aberrant hypermethylation of the promoter at a specific site such as tumor suppressor genes (TSGs) that may benefit re-sensitization to chemotherapy (Schiffmann et al. 2016). To know more about the sensitivity, neither combined decitabine and vinorelbine in both conditions (synchronous and pre-treatment) displayed any significant increase in the caspase 3/7 apoptotic activity, not did the neutral comet assay used here to show any DSB. We suggest future investigations of the mechanism behind sensitivity, using cell cycle flow cytometric analysis with propidium iodide DNA staining to examine the role of combined DAC and VRL in the cell cycle process.

48h VPA pre-treatment sensitize d CALU-6 and SK-LU-1 to gemcitabine, A549, COR-L23, and SK-MES-1 to carboplatin, as well as A549 and SK-LU-1 to vinorelbine and H358 to cisplatin. In contrast, synchronous VPA treatment had an effect on vinorelbine in SK-LU-1 and A549, cisplatin response in SK-LU-1 and carboplatin in COR-L23. To our knowledge, this novel finding demonstrates that VPA can potentially be used for the sensitization of chemotherapies, specifically GM, VRL, Cis, and Carb, in NSCLC. this finding is in accordance with (Hubaux et al. 2010), who determined that VPA has a beneficial effect when used as a first line regimen including Cisplatin plus etoposide in small cell lung cancer (Hubaux et al. 2010). Previous research has provided multiple examples of HDACi anticancer properties when combined with more than 70 combination chemotherapies(Tan et al. 2010; Lane and Chabner 2009). The combination of HDACi with platinum to increase the sensitivity in cancer has also shown interesting results, such as the VPA increased sensitivity to cisplatin in ovarian cancer (Lin et al. 2008) or the GM sensitivity in pancreatic cancer (Ji et al. 2018). Furthermore, HDACi shows a favourable result when combined with cisplatin in gastric cancer (Mutze et al. 2010) as well as with NSCLC (Yamaguchi et al. 2013).

HDACi have multiple biologic effects developing from alterations in patterns of acetylation of histones and various non-histone proteins, which contain proteins complicated in the regulation of gene expression, pathways of extrinsic and intrinsic apoptosis, as well as cell cycle progression (Blackwell et al. 2008). HDACi can induce the death of transformed cells in both proliferative and non-proliferative phases of the cell cycle (Burgess et al. 2004).

Therefore, it can be concluded that the mechanisms of action of HDACi are complex and not completely clear.

HDACi work as microtubule-associated deacetylases and effect acetylation of lysine40 of α-tubulin that cause inhibition of cancer cell growth (Blagosklonny et al. 2002). A previous study conducted by (Yagi et al. 2010) found that VPA has a synergistic effect with PTX microtubule targeting drugs in gastric cancer. Therefore, as shown in this study, synchronous VPA with Vinorelbine (an anti-mitotic) increase sensitivity.

Furthermore, further in vivo pre-clinical studies can be performed by using animals such as zebrafish and mice to analyse the toxicity of the combination and the implication of the drugs.

Following this significant result, we may hypothesize the administration of sodium valproate to the NSCLC patient two days before the chemotherapy, especially patient treated with (platinum or gemcitabine) that may increase the chemosensitivity. As a result, for NSCLC patients who were scheduled to be operated with vinorelbine, the best option is combining VRL with VPA at the same time. Certainly, this hypothesis requires clinical validation in the form of a clinical trial.

Throughout the experiments in this chapter, it has become apparent that concurrent treatment with both VPA and DAC does not have significant advantage. With minor exceptions, VPA has been a much more potent sensitizing compound, therefore making a better candidate for clinical applications. A significant additional factor to this is the differential toxicity of these two compounds, with DAC being severely more toxic to humans than VPA. For example, haematological toxicity (myelosuppression) was observed when DAC was combined with carboplatin in cervical cancer (Stephan and Momparler 2015). In contrast, VPA has been identified as a safe drug to use in treating epilepsy (seizures) and as a mood stabiliser in decays (Detich, Bovenzi, and Szyf 2003). Thus, repurposing this drug for cancer treatment seems much easier. The most recent example is the on-going SAVER trial, led by Prof. R.J. Shaw at the University of Liverpool, which is evaluating the use of VPA to suppress and/or reverse premalignant oral lesions.

Caspases are critical protease mediators of apoptosis triggered by different stimuli. To study the mechanism of epigenetic drugs sensitizing the NSCLC cell lines, we choose the caspase 3/7 activity to examine the influence of VPA and DAC treatment against the apoptosis. This activity was unnoticeable when the NSCLC cell lines were treated with DAC alone in all the tested cell lines, except for SK-MES-1, which manifested a significant increase in the apoptosis activity. Exposure of the NSCLC cell lines to sodium valproate alone determined a substantial decrease in apoptosis activity except in H358 where it shows a considerable increase in caspase 3/7 activity. As expected, chemotherapeutics (cisplatin, carboplatin, gemcitabine and vinorelbine) resulted in a significant increase in the apoptosis activity. A similar trend was recorded when the selected NSCLC cell lines were treated with carboplatin in COR-L23 and cisplatin in H358 combined with decitabine in both synchronous and pre-treated types, while not showing any change when DAC combined with gemcitabine and vinorelbine.

Cisplatin activated caspase-3 activation followed the processing of caspase-9, to produce an inactive p37 form (Checinska et al. 2007). While the mechanism responsible for cisplatin-trigger caspase-3 activation in NSCLC cells is not yet clear, one of the researches has provided evidence that caspase-8 plays a role in starting caspase in this situation in a Fas/FasL-independent manner. They noticed that a minor proportion of caspase-9 was processed into p35 fragment, but it still remained catalytically inactive (Ferreira et al. 2000). Cisplatin is known to enhance apoptosis activity in a p53 dependent manner (Jiang et al. 2004).

Gemcitabine activated the mitochondrial apoptosis pathway downstream of mitochondria without the activation of originator caspases (Pasqualetti et al. 2011).

The noscapine and gemcitabine combination treatment activated initiator caspases, such as caspase-8 (intrinsic pathway) and caspase-9 (extrinsic pathway) followed by the activation of effector caspase-3 (Chougule et al. 2011). Noscapine alone can initiate of apoptosis targeting the mitochondrial pathway through repression of Bcl2 expression and upregulation of proapoptotic genes (Jackson et al. 2008). It has been also shown that a noscapine/ gemcitabine combination treatment leads to stimulation of Bax, BID and p21 genes, inducing apoptosis in lung tumours cells (Chougule et al. 2011).

The combination of metronomic, vinorelbine and endostar significantly increased antitumor activity as compared to the drugs alone, and stimulated apoptosis by down-regulating Bcl-2 expression and up-regulating expression of Bax and caspase 3/7.(Qin et al. 2018). Vinorelbine enhanced apoptosis (Faller and Pandit 2011).

Impaired apoptosis is mutually critical in cancer development and a major difficulty in effective treatment in response to various intracellular damage signals, involving those induced by cancer therapy.

Interestingly, while synchronous treatment with VPA and platin compounds increases apoptosis in all tested cell lines, pre-treatment with VPA resulted in no change for SK-LU-1 and H358 and even showed a drop of this activity in SK-MES-1 and CORL-23 or (Figure 3.8). Apart from further providing further evidence of the fact that different cell lines (i.e. different genotypes) will respond differently to intervention, this may imply that pre-treatment with VPA potentially triggers cell cycle arrest (Kaiser et al. 2006) which stops the cell from recognising the damage and proceeding apoptosis, which in turn may restrict its apoptosis potential. Apparently, apoptosis naturally removes most cells whose cell cycle control is disturbed by oncogenic mutations (Adams and Cory 2007). In contrast, synchronous treatment increases chemotherapy-induced apoptosis by re-activating pro-apoptotic gene expression as has been previously shown (Zhang et al. 2012).

In this study, the epigenetic pre-treatment followed by the four chemotherapeutic agents (gemcitabine, vinorelbine, cisplatin and carboplatin) is suggested due to its capacity to put cells in an alternative condition by deacetylation and increase the expression of important genes that play a role in the pathways of extrinsic and intrinsic apoptosis and cell cycle progression (Blackwell et al. 2008). Research shows that the HDAC inhibitor can increase the chemosensitivity of lung cancer to cisplatin (Diyabalanage, Granda, and Hooker 2013) and has an anti-proliferation effect through cell cycle regulation and apoptosis.

The effect of VPA on increased chemotherapy-induced apoptosis of NSCLC cells triggered a question whether this was mediated by increased DNA damage. It was fully appreciated at this point that some of this chemotherapeutics alone induce DNA damage. It was also appreciated that the neutral comet assay used here assesses DSBs and would not provide information on accumulation of single strand breaks (SSBs) or DNA adducts.

Gemcitabine lead to profound DNA damage in three out of eight NSCLC cell lines tested, showing evidence of DNA strand breaks. Gemcitabine (GM) is a well-known anti-neoplastic drug that can stop cell division. It is a replication inhibitor used to treat cancers with mutations in homologous recombination HR genes such as BRCA2. GM causes replication fork stalling and double-strand breaks (DSB) that result from the processing of stalled forks. The homologous recombination (HR) factor RAD51 mediates fork restart and DSB repair during recovery from replication blocks. Moreover, HR defects may lead to sensitize cells to replication inhibitors such as GM (Jones et al. 2014). Previous evidence on GM-induced DSBs also comes from a Phase I trial on uveal melanoma (Corrie et al. 2005).

Of importance is the observation that VPA pre-treatment significantly enhanced the presence of DSBs. The most probable explanation is that VPA alters the expression of genes that influence GM-induced DSBs, however, future work is required to identify those genes that may mediate this effect and prove the above hypothesis.

Fendiline is an anti-arrhythmic, antianginal agent and a coronary vasodilator which works by inhibiting the calcium channel function in muscle cells on the excitation-contraction coupling. Calcium is a ubiquitous cellular signal, which is vital in cancer. The changed expression of specific calcium channels and calcium binding proteins are distinguishing features of lung cancer, which control the cell signalling pathway leading to cell proliferation or apoptosis. Chemoresistance is common in lung cancer. Changed endoplasmic reticulum calcium homeostasis of lung cancer cells is associated with drug resistance (Yang et al. 2010). Calcium signalling can reverse epigenetic silencing of tumor suppressor genes (Raynal et al. 2016).

Our results showed an original finding that fendiline causes a significant reduction in cell viability when combined with GM in SK-LU-1, but not in CALU-6. Furthermore, significant reduction in cell viability occurred in SK-MES-1 when fendiline was combined with carboplatin, though this did not work with COR-L23. However, fendiline combined with cisplatin did not work with SK-LU-1 and H358.

Gemcitabine, vinorelbine, and carboplatin sensitization in NSCLC cells found in this study has not previously been reported. Fendiline showed a significant effect in reducing proliferation of pancreatic cancer when combined with gemcitabine (Woods et al. 2015). Moreover, the mechanism of fendiline in prostatic cancer showed that fendiline induces intra cellular Ca^{+2} release and external Ca^{+2} entry. A long period of Ca^{+2} increase inside the cell may lead to cell injury and death (Jan et al. 2001). Furthermore, Van der Hoeven *et al*. (2013) provided a novel report in which fendiline blocked the proliferation of lung and other cancers through present oncogenic mutant K-Ras (van der Hoeven et al. 2013).

It has been suggested (van der Hoeven et al. 2013; Woods et al. 2015; Jan et al. 2001) that using fendiline as an anti-cancer agent combining with chemotherapeutics in several researches. Fendiline has advantage in protecting the cardiomyocytes from cell death to avoid cardiotoxicity; while treated with agents, no untoward side effects have been observed even at high dosage levels. As showed in the results, combined fendiline with GM, VRL, Carb increases NSCLC sensitivity. Fendiline can reduce the clinical application of the chemotherapeutics by reducing the dose of agents required to achieve high efficiency.

It has been approved that fendiline treatment induces G1 arrest in pancreatic cancer cells. Treating pancreatic cells (PDAC) with fendiline for 24h shows an accumulation of the cells in the G1 phase and cells reduction in S and G2 phase, meaning that fendiline arrest the cell cycle in G1 phase which stops the proliferation. As a result, combined fendiline with Gemcitabine which works in S/G2 and vinorelbine work in G2/M may increase the drug productivity (Woods et al. 2015).

To move the combination therapy of fendiline with chemotherapeutics from the bench to the bedside, many preclinical studies are needed to be designed to yield preliminary efficacy, toxicity, pharmacokinetics, and safety information. Different doses of the drug are tested using in vitro (test tube or cell culture) as in pancreatic cells mentioned before and in vivo (animal, e.g. zebrafish and mice) experiments which required as a next step, and it is also possible to perform in silico profiling using computer models of the drug-target interactions. AMPA arrested cancer cells in G1/G0, blocked their entry to S phase, and promoted apoptosis, upregulating p53, p21, and procaspase 9 (Li et al. 2013). AMPA can phosphorylate CAMP, which is responsible for increased cell cycle regulators, while tumour suppressor genes proteins lead to decreased ADC cells in the G2 and S phases (Stepulak et al. 2007). Moreover, AMPA is safe and does not reduce cell proliferation in any NSCLC resistant cell lines, except for H358. Our results showed a significant reduction in viable cells in SK-LU-1 and H358 when AMPA was combined with cisplatin. The combined effect of AMPA with drugs revealed an additive effect, which does not indicate any synergetic affect (figure 3.11).

3.4 Conclusion

After having identified the IC50 of the selected chemotherapeutics (cisplatin, carboplatin, gemcitabine and vinorelbine) in eight NSCLC cell lines. The epigenetic drugs VPA and DAC have no cytotoxicity on selected NSCLC, as well as showing a reduction in the 3/7 activity in NSCLC cell lines, while DAC did not have any effect in apoptotic activity. Then, we combined them with selected chemotherapeutics in two different conditions, pre-treatment and synchronous, based on the results of the pilot test.

To sum up, this study has determined a potential synergetic interaction between VPA and the four chemotherapies, namely gemcitabine, vinorelbine, cisplatin, and carboplatin, as well as decitabine sensitize d vinorelbine. Fendiline has a potential benefit with gemcitabine and vinorelbine.

Moreover, this study has determined that the mechanism behind sensitization of the NSCLC cell lines with epigenetic agents VPA and DAC is increasing apoptosis though enhanced caspase 3/7 activity. Additionally, it has indicated that gemcitabine causes DNA double strand break induction, although more research is required to identify the mechanism through which this is achieved.

Chapter 4: Impact of LANCL1 and LANCL1-AS1 in Drug Resistance

4.1 Introduction

Antisense *LANCL1-AS1* lncRNA was chosen from the array results (Acha-Sagredo et al. 2020). To my knowledge, there is not currently any published research about *LANCL1-AS1* presuming a role in cancer, especially lung cancer. Following the observation of extensive *LANCL1-AS1* loss of expression in NSCLC specimens, we aimed to investigate the potential functional significance of this loss in the disease, including tumour phenotype and drug resistance. In this effort, we chose to examine the expression and function of the coding counterpart gene, *LANCL1*. Therefore, the *LANCL1* gene was chosen to study whether *LANCL1-AS1* plays any role in regulating *LANCL1* and to elucidate its role in NSCLC cells. Given the previous evidence on the latter influencing oxidative stress in cells (Zhong et al. 2012), this became one of the central points of focus. This chapter determines the experimental work conducted in human lung tissue samples (table 8.1) and NSCNC cell lines to specify in detail *LANCL1* and *LANCL1-AS1* in NSCLC.

Given the virtually complete lack of information for LANCL1 and LANCL1-AS1 in lung cancer, we set a number of interesting research questions:

a) Do the mRNA expression levels of *LANCL1* and *LANCL1-AS1* correlate in lung tissues and cell lines?

b) Are the reported splicing variants present in lung tissues and cell lines?

c) Is expression of *LANCL1* and *LANCL1-AS1* epigenetically regulated?

d) Is LANCL1 protein consistent with the mRNA expression profile?

e) Is expression of *LANCL1* and *LANCL1-AS1* regulated by oxidative stress in lung cancer cells?

f) Does expression of LANCL1 and LANCL1-AS1 affect the sensitivity of NSCLC cells to cisplatin, carboplatin, VRL and Gemcitabine?

In order to provide answers to those questions, we exogenously knocked down *LANCL1* by using shRNA in lung cancer cells and examined the phenotypic responses, including drug sensitivity. Finally, we overexpressed the *LANCL1-AS1* gene, which is completely knocked out in all lung cancer cell lines and investigated the phenotypic changes.

4.2 Results

4.2.1 Expression of *LANCL1* and *LANCL1-AS1* in human lung cancer tissues

RNA from primary NSCLC cancer tissues had already been prepared by the lung group for the lncRNA study (Acha-Sagredo et al. 2020), therefore I investigated the mRNA expression of LANCL1 in 67 lung tumours and paired adjacent normal tissues (Table 8.1), for which *LANCL1-AS1* expression data was already available (Acha-Sagredo et al. 2020). *LANCL1-AS1* is highly expressed in normal tissue with and diminished in tumour paired tissue (Wilcoxon test, P=0.021) (Acha-Sagredo et al. 2020). The mRNA expression level of *LANCL1* was only moderately higher in tumour samples as compared with in paired adjacent normal tissues, a difference which was not significant (Figure 4.1) (Wilcoxon test, P=0.191).

When tested for bivariate correlation, *LANCL1* and *LANCL1-AS1* values did not correlate, either in normal (Spearman correlation, rho=0.003, P=0.981) or tumour tissues (Spearman correlation, rho=0.061, P=0.621). Moreover, the expression of both *LANCL1* and *LANCL1-AS1* did not difference among pathological groups such as histology, pT status and pN status (Kruskal-Wallis test, P=0.1; Figure 4.2).

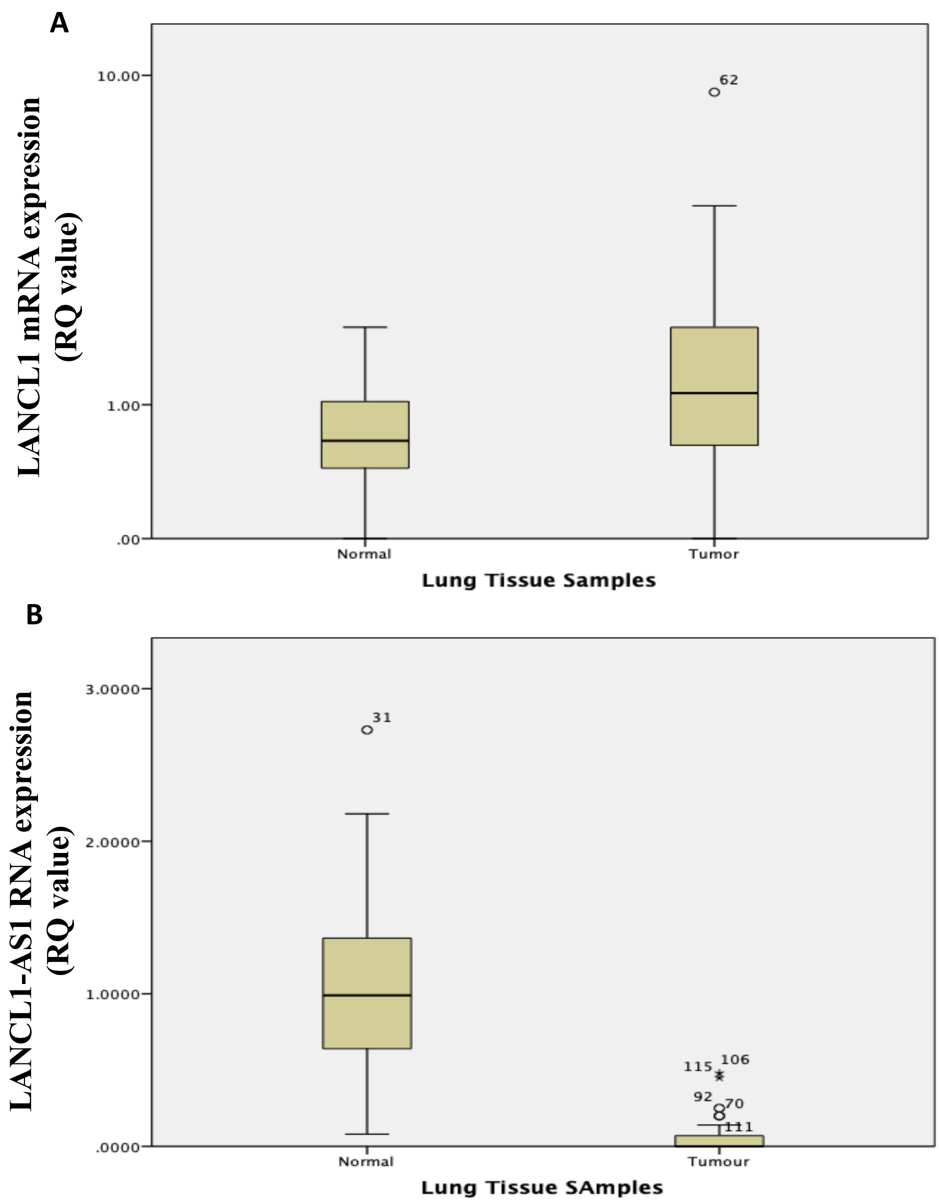

Figure 4.1: *Boxplot representation of expression of both LANCL1 and LANCL1-AS1 in lung tissue samples*. **(A)** *LANCL1* expression is not significantly different in tumour tissues compared to adjacent normal; in contrast, **(B)** *LANCL1-AS1* is highly expressed in normal paired tissue with and diminished in tumour tissue.

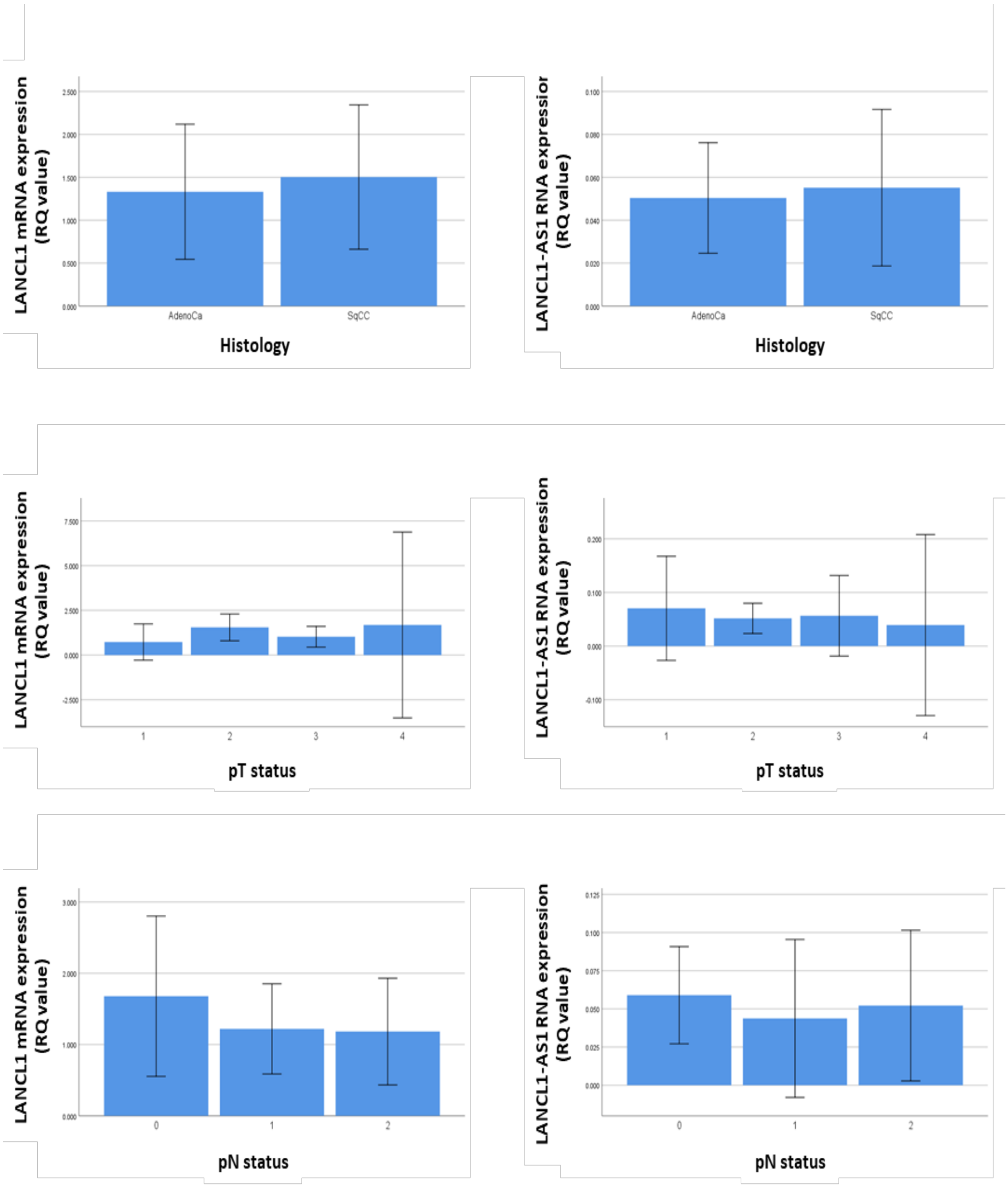

Figure 4.2: *Bar charts demonstrating the expression of LANCL1 and LANCL1-AS1 amongdifferent pathological groups in this study*. AdenoCa: adenocarcinoma, SqCC: squamous cell carcinoma, pT: pathological T status (tumour size), pN: pathological nodal status (0= no involved nodes, 1= proximal nodes, 2= distal nodes). Error pars represent 95% confidence intervals.

4.2.2 Expression of *LANCL1* and *LANCL1-AS1* in NSCLC cell lines

Further investigation of mRNA expression for both *LANCL1* and *LANCL1-AS1* in eight NSCLC cell lines from different histological origins (A549, CALU-3, CALU-6, COR-L23, H348, LUDLU, SK-MES-1, and SK-LU-1) was undertaken by RT-qPCR. *LANCL1* was variably expressed in NSCLC cell lines (Figure 4.3). In contrast, *LANCL1-AS1* was either completely undetectable or detected after the 50th cycle in qPCR.

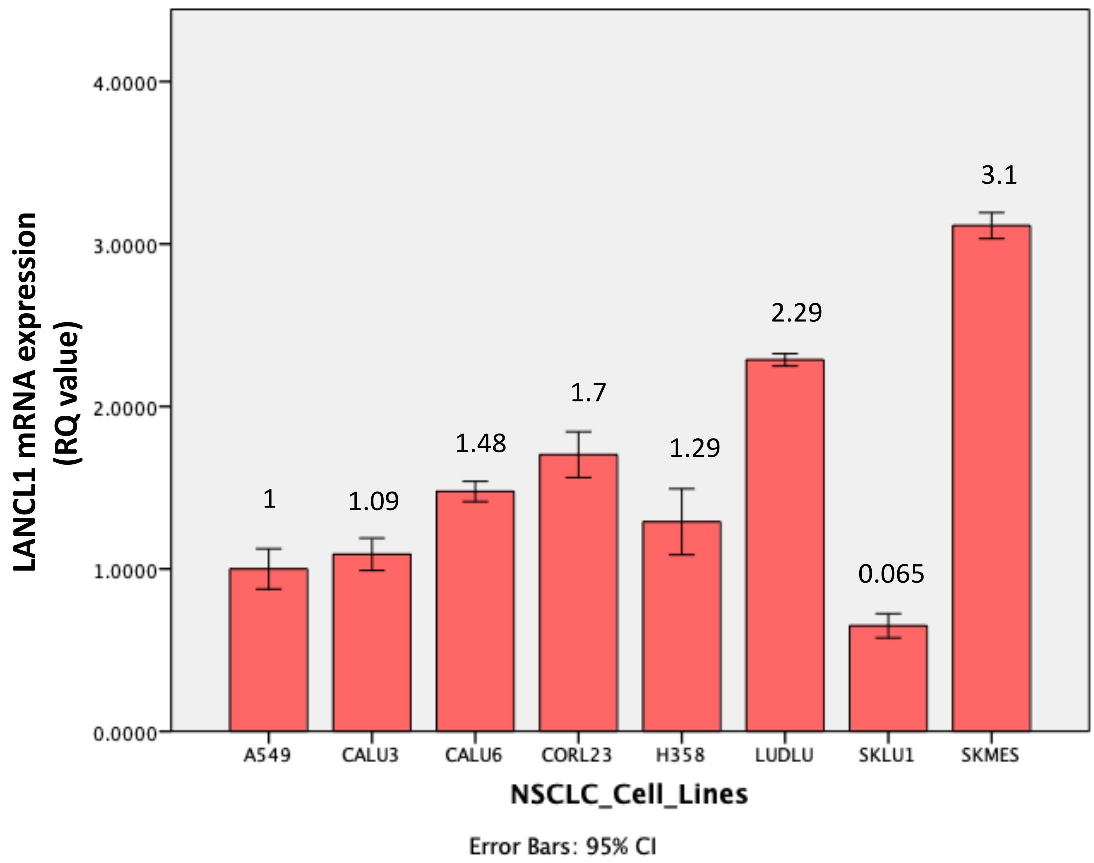

Figure 4.3: *Bar charts exhibiting the mRNA expression of LANCL1 in NSCLC cell lines.* SKMES-1 represent the highest expression while, SK-LU-1 represent the lowest. The mean and error values in all graphs are the triple technical replicates, while the error bars represent 95% confidence intervals. The RQ calibrator is A549.

Western blotting was used to determine and confirm protein expression for *LANCL1* in the eight NSCLC cell lines (Figure 4.4). However, the result was not satisfactory as the antibody showed two faint bands with a very high background signal.

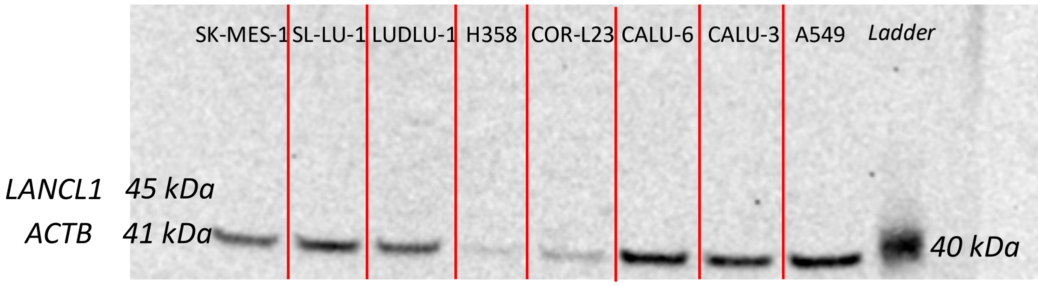

Figure 4.4*: LANCL1 protein expression levels quantified by western blot analysis.* A549 was used as a calibrator (value=1). Band quantitation was undertaken by synGENE. ACTB was used as a loading control Protein Ladder, 10 to 180 kDa.

4.2.3 Splicing variant expression of *LANCL1* in NSCLC

LANCL1 has 6 transcript splice variants; variants 1, 2, 3 and 5 are coding transcripts. Variants 1, 2 & 3 have large size (V1=4270bp, V2=4461 and V3=1385bp) and have been chosen to complete the investigation (Figure 4.5). Variant 5 is a very short (570bp) transcript coding for an incomplete peptide of unknown function, so it was not considered for this study.

Variant 1

cctggcagGAACTGGGCGGTAAAATAGCCCTTCTGTTACTGTCCGGGGCTGCGGGGTGAGAGGCCAGGGCCGAGAAGGGCTTCAGGACGCGGGAGGCGCAC

TTGCTTCAAGTCGCGGGCGTGGGAACGGGGTTGCAAAACGGGGCCTCTTTGTCCGG---

GCTTGCTTCCGGCGTCATGGCTCAAAGGGCCTTCCCGAATCCTTATGCTGATTATAACAAATCCCTGGCCGAAGGCTACTTTGATGCTGCCGGGAGG

Variant 2

cctggcaggaactgggcggtaaaatagcccttctgttactgtccggggctgcggggtgagaggccagggccGAGAAGGGCTTCAGGACGCGGGAGGCGCACTTGCTTCAAGTCGCG

GGCGTGGGAACGGGgttgcaaaacggggcctctttgtccgg---

GCTTGCTTCCGGCGTCATGGCTCAAAGGGCCTTCCCGAATCCTTATGCTGATTATAACAAATCCCTGGCCGAAGGCTACTTTGATGCTGCCGGGAGG

Variant 3

CCTGGCAGGAACTGGGCGGTAAAATAGCCCTTCTGTTACTGTCCGGGGCTGCGGGgtgagaggccagggccgagaagggcttcaggacgcgggaggcgcacttgcttcaagtc

gcgggcgtgggaacggggttgcaaaacggggcctctttgtccgg---

GCTTGCTTCCGGCGTCATGGCTCAAAGGGCCTTCCCGAATCCTTATGCTGATTATAACAAATCCCTGGCCGAAGGCTACTTTGATGCTGCCGGGAGG

Figure 4.5: *Nucleotide sequence demonstrating the differences in exon 1 of the reported LANCL1 transcript variants in Genebank database*. Purple, red and green letters designate exon 1 for variant 1, 2 and 3 respectively. Blue letters denote the common exon 2. Small case letters denote promoter/intron sequences that are not part of the mature transcripts. The highlighted sequences show the location of primers used. One set of primers amplifies both variants 1 and 2, while the other set amplifies only variant 3.

Two assays were designed to amplify the three *LANCL1* transcript variants. The agarose gel electrophoresis analysis of all the samples derived from primary tissues (not showing) and cell lines (Figure 4.6) revealed the presence of V1 and V3, but not V2. No major differences in the variant signals on the gel were detected between normal and tumour tissue to trigger further investigation with a quantitative method such as qPCR.

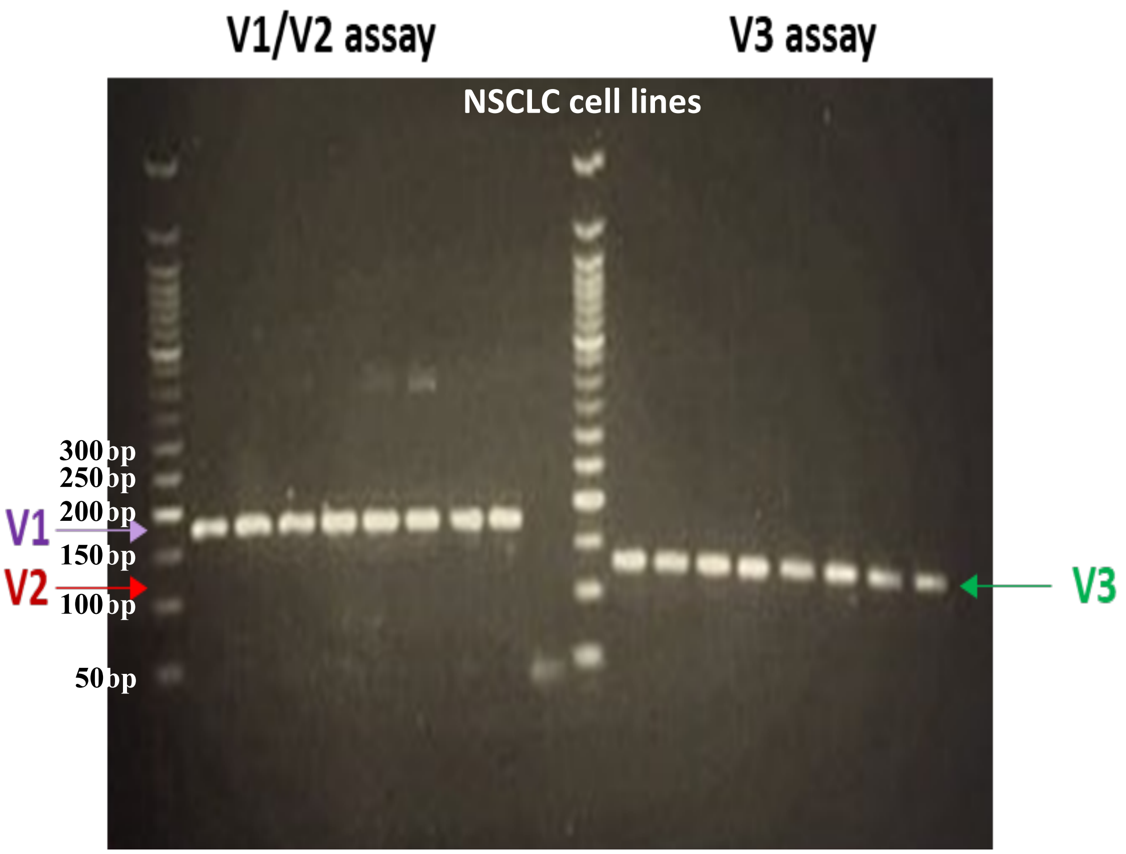

Figure 4.6: *Agarose gel (2% agarose in TBE) electrophoresis of PCR products from LANCL1 transcript variants in NSCLC cell lines*. Variant V1 (173 bp) and variant V3 (145 bp) can be seen in all samples tested, while variant V2 was not detected in any of the samples. The size standard used in this gel is 50 bp ladder.

4.2.4 Methylation state of *LANCL1* in tumour and normal lung samples

The bioinformatic analysis (EMBOSS CpG plot) revealed the presence of a CpG island in the *LANCL1* gene promoter; no CpG island was detected in the promoter of *LANCL1-AS1* gene. We therefore designed a pyrosequencing methylation assay only for *LANCL1* promoter (Figures 4.7, 4.8). We analysed 60 DNA samples, 40 NSCLC tumour samples and 20 normal lung samples, respectively, none of the samples demonstrating any degree of DNA methylation (Figure 4.9). Therefore, DNA methylation is considered absent or, in any case, highly infrequent in lung cancer.

Tggagagacattatccccccacccccgccaaattttatctattgcgaacagcagaaataccagcatgttcagatctaaaagcagtctgtttc
ttctccaggttaaaaaatatatacttcttatgactctggacttaaatttgactttttaaaaataagaaaaattaaagaagggtaggaaatatt
ggtcacatctccgcgtgattctaggtcctcacttctgctacccagtaattaaaataccctgcgttatcctttagaaattacacgcctgtgtcttta
acaaactgtaagagagaagggggcgggtctcgggaacggcgaaggctctgattggccctcctggcaggactgggcggtaaaatagcccttc
tgttACTGTCCGGGGCTGCGGGGTGAGAGGCCAGGGCCGAGAAGGGCTTCAGGACGCGGGAGGCGCACTT
GCTTCAAGTCGCGGGCGTGGGAACGGGGTTGCAAAACGGGGCCTCTTTGTCCGGGTGGGTTAAGGGCCCT
GGCAGCTTTTTCGCGAAGGCGCCATGTCCTAGCAGTTGGGCCGCAGTGGGCCCGAGGTCCACTCGGACCG
CCGAGACGGCTCGATGGCCCTGGAGCTGGAGGAAGGGGGATACCTGGGCGCCGCCGCCGCCCTCGCAAC
TCGGCCGAGGCCCCTATCTCAACCTAGTTTCTGTTTTTCCCCTGTTCTGCAGGCTTGCTTCCGGCGTCATGGC
TCAAAGGGCCTTCCCGAATCCTTATGCTGATTATAACAAATCCCTGGCCGAAGGCTACTTTGATGCTGCCGG
gagggtgagtttaggatatgtctgcctgcatccctgcctctccccacggtgttcggaaaggtgctcatttttgcctgagagagttgagcatcccc
ctttaaaaaaatacatgattcgacgataaatacgtaaattatttaaaaatacatg

Figure 4.7: *Sequence of the promoter and exon 1 of human LANCL1 gene.* Upper case letters denote the exon 1 sequence. Violet letters show the 5’UTR while blue letters show the coding sequence. Cytosines in CG dinucleotides are in red letters. Primer annealing areas for the pyrosequencing assay is shown in yellow highlight and the CpGs interrogated by the assay are indicated in blue highlight. Please note that this is not a bisulphite-converted sequence, therefore, the primer sequence does not match.

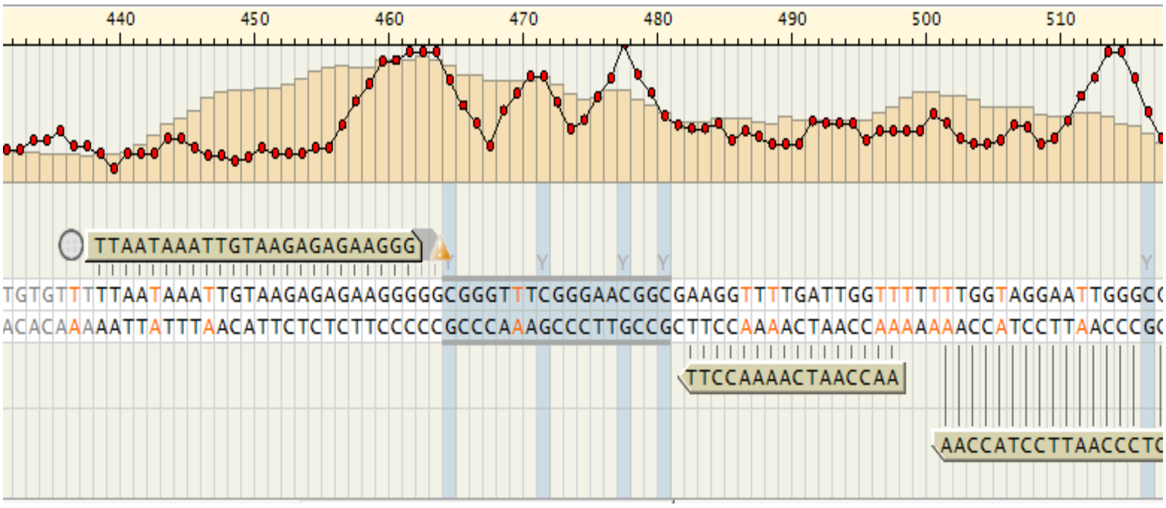

Figure 4.8: *Screen clipping image from Pyromark Assay Design demonstrating the DNA methylation assay design used.* The sequence shown is bisulphite converted DNA; red Ts indicate non CpG cytosines, which are converted to Ts following bisulphite-PCR; the circle at the 5' of the forward primer indicates biotinylation of primer; the interrogated CpGs are shown in blue lanes;

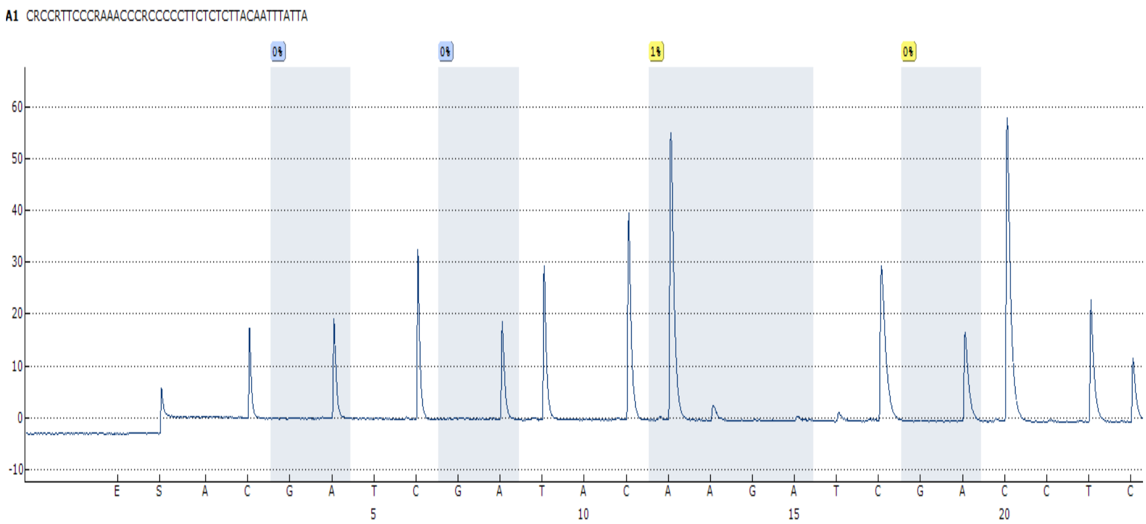

Figure 4.9: *Representative pyrogram demonstrating lack of DNA methylation in all four CpGs examined.* The X axis is the nucleotide dispensation order; the sequence shown on top left is the interrogated sequence; R (=G/A) in this sequence denotes the cytosines tested (reverse strand sequencing) which on the actual pyrogram are shown by the blue strips. The % methylation for each CpG is shown in the box above each one; the colour of this box indicates the confidence of the quantitation (blue is high confidence, yellow is acceptable but moderate confidence).

4.2.5 Oxidative stress response in NCLC cell lines

To investigate whether oxidative stress affected *LANCL1* expression in six NSCLC cell lines, RT-qPCR was run in the NSCLC cell lines following treatment, with two different doses of H_2O_2, 25 µM and 50 µM respectively, for two different durations, three and six hours, respectively. The experiment revealed a gradual increase in *LANCL1* mRNA expression in CALU-3 (the most significant recorded at 50 µM/6h with P=0.004), COR-L23 (the most significant recorded at 50µM/6h post-treatment with P=0.003) and H358 (the most significant recorded at 50µM/6h post-treatment with P=0.005). A549 showed a mild increase in the *LANCL1* mRNA expression (the most significant recorded at 25µM/6h with P=0.003), increase in *LANCL1* mRNA expression in SK-LU-1 after treated with both dose 50 µM and 25 µM at 6h with P= 0.002, while *LANCL1* expression was most significant high in SK-MES-1 after being treated with 25 µM for six hours with P=0.008. The experiment for SK-MES-1 was repeated with six replicates to confirm the result that shows that *LANCL1* increased around four times in SK-MES-1 under the oxidative stress condition (Figure 4.10) (Mann Whitney).

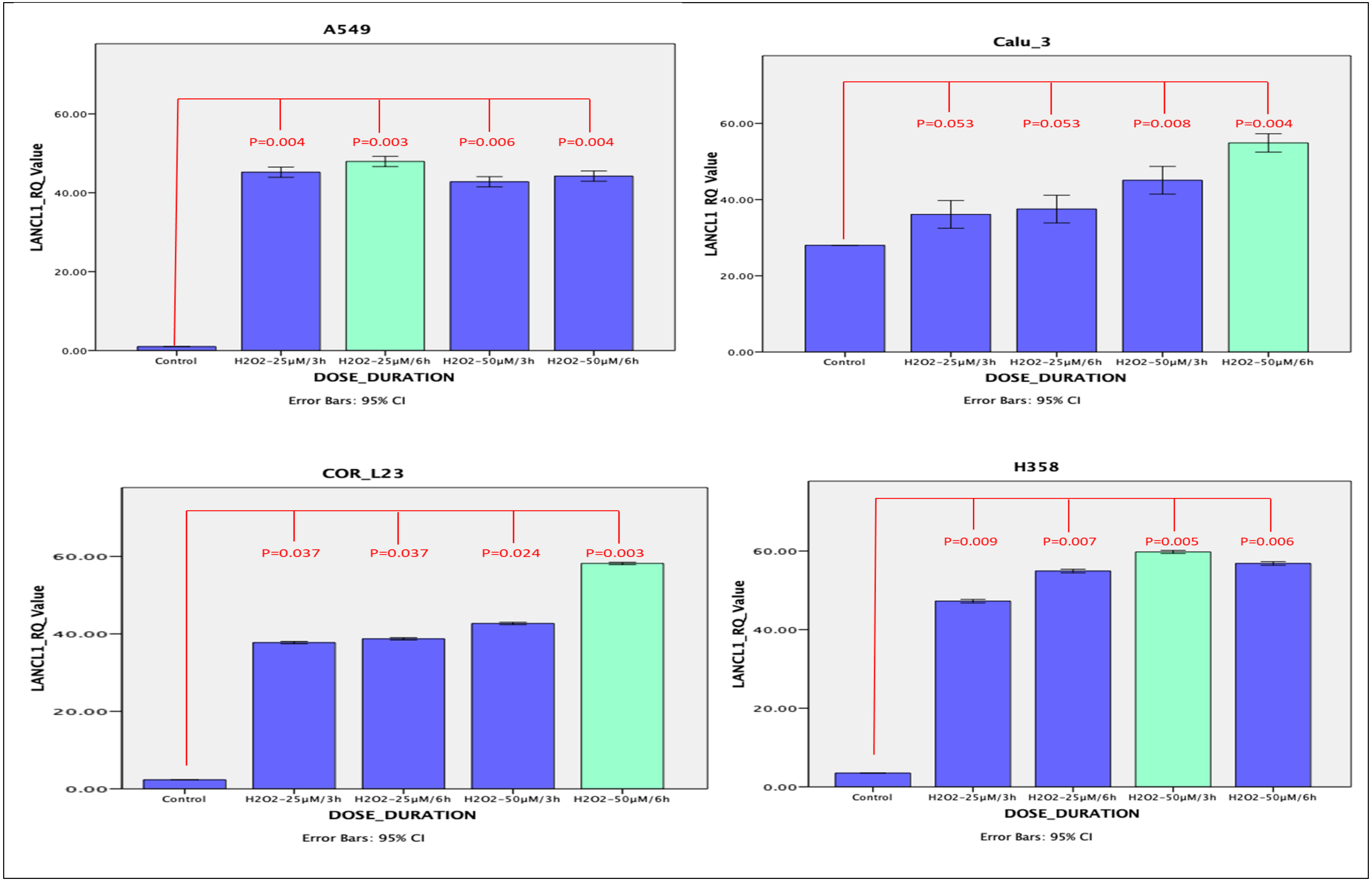
A549
Calu_3
COR_L23
H358
LANCL1_RQ_Value
P=0.004
P=0.003
P=0.006
P=0.004
P=0.053
P=0.053
P=0.008
P=0.004
P=0.037
P=0.037
P=0.024
P=0.003
P=0.009
P=0.007
P=0.005
P=0.006
0.00
20.00
40.00
60.00
Control
H2O2-25µM/3h
H2O2-25µM/6h
H2O2-50µM/3h
H2O2-50µM/6h
DOSE_DURATION
Error Bars: 95% CI

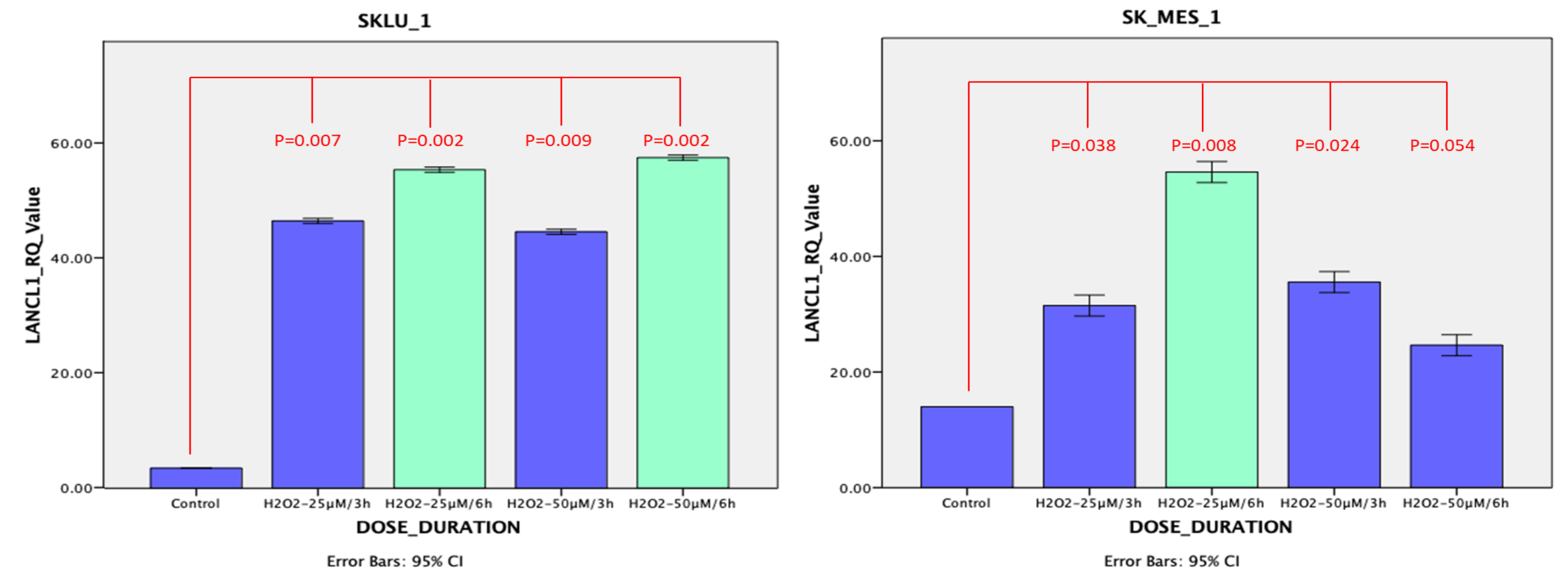

Figure 4.10: *Bar charts displaying mRNA expression of LANCL1 in different NSCLC cell lines treated with two doses of H_2O_2 25 µM/50 µM and incubated for two different periods of three and six hours, respectively*. Green represent the most significant results. The mean and error values in all graphs represent six technical replicates, and the error bars represent 95% confidence intervals. (Mann Whitney).

4.2.6 Overexpressed *LANCL1-AS1* in the SK-MES-1 cell line

As mentioned above, *LANCL1-AS1 expression* was found to be suppressed in tumour lung tissue samples, while completely absent in the eight NSCLC cell lines. The role of *LANCL1-AS1* has not been investigated yet, hence there are not any published papers describing any information relevant to its potential function. Therefore, I exogenously overexpressed the gene in NSCLC cell lines in order to determine the phenotypic effects, including its role in chemotherapy resistance, following expression restoration. SK-MES-1 was selected as the host cell line for this series of experiments, as it had zero expression for *LANCL1-AS1 (as every other cell line tested)* and was the same cell line used to knock down *LANCL1.* This was intended to limit, to the best possible, potential differences originating from the genetic background of different cell lines. In addition, the use of an inducible expression vector, PF12ARM, was selected in order to minimise the effects of the transfection process, mostly insertional mutagenesis by plasmid sequences into the genomic DNA. Therefore, the phenotypic results derived from the inducible clone can directly be attributed to LANCL1-*AS1* expression changes, due to the fact that the genotype does not change, as would be the case comparing a cell line transfected with a recombinant plasmid versus a control transfected with vector only. Following transfection and clone selection, RT-qPCR was used to confirm the overexpression of *LANCL1-AS1*, and only one clone (LS3) successfully achieved inducible expression (Figure 4.11).

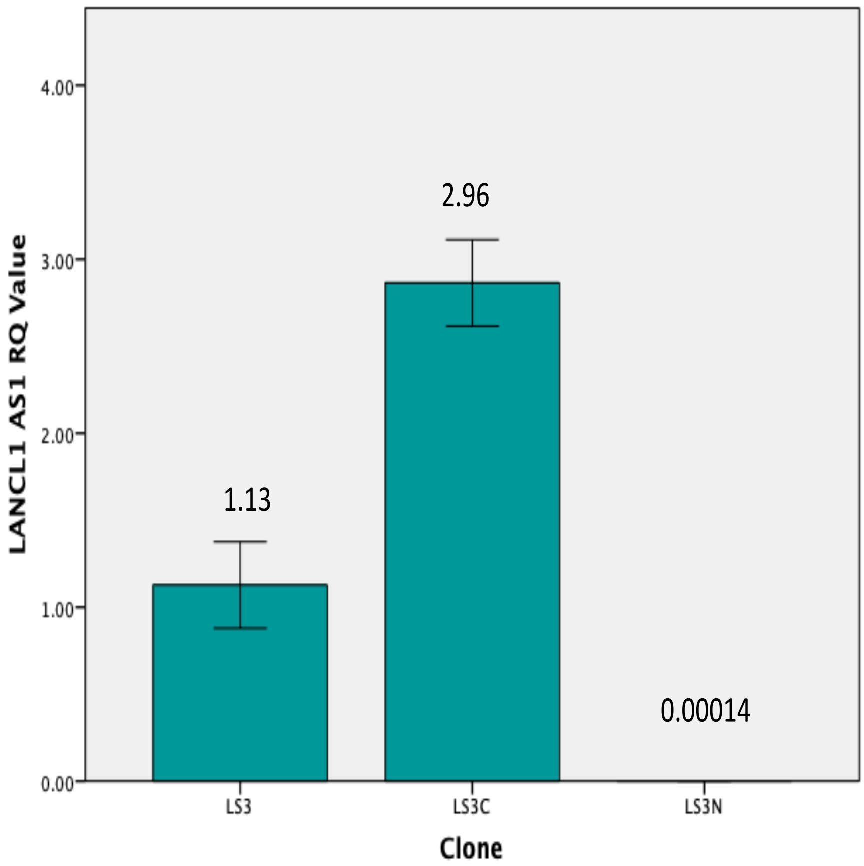

Figure 4.11: Bar chart demonstrating the *coumermycin switch on/off system in overexpressed LANCL1-AS1*. Overexpressed *LANCL1-AS1* (LS3) was the clone, which expressed *LANCL1-AS1* with LS3 treated with coumermycin (LS3C) elevated the expression to triple, while novobiocin decreased *LANCL1-AS1* expression. The numbers over the bars demonstrate the average fold-expression, while error bars represent 95% confidence intervals.

Interestingly, the overexpression of *LANCL1-AS1* in SK-MES-1 resulted in the overexpression of *LANCL1* mRNA (Figure 4.12), which is different from the lack of correlation in primary tissue samples, as shown at the beginning of this chapter. It must be noted that coumermycin and novobiocin exposure of the parental SK-MES cells, which do not carry the PF12ARM-based plasmid, did not affect *LANCL1* expression (data not shown).

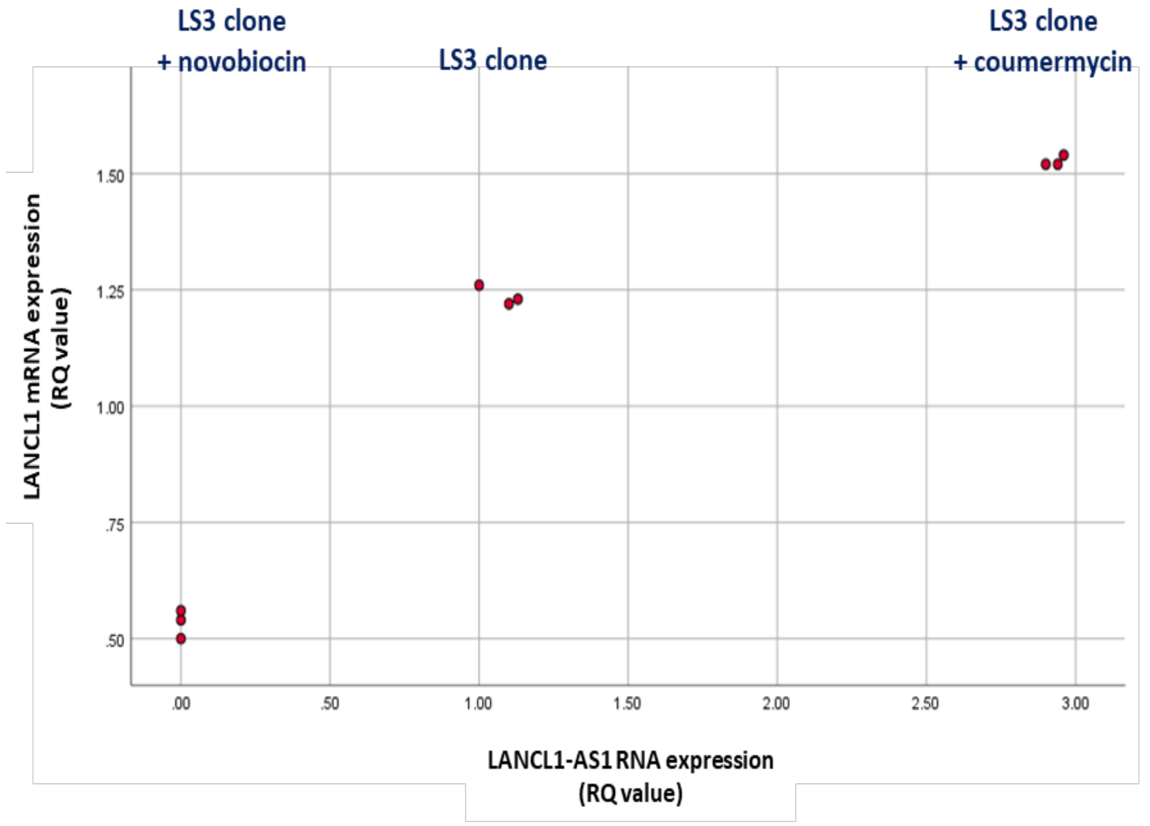

Figure 4.12: *Relationship of LANCL1-AS1 and LANCL1 RNA expression in the inducible clone (LS3) system in SK-MES-1 cells.* Novobiocin, suppresses *LANCL1-AS1* expression and this then suppressed *LANCL1* expression. In contrast, coumermycin exposure induces *LANCL1-AS1* expression and this is caused overexpression of *LANCL1.*

4.2.7 Phenotypic effect on overexpressed *LANCL1-AS1* clone

To investigate the phenotypic effects associated with changing the expression *LANCL1-AS1*, the MTT assay was used to determine the growth rate (proliferation), while wound healing assay was applied to determine cell migration, and invasion assay was employed to analyse cell movement through an extracellular membrane.

4.2.7.1 Proliferation

Proliferation rates were increased by the differential expression of *LANCL1-AS1* (Figure 4.13). The observed difference between transfected cells grown in coumermycin and grown in novobiocin underlines the value of using the inducible system (Mann Whitney at 48 hours P=0.013).

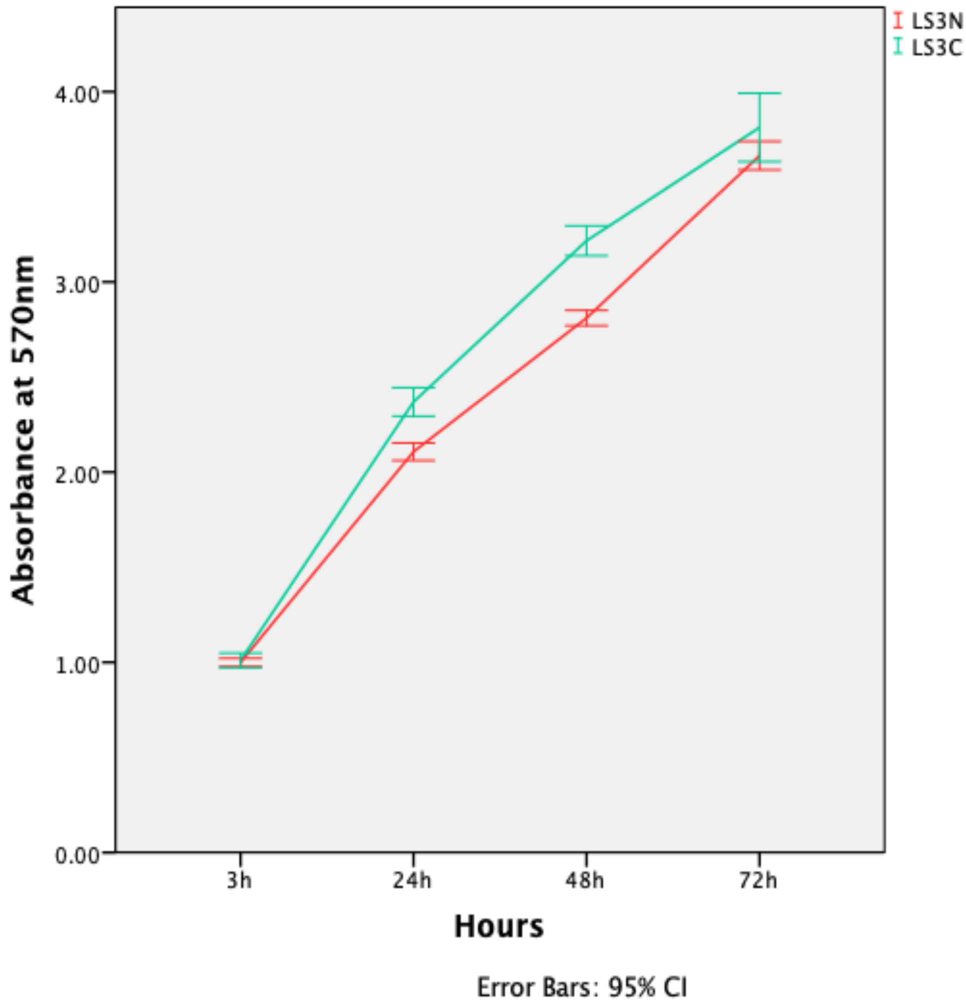

Figure 4.13: *MTT assay to determine the growth rate in the LS3 clone in the presence of coumermycin (green line high LANCL1-AS1 expression) and novobiocin (red line minimised LANCL1-AS1 expression)*. The mean and 95% confidence intervals are derived from six technical replicates.

4.2.7.2 Wound healing assay

Wound healing assay (scratch assay) determined cell migration rate with the use of Fiji software. Interestingly, the cells overexpressing *LANCL1-AS1* (LS3C) demonstrated a significant rapid migration rate compared to those with low *LANCL1-AS1 expression* (LS3N) (Figure 4.14), (Mann Whitney at 72 hours P=0.025) which agreed with the proliferation results.

4.2.7.3 Invasion assay

The Boyden chamber experiments demonstrated faster cell movement through the membrane for the *LANCL1-AS1* overexpressing cells, the result being more pronounced at 48 hours (Figure 4.15).

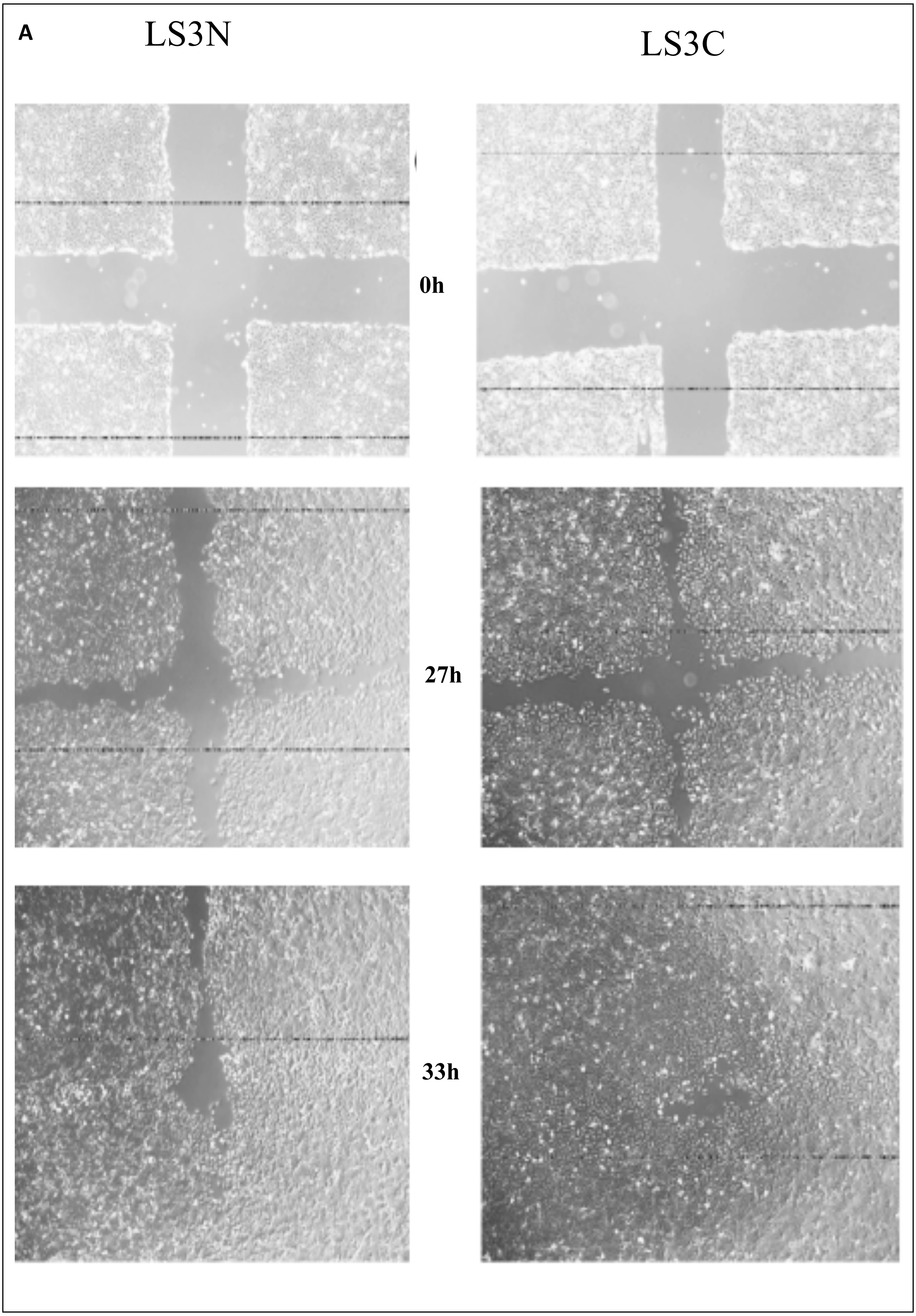
A
LS3N
LS3C
0h
27h
33h

B

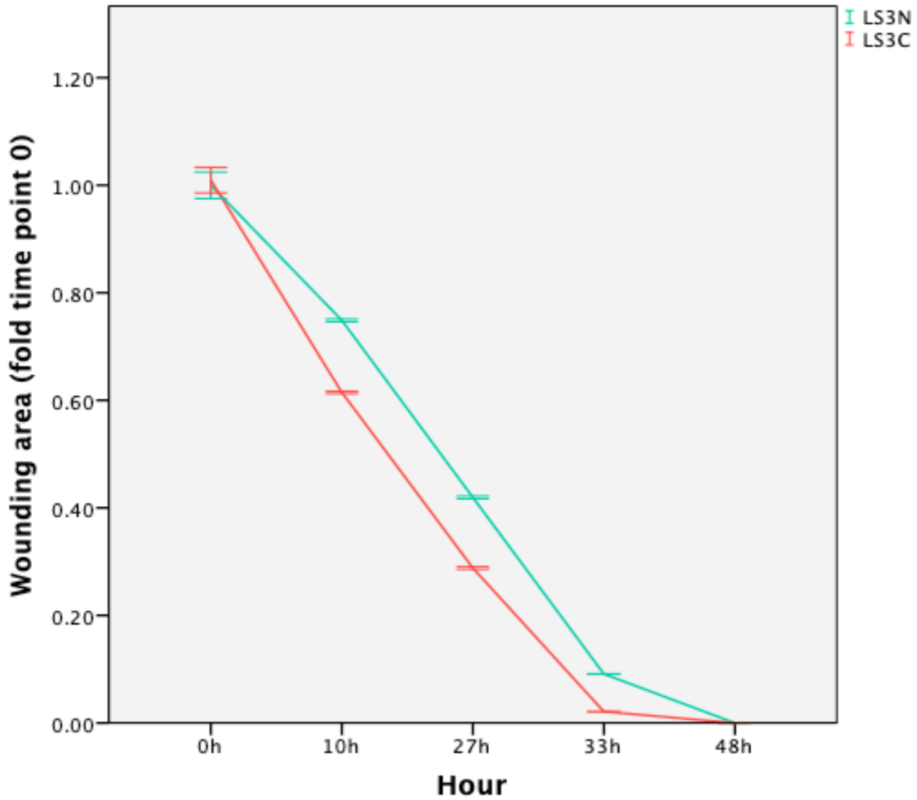

Figure 4.14: *Wound healing assay for 48 hours for cells with differential expression of LANCL1-AS1*. The LS3 clone i*n the presence of coumermycin (red line high LANCL1-AS1 expression) and novobiocin (green line minimised LANCL1-AS1 expression)*. The overexpressed *LANCL1-AS1* clone demonstrates a faster rate of closing the gap in the assay, or potentially is a higher proliferative rate of the LS3C. **A** pictures were taken at different times then **B** analysed by Fiji software.

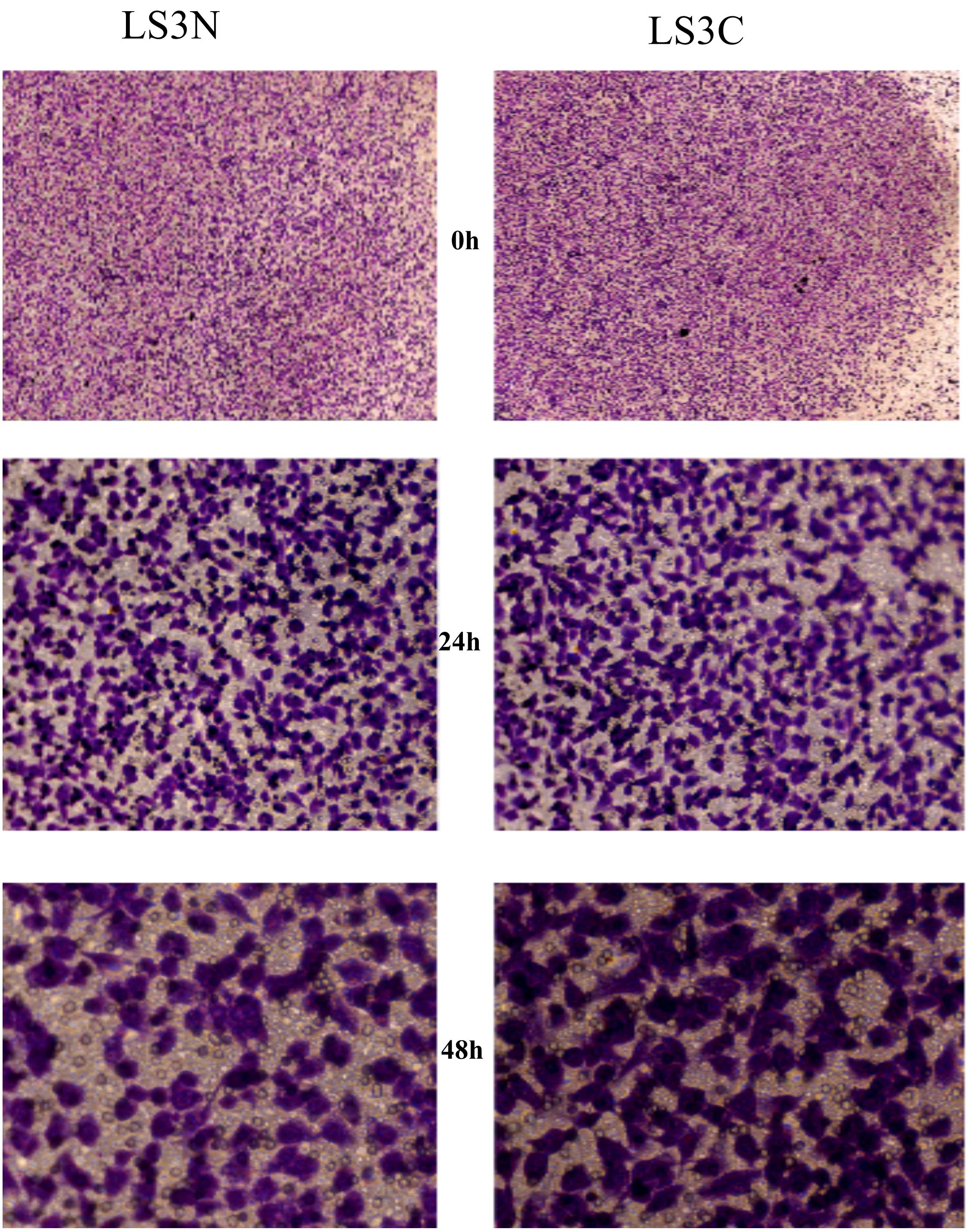

Figure 4.15: *Invasion assay for cells with differential expression of LANCL1-AS1.* LS3C (coumermycin, i.e. highest expression for the gene) demonstrates a higher number of invading cells at 48 hours comparing with LS3N (*novobiocin*, i.e. highest expression for the gene).

4.2.7.4 Oxidative stress response in relation to LANCL1-AS1 overexpression.

LANCL1 seems to play a major role in protecting neural cells from oxidative damage. As shown in various previous studies, there is a relation between oxidative stress and chemotherapy sensitivity (Conklin 2004; Zhen et al. 1992). Therefore, the response to oxidative stress (exposure to H_2O_2) was examined for the cells with differential expression of *LANCL1-AS1.* As a result, we concluded that the survival of cells of overexpressed *LANCL1-AS1* was reduced through treatment with seven different concentrations 0–100µM of H_2O_2 for 48 hours. The overexpressed *LANCL1-AS1* clone was growing with novobiocin (LS3N) and coumermycin (LS3C) to regulate the transgene expression; the LS3C clone become more sensitive to the H_2O_2 oxidative stress (Figure 4.16).

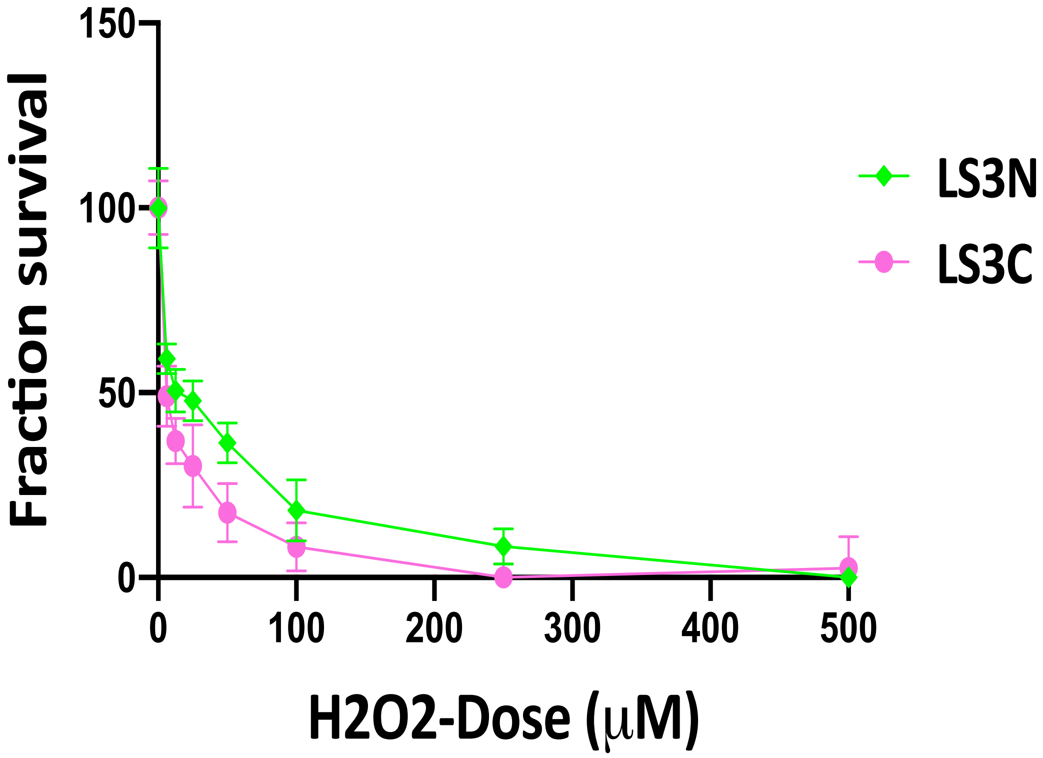

	LS3C	LS3N
IC50 (µM)	6.583	14.67
95% CI (µM)	2.805 to 10.46	9.177 to 21.16

Figure 4.16: *MTT assay demonstrating the sensitivity of the overexpressed LANCL1-AS1 clone to H_2O_2. The LS3 clone in the presence of coumermycin (pink line high LANCL1-AS1 expression) and novobiocin (green line minimised LANCL1-AS1 expression).* The means and error values in all graphs represent six technical replicates, and the error bars represent 95% confidence intervals.

4.2.7.5 Chemotherapeutics response in overexpressed LANCL1-AS1 clones

The treatment of the clones with 0–4μM gemcitabine shows a significant reduction in cell viability in overexpressed *LANCL1-AS1* (LS3C) grown in coumermycin as compared with overexpressed *LANCL1-AS1* (LS3N), which grown in novobiocin and parental cells (Figure 4.17). As displayed, overexpressed *LANCL1-AS1* increases cell sensitivity to gemcitabine.

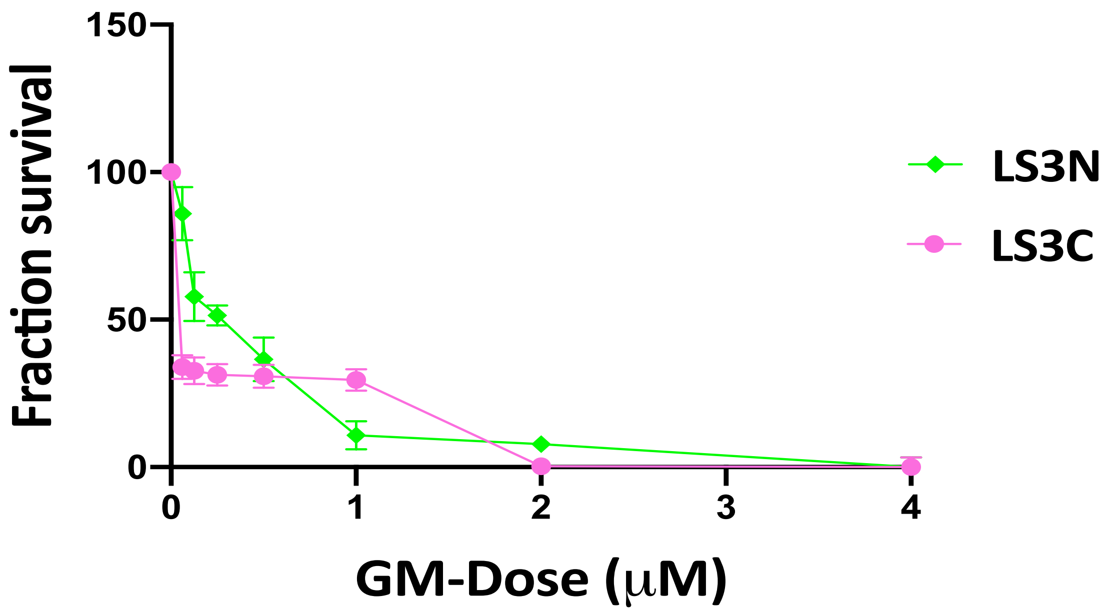

	LS3C	LS3N
IC50 (μM)	0.002	0.59
95% CI (μM)	0.0003 to 0.01	0.14 to 0.90

Figure 4.17: *MTT assay exhibiting the sensitivity of the overexpressed LANCL1-AS1 to gemcitabine.* Overexpression of LANCL1-AS1 sensitize s the SK-MES-1 cells to gemcitabine. The LS3 clone in the presence of coumermycin (pink line high LANCL1-AS1 expression) and novobiocin (green line minimised LANCL1-AS1 expression). The mean and error values in all graphs represent six technical replicates, and the error bars represent 95% confidence interval.

Also, a significant result was found when the clone's were treated with vinorelbine (0–500 nM). The overexpression of *LANCL1-AS1* grown in coumermycin (LS3C) shows an increase in cell sensitivity to vinorelbine as compared with the same clone grown in novobiocin (LS3N) (Figure 4.18).

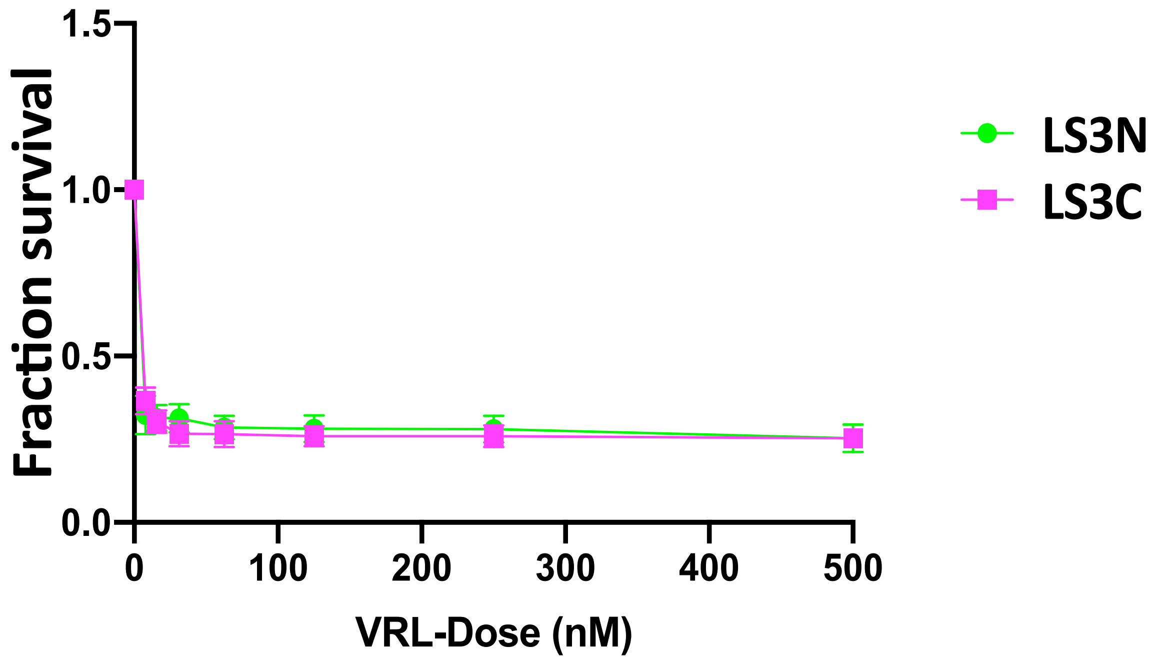

	LS3C	LS3N
IC50 (nM)	0.013	2.6
95% CI (nM)	0.003 to 0.34	0.98 to 5.09

Figure 4.18: MTT assay showing the *response of the overexpressed LANCL1-AS1 to vinorelbine.* Overexpression of LANCL1-AS1 sensitize s the SK-MES-1 cells to vinorelbine. The LS3 clone in the presence of coumermycin (pink line high LANCL1-AS1 expression) and novobiocin (green line minimised LANCL1-AS1 expression). The mean and error values in all graphs represent six technical replicates, and the error bars represent 95% confidence intervals.

Overexpressed *LANCL1-AS1* clones sensitize the SK-MES-1 NSCLC cell line to both gemcitabine and vinorelbine. In contrast, treating the clones with platinum agents shows a significant increase in resistance. As in overexpressed *LANCL1-AS1* grown in coumermycin (LS3C), when treated with cisplatin (0–100µM) showed an IC50 increase compared with the same clone grown in novobiocin (LS3N). The same response was determined when the clones were treated with carboplatin (0–100µM) (Figure 4.19).

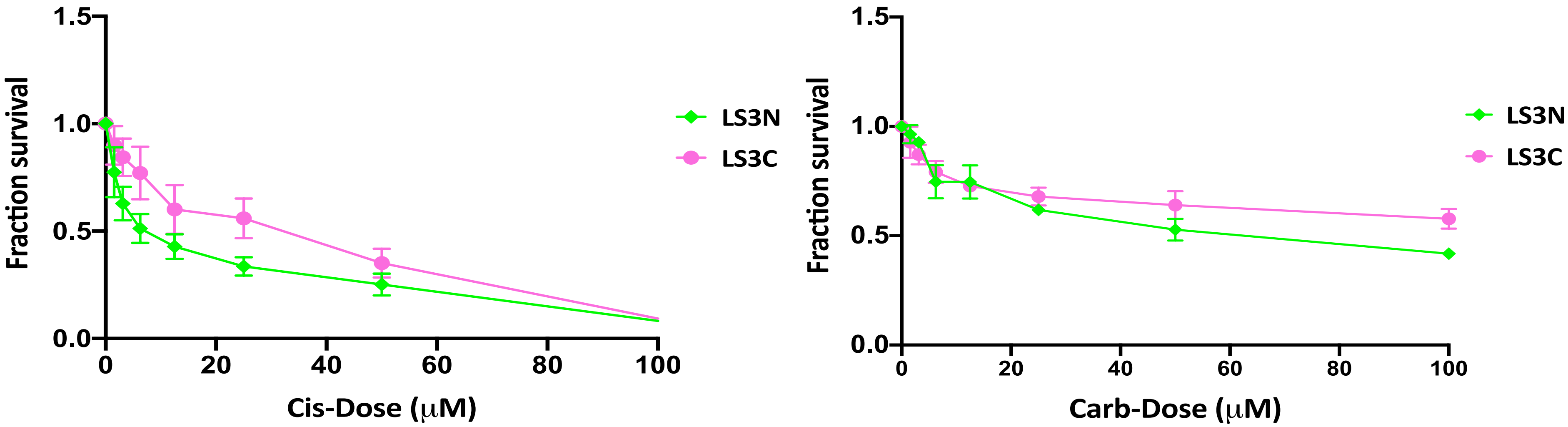

		LS3C	LS3N
Cisplatin	IC50 (µM)	32	5.96
	95% CI (µM)	19.01 to 48.92	1.53 to 9.54
Carboplatin	IC50 (µM	102.12	68.83
	95% CI (µM)	86.21 to 129.80	47.47 to 104.15

Figure 4.19: *MTT assay representing the overexpressed LANCL1-AS1 react against platinum.* Overexpression of *LANCL1-AS1* makes SK-MES-1 cells more resistant to both cisplatin and carboplatin. The LS3 clone in the presence of coumermycin (pink line high LANCL1-AS1 expression) and novobiocin (green line minimised LANCL1-AS1 expression). The mean and error values in all graphs represent six technical replicates, and the error bars represent 95% confidence intervals.

4.2.8 *LANCL1* downregulated in SK-MES-1 NSCLC cell line

LANCL1 mRNA expression was detectable in all normal and tumour tissue samples as well as the examined cell lines, among which SK-MES-1 demonstrated the highest *LANCL1* mRNA expression. Therefore, this cell line was selected for genetic manipulation to silence the *LANCL1* gene by using the small hairpin (shRNA) approach. The aim of this set of experiments was to explore the phenotypic effects that *LANCL1* expression silencing may trigger; more specifically, we measured proliferation, motility and invasion, as well as response to oxidative stress and chemotherapeutic agents.

Five shRNA constructs (materials and methods section2.7.1 Table 10) to knockdown *LANCL1* were used in individual transfections. RT-qPCR was utilized to analyse the mRNA expression level of *LANCL1* in determined clones to confirm the suppression of *LANCL1* expression in SK-MES-1. Four clones were isolated based on the efficiency of silencing: A6-8 and A6-26 clones, derived from TRCN0000011687 plasmid targeting the 3UTR region; A9-10 and A9-28 clone, derived from TRCN 0000011690 plasmid targeting the CDS region (Figure 4.20). It must be noted that the qPCR analysis of *LANCL1-AS1* expression did not show any difference (i.e. undetectable expression) regardless of the *LANCL1* expression level in the examined cell lines.

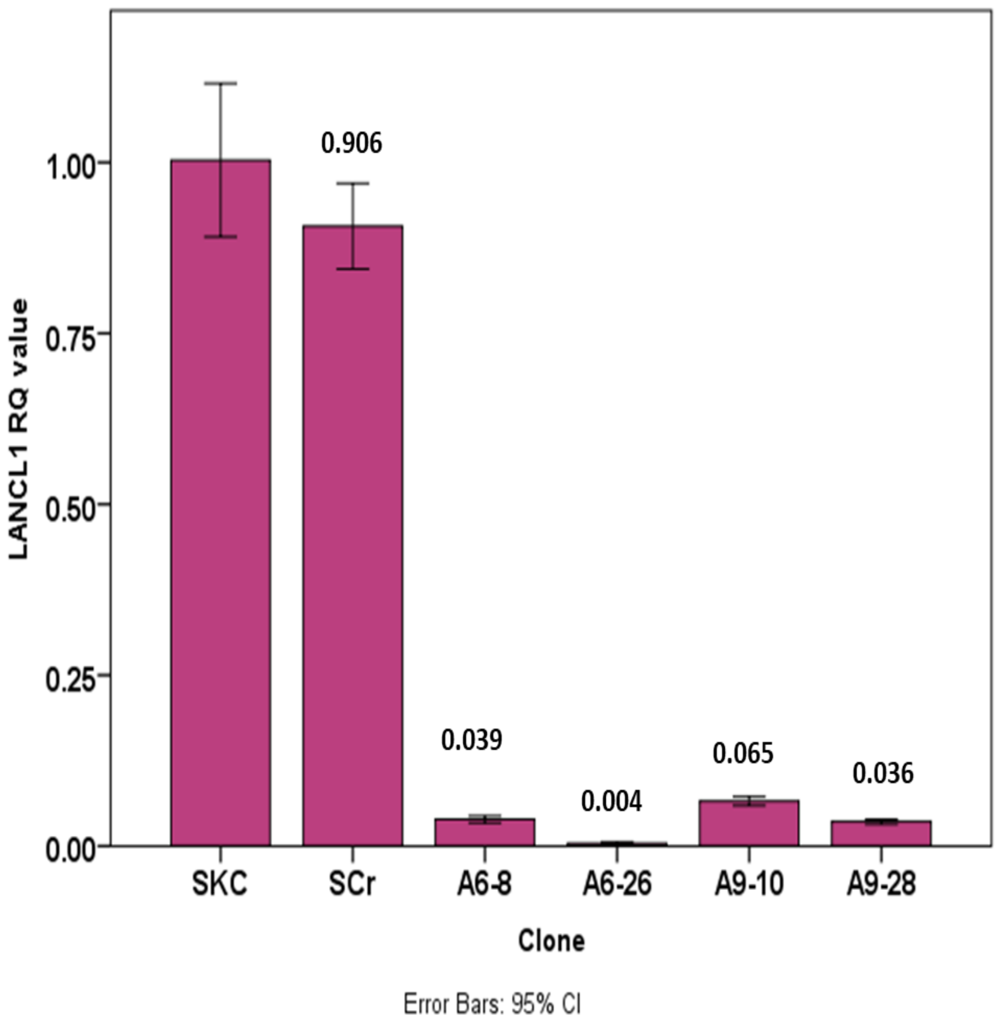

Figure 4.20: *RT-qPCR assessment of LANCL1 mRNA expression in selected SK-MES-1 derived transfectants*. Values are derived from triplicate experiments and are expressed as fold-difference to the parental cell line (shown as SKC). SCr: Scrambled transfectant clone. The numbers over the bars demonstrate the average fold-expression, while error bars represent 95% confidence intervals.

4.2.9 Western blot to validate *LANCL1* silencing at protein level.

Using Western blotting to detect LANCL1, and unfortunately, after using two different antibodies (catalogue no. PA5-57107 & PAS-31080, Thermo Fisher Scientific) and repeating the experiment several times, we could not obtain a successful result demonstrating knockdown of LANCL1 (Figure 4.21).

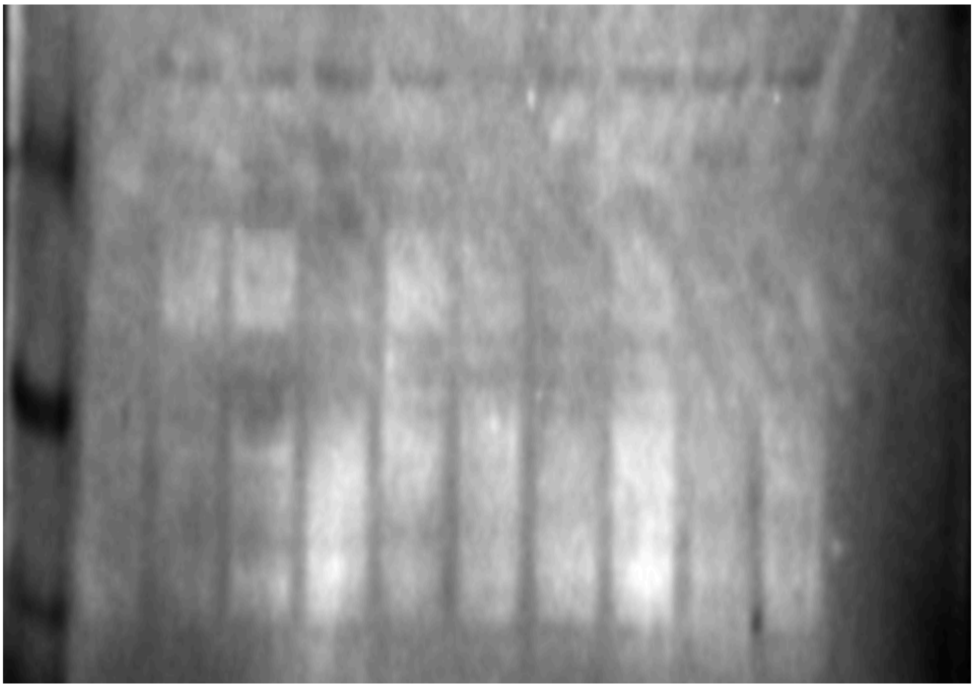

Figure 4.21: *Western blot results of LANCL1 protein expression. The low quality of the result lead to stop the investigation in this area.*

4.2.10 phenotypic effect on *LANCL1* clones

4.2.10.1 Proliferation

LANCL1 knockeddown clones displayed reduction in the cell proliferation in all two picked clones A6/26 and A9/10 (Mann Whitney at 72 hours P=0.003, P=0.005 respectively) compared to the parental and the scramble. Also, the proliferation rate decreased in scramble comparing with parental cells that may because the off-target effect (Mann Whitney at 72 hours P=0.017) (Figure 4.22).

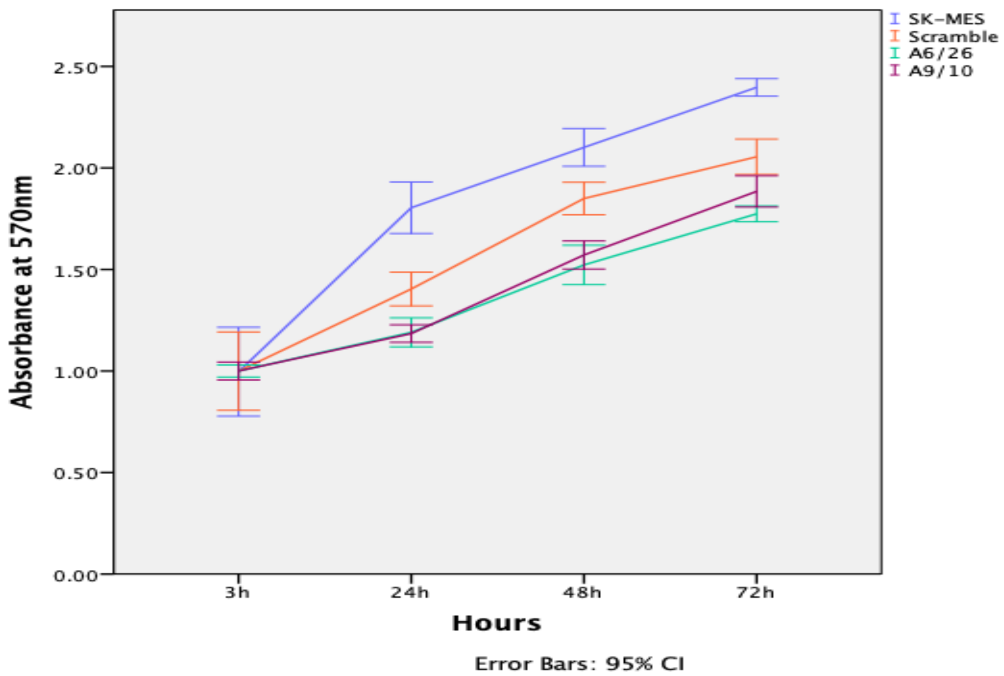

Figure 4.22*: MTT assay to determine the growth rate in knocked down LANCL1.* In knocked down clones: A6/26 and A9/10 reported a reduction in cell proliferation as compared with the parental SK-MES-1 and the scramble. The mean and error values in all graphs represent six technical replicates, and the error bars represent 95% confidence intervals.

4.2.10.2 Wound healing assay

Both knockeddown *LANCL1* clones; A6/26 and A9/10 (Mann Whitney at 27 hours P=0.025, P=0.008 respectively) showed a slow movement in the migration rate for closing the wound versus parental cell SK-MES-1 (Figure 4.23). Parental cells have a higher proliferation rate. Therefore, this result might be expected.

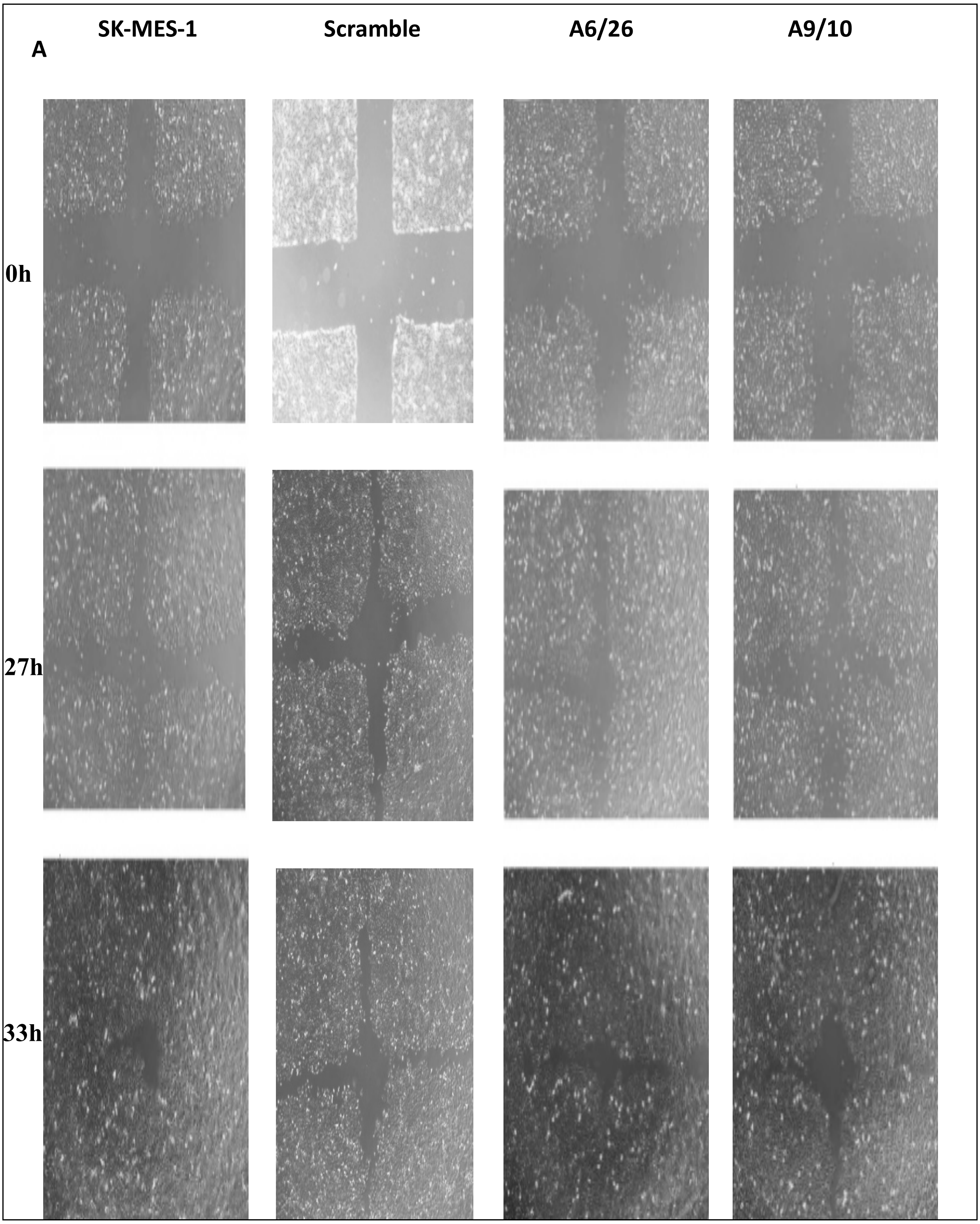
A
SK-MES-1
Scramble
A6/26
A9/10
0h
27h
33h

B

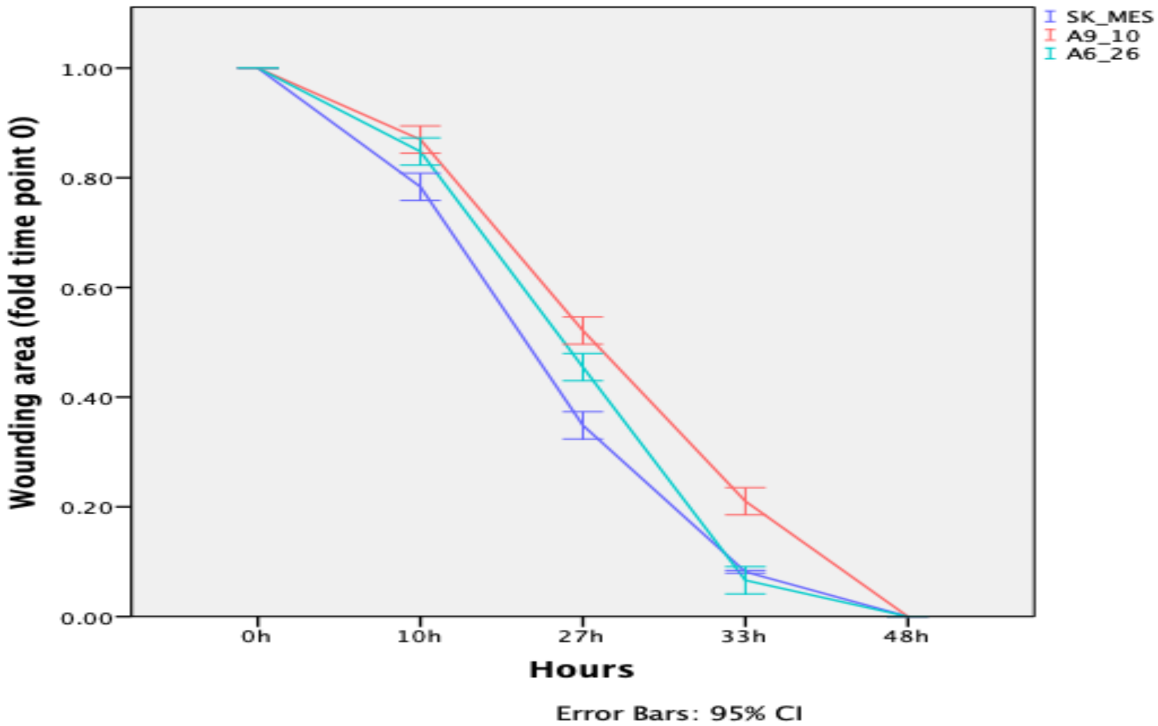

Figure 4.23: *Wound healing assay for 48 hours for cells with differential expression of LANCL1*. The *LANCL1* knocked down clones *(red line A9/10 and green A6/26)* and blue line parental cell line SK-MES-1. The knockdown *LANCL1* clone demonstrates a slow rate of closing the gap in the assay. **A** pictures were taken at different times then **B** analysed by Fiji software.

4.2.10.3 Invasion assay

In the invasion assay, no significant differences were observed between *LANCL1* knocked down clones and parental cells (Figure 4.24).

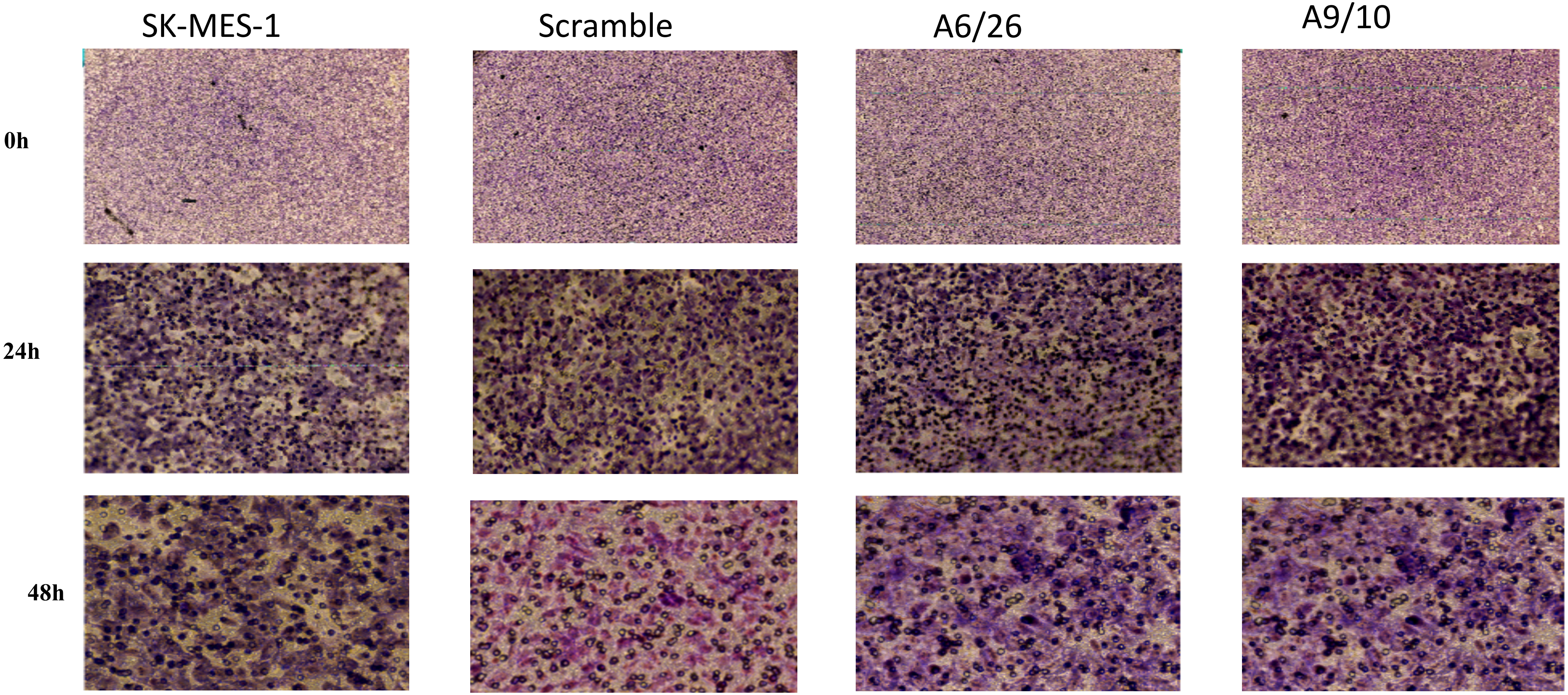

Figure 4.24: *Invasion assay for both LANCL1 (A6/26 and A9/10) clones*. The rate of cell movement through the extracellular membrane for 48 hours.

4.2.10.4 Oxidative stress response in knocked down LANCL1 clones

MTT assay was employed to analyse the H_2O_2 toxicity with seven different concentrations (0–100 µM) on the knockeddown *LANCL1* clones. That showed a reduction in cell viability in both A6/26 and A9/10 clones mean that the clones become more sensitive to H_2O_2. Furthermore, clone A6/26 showed more increase in the sensitivity to H_2O_2 than clone A9/10 (Figure 4.25).

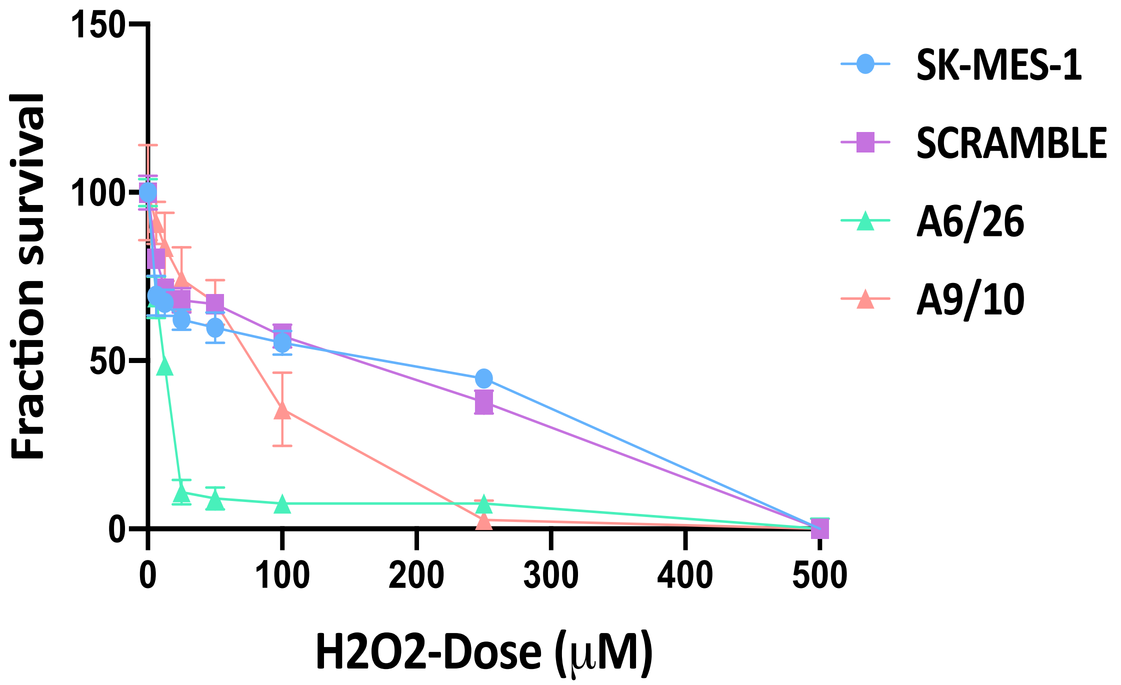

	SK-MES-1	SCRAMBLE	A6/26	A9/10
IC50 (µM)	116.74	174.90	10.58	84.75
95% CI (µM)	84.05 to 134.57	132.61 to 197.1	9.235 to 11.99	59.75 to 129.54

Figure 4.25: *Sensitivity of the knocked down LANCL1 clones to H_2O_2.* In MTT assay both clones (green line A6/26, orange line A910) show a sensitivity to H_2O_2. The mean and error values in all log10 graphs represent six technical replicates, and the error bars represent 95% confidence intervals.

4.2.10.5 Chemotherapeutic response in knocked down LANCL1 clones

Treatment of the parental SK-MES-1 and the clones with (0–4 µM) gemcitabine shows a reduction in cell viability in knockeddown clones show reduction in cell viability in A6/26 and A9/10. As displayed in knocked down *LANCL1*, increases cell sensitivity to gemcitabine (Figure 4. 26).

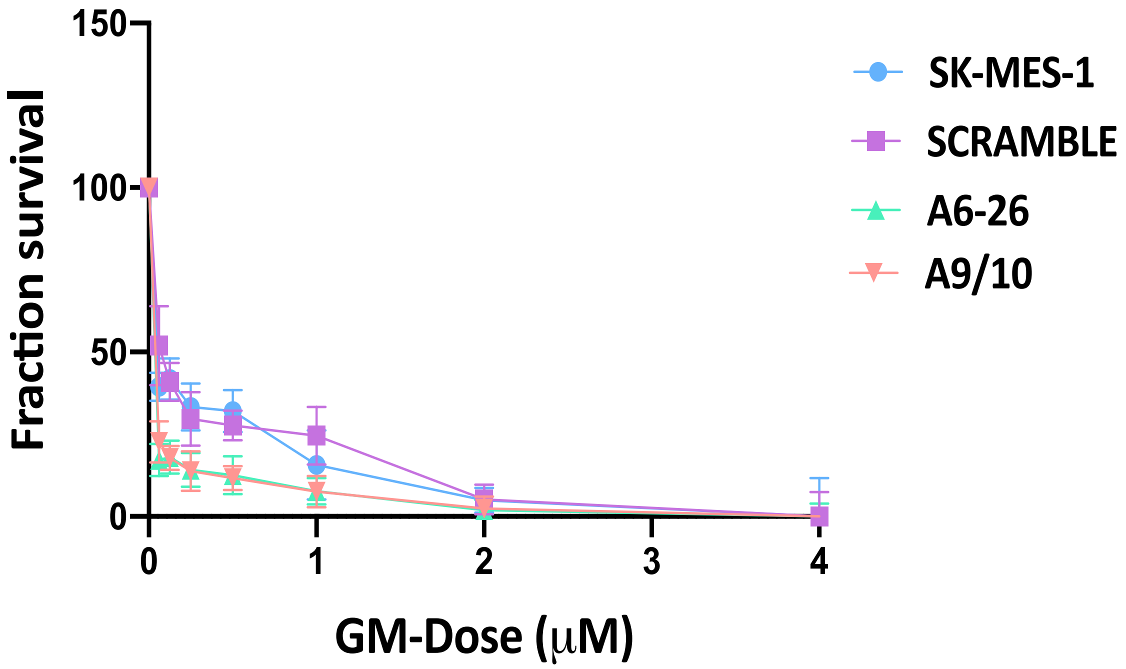

	SK-MES-1	SCRAMBLE	A6/26	A9/10
IC50 (µM)	0.023	0.038	0.001	0.002
95% CI (µM)	0.012 to 0.045	0.001. to 0.068	0.0006 to 0.009	0.001 to 0.014

Figure 4.26: *Sensitivity of the knocked down LANCL1 clones to gemcitabine.* Both clones (green line A6/26, orange line A910) sensitize the SK-MES-1 (blue line) against gemcitabine. The mean and error values in all graphs represent six technical replicates, and the error bars represent 95% confidence intervals.

A significant result was found when the clones was treating with vinorelbine (0–500nM). knockeddown *LANCL1* clones also show a reduction in cell viability when treated with VRL in both clones A6/26 and A9/10 (Figure 4.27).

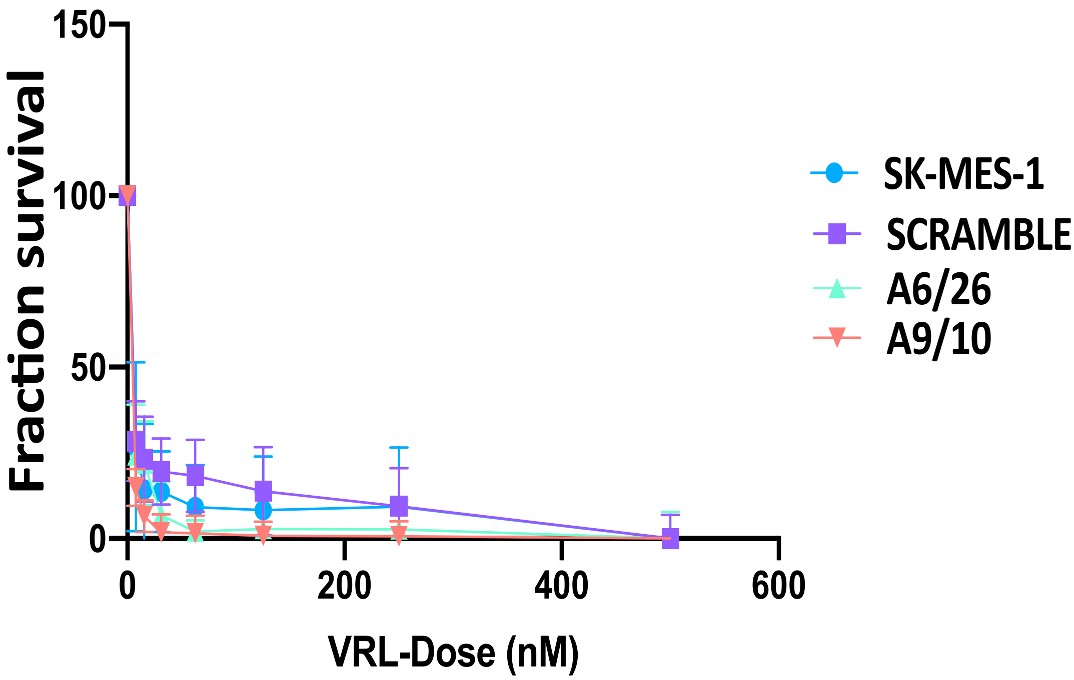

	SK-MES-1	SCRAMBLE	A6/26	A9/10
IC50 (nM)	1.54	3.721	0.065	0.001
95% CI (nM)	0.5867 to 2.666	1.065 to 5.063	0.017 to 0.951	0.002to 0.188

Figure 4.27: *Response of the knocked down LANCL1 clone to vinorelbine.* In MTT assay both clones (green line A6/26, orange line A910) sensitize the SK-MES-1 (blue line) against vinorelbine. The mean and error values in all graphs represent six technical replicates, and the error bars represent 95% confidence intervals.

Surprisingly, resistance was found in knocked down *LANCL1* clones when treated with cisplatin and carboplatin, where the IC50 increased in A6/26 and in A9/10 as compared with both parental SK-MES-1 and scrambled cell line. The same response appeared when the clone was treated with carboplatin: both A6/26 and A9/10 showed an increase in the IC50 compared with the parental cells (Figure 4.28).

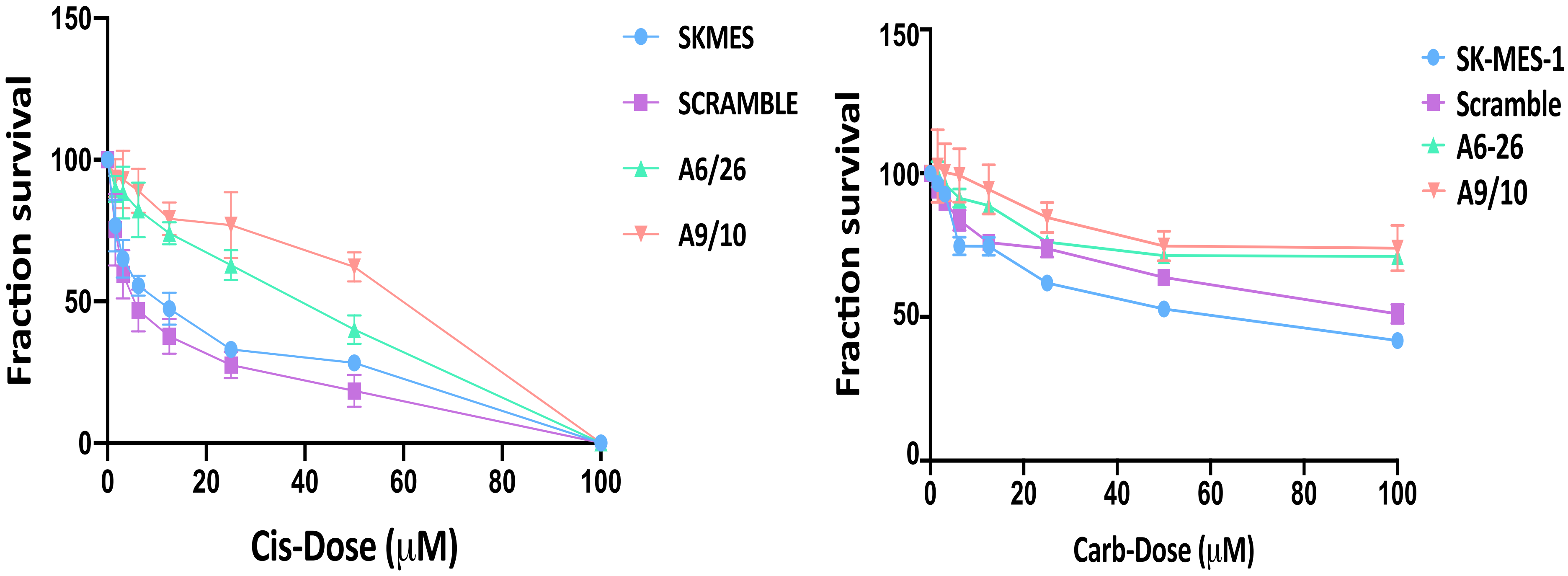

		SK-MES-1	SCRAMBLE	A6/26	A9/10
Cisplatin	IC50 (µM)	13.08	6.08	37.344	48.804
	95% CI (µM)	9.631 to 16.589	1.777 to 9.417	24.9053 to 58.965	24.072 to 79.820
Carboplatin	IC50 (µM	79.53	120.23	184.4	211.76
	95% CI (µM)	47.82 to 106.25	105.72 to 160.63	218.14 to 157.23	256.91 to 198.16

Figure 4.28: *knocked down LANCL1 clones react against platinum.* In MTT assay both clones (green line A6/26, orange line A910) make SK-MES-1 (blue line) more resistance to both cisplatin and carboplatin. The mean and error values in all graphs represent six technical replicates, and the error bars represent 95% confidence intervals.

4.2.11 Effect of sodium valproate on *LANCL1* expression

LANCL1 is overexpressed in lung tumours and NSCLC cell lines. Given the highly deregulated epigenetic control of lung tumours, an interesting research question arising is whether *LANCL1* expression is under epigenetic control. Previously in this chapter, we observed lack of DNA methylation in the promoter of the gene in primary NSCLCs. Therefore, it was decided to examine another major epigenetic factor, which is histone deacetylation. For this purpose, eight NSCLC cell lines were treated with valproic acid, which is a well-known HDAC inhibitor, for 48 hours. Interestingly, all but H358 cell lines showed elevated *LANCL1* expression with VPA (Figure 4.29).

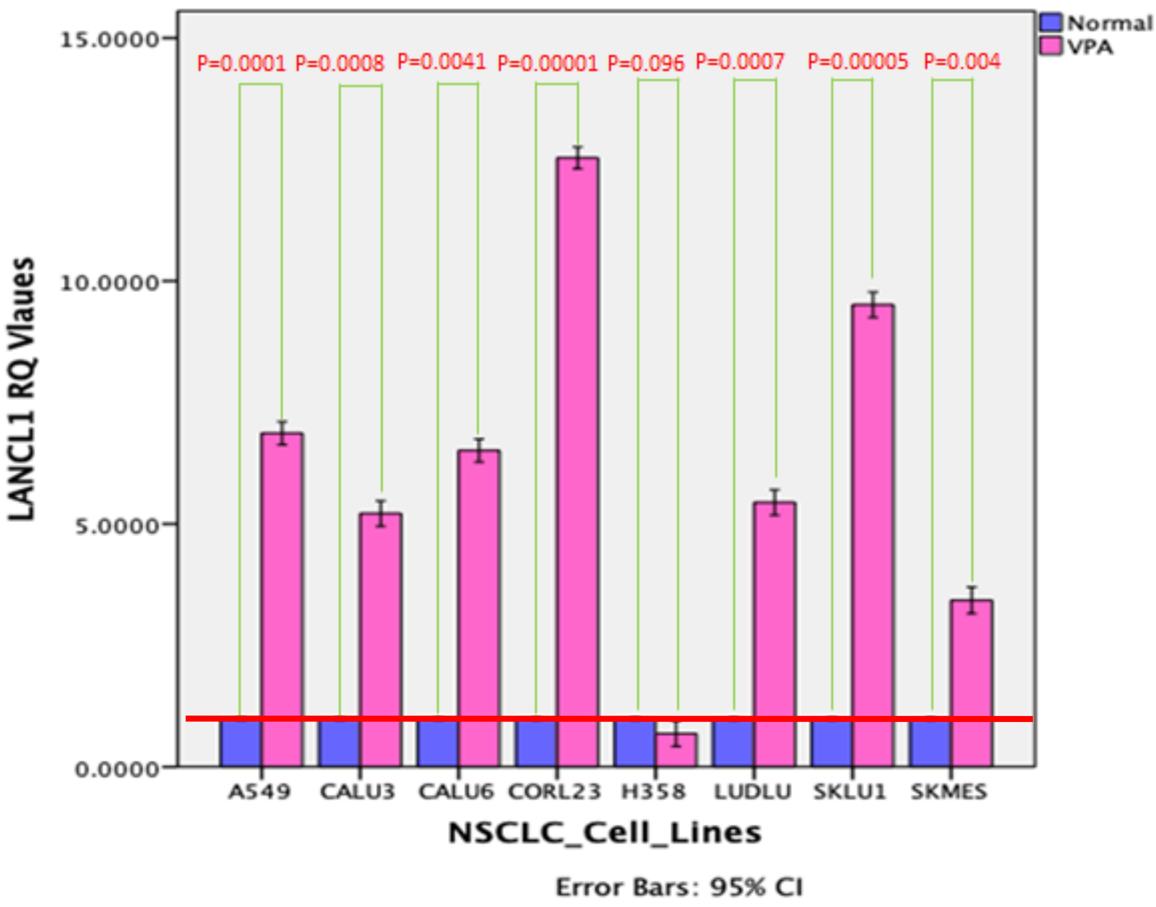

Figure 4.29: Bar chart showing the *LANCL1 expression under exposure to sodium valproate.* Eight NSCLC cell lines were treated with VPA for 48 hours and then the mRNA expression was determined by RT-qPCR. The numbers over the bars demonstrate the average fold-expression, while error bars represent 95% confidence intervals (Mann Whitney).

4.3 Discussion

Following the observation of *LANCL1-AS1* loss of expression in NSCLC tissue and cell lines, we examined the potential functional significance of this alteration in the tumour phenotype and drug resistance. Currently, the relationship between *LANCL1-AS1 and LANCL1* (coding) gene is completely unexplored, hence the decision to examine the expression and function of this coding (potential) counterpart gene. *LANCL1,* a GSH-binding protein, plays a fundamental role in neural development, more specifically in signalling and differentiation (Zhang et al. 2009). Given the previous reports showing that *LANCL1* influences oxidative stress in cells (Zhong et al. 2012), this became one of the central points of focus in this chapter.

LANCL1 was overexpressed in the NSCLC tissue compared to the normal lung counterpart tissue. While *LANCL1-AS1* expression is reduced in the same tumours, no direct correlation was observed between the two genes, which is not necessarily surprising and can be attributed to the multiplicity of factors controlling the expression of the two genes in the lung tissue. When, however, *LANCL1-AS1* was overexpressed in a very well controlled system (inducible expression in SK-MES-1), *LANCL1* expression was increased.

The mechanism underlining this observation is not known. lncRNAs control the abundance of their coding targets in a number of ways, including transcriptional control (e.g. used as scaffolds between transcription factors and guides to transcription complexes to the targets promoter) as well as controlling the half-life of the nascent mRNA, for example by sponging miRNAs (Table 4.1) (Fang and Fullwood 2016). Since the exonic sequence overlap of LANCL1 and LANCL1-AS1 is zero (Figure 1.14), one can probably exclude the miRNA sponging scenario, leaving thus more room towards a transcriptional control hypothesis. This theory needs to be experimentally established in future studies.

Table 4.1: *Function of LncRNA in transcription regulation* (Fang and Fullwood 2016).

Signal RNA	Signal in response to different stimuli
Decoy RNA	Reduce the availability of regulating factors by using decoy binding sites, catalysis proteins, and subunit of long chromatin modification complex
Scaffold RNA	Provide the platform to structure multicomponent complexes, e.g. ribonucleoprotein (RNP)
Guide RNA	Drive the complex component RNP to the target gene
Enhance RNA	Signal the production from the enhancer region (chromatin interaction)
Tethers RNA	Take the interacting protein from the enhancer region to the target place

LANCL1 promoter bears a CpG island, which triggered the question of a potential methylation-dependent deregulation. Pyrosequencing analysis demonstrated, however, that LANCL1 promoter was unmethylated in both tumour and normal lung samples, excluding this scenario. Two of the three reported splice splicing variants (variant 1 and variant 3) were detectable in both lung normal and tumour tissues, while variant 2 was not detected in any of the tissue or cell line samples. The absence of variant 2 on the gel means that it is either a variant not expressed in the lung tissue, or that it is expressed at such low levels that it could not be compared to the very high abundance of variant 1 transcripts in a common tube. Nonetheless, at this point, variant 2 was considered insignificant to follow; in fact, the general absence of any difference in the PCR signals from normal and tumour samples, despite the full appreciation that endpoint PCR is not quantitative, led us to abandon this question and concentrate on more interesting findings.

In the complete absence of information regarding the role of *LANCL1 in* NSCLC, we decided to suppress *LANCL1* using shRNA in a NSCLC cell line and study its phenotypic effects, such as proliferation, migration, invasion, sensitivity to drugs and oxidative stress. SK-MES-1 cell line was chosen as the highest *LANCL1* expressor among the available NSCLC cell lines in our lab. In order to minimise the off-target effects by the shRNA action, we selected clones from two different oligos, namely A6 targeting the 3'UTR and A9 targeting the coding area. It is of note that all the phenotypic results observed were common for the two clones, providing high confidence for their specificity to the knocked down gene. As a result, the LANCL1 knock down led to lower proliferation and migration, however without having any effect on invasion. This agrees with the observation of the overexpression of LANCL1 mRNA in primary NSCLC in this study and suggests that LANCL1 may provide a selective growth advantage in lung tumour cells. LANCL1-AS1 overexpression, which caused increase of LANCL1 expression, led to increased migration and invasion but did not affect proliferation. *LANCL1* has previously been reported to increase cell proliferation (Zhang et al. 2009), the discrepancy of the results between LANCL1 and LANCL1-AS1 induced proliferation probably reflecting an independent role for the LANCL1-AS1 gene.

Exposure of all six NSCLC cell lines to different H_2O_2 concentrations triggered an increase of *LANCL1* mRNA expression, indicating the direct effect of oxidative stress in the transcriptional regulation of *LANCL1* expression; this may protect lung cancer cells from the damage, as has been previously shown for other cell types (Zhong et al. 2012). While it is currently not clear how oxidative stress stimulates LANCL1 transcription, there is a report on prostate cancer cells indicating that this is accomplished through the inhibition of the c-Jun NH2-terminal kinases (JNK) pathway (Wang et al. 2018). The proximal promoter sequence (1000 nucleotides from transcription start site [TSS]) was subjected to transcription factor binding prediction in one of the available online tools: http://tfbind.hgc.jp/. The potential transcription factors

(TFs) with binding motifs on LANCL1 promoter. Among the predicated TFs (AP1 and p53) belong to the JNK pathway. Especially, JNK activity in *LANCL1* knockdown prostatic cells showed a significant increase in the number of cell death produced by H2O2 treatment (Wang et al. 2018). Investigators determined JNK as a core mediator of ROS and oxidative stress stimulating apoptosis in several cell types. They report that ROS stimulates the initiation of JNK and DNA damage and increases growth arrest/senescence to apoptosis in prostate cancer cells. JNK regulates AP-1 and downstream apoptosis pathways, such as p53, PARP-1 activation. Consequently, JNK pathway is an essential mediator in ROS stimulating prostate cancer apoptosis and is a potential therapeutic target (Wang et al. 2018).

Interestingly, oxidative stress did not affect LANCL1-AS1 expression at all, a point that will be discussed further below when looking into the opposite direction, i.e. the effect of LANCL1-AS1 expression on the sensitivity of cells to oxidative stress.

The overexpressed *LANCL1-AS1* clones showed increased proliferation, migration and invasion properties, which, at first sight, seems contradictory to the finding that *LANCL1-AS1* expression is reduced in primary lung cancer and eliminated in NSCLC cell lines. Such a reduction could point to the hypothesis that loss of LANCL1-AS1 expression is a selective advantage for lung cancer cells, both *in vivo* and *in vitro*. Since the function of *LANCL1-AS1* is virtually unknown, it is very difficult currently to create hypotheses behind this contradiction. One could speculate that the loss of *LANCL1-AS1* expression in primary NSCLC is a passenger effect, i.e. it is due to alterations affecting its transcriptional regulation, however, its overall contribution to tumour phenotype is minor, as it is one among thousands of genetic and epigenetic changes occurring in NSCLC. In contrast, in a well-controlled experimental environment, such as an inducible expression system, its phenotypic effects may be clearer.

It is also important to note that we have only observed this effect in a single cell line (i.e. a specific genotype), therefore, a universal such effect cannot be claimed.

On the other hand, it is of interest that *LANCL1-AS1* overexpression resulted in *LANCL1* overexpression in human cancers, including NSCLC specimens examined in this study, as well as many NSCLC cell lines. Therefore, the effect of the antisense gene might be a result of the modification of the coding counterpart. This is supported by the fact that *LANCL1* downregulation in this study resulted in lower proliferation and migration. No such effect was seen for invasion, but this is a difference potentially attributed to the variability occurring in experimental system (e.g. effects produced by transfection).

The overexpression of *LANCL1-AS1,* provided a rather puzzling result in relation to the sensitivity to oxidative stress. Overexpressing *LANCL1-AS1* cells became more sensitive to H_2O_2. As noted above, however, *LANCL1-AS1* overexpression leads to *LANCL1* overexpression (Figure 4.12). While currently this cannot be clearly explained, it implies that *LANCL1-AS1* may have LANCL1-independent functions which may outweigh the LANCL1 overexpression effect in relation to oxidative stress. A separate series of experiments involving more cell lines are needed to clarify those mechanisms, studying the effects of LANCL1-AS1 in LANCL1 knockout cell lines.

After having indicated that *LANCL1* plays a role in protecting lung cancer cells from oxidative stress, further research is required to determine how the oxidative stress produced from the chemotherapies can increase the resistance against them. We explored the effect of *LANCL1-AS1* and *LANCL1* expression modulation on chemotherapy sensitivity. Remarkably, our result shows significant sensitization to gemcitabine and vinorelbine of the SK-MES-1 NSCLC cell line in both overexpressed *LANCL1-AS1* and both the knocked down *LANCL1* clones (A6/26 and A9/10).

In contrast, the same modulation of *LANCL1-AS1* and *LANCL1* expression triggered a significant increase in SK-MES-1 resistance against platinum compounds (both cisplatin and carboplatin). It has been determined that oxidative metabolic characteristics increased in platinum resistance cells as compared with in the sensitive cells in ovarian cancer (Matassa et al. 2016). Oxidative stress works usually to overproduce ROS and damage the function of the antioxidative defence (Ma et al. 2014).

Almost all chemotherapeutic agents create some ROS through the generation of apoptosis in cancer cells, which explains the apoptosis generation by one of the chemotherapies through the release of cytochrome C from the mitochondria leaf part of ETS, resulting in the production of superoxide radicals. The generation of ROS during chemotherapeutic treatment can reduce the affinity of anticancer therapy (Debatin 2000). Platinum alkylating antineoplastic agents can produce a higher level of ROS compared with vinca alkaloid, which produces a low level of ROS (Conklin 2004).

Moreover, chemotherapy may also induce oxidative stress in cancer cells. In other words, increased oxidative stress increases the production of lipid peroxidation, which creates multiple electrophilic aldehyde that can target many cellular molecules. The presence of oxidative stress leads to the reduced ability of chemotherapy to induce cell death, due to the ability oxidative stress can slow cell cycle progresses through checkpoint arrest (Conklin 2004). Another way oxidative stress can affect the affinity of the chemotherapy to inhibit apoptosis is through stopping caspase activity or death receptor inactivation. Therefore, using antioxidative agents with chemotherapy may increase drug productivity through the inhibition of creation aldehyde from the oxidative stress (Conklin 2004).

Furthermore, oxidative stress reduces cell proliferation and limits the transaction from the G0/G1 lead to slow progressing from the S-phase lead to inhibit cell cycle passage though the restriction point to cause chick point arrest in the cell. Therefore, chemotherapeutic antineoplastic cytotoxicity will be diminished due to the chemotherapeutic agents which work to increase cell cycle progression through a specific phase and oxidative stress will reduce the cytotoxicity. Platinum does not work with the specific phases of other cell cycles; however, it regulates the cell rich G2 phase to recognise the damage attributed to platinum and induce apoptosis. Therefore, using antioxidants during chemotherapy may increase the affinity of the drug (Conklin 2004).

The consequences of oxidative stress on cell proliferation are almost certainly related to block of critical enzymes by the aldehydes, and selective inhibition of DNA polymerases by 4-hydroxyalkenals has been confirmed (Conklin 2004). The cyclin-dependent kinases (CDKs) are other likely targets of the aldehydes (Shackelford, Kaufmann, and Paules 2000).

Part of chemotherapy induces cell apoptosis through either initial apoptosis from the mitochondrial by the release of cytochrome C or the activities of death receptor CD95 by ligate with dead receptor ligation CD95L (Debatin 2000). The apoptosis process is mediated by caspase, which is a protease that induce cysteine residue interactive sites and requires a special environment to initiate the activity. Usually, chemotherapeutics, which targets to upregulate death receptor signalling, activates caspase 8 or releases cytochrome C to interact with caspase 9 and activate the downstream caspases (3, 6, and 7) that lead to cell death apoptosis (Thornberry and Lazebnik 1998).

It was proven that ROS is a late event after the cell decides to activate the death program for cell death. ROS generation after apoptosis releases cytochrome C. Furthermore, an increase in oxidative stress leads to inhibition of caspase activity, which in turn reduces the efficiency of other chemotherapeutics to induce apoptosis (Conklin 2004).

Therefore, oxidative stress may reduce the affinity of agents, inducing apoptosis and generating aldehyde to block the caspase activity. The other way oxidative stress reduces the agent's efficiency is by generating lipid peroxidase that targets the death receptor CD95 pathway (Ashkenazi and Dixit 1998).

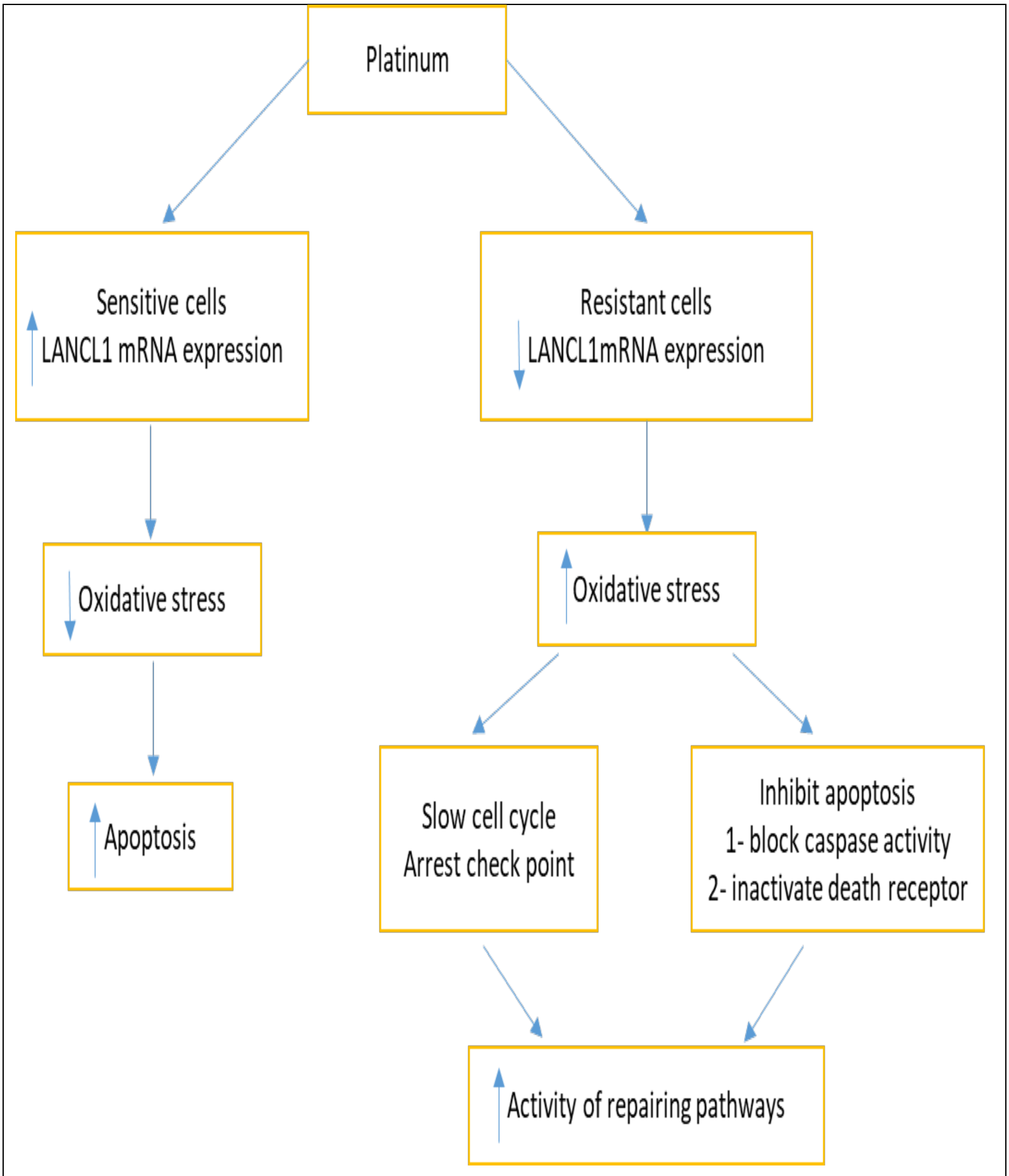

Figure 4.30: A proposed model for the oxidative stress-mediated activation of survival pathways in low versus high *LANCL1* express in NSCLC treated with platinum, based on data in the current study.

LANCL1 can be used as a good marker for NSCLC progression under the platinum therapy, due to the fact that low *LANCL1* mRNA expression can be used as a marker for poor NSCLC progression. *LANCL1* expression regulator the defence against oxidative stress. Therefore, NSCLC patients who have low LANCL1 expression and are treated with platinum, may show increase in oxidative stress levels, which may affect chemosensitivity. As mentioned previously, decreased LANCL1 mRNA expression lead to reduced cell defence against oxidative stress which is elevated under platinum therapy. Therefore, using antioxidants during chemotherapy will increase the affinity of the drug (Conklin 2004; Zhen et al. 1992).

Most likely, deregulated epigenetic control of lung tumours depend on what is shown before overexpressing of *LANCL1* in lung tumours and NSCLC cell lines, that led us to investigate more whether *LANCL1* expression is under epigenetic control. We previously investigate the methylation state of *LANCL1,* and we determined that lack of DNA methylation in the promoter of the gene in NSCLCs (Figure 4.9). Consequently, it was obvious to examine another major epigenetic factor, which is histone deacetylation.

Our investigation showed the sodium valproate treatment of all, but one NSCLC cell line tested resulted in an increase in *LANCL1* expression compared to the untreated cells (Figure 4.29). Sodium valproate (VPA) is a histone deacetylace inhibitor (HDACi) and can therefore activate the expression of a large number of genes, subsequently altering various phenotypic characteristics, such as cell proliferation or apoptosis (Figure 1.8) (Bose, Dai, and Grant 2014). At this moment, it is not clear whether VPA has a direct effect on the LANCL1 promoter (i.e. whether this promoter is subject to histone deacetylation) or it is a secondary effect, i.e. as a result of other overexpressed proteins, following HDAC inhibition, binding LANCL1 promoter.

4.4 Conclusion

To sum up, the results found that *LANCL1-AS1* diminished in both lung cancer tissues and NSCLC cell lines, therefore we discovered that *LANCL1* is highly expressed in lung cancer tissues and NSCLC cell lines. However, there was no correlation between *LANCL1-AS1* and *LANCL1*. Also, lack of DNA methylation in the promoter of the gene in NSCLCs. We determined that *LANCL1* expression increases in NSCLC cell lines after exposure to H2O2, which means *LANCL1* may play a role in protecting NSCLC cell lines from oxidative stress.

Furthermore, overexpressed *LANCL1-AS1* increased cell proliferation, migration and invasion, while knocked down *LANCL1* reduced in cell proliferation and migration. Following, we found that both overexpressed *LANCL1-AS1* and knocked down *LANCL1* clones increase the NSCLC sensitivity from the H_2O_2. Also, both clones had sensitized SK-MES-1 NSCLC cell line for gemcitabine and vinorelbine. In contrast, both clones increase the resistance to platinum.

Chapter 5: Exosomes' Role in Drug Resistance

5.1 Introduction

We have previously seen in chapter 4, that modulation of *LANCL1-AS1* expression affected the response of NSCLC cells to gemcitabine and VRL (figures 4.17, 4.18). Given the bystander effect that exosomes can induce (Samuel et al. 2017), we therefore decided to assess this in relation to *LANCL1-AS1* expression and test whether the observed *LANCL1-AS1*-dependent sensitivity modification can be transferred through exosomes.

It is now well established that EVs function as cargo transporters between cells, carrying multiple components and facilitating cell-cell communication. The list of protein and nucleic acid cargo of EVs is constantly growing in the literature. Interestingly, *LANCL1* was identified as one of the cargo proteins in extracellular vesicles (ExoCarta 2016). While this observation does not necessitate a role for *LANCL1* in EV biogenesis, it was certainly an intriguing research question to ask: does it affect exosome release?

Therefore, w*e set up a series of experiments to provide answers for the following questions.*

a) Do *LANCL1* and *LANCL1-AS1* expression levels determine the number of EVs released from cells?

b) Oxidative stress is known to trigger EVs release; do *LANCL1* and *LANCL1-AS1* interfere in this process?

c) *LANCL1* knock-down and *LANCL1-AS1* overexpression increase the sensitivity to gemcitabine; is this effect associated with an alteration in EV biogenesis?

d) Can *LANCL1-AS1* induced sensitivity to gemcitabine be transferred through conditioned media and/or EV transfer to cells with low *LANCL1-AS1* expression?

5.2 Results

5.2.1 Pilot test to select EVs Harvesting time.

At first, we assessed the effect of *LANCL1* and *LANCL1-AS1* expression on EVs release. A preliminary experiment was performed to establish the time of culture required to gain an EVs count high enough to be measurable by Nanosight (Malvern). As described in the methods section, once the medium had been harvested for EVs quantification, the total cellular protein was measured (BCA assay), in order to obtain an accurate estimate of the number of cells producing the EVs. In all analyses presented below, we have utilised a Normalised EVs Count, conducted using Nanosight, divided by the protein concentration of the producing cells. As can be seen in Figure 5.1, there is an increasing number EVs count in relation to time of culture, as expected. However, differences were observed in this pilot regarding the EVs count per time slot in relation to *LANCL1,* increase in EV count is only observed at 12 and 24 h. In fact, a difference is observed in the knockdown clones (A6/26 and A9/10), however a similar reduction was observed in the scrambled, therefore it can by hypothesised that this difference is related to transfection stress rather than the *LANCL1* expression. Indeed, an independent experiment (Figure 5.2) at 9 hours harvesting confirmed this lack of difference; more specifically, only one of the two clones (A6/26) showed a borderline reduction compared to scrambled, thus there is no strong evidence to support the involvement of *LANCL1* in the EV biogenesis.

In contrast, *LANCL1-AS1* overexpression in the pilot experiment (Figure 5.1) seemed to exert a certain positive effect on the EVs count. This was also confirmed by an independent experiment at 9h harvesting (Figure 5.3). As *LANCL1-AS1* expression in this inducible model is manipulated by coumermycin/novobiocin, the parental SK-MES-1 cells were also exposed to these reagents, demonstrating no differences in the normalised EVs count (Figure 5.4). The reason for choosing harvesting at 9 hours is that the aim of the experiment is to assess the potential effect of exosomes representing cells early reaction to drug exposure rather than the exosomes representing just the surviving fraction after prolonged exposure. At the same time, we wanted to have a count high enough to measure on the Nanosight, and the 9-hour slot combines these two characteristics.

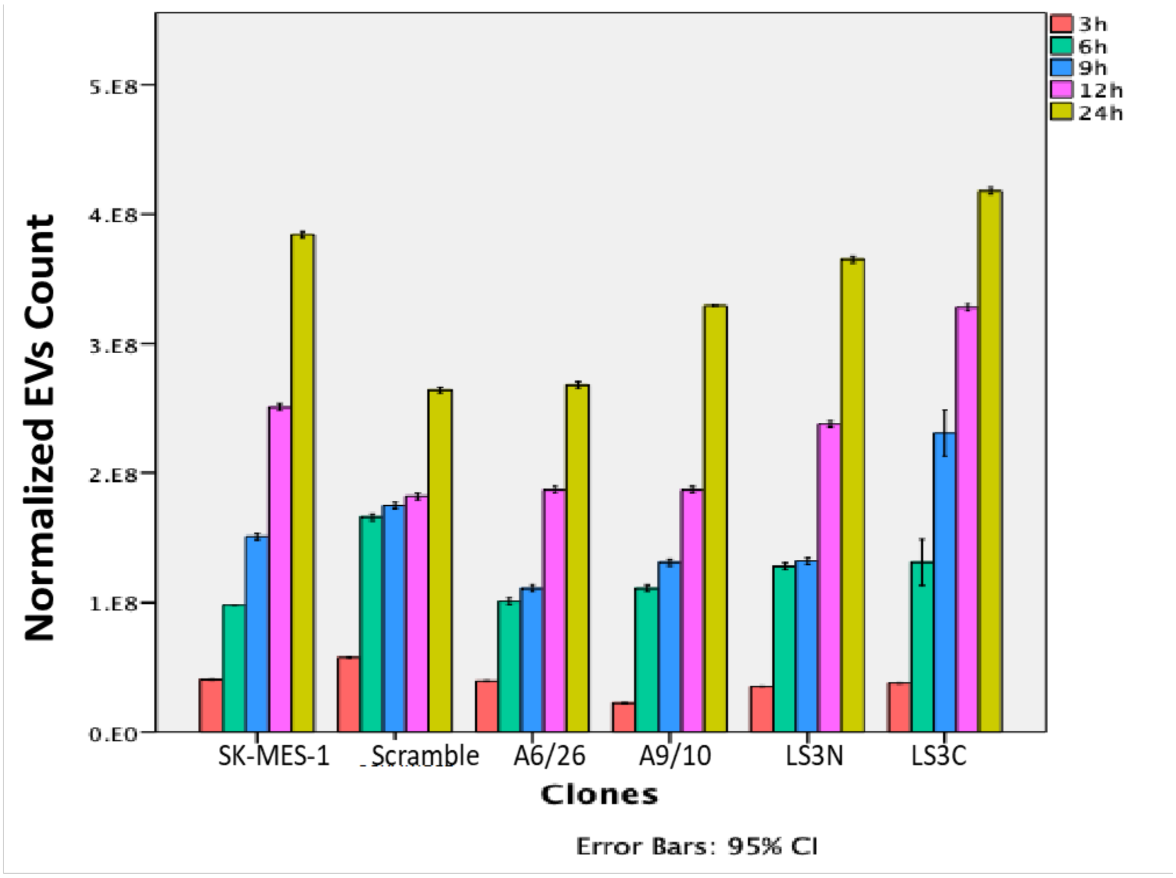

Figure 5.1: *The bar charts represent the variable values of exosomes released from parental, scramble and clones' cells in different incubation period.* The mean and error values in all graphs are the six technical replicates, and the error bars represent 95% confidence intervals.

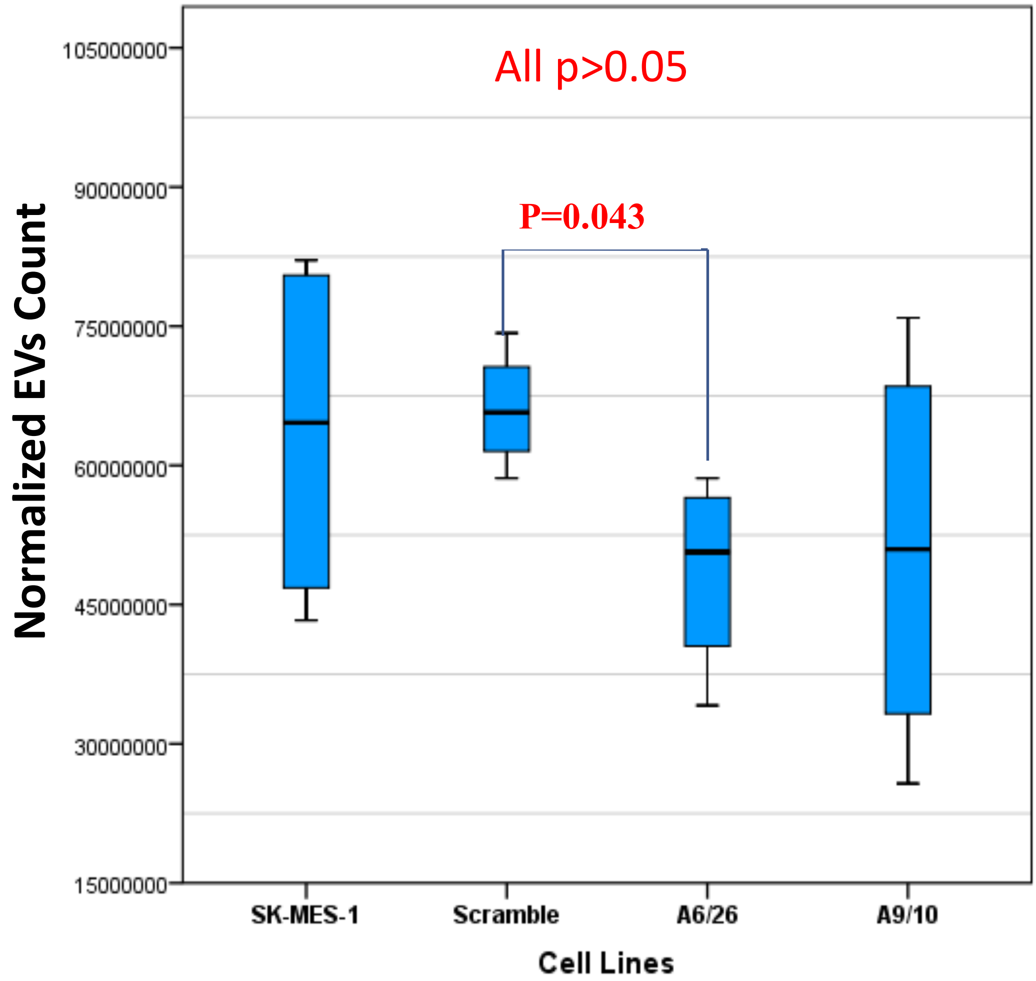

Figure 5.2: *Boxplots displaying the number of the EVs released by parental, scrambled and knocked down LANCL1 clones, nine hours post seeding*. No significant statistical difference is observed, with the exception of a borderline trend between scrambled and A6/26. In the absence of reproducing such a difference with the second shRNA oligo (A9), this borderline difference was considered as an off-target effect.

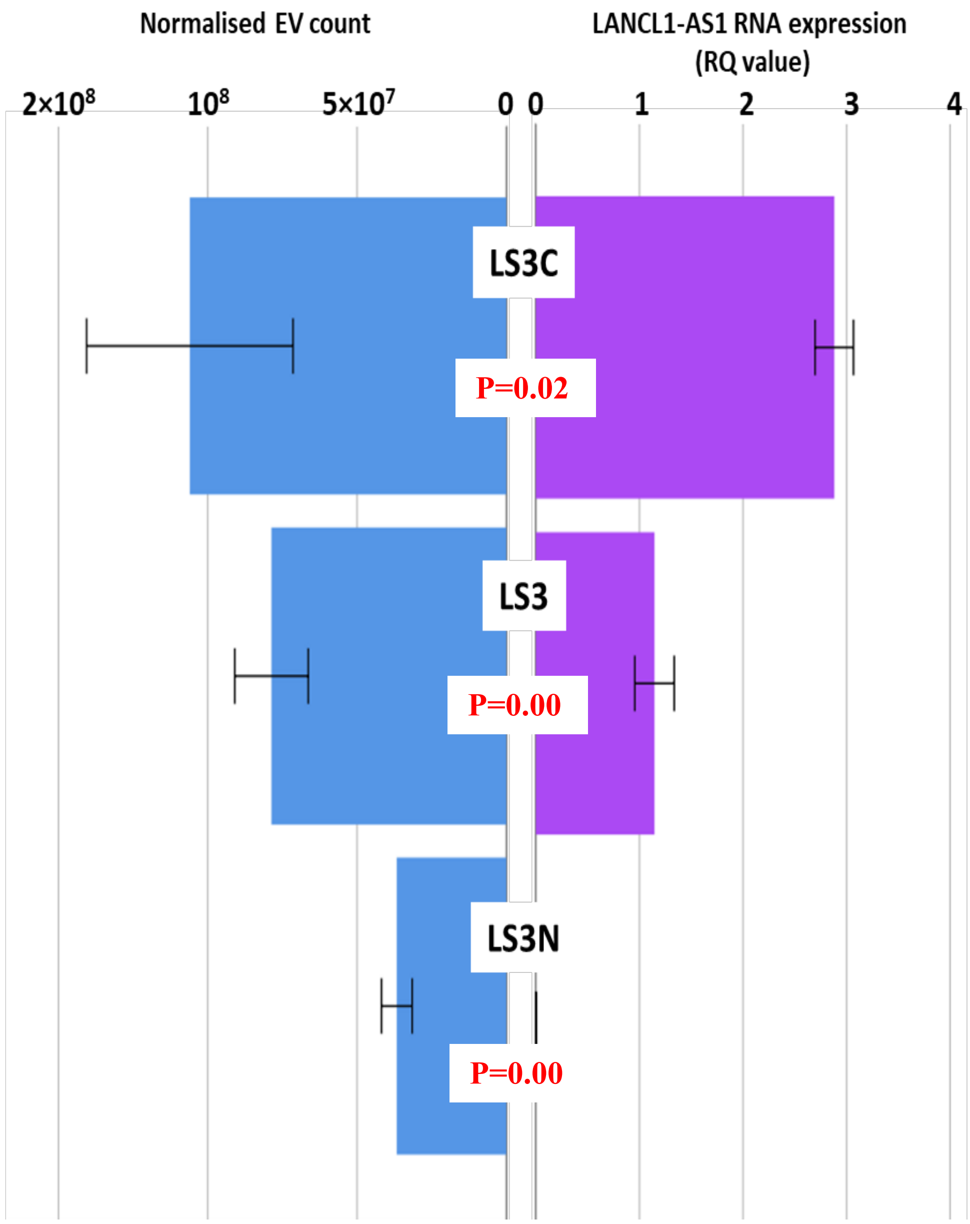

Figure 5.3: *The EV release is affected by LANCL1-AS1 expression in a dose-dependent manner.* There is an apparent increase of released EVs (normalised by total protein of producing cells) corresponding to the expression of *LANCL1 -AS1* in LS3 cells exposed to novobiocin (LS3N), controls LS3 cells and LS3 cells exposed to coumermycin (LS3C). Error bars represent 95% confidence intervals. (Mann Whitney).

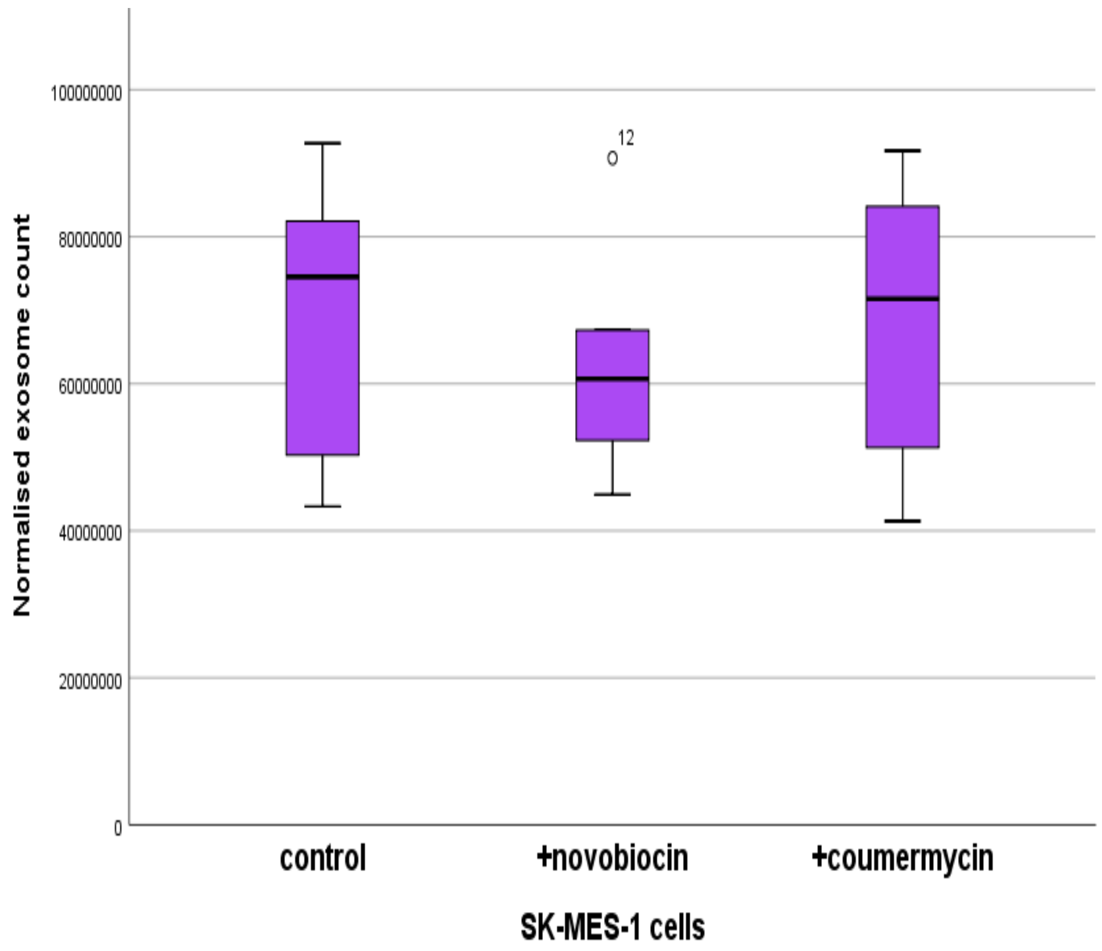

Figure 5.4: *Boxplots demonstrating that EVs release by parental cell in response to exposure to coumermycin/novobiocin*.

5.2.2 EVs release under oxidative stress on cells containing knocked-down *LANCL1*

Having assessed the EVs count changes in relation to *LANCL1* and *LANCL1-AS1* expression under normal conditions, we performed a series of experiments to study the release of exosomes under oxidative stress. We therefore exposed parental cells, scramble and clones to H2O2 for nine hours. The results revealed a significant increase in the amount of EVs release under oxidative stress in both clones A6/26 and A9/10, as well as the parental and the scrambled cell lines (Mann-Whitney test, $p=0.014$, $p=0.019$, $p=0.021$ and $p=0.02$ respectively) (Figure 5.5). As in the case of normal conditions, *LANCL1* expression did not affect the EVs count under oxidative stress ($p>0.05$).

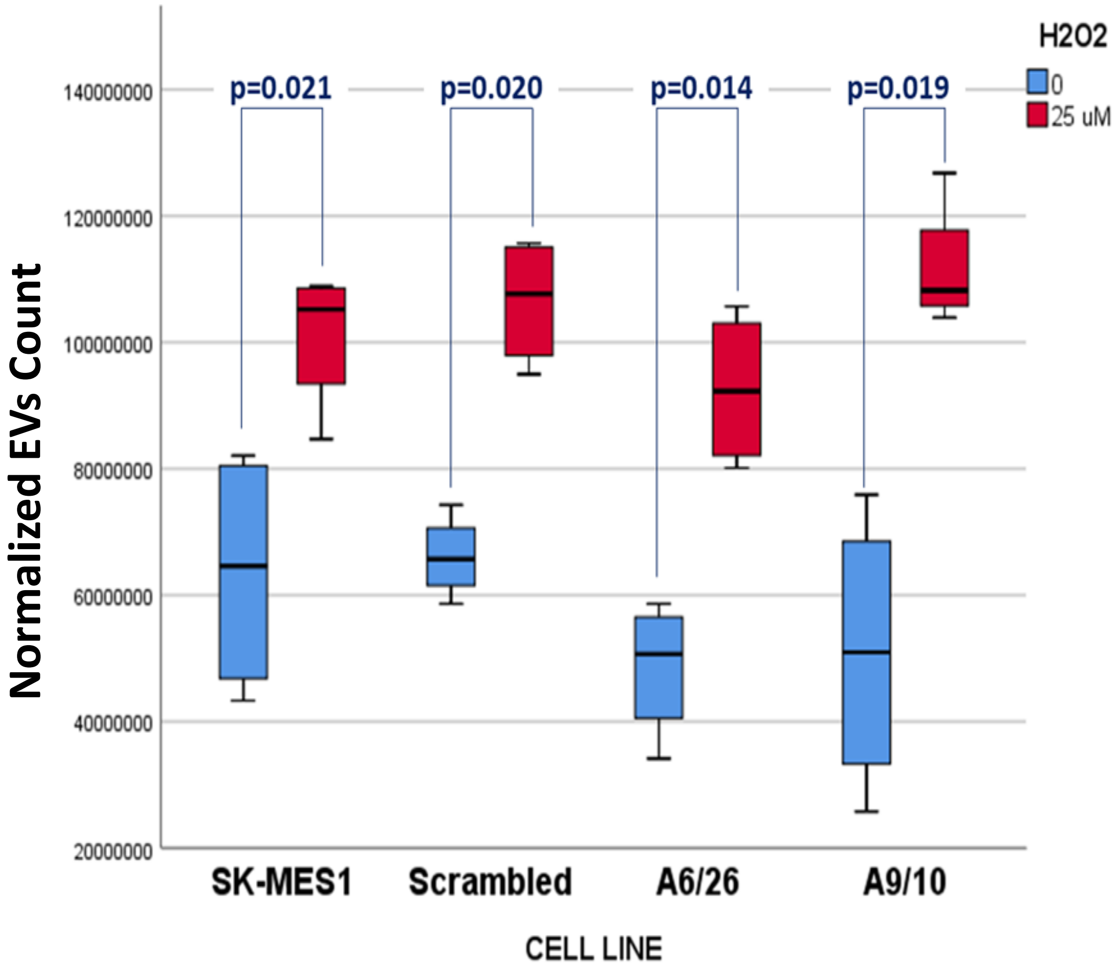

Figure 5.5: *Boxplots demonstrating the number of EVs released after treatment of the parental, scrambled and the LANCL1 knock-down clones with 25 µM of H2O2 for nine hours.* The number of EVs released increases significantly in all the cell lines under oxidative stress. The parental, scramble and LANCL1 knock-down clones behave similarly under oxidative stress.

5.2.3 EV Release under Oxidative Stress on overexpressed *LANCL1-AS1*

The same procedure was followed in this experiment for incubation of the overexpressed *LANCL1-AS1* clones for nine hours with 25 µM of H2O2, to assess the effects of oxidative stress. Interestingly, the LS3N clone (low *LANCL1-AS1* expression) demonstrated a significant increase under the oxidative stress (Mann Whitney test, $p=0.004$). However, this difference was significantly reduced in the LS3C (high *LANCL1-AS1* expression) clone ($p=0.083$) (Figure 5.6).

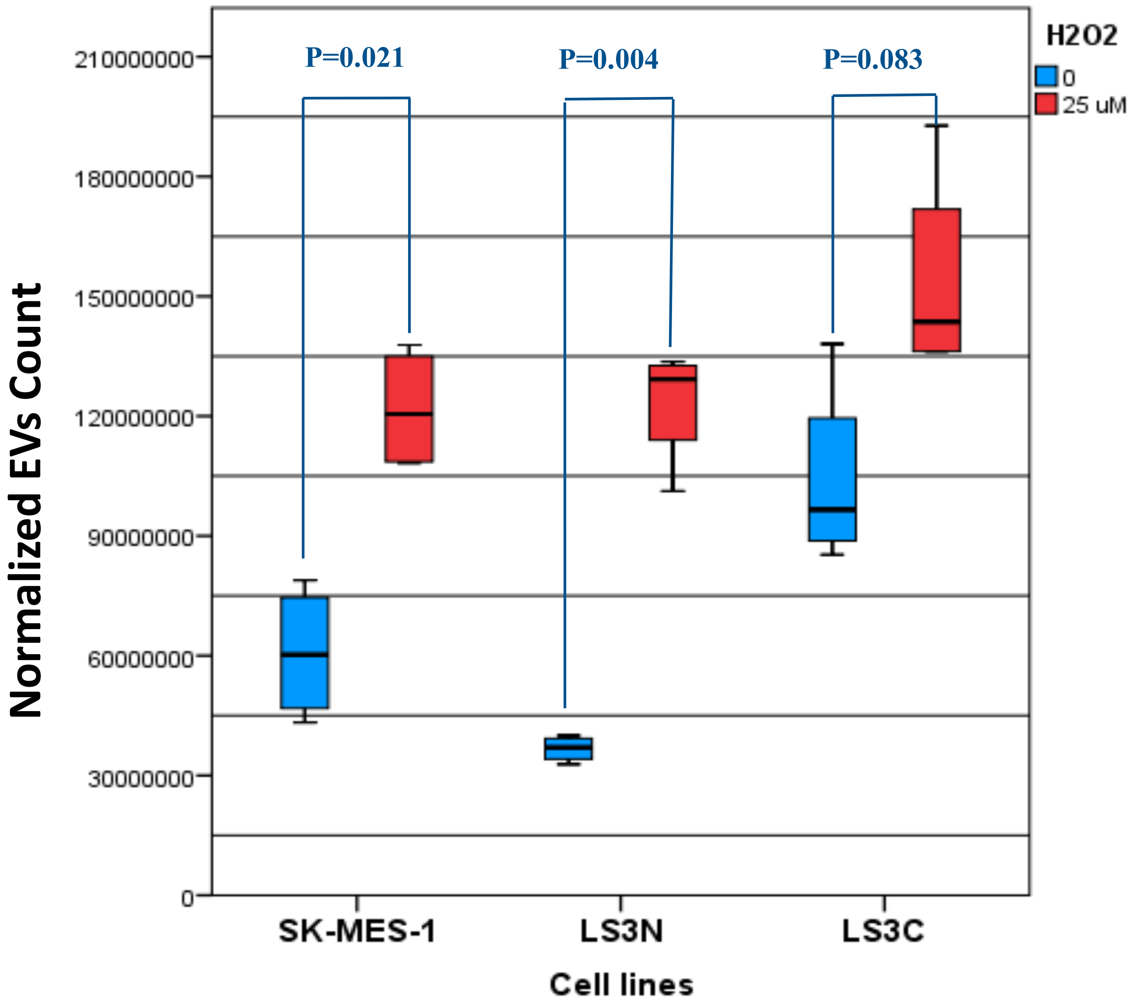

Figure 5.6: *Boxplots representing the number of EVs released in overexpressed LANCL1-AS1 after treatment with 25 µM of H2O2 for nine hours.* The number of the EVs released increases significantly in the parental and the lower expression of LANCL1-AS1 (LS3N) clone under oxidative stress, while it doesn't change in high expression of LANCL1-AS1 (LS3C) clone under the oxidative stress.

5.2.4 Rate of Releasing Extracellular vesicles under Gemcitabine treatment on cells containing knocked-down *LANCL1*

The *LANCL1* knocked-down clones treated with 0.06 µM of gemcitabine and incubated for nine hours. The result showed a slight increase in the rate of releasing EVs from the knocked-down *LANCL1* clones A6/26 and A9/10 after treatment with gemcitabine compared with the unexposed cells, while the SK-MES-1 parent cell line shows no difference in the number of EVs release after treated with GM. Mann Whitney test, $P>0.004$ in all the results (Figure 5.7).

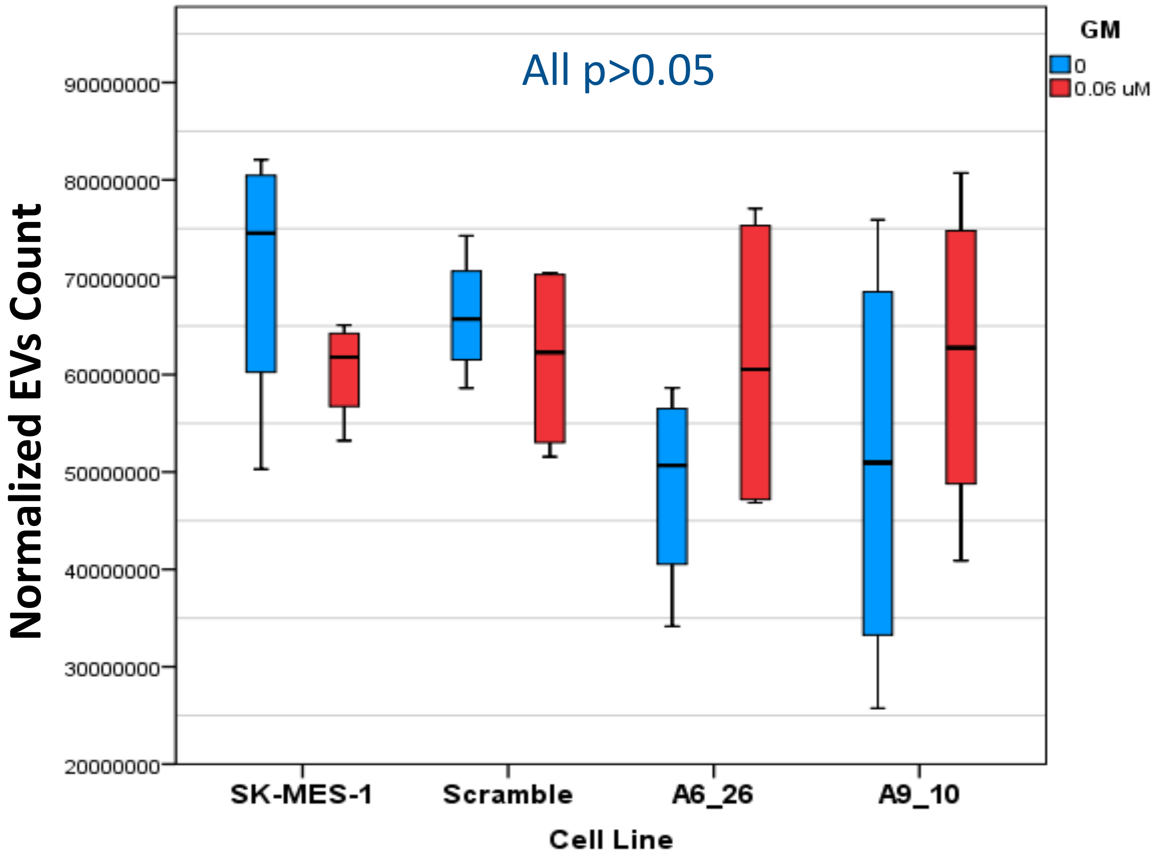

Figure 5.7: Boxplots displaying *the number of EVs released after parental, scramble and knocked-down LANCL1 expression clone's treatment with* 0.06 µM *gemcitabine for nine hours*. The number of EVs released does not change significantly in all the cell lines under the treatment with gemcitabine.

5.2.5 Rate of Releasing Extracellular vesicles under Gemcitabine treatment on overexpressed *LANCL1-AS1* clone

The *LANCL1-AS1* overexpression clones were treated with 0.06 µM of gemcitabine and incubate for nine hours. The result revealed that overexpression of *LANLC1-AS1* clones (LS3C) showed a slight decrease in the number of EVs released after treatment, with gemcitabine comparison with unexposed counterpart, while there was no significant change in the number of EVs released from (LS3N) lower expression of *LANCL1-AS1*. Mann Whitney test, P>0.004 in all the results (Figure 5.8).

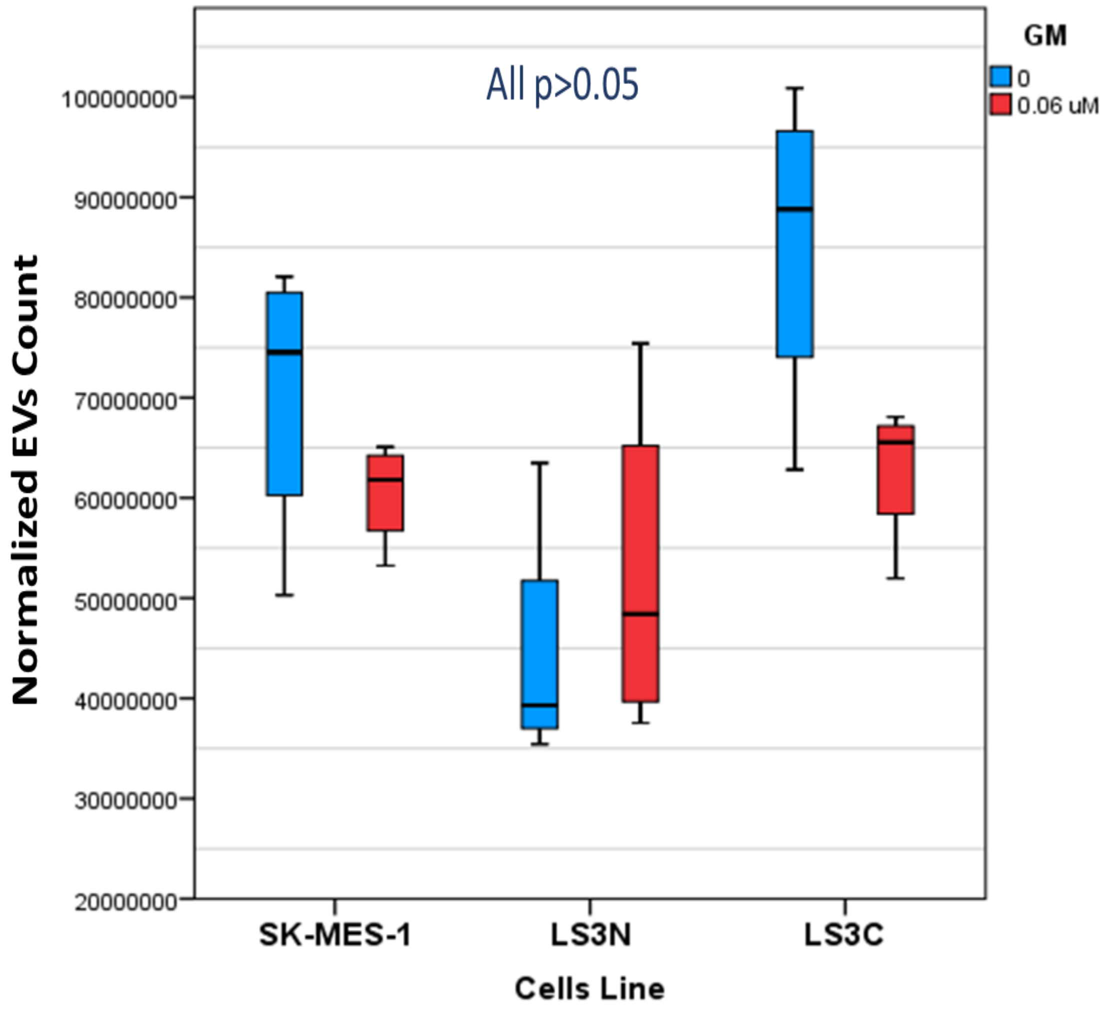

Figure 5.8: *Boxplots demonstrating the number of EVs released after treatment with 0.06 μM gemcitabine incubate for nine hours in overexpressed LANCL1-AS1 clone.* The number of EVs released does not change significantly in all the cell lines under the treatment with gemcitabine.

5.2.6 Exchange of conditioned medium between clones with different *LANCL1-AS1* expression.

As mentioned in Chapter 4 (section 4.2.7.1), the rate of cell growth increased in high expressed *LANCL1-AS1* clone LS3C in comparison with the low expressed *LANCL1-AS1* LS3N (Figure 4.13). Having seen the effect of *LANCL1-AS1* in EV release, we decided to examine whether exchanging of serum free (SF) conditioned media between high and low *LANCL1-AS1* expressing cells might have an effect on proliferation (Figure 5.9). The results showed that, in comparison to control (LS3 supplemented with fresh SF medium and novobiocin), the addition of medium conditioned in LS3 cells with novobiocin (autologous, low *LANCL1-AS1* expression) triggered a reduction in proliferation (Figure 5.9). This most likely represents the exhaustion of the growth factor cocktail (see materials and methods) used to supplement the SF medium, as all these are quite liable and they have been at 37oC for the 48h of conditioning. However, the addition in the LS3 cells of the medium conditioned in LS3-coumermycin cells (heterologous – high *LANCL1* expression) triggered a massive reduction in cell proliferation (Figure 5.9).

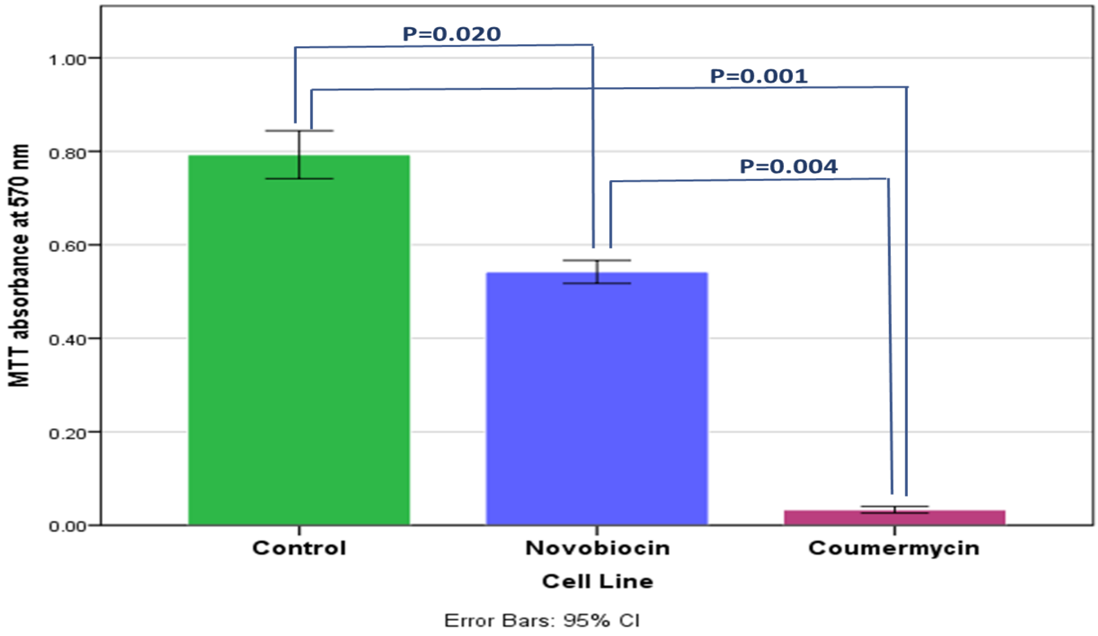

Figure 5.9: The effect of conditioned media exchanging between cells with different *LANCL1-AS1* expression. LS3 cells were grown in serum free medium containing novobiocin (control – green bar). When confluence reached 40%, the medium was replaced by serum free media conditioned for 48h in LS3 cells grown in novobiocin (autologous – blue bar) or coumermycin (heterologous – purple bar). Cells were grown in pre-conditioned media for 48 hours before the MTT assay. The reduction in replication shown in the autologous medium replacement most probably reflects the partial exhaustion of medium resources as the growth factors in SF-media are being degraded (control receives fresh SF medium with supplements for the corresponding 48h incubation). In contrast, the heterologous replacement with media from cells with high *LANCL1-AS1* expression, causes a significant reduction on the target cells (with low expression of *LANCL1 -AS1*). The mean and error values in all graphs represent six technical replicates, and the error bars represent 95% confidence intervals. (Mann Whitney test).

Moreover, we tested whether exchanging of serum free (SF) conditioned media might affect the action of gemcitabine (0.06 μM) between high (coumermycin) and low (novobiocin) *LANCL1-AS1* expressing cells. The results showed that the proliferation inhibition caused by media conditioned in LS3 cells with novobiocin (Mann Whitney test, P=0.043) or coumermycin (Mann Whitney test, P=0.053) cause a reduction of the relative toxicity of gemcitabine (Figure 5.10).

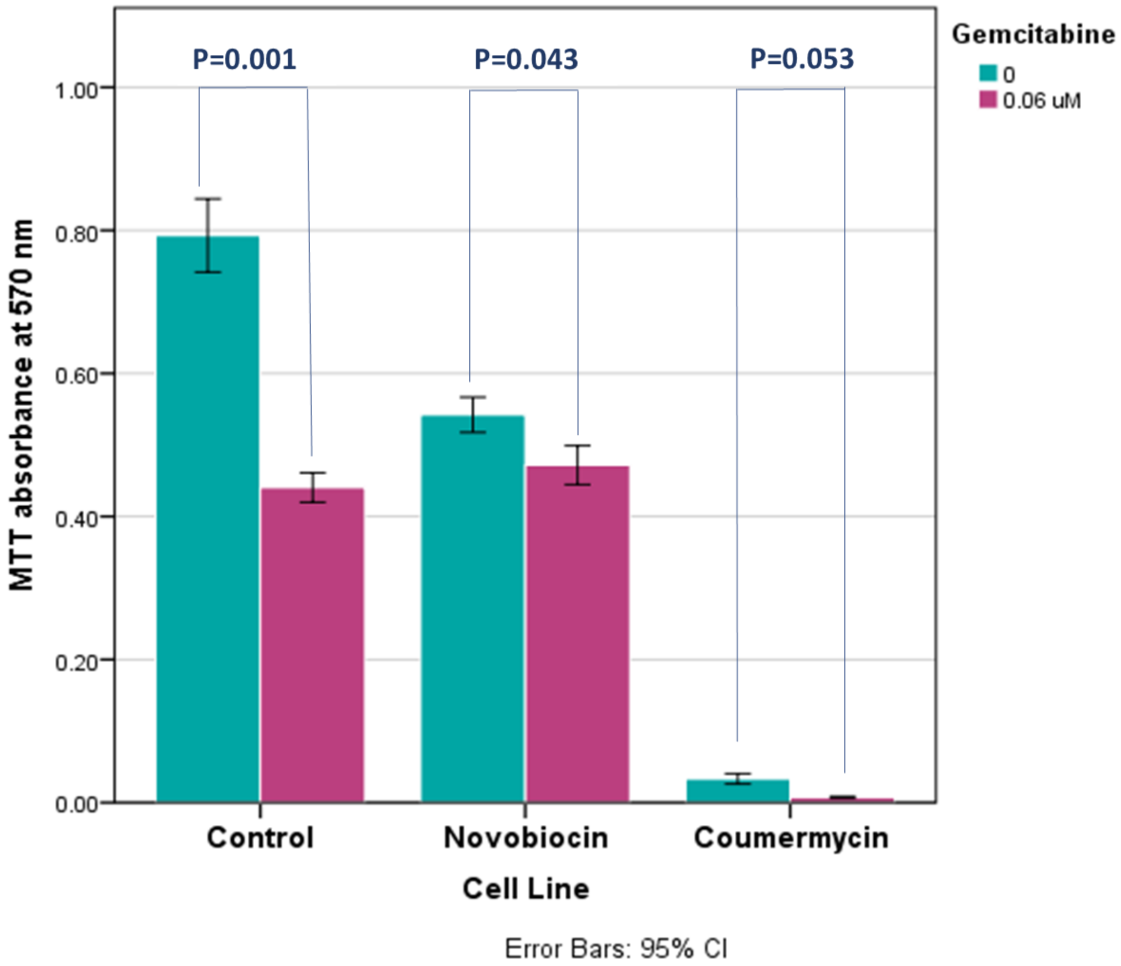

Figure 5.10: *Exchange the unconditional medium added to 0.06 µM of gemcitabine to overexpressed LANCL1-AS1 clone.* A significant reduction in cell replication was shown in the parental after being treated with gemcitabine. Borderline reduction was shown in autologous medium replacement from cells with low LANCL1-AS1 expression (novobiocin) with GM, and heterologous medium replacement from cells with high LANCL1-AS1 expression (coumermycin) with gemcitabine. The mean and error values in all graphs represent six technical replicates, and the error bars represent 95% confidence intervals.

5.2.7 Exchange EVs from Sensitive to Resistance Cell Line

The conditioned media contain both soluble growth factors and small EVs, as the large EVs have been removed during filtration through 0.22 μm filter. We therefore extended our experiments to investigate the effects of supplementing only EVs from LS3 cells with high (coumermycin) and low (novobiocin) *LANCL1-AS1* expression. EVs' input was normalized by protein quantification prior to supplementation as the Nanosight measurement accuracy is not high enough to support this experiment. In contrast to the conditioned media experiment (Figure 5.13), the supplementation of EVs does not demonstrate any significant difference between high and low *LANCL1-AS1* expression of the donor cells (Figure 5.11).

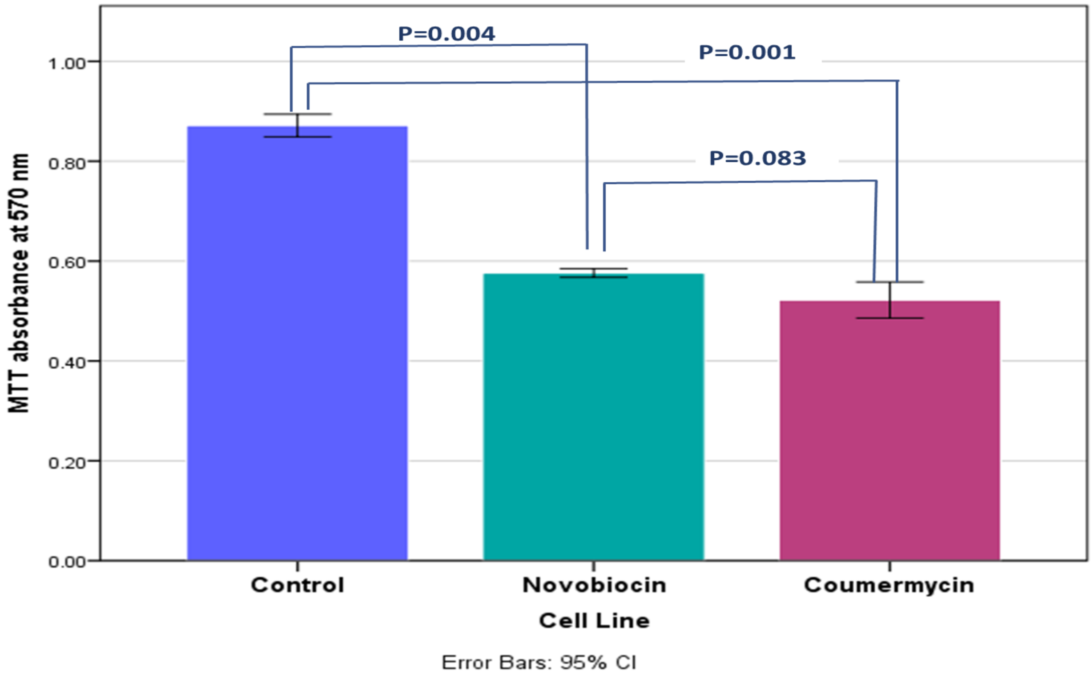

Figure 5.11: The effect of autologous and heterologous EV supplementation comparing cell sources with high and low *LANCL1-AS1* expression. LS3 cells were grown in serum free medium containing novomycin (control – blue bar). Once confluence had reached 40%, the medium was replaced by serum-free media supplemented with EVs from LS3 cells grown in novomycin (autologous – green bar) or coumermycin (heterologous – purple bar). Cells were grown for further 48 hours prior to the MTT assay. The reduction in replication shown in the autologous medium most probably reflects the toxicity from the EVs elution buffer, indicating that longer dialysis in PBS should have been performed prior to supplementation. The heterologous supplementation does not confer a different effect in proliferation. The mean and error values in all graphs represent six technical replicates, and the error bars represent 95% confidence intervals.

5.2.8 Exchange of Exosomes from Sensitive Cell Line to Resistance Cell Line Treated with Gemcitabine

In this experiment, we aimed to determine the effects of gemcitabine 0.06 μM added only to EVs from LS3 cells with high (coumermycin) and low (novobiocin) *LANCL1-AS1* expression, EVs input was normalized by protein quantification. Similar to the conditioned media experiment with gemcitabine (Figure 5.10), the supplementation of EVs with of gemcitabine does not demonstrate a significant difference between high and low *LANCL1-AS1* expression of the donor cells (Figure 5.12).

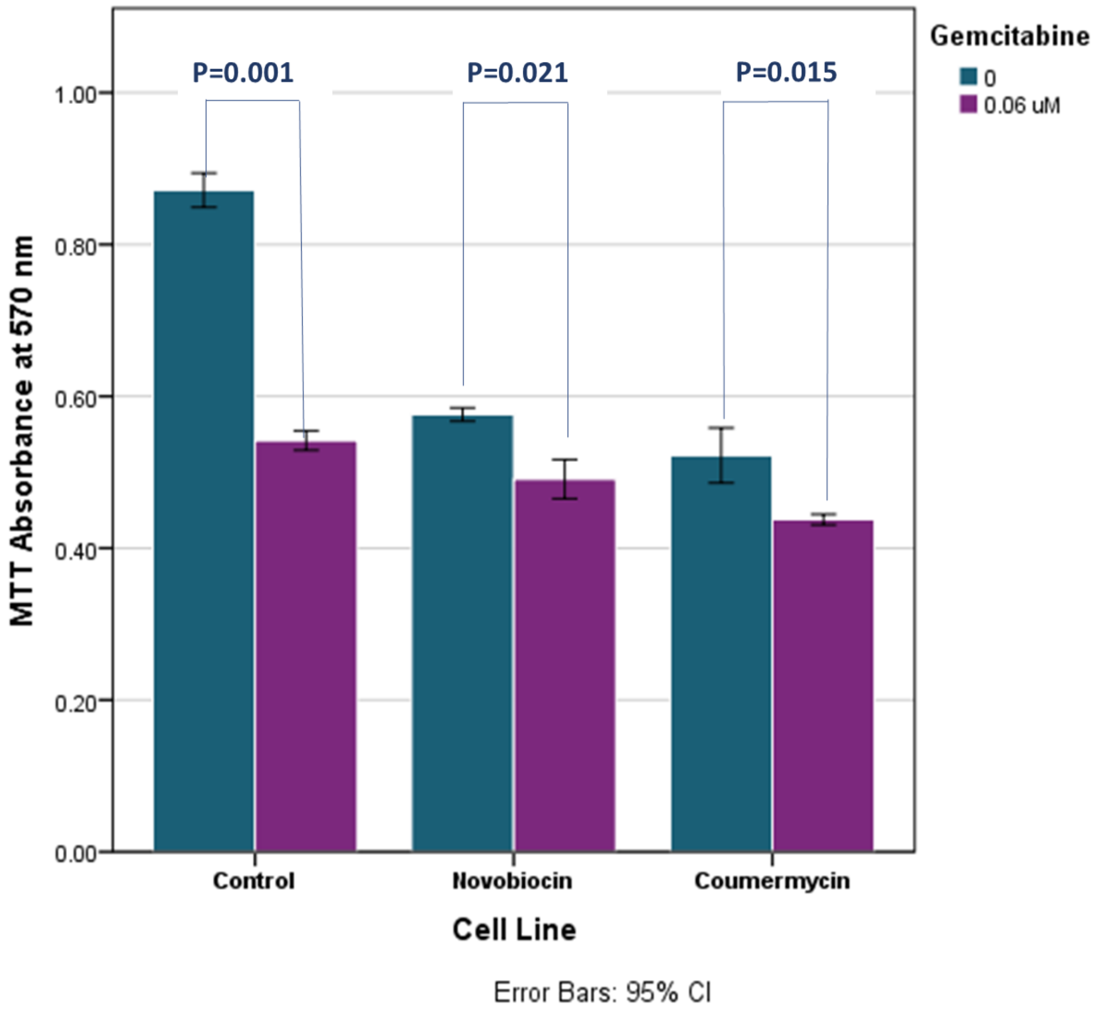

Figure 5.12: *The exosomes were exchanged with 0.06 µM of gemcitabine in overexpressed LANCL1-AS1 clone.* A significant reduction in cell replication was shown in the parental after being treated with GM. Also, a significant reduction was shown in autologous (novobiocin) and heterologous (coumermycin) EVs supplements with gemcitabine. The mean and error values in all graphs represent six technical replicates, and the error bars represent 95% confidence intervals.

5.3 Discussion

Extracellular vesicles (EVs) play an essential role in cell communication as well as the pathogenesis of many diseases including cancer (Riches et al. 2014). It has been determined that EVs release is frequently higher in cancer cells. Furthermore, elevated EV release may influence chemotherapy resistance and even mediate the transfer of resistance information between cells (Sweeney, Richards, and Hill 2017). In view of this study's results, namely that *LANCL1* and *LANCL1-AS1* expression changes can influence the resistance to gemcitabine and VRL, we have investigated the hypothesis that EVs may mediate this action. First, we examined the role of *LANCL1* and *LANCL1-AS1* expression in the rate of EVs release. In addition, the effect of oxidative stress and chemotherapy with regard to the number of EVs discharge was explored. Finally, we designed an experiment to investigate whether exchanging EVs between cells with different *LANCL1-AS1* expression and consequent sensitivity to gemcitabine demonstrate a bystander effect; in other words, LS3 grown in coumermycin overexpresses *LANCL1-AS1* and is more sensitive while LS3 grown in novobiocin has a low *LANCL1-AS1* expression and is less sensitive to gemcitabine.

Our results showed no major difference in the number of EVs released by the knockeddown *LANCL1* clones compared to the scrambled and parental cell line SK-MES-1. Only a borderline effect was seen in one of the two clones. *LANCL1* protein has been identified as a frequent cargo of human exosomes from different tissues (including lung and kidney) and cell lines (ExoCarta 2016). This fact, of course, does not necessitate the dependence of exosome biogenesis to *LANCL1*. Currently, there is no published information regarding the role of *LANCL1* in EV regulation, therefore we are conscious that our result comes from a single cell line, i.e. a single genotype. As a result, *LANCL1* may contain certain effectors in its EV-related function that are missing from SK-MES-1. The cell line's karyotype reveals that normal X, 13, and 19 chromosomes were absent and chromosomes 2, 3, 14, 17 and 20 were generally monosomic (ATCC 2019). Therefore, this question ought to be expanded in many other cell lines before a clearly shaped conclusion can be reached.

In contrast, to the non-significant EV changes seen in *LANCL1* knockdown, the difference in expression of *LANCL1-AS1* in the inducible LS3 clone triggered a substantial corresponding difference in EV release. More specifically, it is worth mentioning that EV count shows a dose response effect to *LANCL1-AS1* expression (Figure 5.3). While high *LANCL1-AS1* expression results in high *LANCL1* expression in LS3 cells, the absent or moderate effect of the latter on the EV count suggests that the EV effect of *LANCL1-AS1* is probably a *LANCL1*-independent function.

The next question posed in this study was whether *LANCL1/LANCL1-AS1* expression influences the EV release under the conditions of oxidative stress. According to (Szypowska et al. 2011), the defence to oxidative stress depends on reprogramming the transcriptional profile of the cell. In addition, it has been suggested that exosomes may mediate protective signals in response to oxidative stress, based on the argument that exosomes released from cells exposed to oxidative stress can transfer protection from oxidative stress to recipient cells, which were not exposed to the stress (Eldh et al. 2010). The alteration in exosomes phosphoprotein content under oxidative stress has emphasised the role played by exosomes in mediating cell–cell signalling during physiopathological events (Biasutto et al. 2013). It has also been demonstrated that oxidative stress can enhance EVs secretion, while soluble NKG2D ligands stimulate the impairment of the cytotoxic response (Hedlund et al. 2011).

In agreement with all the relevant literature so far, including SK-MES cells (Saeed-Zidane et al. 2017), our result shows that under oxidative stress, EVs release increased significantly in all of the tested cell lines. *LANCL1* has a well-established role in protecting cells, particularly neurons, from oxidative stress (Zhong et al. 2012) and this was also confirmed in our cells in chapter 4 (Figure 4.25). However, *LANCL1* knockdown did not have an effect on the EV count released under oxidative stress, thus suggesting that this function is probably not accomplished through changing the released EV count.

Moreover, *LANCL1-AS1* overexpression results in a significantly higher EV count under normal conditions, while high *LANCL1-AS1* expression has only a moderate effect under oxidative stress (Figure 5.5). At this moment, it is difficult to assess the significance of this observation, especially as *LANCL1-AS1* function is largely not known, therefore the need for further research. One hypothesis may be that overexpressing *LANCL1-AS1* cells approach the EV production capacity of these cells under normal conditions, therefore the EV release reaches a plateau, a hypothesis which, of course, requires experimental verification.

It has been previously shown that cells release more EVs when exposed to chemotherapeutics (Sweeney, Richards, and Hill 2017). In this study, we tested the effect of gemcitabine on EV count, given the fact that both *LANCL1* knock-down and *LANCL1-AS1* changed the response of cells to this drug. However, the findings presented in this chapter show no significant change in the EV count of any of the cell lines/clones treated with gemcitabine; in fact, only limited information on gemcitabine's influence on EV release is provided within specialised literature, such as a few studies showing that gemcitabine exposure increases EV release in pancreatic cancer cells (Sweeney, Richards, and Hill 2017) and cancer-associated fibroblasts (CAF) (Richards et al. 2017), with no relevant results on any other cancer cell type.

Despite the lack of quantitative changes in the EV count by gemcitabine, the question whether qualitative changes in EV cargo might be influenced by the drug and to what extent this might be communicated to other cells arose. Even if this question occurred at a late stage of this PhD study, with limited time and resources to explore the cargo profile, it was possible to assess the ability of EV-mediated phenotypic alterations in recipient cells induced by EVs with different *LANCL1-AS1* levels. As *LANCL1-AS1* affected proliferation (Figure 4.13), we tested the hypothesis that this effect might be transferred through EVs. The first pilot set of experiments was to test medium conditioned in LS3 cells grown in novobiocin (low *LANCL1-AS1*) and coumermycin (high *LANCL-AS1*). The recipient cells were LS3 cells grown in novobiocin, therefore the transfer of EVs from cells with novobiocin (LS3N) is considered autologous, while the transfer from cells grown in coumermycin (LS3C) as heterologous. Interestingly, the heterologous transfer caused a significant reduction in proliferation, greatly differing from the observed autologous one. The reduction seen in the autologous media transfer is most likely due to the weakening of the labile growth factor supplements during the 48 hours of conditioning (Figure 5.8).

However, the subsequent experiment using isolated EV supplementation did not confirm this finding (Figure 5.10), for which there are a number of possible explanations for this, both technical and biological. First, from a technical point of view, the observed reduction in the autologous supplementation (Figure 5.10) can only be explained as toxicity by the EV elution buffer, as cells were supplemented with fresh growth factors in this experiment. Indeed, we are aware that the elution buffer (XE buffer, Qiagen) is highly toxic to the cells from early pilot experiments. Therefore, for this experiment, EVs eluates were dialysed twice against 1 L of PBS for 30 min each. However, it became apparent that this is not enough to remove all the

XE buffer, therefore leaving residual toxins. As these were the last set of experiments in this PhD study, unfortunately there was no time to repeat the experiments with altered conditions.

Another technical reason is that EVs isolated with the ExoEasy kit tend to aggregate in larger complexes, which may significantly reduce the absorption of EVs in recipient cells, a result based on Nanosight readings, communicated by Dr Amelia Acha Sagredo. However, from a biological point of view, looking at the result of the conditioned medium exchange, there is a significant negative effect on proliferation exerted by medium conditioned in high *LANCL1-AS1* expressing cells. Apart the technical difficulty discussed above, the lack of reproduction of this effect in EVs suggests that the effect may be due to soluble factors and/or >220nm EVs released by LS3C cells. It must be reminded that EV isolation includes an initial filtration through 0.22 µm filters.

The final experiments in this chapter addressed the question of *LANCL1-AS1* expression, which changes the sensitivity of cells to gemcitabine, to influence the EV-mediated phenotypic response of cells to this drug. Our experiment, which used either filtered conditioned media or isolated EVs, demonstrated only borderline changes. Therefore, the potential technical difficulties explained above are deemed to hinder the ability to draw clear conclusions. One can speculate though that the reduction in proliferation induced EV supplementation from *LANCL1-AS1* overexpressing cells might be a reason for the moderated sensitivity to gemcitabine, as the effectiveness of the drug is increased by high proliferation levels.

5.4 Conclusion

To summarize, our experimental evidence demonstrates that that *LANCL1* expression does not affect the rate of EVs released. In contrast, *LANCL1-AS1* expression appears to stimulate EV release. Moreover, our results are concordant with the literature showing increased EVs release under oxidative stress. Finally, exposure to gemcitabine had no significant result on the rate of EVs released.

Furthermore, exchanging filtered conditioned media between low expression *LANCL1-AS1* (LS3N) and high expression *LANCL1-AS1* (LS3C) showed a significant reduction in cell proliferation. However, this effect was not reproduced by isolated EVs exchange. It is appreciated that the technical difficulties we recognised may have interfered with this result, thus further investigation is required to provide a definite answer on this aspect.

Chapter 6: Summary of conclusions and future prospects

Lung cancer is responsible for the highest malignancy-related mortality rate worldwide and the resistance to classical chemotherapeutics and targeted therapies being one of the main factors for its very high death rate. While numerous studies so far have attempted to identify the determinants of resistance, our knowledge is still poor and confined to only a few clinical measures (e.g. K-Ras mutant neoplasms are excluded from TKI therapies).

The main aim of this study was to explore various means to sensitize NSCLC cells to chemotherapeutics commonly used in clinical practice today. While there is promise for new therapies (targeted and immunotherapy), one can easily estimate that classical chemotherapy will continue to be perceived as the main line of therapy, especially in low-income countries. In this respect, our starting point was the IC50 profile calculated in eight NSCLC cell line (A549, CALU-1, CALU-3, CO-RL23, H358, LUDLU, SK-MES-1, SK-LU-1) for the selected chemotherapeutic agents (cisplatin, carboplatin, gemcitabine and vinorelbine). The study subsequently focused on the two cells with the highest IC50 for each chemotherapeutic, in an effort to assess epigenetic sensitization by Valproic acid (VPA) and decitabine (DAC), as well as sensitization by fendiline and AMPA, which have previously been reported to demonstrate such a function.

It is noteworthy to mention that VPA treatment induced a drop in the IC50 in all the four chemotherapeutics, suggesting that histone deacetylation inhibition increases the expression of essential genes in the apoptosis and proliferation pathway, thus enhancing the chemotherapeutic effect. Furthermore, we observed that VPA showed an increased potential when used to treat the cells prior to the chemotherapeutic addition. 3/7 caspase activity exhibited a significant increase when NSCLC cell lines were exposed to platinum (cisplatin and carboplatin) with epigenetic drug, either pre-treated or synchronous, suggesting that the increased apoptotic capacity is a significant mediator of this sensitization.

The results of this activity of VPA in lung cancer cells is novel; keeping in mind that VPA is reported to be a safe and well-established drug, its clinical application can be achieved in an easier manner through appropriate clinical trials. Another new finding in this study was the DNA damage caused by gemcitabine, as reported by the comet assays. Interestingly, the co-treatment with VPA further induced DNA damaging, therefore providing evidence for further exploitation of this result in preclinical and clinical models.

Recent improvements in sequencing technology have led to a more consistent exploration of the transcriptional map of the entire human genome, showing that 70 to 90% of the mammalian genes are transcribed (Fang and Fullwood 2016; Lu et al. 2013; Sun et al. 2014). Around 2% of the transcribed genome encode proteins; while most transcribed genes produce noncoding RNA (Villegas and Zaphiropoulos 2015).

Long non-coding RNAs (lncRNAs) compose a class of particular interest due to their multiplicity of functions in many aspects of normal physiology. It is, therefore, not surprising that their deregulation is involved in many human cancers, including glioblastoma, leukaemia, breast, colon, liver, prostatic, and bladder. LncRNAs can serve as proto-oncogenes or tumour suppressors (Lu et al. 2013). While research into the function of lncRNAs is increasing exponentially, we only understand the functions of a small minority of the lncRNA transcriptome, which contain over 9,000 genes (Fang and Fullwood 2016).

The lung cancer research group at the University of Liverpool has recently evaluated LncRNA deregulation in non-small-cell lung cancer (NSCLC) to support the existing data, determining that the 14 LncRNA profile remarkably discriminated NSCLC tissue from normal lung tissue. One of them, *LANCL1-AS1*, which is absent in NSCLC (Figure 1.10), is a lncRNA classified in the antisense RNA subgroup, as it is transcribed from the opposite strand of a coding gene, in this case, *LANCL1*. Apart from being significantly decreased in NSCLC tissue, *LANCL1-AS1* was found to be completely absent in all the NSCLC cell lines studied by the research group (Acha-Sagredo et al. 2020) This suggested a potential inhibitory role in tumour development, although we can never exclude the possibility of this being a passenger alteration.

Following these observations, the overarching hypothesis of this PhD study was that *LANCL1* and *LANCL1-AS1* might contribute to a cancer phenotype. Having no publications available for *LANCL1-AS1* and only a small number for LANCL1, we had a very large number of research questions to answer, starting from whether *LANCL1-AS1* could regulate *LANCL1* transcription and vice versa. Furthermore, knowing that *LANCL1* protects the neurons against oxidative stress, we wondered whether this characteristic suggests a role for the gene in chemotherapy resistance (Zhang et al. 2009).

LANCL1 and *LANCL1-AS1* expression alteration increase the cell NSCLC sensitivity to oxidative stress and also increased the sensitivity of gemcitabine and vinorelbine, while reducing the sensitivity to platinum, which is known to be dependent on the oxidative stress levels.

The changes in chemosensitivity induced by *LANCL1* and *LANCL1-AS1* expression, led us to ask one more question: whether there are any changes in the extracellular vesicles (EVs) that may be mediating this effect. EVs are known to facilitate cell communication and induce chemotherapy-related bystander effects and it’s been shown that releasing of EVs increase in the cancer cell and that can transfer drug resistance from one cell to another.

We have found, that *LANCL1* expression does not present any significant change in the number of EVs released. In contrast, *LANCL1-AS1* expression affects, in a dose-dependent manner, the release of EVs. However, there was no conclusive evidence from exchanging EVs between different expressing *LANCL1-AS1* cells (i.e. sensitive and resistant to GM) due to technical issues. These have now been recognised and will certainly serve as the basis for the next research project in the lab.

Future work regarding increased chemosensitivity with valproic acid can be continued from different angles. The drug sensitivity results can be confirmed by proceeding to a preclinical test to examine the efficiency of the combined drugs in animals.

As already known, valproic acid has been used for a decade to treat epilepsy patients. Therefore, by looking at the record of overall survival rate of NSCLC patients who have epilepsy and were treated with valproic acid and chemotherapeutics and comparing them with the overall survival rate of NSCLC who were treated with chemotherapeutics only, we can gain useful information.

Overall, I believe that the present study was successful in adding new evidence to the existing preclinical information relevant to lung cancer treatment and provided leads for future research work to move this area further forward.

Chapter7: References

Abrami, Laurence, Lucia Brandi, Mahtab Moayeri, Michael J Brown, Bryan A Krantz, Stephen H Leppla, and F Gisou van der Goot. 2013. 'Hijacking multivesicular bodies enables long-term and exosome-mediated long-distance action of anthrax toxin', *Cell reports*, 5: 986-96.

Acha-Sagredo, Amelia , Bubaraye Uko, Paschalia Pantazi, Naiara Bediaga, Chryssanthi Moschandrea, Lucille Rainbow, Michael Marcus, Michael Davies, John Field, and Triantafillos Liloglou. 2020. 'Long non-coding RNA dysregulation is a frequent event in non-small cell lung carcinoma pathogenesis ', *Brit. J. Cancer*.

Adams, Jerry M, and Suzanne Cory. 2007. 'The Bcl-2 apoptotic switch in cancer development and therapy', *Oncogene*, 26: 1324.

Agrawal, Khushboo, Viswanath Das, Pankhuri Vyas, and Marian Hajduch. 2018. 'Nucleosidic DNA demethylating epigenetic drugs–a comprehensive review from discovery to clinic', *Pharmacology & therapeutics*, 188: 45-79.

Alberg, A. J., M. V. Brock, J. G. Ford, J. M. Samet, and S. D. Spivack. 2013. 'Epidemiology of lung cancer: Diagnosis and management of lung cancer, 3rd ed: American College of Chest Physicians evidence-based clinical practice guidelines', *Chest*, 143: e1S-e29S.

Alló, Mariano, Valeria Buggiano, Juan P Fededa, Ezequiel Petrillo, Ignacio Schor, Manuel De La Mata, Eneritz Agirre, Mireya Plass, Eduardo Eyras, and Sherif Abou Elela. 2009. 'Control of alternative splicing through siRNA-mediated transcriptional gene silencing', *Nature structural & molecular biology*, 16: 717-24.

Althubiti, M, L Lezina, S Carrera, R Jukes-Jones, SM Giblett, A Antonov, N Barlev, GS Saldanha, CA Pritchard, and K Cain. 2014. 'Characterization of novel markers of senescence and their prognostic potential in cancer', *Cell death & disease*, 5: e1528.

Alvarez-Erviti, Lydia, Yiqi Seow, HaiFang Yin, Corinne Betts, Samira Lakhal, and Matthew JA Wood. 2011. 'Delivery of siRNA to the mouse brain by systemic injection of targeted exosomes', *Nature biotechnology*, 29: 341.

Anderson, Donald D, and Patrick J Stover. 2009. 'SHMT1 and SHMT2 are functionally redundant in nuclear de novo thymidylate biosynthesis', *PloS one*, 4.

Apel, Klaus, and Heribert Hirt. 2004. 'Reactive oxygen species: metabolism, oxidative stress, and signal transduction', *Annu. Rev. Plant Biol.*, 55: 373-99.

Armstrong, James PK, Margaret N Holme, and Molly M Stevens. 2017. 'Re-engineering extracellular vesicles as smart nanoscale therapeutics', *ACS nano*, 11: 69-83.

Ashkenazi, Avi, and Vishva M Dixit. 1998. 'Death receptors: signaling and modulation', *science*, 281: 1305-08.

ATCC. 2019. 'SK-MES-1'.

Azmi, Asfar S, Bin Bao, and Fazlul H Sarkar. 2013. 'Exosomes in cancer development, metastasis, and drug resistance: a comprehensive review', *Cancer and Metastasis Reviews*, 32: 623-42.

Balaj, Leonora, Ryan Lessard, Lixin Dai, Yoon-Jae Cho, Scott L Pomeroy, Xandra O Breakefield, and Johan Skog. 2011. 'Tumour microvesicles contain retrotransposon elements and amplified oncogene sequences', *Nature communications*, 2: 180.

Batista, Pedro J, and Howard Y Chang. 2013. 'Long noncoding RNAs: cellular address codes in development and disease', *Cell*, 152: 1298-307.

Baxevanos, Panagiotis, and Giannis Mountzios. 2018. 'Novel chemotherapy regimens for advanced lung cancer: have we reached a plateau?', *Annals of translational medicine*, 6.
Bebelman, Maarten P, Martine J Smit, D Michiel Pegtel, and S Rubina Baglio. 2018. 'Biogenesis and function of extracellular vesicles in cancer', *Pharmacology & therapeutics*, 188: 1-11.
Berridge, Michael V, Patries M Herst, and An S Tan. 2005. 'Tetrazolium dyes as tools in cell biology: new insights into their cellular reduction', *Biotechnology annual review*, 11: 127-52.
Biasutto, Lucia, Antonella Chiechi, Robin Couch, Lance A Liotta, and Virginia Espina. 2013. 'Retinal pigment epithelium (RPE) exosomes contain signaling phosphoproteins affected by oxidative stress', *Experimental cell research*, 319: 2113-23.
Biesalski, Hans Konrad, Bas Bueno De Mesquita, Andrew Chesson, Frank Chytil, Robert Grimble, RJJ Hermus, Jochen Köhrle, Reuben Lotan, Karl Norpoth, and Ugo Pastorino. 1998. 'European consensus statement on lung cancer: risk factors and prevention. lung cancer panel', *CA: a cancer journal for clinicians*, 48: 167-76.
BiotechAdvisers. 2019. 'Comet assay '.
Blackwell, Leonard, Jacqueline Norris, Carla M Suto, and William P Janzen. 2008. 'The use of diversity profiling to characterize chemical modulators of the histone deacetylases', *Life sciences*, 82: 1050-58.
Blagosklonny, Mikhail V, Robert Robey, Dan L Sackett, Litong Du, Frank Traganos, Zbigniew Darzynkiewicz, Tito Fojo, and Susan E Bates. 2002. 'Histone deacetylase inhibitors all induce p21 but differentially cause tubulin acetylation, mitotic arrest, and cytotoxicity', *Molecular cancer therapeutics*, 1: 937-41.
Boelens, Mirjam C, Tony J Wu, Barzin Y Nabet, Bihui Xu, Yu Qiu, Taewon Yoon, Diana J Azzam, Christina Twyman-Saint Victor, Brianne Z Wiemann, and Hemant Ishwaran. 2014. 'Exosome transfer from stromal to breast cancer cells regulates therapy resistance pathways', *Cell*, 159: 499-513.
Bose, Prithviraj, Yun Dai, and Steven Grant. 2014. 'Histone deacetylase inhibitor (HDACI) mechanisms of action: emerging insights', *Pharmacology & therapeutics*, 143: 323-36.
Brady, Anna K, Jonathan D McNeill, Brendan Judy, Joshua Bauml, Tracey L Evans, Roger B Cohen, Corey Langer, Anil Vachani, and Charu Aggarwal. 2015. 'Survival outcome according to KRAS mutation status in newly diagnosed patients with stage IV non-small cell lung cancer treated with platinum doublet chemotherapy', *Oncotarget*, 6: 30287.
Bunn, Paul A, and Karen Kelly. 1998. 'New chemotherapeutic agents prolong survival and improve quality of life in non-small cell lung cancer: a review of the literature and future directions', *Clinical cancer research*, 4: 1087-100.
Burdett, Sarah, Lesley A Stewart, and Larysa Rydzewska. 2006. 'A systematic review and meta-analysis of the literature: chemotherapy and surgery versus surgery alone in non-small cell lung cancer', *Journal of Thoracic Oncology*, 1: 611-21.
Burgess, Andrew, Astrid Ruefli, Heather Beamish, Robyn Warrener, Nicholas Saunders, Ricky Johnstone, and Brian Gabrielli. 2004. 'Histone deacetylase inhibitors specifically kill nonproliferating tumour cells', *Oncogene*, 23: 6693.
Cadranel, Jacques, Jean-Marc Naccache, Marie Wislez, and Charles Mayaud. 1999. 'Pulmonary malignancies in the immunocompromised patient', *Respiration*, 66: 289-309.
CancerResearchUK. 2019.

Catalano, Maria G, Nicoletta Fortunati, Mariateresa Pugliese, Lucia Costantino, Roberta Poli, Ornella Bosco, and Giuseppe Boccuzzi. 2005. 'Valproic acid induces apoptosis and cell cycle arrest in poorly differentiated thyroid cancer cells', *The Journal of Clinical Endocrinology & Metabolism*, 90: 1383-89.

Checinska, Agnieszka, Bas SJ Hoogeland, Jose A Rodriguez, Giuseppe Giaccone, and Frank AE Kruyt. 2007. 'Role of XIAP in inhibiting cisplatin-induced caspase activation in non-small cell lung cancer cells: a small molecule Smac mimic sensitizes for chemotherapy-induced apoptosis by enhancing caspase-3 activation', *Experimental cell research*, 313: 1215-24.

Chen, Bin, Ling He, Van H Savell, Jesse J Jenkins, and David M Parham. 2000. 'Inhibition of the interferon-γ/signal transducers and activators of transcription (STAT) pathway by hypermethylation at a STAT-binding site in the p21WAF1 promoter region', *Cancer research*, 60: 3290-98.

Chen, Ping, Jian-Nong Wu, Yang Shu, He-Guo Jiang, Xiao-Hui Zhao, Hai Qian, Kang Chen, Ting Lan, Chen-Guo Chen, and Jian Li. 2018. 'Gemcitabine resistance mediated by ribonucleotide reductase M2 in lung squamous cell carcinoma is reversed by GW8510 through autophagy induction', *Clinical Science*, 132: 1417-33.

Chougule, Mahavir B, Apurva Patel, Pratik Sachdeva, Tanise Jackson, and Mandip Singh. 2011. 'Enhanced anticancer activity of gemcitabine in combination with noscapine via antiangiogenic and apoptotic pathway against non-small cell lung cancer', *PloS one*, 6.

Clayton, Aled, J Paul Mitchell, Malcolm D Mason, and Zsuzsanna Tabi. 2007. 'Human tumor-derived exosomes selectively impair lymphocyte responses to interleukin-2', *Cancer research*, 67: 7458-66.

Conklin, Kenneth A. 2004. 'Chemotherapy-associated oxidative stress: impact on chemotherapeutic effectiveness', *Integrative cancer therapies*, 3: 294-300.

Conroy, Thierry, Françoise Desseigne, Marc Ychou, Olivier Bouché, Rosine Guimbaud, Yves Bécouarn, Antoine Adenis, Jean-Luc Raoul, Sophie Gourgou-Bourgade, and Christelle de la Fouchardière. 2011. 'FOLFIRINOX versus gemcitabine for metastatic pancreatic cancer', *New England Journal of Medicine*, 364: 1817-25.

Cooper, Wendy A, David CL Lam, Sandra A O'Toole, and John D Minna. 2013. 'Molecular biology of lung cancer', *Journal of thoracic disease*, 5: S479.

Corrie, PG, J Shaw, VJ Spanswick, R Sehmbi, A Jonson, A Mayer, R Bulusu, JA Hartley, and IA Cree. 2005. 'Phase I trial combining gemcitabine and treosulfan in advanced cutaneous and uveal melanoma patients', *British journal of cancer*, 92: 1997.

Cullen, M. 2003. 'Lung cancer• 4: Chemotherapy for non-small cell lung cancer: the end of the beginning', *Thorax*, 58: 352-56.

d'Amato, Thomas A, Rodney J Landreneau, William Ricketts, Weidong Huang, Ricardo Parker, Eugene Mechetner, Ru Yu, and James D Luketich. 2007. 'Chemotherapy resistance and oncogene expression in non–small cell lung cancer', *The Journal of thoracic and cardiovascular surgery*, 133: 352-63.

Davidson, Jennifer D, Liandong Ma, Michael Flagella, Sandaruwan Geeganage, Lawrence M Gelbert, and Christopher A Slapak. 2004. 'An increase in the expression of ribonucleotide reductase large subunit 1 is associated with gemcitabine resistance in non-small cell lung cancer cell lines', *Cancer research*, 64: 3761-66.

Davies, Marianne. 2014. 'New modalities of cancer treatment for NSCLC: focus on immunotherapy', *Cancer management and research*, 6: 63.

Debatin, Klaus-Michael. 2000. 'Activation of apoptosis pathways by anticancer treatment', *Toxicology letters*, 112: 41-48.

Del Bufalo, Donatella, Marianna Desideri, Teresa De Luca, Marta Di Martile, Chiara Gabellini, Valentina Monica, Simone Busso, Adriana Eramo, Ruggero De Maria, and Michele Milella. 2014. 'Histone deacetylase inhibition synergistically enhances pemetrexed cytotoxicity through induction of apoptosis and autophagy in non-small cell lung cancer', *Molecular cancer*, 13: 230.

Detich, Nancy, Veronica Bovenzi, and Moshe Szyf. 2003. 'Valproate induces replication-independent active DNA demethylation', *Journal of Biological Chemistry*, 278: 27586-92.

Diyabalanage, Himashinie VK, Michael L Granda, and Jacob M Hooker. 2013. 'Combination therapy: histone deacetylase inhibitors and platinum-based chemotherapeutics for cancer', *Cancer letters*, 329: 1-8.

Drugbanck. 2019a. 'Platinum'.

———. 2019b. 'Vinorelbine'.

Eggert, Angelika, Michael A Grotzer, Tycho J Zuzak, Barbara R Wiewrodt, Ruth Ho, Naohiko Ikegaki, and Garrett M Brodeur. 2001. 'Resistance to tumor necrosis factor-related apoptosis-inducing ligand-induced apoptosis in neuroblastoma cells correlates with a loss of caspase-8 expression', *Cancer research*, 61: 1314-19.

Eldh, Maria, Karin Ekström, Hadi Valadi, Margareta Sjöstrand, Bob Olsson, Margareta Jernås, and Jan Lötvall. 2010. 'Exosomes communicate protective messages during oxidative stress; possible role of exosomal shuttle RNA', *PloS one*, 5: e15353.

England, Robert, and Monica Pettersson. 2005. 'Pyro Q-CpG™: quantitative analysis of methylation in multiple CpG sites by Pyrosequencing®', *Nature Methods*, 2: 798.

ExoCarta. 2016. 'Gene summary'.

Fahmy, HA, and OA Gharib. 2014. 'Effect of low radiation dose on cisplatin induced hepato-testicular damage in male rats', *British Journal of Pharmaceutical Research*, 4: 1053.

Faller, Bryan A, and Trailokya N Pandit. 2011. 'Safety and efficacy of vinorelbine in the treatment of non-small cell lung cancer', *Clinical Medicine Insights: Oncology*, 5: CMO. S5074.

Fang, Yiwen, and Melissa J Fullwood. 2016. 'Roles, functions, and mechanisms of long non-coding RNAs in cancer', *Genomics, proteomics & bioinformatics*, 14: 42-54.

Ferreira, Carlos G, Christos Tolis, Simone W Span, Godefridus J Peters, Thea Van Lopik, Alain J Kummer, Herbert M Pinedo, and Giuseppe Giaccone. 2000. 'Drug-induced apoptosis in lung cancer cells is not mediated by the Fas/FasL (CD95/APO1) signaling pathway', *Clinical cancer research*, 6: 203-12.

Février, Benoit, and Graça Raposo. 2004. 'Exosomes: endosomal-derived vesicles shipping extracellular messages', *Current opinion in cell biology*, 16: 415-21.

Gajra, Ajeet, Arthur H Tatum, Nancy Newman, Gary P Gamble, Sonja Lichtenstein, Michele T Rooney, and Stephen L Graziano. 2002. 'The predictive value of neuroendocrine markers and p53 for response to chemotherapy and survival in patients with advanced non-small cell lung cancer', *Lung Cancer*, 36: 159-65.

Gallo, Alessia, Mayank Tandon, Ilias Alevizos, and Gabor G Illei. 2012. 'The majority of microRNAs detectable in serum and saliva is concentrated in exosomes', *PloS one*, 7: e30679.

Garcia-Blanco, Mariano A, Andrew P Baraniak, and Erika L Lasda. 2004. 'Alternative splicing in disease and therapy', *Nature biotechnology*, 22: 535-46.

Ghoshal, Kalpana, Jharna Datta, Sarmila Majumder, Shoumei Bai, Huban Kutay, Tasneem Motiwala, and Samson T Jacob. 2005. '5-Aza-deoxycytidine induces selective degradation of DNA methyltransferase 1 by a proteasomal pathway that requires the KEN box, bromo-adjacent homology domain, and nuclear localization signal', *Molecular and cellular biology*, 25: 4727-41.

Giallombardo, Marco, Simona Taverna, Riccardo Alessandro, David Hong, and Christian Rolfo. 2016. "Exosome-mediated drug resistance in cancer: the near future is here." In.: SAGE Publications Sage UK: London, England.
Gibbings, Derrick J, Constance Ciaudo, Mathieu Erhardt, and Olivier Voinnet. 2009. 'Multivesicular bodies associate with components of miRNA effector complexes and modulate miRNA activity', *Nature cell biology*, 11: 1143.
Glasspool, RM, R Brown, ME Gore, GJS Rustin, IA McNeish, RH Wilson, S Pledge, J Paul, M Mackean, and GD Hall. 2014. 'A randomised, phase II trial of the DNA-hypomethylating agent 5-aza-2′-deoxycytidine (decitabine) in combination with carboplatin vs carboplatin alone in patients with recurrent, partially platinum-sensitive ovarian cancer', *British journal of cancer*, 110: 1923.
Goffin, Jan, and E Eisenhauer. 2002. 'DNA methyltransferase inhibitors—state of the art', *Annals of Oncology*, 13: 1699-716.
Golding, Brandon, Anita Luu, Robert Jones, and Alicia M Viloria-Petit. 2018. 'The function and therapeutic targeting of anaplastic lymphoma kinase (ALK) in non-small cell lung cancer (NSCLC)', *Molecular cancer*, 17: 52.
Gurvich, Nadia, Oxana M Tsygankova, Judy L Meinkoth, and Peter S Klein. 2004. 'Histone deacetylase is a target of valproic acid-mediated cellular differentiation', *Cancer research*, 64: 1079-86.
Ha, Dinh, Ningning Yang, and Venkatareddy Nadithe. 2016. 'Exosomes as therapeutic drug carriers and delivery vehicles across biological membranes: current perspectives and future challenges', *Acta Pharmaceutica Sinica B*, 6: 287-96.
Hallberg, Bengt, and Ruth H Palmer. 2011. 'ALK and NSCLC: Targeted therapy with ALK inhibitors', *F1000 medicine reports*, 3.
Hedlund, Malin, Olga Nagaeva, Dominic Kargl, Vladimir Baranov, and Lucia Mincheva-Nilsson. 2011. 'Thermal-and oxidative stress causes enhanced release of NKG2D ligand-bearing immunosuppressive exosomes in leukemia/lymphoma T and B cells', *PloS one*, 6: e16899.
Heighway, Jim, and Daniel C Betticher. 2004. 'Lung: Non-small cell carcinoma', *Atlas of Genetics and Cytogenetics in Oncology and Haematology*.
Heijnen, Harry FG, Anja E Schiel, Rob Fijnheer, Hans J Geuze, and Jan J Sixma. 1999. 'Activated Platelets Release Two Types of Membrane Vesicles: Microvesicles by Surface Shedding and Exosomes Derived From Exocytosis of Multivesicular Bodies and □-Granules', *Blood*, 94: 3791-99.
Henne, William M, Nicholas J Buchkovich, and Scott D Emr. 2011. 'The ESCRT pathway', *Developmental cell*, 21: 77-91.
Hoshino, Daisuke, Kellye C Kirkbride, Kaitlin Costello, Emily S Clark, Seema Sinha, Nathan Grega-Larson, Matthew J Tyska, and Alissa M Weaver. 2013. 'Exosome secretion is enhanced by invadopodia and drives invasive behavior', *Cell reports*, 5: 1159-68.
Howington, John A, Matthew G Blum, Andrew C Chang, Alex A Balekian, and Sudish C Murthy. 2013. 'Treatment of stage I and II non-small cell lung cancer: Diagnosis and management of lung cancer: American College of Chest Physicians evidence-based clinical practice guidelines', *Chest*, 143: e278S-e313S.
Hu, Zhibin, Xi Chen, Yang Zhao, Tian Tian, Guangfu Jin, Yongqian Shu, Yijiang Chen, Lin Xu, Ke Zen, and Chenyu Zhang. 2010. 'Serum microRNA signatures identified in a genome-wide serum microRNA expression profiling predict survival of non-small-cell lung cancer', *J Clin Oncol*, 28: 1721-26.
Huang, Chao, Mina Chen, Dejiang Pang, Dandan Bi, Yi Zou, Xiaoqiang Xia, Weiwei Yang, Liping Luo, Rongkang Deng, and Honglin Tan. 2014. 'Developmental and activity-

dependent expression of LanCL1 confers antioxidant activity required for neuronal survival', *Developmental cell*, 30: 479-87.
Hubaux, Roland, Fabian Vandermeers, Cecilia Crisanti, Veena Kapoor, Arsène Burny, Céline Mascaux, Steven M Albelda, and Luc Willems. 2010. 'Preclinical evidence for a beneficial impact of valproate on the response of small cell lung cancer to first-line chemotherapy', *European journal of cancer*, 46: 1724-34.
Ingato, Dominique, Jong Uk Lee, Sang Jun Sim, and Young Jik Kwon. 2016. 'Good things come in small packages: Overcoming challenges to harness extracellular vesicles for therapeutic delivery', *Journal of Controlled Release*, 241: 174-85.
Iwai, Yoshiko, Masayoshi Ishida, Yoshimasa Tanaka, Taku Okazaki, Tasuku Honjo, and Nagahiro Minato. 2002. 'Involvement of PD-L1 on tumor cells in the escape from host immune system and tumor immunotherapy by PD-L1 blockade', *Proceedings of the National Academy of Sciences*, 99: 12293-97.
Jackson, Tanise, Mahavir B Chougule, Nkechi Ichite, Ram R Patlolla, and Mandip Singh. 2008. 'Antitumor activity of noscapine in human non-small cell lung cancer xenograft model', *Cancer chemotherapy and pharmacology*, 63: 117-26.
Jan, C, K Lee, K Chou, J Cheng, J Wang, Y Lo, H Chang, K Tang, C Yu, and J Huang. 2001. 'Fendiline, an anti-anginal drug, increases intracellular Ca 2+ in PC3 human prostate cancer cells', *Cancer chemotherapy and pharmacology*, 48: 37-41.
Ji, Meiying, Zhenling Li, Zhenhua Lin, and Liyan Chen. 2018. 'Antitumor activity of the novel HDAC inhibitor CUDC-101 combined with gemcitabine in pancreatic cancer', *American journal of cancer research*, 8: 2402.
Jiang, Man, Xiaolan Yi, Stephen Hsu, Cong-Yi Wang, and Zheng Dong. 2004. 'Role of p53 in cisplatin-induced tubular cell apoptosis: dependence on p53 transcriptional activity', *American Journal of Physiology-Renal Physiology*, 287: F1140-F47.
Johnson, David G, and CL Walker. 1999. 'Cyclins and cell cycle checkpoints', *Annual review of pharmacology and toxicology*, 39: 295-312.
Jones, Rebecca M, Panagiotis Kotsantis, Grant S Stewart, Petra Groth, and Eva Petermann. 2014. 'BRCA2 and RAD51 promote double-strand break formation and cell death in response to gemcitabine', *Molecular cancer therapeutics*, 13: 2412-21.
Kaiser, Martin, Ivana Zavrski, Jan Sterz, Christian Jakob, Claudia Fleissner, Peter-Michael Kloetzel, Orhan Sezer, and Ulrike Heider. 2006. 'The effects of the histone deacetylase inhibitor valproic acid on cell cycle, growth suppression and apoptosis in multiple myeloma', *haematologica*, 91: 248-51.
Kanda, Tatsuo, Motohisa Tada, Fumio Imazeki, Osamu Yokosuka, Keiichi Nagao, and Hiromitsu Saisho. 2005. '5-aza-2'-deoxycytidine sensitizes hepatoma and pancreatic cancer cell lines', *Oncology reports*, 14: 975-79.
Karppinen, Sari, Sandra L Hänninen, Risto Rapila, and Pasi Tavi. 2018. 'Sarcoplasmic reticulum Ca2+-induced Ca2+ release regulates class II a HDAC localization in mouse embryonic cardiomyocytes', *Physiological reports*, 6: e13522.
Kashi, Kaori, Lindsey Henderson, Alessandro Bonetti, and Piero Carninci. 2016. 'Discovery and functional analysis of lncRNAs: methodologies to investigate an uncharacterized transcriptome', *Biochimica et Biophysica Acta (BBA)-Gene Regulatory Mechanisms*, 1859: 3-15.
Katzmann, David J, Greg Odorizzi, and Scott D Emr. 2002. 'Receptor downregulation and multivesicular-body sorting', *Nature reviews Molecular cell biology*, 3: 893.
Kazantsev, Aleksey G, and Leslie M Thompson. 2008. 'Therapeutic application of histone deacetylase inhibitors for central nervous system disorders', *Nature reviews Drug discovery*, 7: 854.

Khan, Nagma, Michael Jeffers, Sampath Kumar, Craig Hackett, Ferenc Boldog, Nicholai Khramtsov, Xiaozhong Qian, Evan Mills, Stanny C Berghs, and Nessa Carey. 2008. 'Determination of the class and isoform selectivity of small-molecule histone deacetylase inhibitors', *Biochemical Journal*, 409: 581-89.

Kim, Sungeun, S Swaminathan, Li Shen, SL Risacher, Kwangsik Nho, Tatiana Foroud, LM Shaw, JQ Trojanowski, SG Potkin, and MJ Huentelman. 2011. 'Genome-wide association study of CSF biomarkers Aβ1-42, t-tau, and p-tau181p in the ADNI cohort', *Neurology*, 76: 69-79.

Koliopanos, Alexander, Helmut Friess, Jörg Kleeff, Xin Shi, Quan Liao, Iris Pecker, Israel Vlodavsky, Arthur Zimmermann, and Markus W Büchler. 2001. 'Heparanase expression in primary and metastatic pancreatic cancer', *Cancer Research*, 61: 4655-59.

Koukourakis, Michael I, Dimitrios Papazoglou, Alexandra Giatromanolaki, George Bougioukas, Efstratios Maltezos, and Efthimios Siviridis. 2004. 'VEGF gene sequence variation defines VEGF gene expression status and angiogenic activity in non-small cell lung cancer', *Lung cancer*, 46: 293-98.

Krämer, Oliver H, Ping Zhu, Heather P Ostendorff, Martin Golebiewski, Jens Tiefenbach, Marvin A Peters, Boris Brill, Bernd Groner, Ingolf Bach, and Thorsten Heinzel. 2003. 'The histone deacetylase inhibitor valproic acid selectively induces proteasomal degradation of HDAC2', *The EMBO journal*, 22: 3411-20.

Lane, Andrew A, and Bruce A Chabner. 2009. 'Histone deacetylase inhibitors in cancer therapy', *Journal of clinical oncology*, 27: 5459-68.

Lardinois, Didier, Walter Weder, Thomas F Hany, Ehab M Kamel, Stephan Korom, Burkhardt Seifert, Gustav K von Schulthess, and Hans C Steinert. 2003. 'Staging of non–small-cell lung cancer with integrated positron-emission tomography and computed tomography', *New England Journal of Medicine*, 348: 2500-07.

Larsen, Jill E, and John D Minna. 2011. 'Molecular biology of lung cancer: clinical implications', *Clinics in chest medicine*, 32: 703-40.

Lazzari, Chiara, Niki Karachaliou, Alessandra Bulotta, Mariagrazia Viganó, Aurora Mirabile, Elena Brioschi, Mariacarmela Santarpia, Luca Gianni, Rafael Rosell, and Vanesa Gregorc. 2018. 'Combination of immunotherapy with chemotherapy and radiotherapy in lung cancer: is this the beginning of the end for cancer?', *Therapeutic advances in medical oncology*, 10: 1758835918762094.

Li, Qingli, Mark J Lambrechts, Qiuyang Zhang, Sen Liu, Dongxia Ge, Rutie Yin, Mingrong Xi, and Zongbing You. 2013. 'Glyphosate and AMPA inhibit cancer cell growth through inhibiting intracellular glycine synthesis', *Drug design, development and therapy*, 7: 635.

Lin, Ching-Tai, Hung-Cheng Lai, Hsin-Yi Lee, Wei-Hsin Lin, Cheng-Chang Chang, Tang-Yuan Chu, Ya-Wen Lin, Kuan-Der Lee, and Mu-Hsien Yu. 2008. 'Valproic acid resensitizes cisplatin-resistant ovarian cancer cells', *Cancer science*, 99: 1218-26.

Lu, Kai-hua, Wei Li, Xiang-hua Liu, Ming Sun, Mei-ling Zhang, Wei-qin Wu, Wei-ping Xie, and Ya-yi Hou. 2013. 'Long non-coding RNA MEG3 inhibits NSCLC cells proliferation and induces apoptosis by affecting p53 expression', *BMC cancer*, 13: 461.

Lv, Lin-Li, Yuhan Cao, Dan Liu, Min Xu, Hong Liu, Ri-Ning Tang, Kun-Ling Ma, and Bi-Cheng Liu. 2013. 'Isolation and quantification of microRNAs from urinary exosomes/microvesicles for biomarker discovery', *International journal of biological sciences*, 9: 1021.

Ma, Jun, Jie Yang, Chao Wang, Nan Zhang, Ying Dong, Chengjie Wang, Yu Wang, and Xinjian Lin. 2014. 'Emodin augments cisplatin cytotoxicity in platinum-resistant

ovarian cancer cells via ROS-dependent MRP1 downregulation', *BioMed research international*, 2014.
Martin, Lainie P, Thomas C Hamilton, and Russell J Schilder. 2008. 'Platinum resistance: the role of DNA repair pathways', *Clinical cancer research*, 14: 1291-95.
Marullo, Rossella, Erica Werner, Natalya Degtyareva, Bryn Moore, Giuseppe Altavilla, Suresh S Ramalingam, and Paul W Doetsch. 2013. 'Cisplatin induces a mitochondrial-ROS response that contributes to cytotoxicity depending on mitochondrial redox status and bioenergetic functions', *PloS one*, 8.
Massion, Pierre P, and David P Carbone. 2003. 'The molecular basis of lung cancer: molecular abnormalities and therapeutic implications', *Respiratory research*, 4: 12.
Matakidou, A, T Eisen, and RS Houlston. 2005. 'Systematic review of the relationship between family history and lung cancer risk', *British journal of cancer*, 93: 825.
Matassa, DS, MR Amoroso, H Lu, R Avolio, D Arzeni, C Procaccini, D Faicchia, Francesca Maddalena, V Simeon, and I Agliarulo. 2016. 'Oxidative metabolism drives inflammation-induced platinum resistance in human ovarian cancer', *Cell death and differentiation*, 23: 1542.
Mayer, Herbert, Hemma Bauer, Johannes Breuss, Sophie Ziegler, and Rainer Prohaska. 2001. 'Characterization of rat LANCL1, a novel member of the lanthionine synthetase C-like protein family, highly expressed in testis and brain', *Gene*, 269: 73-80.
Meier, Jordan L. 2013. 'Metabolic mechanisms of epigenetic regulation', *ACS chemical biology*, 8: 2607-21.
Molina, Julian R, Ping Yang, Stephen D Cassivi, Steven E Schild, and Alex A Adjei. 2008. "Non-small cell lung cancer: epidemiology, risk factors, treatment, and survivorship." In *Mayo Clinic Proceedings*, 584-94. Elsevier.
Momparler, Richard L. 2013. 'Epigenetic therapy of non-small cell lung cancer using decitabine (5-aza-2′-deoxycytidine)', *Frontiers in oncology*, 3: 188.
Momparler, Richard L, and J Ayoub. 2001. 'Potential of 5-aza-2′-deoxycytidine (Decitabine) a potent inhibitor of DNA methylation for therapy of advanced non-small cell lung cancer', *Lung cancer*, 34: 111-15.
Momparler, Richard L, David Y Bouffard, Louise F Momparler, Jeanne Dionne, Karl Bélanger, and Joseph Ayoub. 1997. 'Pilot phase I-II study on 5-aza-2'-deoxycytidine (Decitabine) in patients with metastatic lung cancer', *Anti-cancer drugs*, 8: 358-68.
Muntasell, Aura, Adam C Berger, and Paul A Roche. 2007. 'T cell-induced secretion of MHC class II–peptide complexes on B cell exosomes', *The EMBO journal*, 26: 4263-72.
Mutze, Kathrin, Rupert Langer, Karen Becker, Katja Ott, Alexander Novotny, Birgit Luber, Alexander Hapfelmeier, Martin Göttlicher, Heinz Höfler, and Gisela Keller. 2010. 'Histone deacetylase (HDAC) 1 and 2 expression and chemotherapy in gastric cancer', *Annals of surgical oncology*, 17: 3336-43.
Nascimento, ASF, S Côté, LS Jeong, J Yu, and RL Momparler. 2016. 'Synergistic antineoplastic action of 5-aza-2'deoxycytidine (decitabine) in combination with different inhibitors of enhancer of zeste homolog 2 (EZH2) on human lung carcinoma cells', *J Cancer Res Ther*, 4: 42-49.
Naseer, Aisha, Arum Parthipun, Athar Haroon, and Stephen Ellis. 2018. 'Lung Cancer: An Overview.' in Archi Agrawal and Venkatesh Rangarajan (eds.), *PET/CT in Lung Cancer* (Springer International Publishing: Cham).
Nasser, Nicola J. 2010. 'Stages of Non Small Cell Lung Cancer (NSCLC)', *The Best Oncologist TM*.
NationalCancerInstitute. 2019. ***The National Institutes of Health***.

Nolan, L, PWM Johnson, A Ganesan, G Packham, and SJ Crabb. 2008. 'Will histone deacetylase inhibitors require combination with other agents to fulfil their therapeutic potential?', *British journal of cancer*, 99: 689.
Ostrowski, Matias, Nuno B Carmo, Sophie Krumeich, Isabelle Fanget, Graça Raposo, Ariel Savina, Catarina F Moita, Kristine Schauer, Alistair N Hume, and Rui P Freitas. 2010. 'Rab27a and Rab27b control different steps of the exosome secretion pathway', *Nature cell biology*, 12: 19.
Pan, Bin-Tao, and Rose M Johnstone. 1983. 'Fate of the transferrin receptor during maturation of sheep reticulocytes in vitro: selective externalization of the receptor', *Cell*, 33: 967-78.
Parajuli, Keshab Raj, Qiuyang Zhang, Sen Liu, and Zongbing You. 2016. 'Aminomethylphosphonic acid inhibits growth and metastasis of human prostate cancer in an orthotopic xenograft mouse model', *Oncotarget*, 7: 10616.
Plunkett, William, Peng Huang, Catherine E Searcy, and Varsha Gandhi. 1996. "Gemcitabine: preclinical pharmacology and mechanisms of action." In *Seminars in oncology*, 3-15.
Png, Kim J, Nils Halberg, Mitsukuni Yoshida, and Sohail F Tavazoie. 2012. 'A microRNA regulon that mediates endothelial recruitment and metastasis by cancer cells', *Nature*, 481: 190.
Pohlmann, Paula, Luciane Pons DiLeone, Anna Isabel Cancella, Ana Paula F Caldas, Lissandra Dal Lago, Jr Ormando Campos, Eleusa Monego, Waldemar Rivoire, and Gilberto Schwartsmann. 2002. 'Phase II trial of cisplatin plus decitabine, a new DNA hypomethylating agent, in patients with advanced squamous cell carcinoma of the cervix', *American journal of clinical oncology*, 25: 496-501.
Ponting, Chris P, Peter L Oliver, and Wolf Reik. 2009. 'Evolution and functions of long noncoding RNAs', *Cell*, 136: 629-41.
Promega. 2019a. 'Caspase-Glo® 3/7 Assay System'.
———. 2019b. 'coumermycin-regulated system'.
Qin, Rong-Sheng, Zhen-Hua Zhang, Neng-Ping Zhu, Fei Chen, Qian Guo, Hao-Wen Hu, Shao-Zhi Fu, Shan-Shan Liu, Yue Chen, and Juan Fan. 2018. 'Enhanced antitumor and anti-angiogenic effects of metronomic Vinorelbine combined with Endostar on Lewis lung carcinoma', *BMC cancer*, 18: 1-12.
Raaschou-Nielsen, Ole, Zorana J Andersen, Rob Beelen, Evangelia Samoli, Massimo Stafoggia, Gudrun Weinmayr, Barbara Hoffmann, Paul Fischer, Mark J Nieuwenhuijsen, and Bert Brunekreef. 2013. 'Air pollution and lung cancer incidence in 17 European cohorts: prospective analyses from the European Study of Cohorts for Air Pollution Effects (ESCAPE)', *The lancet oncology*, 14: 813-22.
Rao's, Zihe. 2009. *Institute of Biophysics*.
Raparia, Kirtee, Celina Villa, Malcolm M DeCamp, Jyoti D Patel, and Minesh P Mehta. 2013. 'Molecular profiling in non–small cell lung cancer: a step toward personalized medicine', *Archives of pathology & laboratory medicine*, 137: 481-91.
Rasband, Wayne S. 1997-2018. 'National Institutes of Health, Bethesda, Maryland, USA', *http://imagej. nih. gov/ij/*.
Rastogi, Rajesh P, Ashok Kumar, Madhu B Tyagi, and Rajeshwar P Sinha. 2010. 'Molecular mechanisms of ultraviolet radiation-induced DNA damage and repair', *Journal of nucleic acids*, 2010.
Raynal, Noël J-M, and Jean-Pierre J Issa. 2016. 'DNA methyltransferase inhibitors.' in, *Drug Discovery in Cancer Epigenetics* (Elsevier).
Raynal, Noël J-M, Justin T Lee, Youjun Wang, Annie Beaudry, Priyanka Madireddi, Judith Garriga, Gabriel G Malouf, Sarah Dumont, Elisha J Dettman, and Vazganush

Gharibyan. 2016. 'Targeting calcium signaling induces epigenetic reactivation of tumor suppressor genes in cancer', *Cancer research*, 76: 1494-505.
Richards, Katherine E, Ann E Zeleniak, Melissa L Fishel, Junmin Wu, Laurie E Littlepage, and Reginald Hill. 2017. 'Cancer-associated fibroblast exosomes regulate survival and proliferation of pancreatic cancer cells', *Oncogene*, 36: 1770.
Riches, Andrew, Elaine Campbell, Eva Borger, and Simon Powis. 2014. 'Regulation of exosome release from mammary epithelial and breast cancer cells–a new regulatory pathway', *European journal of cancer*, 50: 1025-34.
Rolfo, Christian, Christian Caglevic, Mariacarmela Santarpia, Antonio Araujo, Elisa Giovannetti, Carolina Diaz Gallardo, Patrick Pauwels, and Mauricio Mahave. 2017. 'Immunotherapy in NSCLC: a promising and revolutionary weapon.' in, *Immunotherapy* (Springer).
Saayman, Sheena, Amanda Ackley, Anne-Marie W Turner, Marylinda Famiglietti, Alberto Bosque, Matthew Clemson, Vicente Planelles, and Kevin V Morris. 2014. 'An HIV-encoded antisense long noncoding RNA epigenetically regulates viral transcription', *Molecular Therapy*, 22: 1164-75.
Saeed-Zidane, Mohammed, Lea Linden, Dessie Salilew-Wondim, Eva Held, Christiane Neuhoff, Ernst Tholen, Michael Hoelker, Karl Schellander, and Dawit Tesfaye. 2017. 'Cellular and exosome mediated molecular defense mechanism in bovine granulosa cells exposed to oxidative stress', *PloS one*, 12: e0187569.
Safaei, Roohangiz, Barrett J Larson, Timothy C Cheng, Michael A Gibson, Shinji Otani, Wiltrud Naerdemann, and Stephen B Howell. 2005. 'Abnormal lysosomal trafficking and enhanced exosomal export of cisplatin in drug-resistant human ovarian carcinoma cells', *Molecular cancer therapeutics*, 4: 1595-604.
Sallmyr, Annahita, Jinshui Fan, Kamal Datta, Kyu-Tae Kim, Dan Grosu, Paul Shapiro, Donald Small, and Feyruz Rassool. 2008. 'Internal tandem duplication of FLT3 (FLT3/ITD) induces increased ROS production, DNA damage, and misrepair: implications for poor prognosis in AML', *Blood, The Journal of the American Society of Hematology*, 111: 3173-82.
Samuel, Priya, Laura Ann Mulcahy, Fiona Furlong, Helen O McCarthy, Susan Ann Brooks, Muller Fabbri, Ryan Charles Pink, and David Raul Francisco Carter. 2017. 'Cisplatin induces the release of extracellular vesicles from ovarian cancer cells that can induce invasiveness and drug resistance in bystander cells', *Philosophical Transactions of the Royal Society B: Biological Sciences*, 373: 20170065.
Sansone, Pasquale, Claudia Savini, Ivana Kurelac, Qing Chang, Laura Benedetta Amato, Antonio Strillacci, Anna Stepanova, Luisa Iommarini, Chiara Mastroleo, and Laura Daly. 2017. 'Packaging and transfer of mitochondrial DNA via exosomes regulate escape from dormancy in hormonal therapy-resistant breast cancer', *Proceedings of the National Academy of Sciences*, 114: E9066-E75.
Scaletti, Emma, Ann-Sofie Jemth, Thomas Helleday, and Pål Stenmark. 2019. 'Structural basis of inhibition of the human serine hydroxymethyltransferase SHMT 2 by antifolate drugs', *FEBS letters*, 593: 1863-73.
Scheff, Ronald J, and Bryan J Schneider. 2013. "Non–Small-Cell Lung Cancer: Treatment of Late Stage Disease: Chemotherapeutics and New Frontiers." In *Seminars in interventional radiology*, 191-98. Thieme Medical Publishers.
Schiffmann, Insa, Gabriele Greve, Manfred Jung, and Michael Lübbert. 2016. 'Epigenetic therapy approaches in non-small cell lung cancer: update and perspectives', *Epigenetics*, 11: 858-70.
Schulz, Thomas F. 2009. 'Cancer and viral infections in immunocompromised individuals', *International journal of cancer*, 125: 1755-63.

Sève, Pascal, Sylvie Isaac, Olivier Trédan, Pierre-Jean Souquet, Yves Pachéco, Maurice Pérol, Laurence Lafanéchère, Aurélie Penet, Eva-Laure Peiller, and Charles Dumontet. 2005. 'Expression of class III β-tubulin is predictive of patient outcome in patients with non–small cell lung cancer receiving Vinorelbine-based chemotherapy', *Clinical Cancer Research*, 11: 5481-86.

Sève, Pascal, Raymond Lai, Keyue Ding, Timothy Winton, Charles Butts, John Mackey, Charles Dumontet, Laith Dabbagh, Sarit Aviel-Ronen, and Lesley Seymour. 2007. 'Class III β-tubulin expression and benefit from adjuvant cisplatin/vinorelbine chemotherapy in operable non–small cell lung cancer: analysis of NCIC JBR. 10', *Clinical Cancer Research*, 13: 994-99.

Shackelford, Rodney E, William K Kaufmann, and Richard S Paules. 2000. 'Oxidative stress and cell cycle checkpoint function', *Free Radical Biology and Medicine*, 28: 1387-404.

Sharma, Alok, Hieu Nguyen, Cuiyu Geng, Melissa N Hinman, Guangbin Luo, and Hua Lou. 2014. 'Calcium-mediated histone modifications regulate alternative splicing in cardiomyocytes', *Proceedings of the National Academy of Sciences*, 111: E4920-E28.

Simons, Mikael, and Graça Raposo. 2009. 'Exosomes–vesicular carriers for intercellular communication', *Current opinion in cell biology*, 21: 575-81.

SinoBiological. 2019. 'Basic principle of SYBR Green dye method'.

Snyder, Deborah A, Marie L Kelly, and Dixon J Woodbury. 2006. 'SNARE complex regulation by phosphorylation', *Cell biochemistry and biophysics*, 45: 111-23.

Soldà, Francesca, Mark Lodge, Sue Ashley, Alastair Whitington, Peter Goldstraw, and Michael Brada. 2013. 'Stereotactic radiotherapy (SABR) for the treatment of primary non-small cell lung cancer; systematic review and comparison with a surgical cohort', *Radiotherapy and Oncology*, 109: 1-7.

Šorm, F, A Piskala, A Čihák, and J Veselý. 1964. '5-Azacytidine, a new, highly effective cancerostatic', *Cellular and Molecular Life Sciences*, 20: 202-03.

Spizzo, Riccardo, Maria In^es Almeida, A Colombatti, and George A Calin. 2012. 'Long non-coding RNAs and cancer: a new frontier of translational research?', *Oncogene*, 31: 4577.

Steinhardt, James J, and Ronald B Gartenhaus. 2013. 'Epigenetic approaches for chemosensitization of refractory diffuse large B-cell lymphomas', *Cancer discovery*, 3: 968-70.

Stephan, L, and R Momparler. 2015. 'Combination chemotherapy of cancer using the inhibitor of DNA methylation 5-aza-2'-deoxycytidine (decitabine)', *J Cancer Res Ther*, 3: 56-65.

Stepulak, Andrzej, Marco Sifringer, Wojciech Rzeski, Katja Brocke, Alexander Gratopp, Elena E Pohl, Lechoslaw Turski, and Chrysanthy Ikonomidou. 2007. 'AMPA antagonists inhibit the extracellular signal regulated kinase pathway and suppress lung cancer growth', *Cancer biology & therapy*, 6: 1908-15.

Stuckler, David, Jyotsana Singhal, Sharad S Singhal, Sushma Yadav, Yogesh C Awasthi, and Sanjay Awasthi. 2005. 'RLIP76 Transports Vinorelbine and Mediates Drug Resistance in Non–Small Cell Lung Cancer', *Cancer research*, 65: 991-98.

Studio, DensityDesign Integrated Course Final Synthesis. 2014. 'pyrosequencing', *Polytechnic University of Milan*.

Sun, M, XH Liu, KH Lu, FQ Nie, R Xia, R Kong, JS Yang, TP Xu, YW Liu, and YF Zou. 2014. 'EZH2-mediated epigenetic suppression of long noncoding RNA SPRY4-IT1 promotes NSCLC cell proliferation and metastasis by affecting the epithelial–mesenchymal transition', *Cell death & disease*, 5: e1298.

Sweeney, Ryan, Katherine E Richards, and Reginald Hill. 2017. 'Gemcitabine-Induced Exosome Hypersecretion Increases the Chemoresistance and Migration of Pancreatic Cancer Cells', *The FASEB Journal*, 31: 775.20-75.20.

Szyf, Moshe. 2009. 'Epigenetics, DNA methylation, and chromatin modifying drugs', *Annual review of pharmacology and toxicology*, 49: 243-63.

Szypowska, Anna A, Hesther de Ruiter, Lars AT Meijer, Lydia MM Smits, and Boudewijn MT Burgering. 2011. 'Oxidative stress-dependent regulation of Forkhead box O4 activity by nemo-like kinase', *Antioxidants & redox signaling*, 14: 563-78.

Takenaka, Tomoyoshi, Ichiro Yoshino, Hidenori Kouso, Taro Ohba, Tomofumi Yohena, Atsushi Osoegawa, Fumihiro Shoji, and Yoshihiko Maehara. 2007. 'Combined evaluation of Rad51 and ERCC1 expressions for sensitivity to platinum agents in non-small cell lung cancer', *International journal of cancer*, 121: 895-900.

Tan, Jiahuai, Shundong Cang, Yuehua Ma, Richard L Petrillo, and Delong Liu. 2010. 'Novel histone deacetylase inhibitors in clinical trials as anti-cancer agents', *Journal of hematology & oncology*, 3: 5.

Tang, Qingfeng, Zhenhua Ni, Zhuoan Cheng, Jianhua Xu, Hui Yu, and Peihao Yin. 2015. 'Three circulating long non-coding RNAs act as biomarkers for predicting NSCLC', *Cellular Physiology and Biochemistry*, 37: 1002-09.

Thornberry, Nancy A, and Yuri Lazebnik. 1998. 'Caspases: enemies within', *Science*, 281: 1312-16.

Tian, Yanhua, Suping Li, Jian Song, Tianjiao Ji, Motao Zhu, Gregory J Anderson, Jingyan Wei, and Guangjun Nie. 2014. 'A doxorubicin delivery platform using engineered natural membrane vesicle exosomes for targeted tumor therapy', *Biomaterials*, 35: 2383-90.

Trajkovic, Katarina, Chieh Hsu, Salvatore Chiantia, Lawrence Rajendran, Dirk Wenzel, Felix Wieland, Petra Schwille, Britta Brügger, and Mikael Simons. 2008. 'Ceramide triggers budding of exosome vesicles into multivesicular endosomes', *Science*, 319: 1244-47.

Travis, William D, Elisabeth Brambilla, Masayuki Noguchi, Andrew G Nicholson, Kim Geisinger, Yasushi Yatabe, Yuichi Ishikawa, Ignacio Wistuba, Douglas B Flieder, and Wilbur Franklin. 2012. 'Diagnosis of lung adenocarcinoma in resected specimens: implications of the 2011 International Association for the Study of Lung Cancer/American Thoracic Society/European Respiratory Society classification', *Archives of Pathology and Laboratory Medicine*, 137: 685-705.

Uchiumi, Fumiaki, Jun Arakawa, Yutaka Takihara, Motohiro Akui, Hiroshi Hamada, and Sei-ichi Tanuma. 2017. 'A New Insight into the Development of Novel Anti-Cancer Drugs that Improve the Expression of Mitochondrial Function-Associated Genes.' in, *Mitochondrial Diseases* (IntechOpen).

Ueno, H, K Kiyosawa, and N Kaniwa. 2007. 'Pharmacogenomics of gemcitabine: can genetic studies lead to tailor-made therapy?', *British journal of cancer*, 97: 145.

Ulivi, Paola, Wainer Zoli, Laura Capelli, Elisa Chiadini, Daniele Calistri, and Dino Amadori. 2013. 'Target therapy in NSCLC patients: Relevant clinical agents and tumour molecular characterisation', *Molecular and clinical oncology*, 1: 575-81.

van der Hoeven, Dharini, Kwang-jin Cho, Xiaoping Ma, Sravanthi Chigurupati, Robert G Parton, and John F Hancock. 2013. 'Fendiline inhibits K-Ras plasma membrane localization and blocks K-Ras signal transmission', *Molecular and cellular biology*, 33: 237-51.

Vansteenkiste, Johan, Dirk De Ruysscher, WEE Eberhardt, E Lim, S Senan, E Felip, S Peters, and ESMO Guidelines Working Group. 2013. 'Early and locally advanced

non-small-cell lung cancer (NSCLC): ESMO Clinical Practice Guidelines for diagnosis, treatment and follow-up', *Annals of oncology*, 24: vi89-vi98.
Vendetti, Frank P, Michael Topper, Peng Huang, Irina Dobromilskaya, Hariharan Easwaran, John Wrangle, Stephen B Baylin, JT Poirier, and Charles M Rudin. 2015. 'Evaluation of azacitidine and entinostat as sensitization agents to cytotoxic chemotherapy in preclinical models of non-small cell lung cancer', *Oncotarget*, 6: 56.
Verweij, Frederik Johannes, Maarten P Bebelman, Connie R Jimenez, Juan J Garcia-Vallejo, Hans Janssen, Jacques Neefjes, Jaco C Knol, Richard de Goeij-de Haas, Sander R Piersma, and S Rubina Baglio. 2018. 'Quantifying exosome secretion from single cells reveals a modulatory role for GPCR signaling', *J Cell Biol*, 217: 1129-42.
Viet, Chi T, Dongmin Dang, Stacy Achdjian, Yi Ye, Samuel G Katz, and Brian L Schmidt. 2014. 'Decitabine rescues cisplatin resistance in head and neck squamous cell carcinoma', *PLoS One*, 9: e112880.
Villarroya-Beltri, Carolina, Cristina Gutiérrez-Vázquez, Fátima Sánchez-Cabo, Daniel Pérez-Hernández, Jesús Vázquez, Noa Martin-Cofreces, Dannys Jorge Martinez-Herrera, Alberto Pascual-Montano, María Mittelbrunn, and Francisco Sánchez-Madrid. 2013. 'Sumoylated hnRNPA2B1 controls the sorting of miRNAs into exosomes through binding to specific motifs', *Nature communications*, 4: 2980.
Villegas, Victoria E, and Peter G Zaphiropoulos. 2015. 'Neighboring gene regulation by antisense long non-coding RNAs', *International journal of molecular sciences*, 16: 3251-66.
Wang, Haolu, Xinxing Li, Tao Chen, Wei Wang, Qiang Liu, Hui Li, Jing Yi, and Jian Wang. 2013. 'Mechanisms of verapamil-enhanced chemosensitivity of gallbladder cancer cells to platinum drugs: glutathione reduction and MRP1 downregulation', *Oncology reports*, 29: 676-84.
Wang, Jianqing, Qianyi Xiao, Xu Chen, Shijun Tong, Jianliang Sun, Ruitu Lv, Siqing Wang, Yuancheng Gou, Li Tan, and Jianfeng Xu. 2018. 'LanCL1 protects prostate cancer cells from oxidative stress via suppression of JNK pathway', *Cell death & disease*, 9: 197.
Wang, Luo, Jiachun Lu, Jiaze An, Qiuling Shi, Margaret R Spitz, and Qingyi Wei. 2007. 'Polymorphisms of cytosolic serine hydroxymethyltransferase and risk of lung cancer: a case–control analysis', *Lung Cancer*, 57: 143-51.
Wangari-Talbot, Janet, and Elizabeth Hopper-Borge. 2013. 'Drug resistance mechanisms in non-small cell lung carcinoma', *Journal of cancer research updates*, 2: 265.
Woods, Neha, Jose Trevino, Domenico Coppola, Srikumar Chellappan, Shengyu Yang, and Jaya Padmanabhan. 2015. 'Fendiline inhibits proliferation and invasion of pancreatic cancer cells by interfering with ADAM10 activation and β-catenin signaling', *Oncotarget*, 6: 35931.
Yagi, Yasumichi, Sachio Fushida, Shinichi Harada, Jun Kinoshita, Isamu Makino, Katsunobu Oyama, Hidehiro Tajima, Hideto Fujita, Hiroyuki Takamura, and Itasu Ninomiya. 2010. 'Effects of valproic acid on the cell cycle and apoptosis through acetylation of histone and tubulin in a scirrhous gastric cancer cell line', *Journal of Experimental & Clinical Cancer Research*, 29: 149.
Yamaguchi, Hirohito, Jennifer L Hsu, Chun-Te Chen, Ying-Nai Wang, Ming-Chuan Hsu, Shih-Shin Chang, Yi Du, How-Wen Ko, Roy Herbst, and Mien-Chie Hung. 2013. 'Caspase-independent cell death is involved in the negative effect of EGF receptor inhibitors on cisplatin in non–small cell lung cancer cells', *Clinical cancer research*, 19: 845-54.
Yang, Haihong, Qi Zhang, Jianxing He, and Wenju Lu. 2010. 'Regulation of calcium signaling in lung cancer', *Journal of thoracic disease*, 2: 52.

Zhang, Jian, Sha Li, Lu Li, Meng Li, Chongye Guo, Jun Yao, and Shuangli Mi. 2015. 'Exosome and exosomal microRNA: trafficking, sorting, and function', *Genomics, proteomics & bioinformatics*, 13: 17-24.

Zhang, Wenchi, Liang Wang, Yijin Liu, Jiwei Xu, Guangyu Zhu, Huaixing Cang, Xuemei Li, Mark Bartlam, Kenneth Hensley, and Guangpu Li. 2009. 'Structure of human lanthionine synthetase C-like protein 1 and its interaction with Eps8 and glutathione', *Genes & development*, 23: 1387-92.

Zhang, Xiang-Zhong, Ai-Hua Yin, Dong-Jun Lin, Xiao-Yu Zhu, Qian Ding, Chun-Huai Wang, and Yun-Xian Chen. 2012. 'Analyzing gene expression profile in K562 cells exposed to sodium valproate using microarray combined with the connectivity map database', *BioMed Research International*, 2012.

Zhen, WEIPING, CJ Link, PM O'connor, E Reed, R Parker, SB Howell, and VA Bohr. 1992. 'Increased gene-specific repair of cisplatin interstrand cross-links in cisplatin-resistant human ovarian cancer cell lines', *Molecular and Cellular Biology*, 12: 3689-98.

Zhong, Wei-xia, Yu-bin Wang, Lin Peng, Xue-zhen Ge, Jie Zhang, Shuang-shuang Liu, Xiang-nan Zhang, Zheng-hao Xu, Zhong Chen, and Jian-hong Luo. 2012. 'Lanthionine Synthetase C-like Protein 1 Interacts with and Inhibits Cystathionine β-Synthase A TARGET FOR NEURONAL ANTIOXIDANT DEFENSE', *Journal of Biological Chemistry*, 287: 34189-201.

Zhou, Caicun, Yi-Long Wu, Gongyan Chen, Jifeng Feng, Xiao-Qing Liu, Changli Wang, Shucai Zhang, Jie Wang, Songwen Zhou, and Shengxiang Ren. 2011. 'Erlotinib versus chemotherapy as first-line treatment for patients with advanced EGFR mutation-positive non-small-cell lung cancer (OPTIMAL, CTONG-0802): a multicentre, open-label, randomised, phase 3 study', *The lancet oncology*, 12: 735-42.

Chapter 8: Appendix

Table 8.1 Human lung tissue samples to specify in detail *LANCL1* and *LANCL1-AS1* in NSCLC.

PD_MPI	Meth Data	Microarray	HistNo	SampleID	Histology MD	Histo_coded	Diff_old	Diff	T_stat	N_stat	gender	Sex	DOB	DOOP	Age	DLS	DOD	Status	Follow-up	LANCL1-AS1_N	LANCL1-AS1_T	LANCL1_N
91505	0	0		91505	SqCC	1			2	0	M	0	03/06/1937	17/05/2011	74.0		22/05/2011	2	0.2	0.92	0.00	0.09
20807	1	0	L269	269	AdenoCa	0	1	1	2	2	M	0	02/09/1930	27/11/1997	67.2		04/12/1997	1	0.2	1.13	0.12	0.41
20709	0	0	L208	208	AdenoCa	0	3	5	1	0	M	0	21/09/1922	12/06/1997	74.7		22/06/1997	1	0.3	1.45	0.20	0.74
20732	0	0	L215	215	SqCC	1	1	1	2	0	M	0	12/11/1920	26/06/1997	76.6		14/07/1997	1	0.6	0.75	0.00	0.91
20640	1	0	L183	183	AdenoCa	0			3	0	M	0	29/03/1942	19/02/1997	54.9		06/04/1997	1	1.5	0.89	0.00	0.51
20785	0	0	L252	252	AdenoCa	0	1	1	4	2	M	0	22/05/1929	21/10/1997	68.4		10/12/1997	1	1.7	0.94	0.00	0.45
20638	1	0	L181	181	NSCLC		1	1	3	1	M	0	12/04/1923	17/02/1997	73.9		23/04/1997	1	2.2	0.60	0.00	1.12
20628	0	1	L175	175	AdenoCa	0	1	1	2	0	M	0	21/01/1926	30/01/1997	71.0		07/04/1997	1	2.2	0.64	0.00	0.50
78749	0	0		78749	SqCC	1			2	1	F	1	11/09/1931	18/09/2008	77.0	11/12/2008		0	2.8	2.04	0.00	0.66
20753	1	1	L236	236	AdenoCa	0	2	3	3	1	M	0	20/05/1930	18/08/1997	67.2		18/11/1997	1	3.1	1.01	0.00	0.63
20624	1	1	L171	171	SqCC	1	1	1	2	0	M	0	10/04/1929	23/01/1997	67.8		13/05/1997	1	3.7	0.75	0.00	0.59
20773	1	1	L240	240	SqCC	1	1	1	3	2	F	1	07/02/1932	15/09/1997	65.6		23/01/1998	1	4.3	1.28	0.00	0.86
20735	0	1	L218	218	AdenoCa	0	2	3	2	0	F	1	15/03/1942	07/07/1997	55.3		18/11/1997	1	4.5	0.60	0.00	1.14
20580	0	0	L154	154	SqCC	1	1.5	2	2	2	M	0	11/06/1924	11/11/1996	72.4		09/05/1997	1	6.0	1.52	0.00	0.59
20733	1	0	L216	216	AdenoCa	0	1	1	2	0	M	0	18/12/1909	26/06/1997	87.5		23/12/1997	1	6.0	1.16	0.14	1.10
21021	1	0	L288	288	AdenoCa	0	2	3	2	1	F	1	25/05/1950	16/02/1998	47.7		22/09/1998	1	7.3	1.19	0.00	1.34
20631	1	0	L178	178	AdenoCa	0	1	1	2	1	F	1	16/11/1927	10/02/1997	69.2		17/09/1997	1	7.3	0.82	0.00	0.94
20434	1	0	L127	127	SqCC	1	2	3	2	2	M	0	06/09/1924	22/07/1996	71.9		07/03/1997	1	7.6	0.90	0.00	0.99
20682	0	1	L198	198	AdenoCa	0	1	1	4	0	M	0	15/05/1946	28/04/1997	51.0		20/03/1998	1	10.9	1.66	0.12	0.72
20565	1	1	L146	146	SqCC	1	2	3	2	0	M	0	04/04/1917	16/10/1996	79.5		12/09/1997	1	11.0	1.76	0.08	1.10
21023	1	1	L289	289	AdenoCa	0	3	5	2	2	M	0	18/07/1939	16/02/1998	58.6		01/02/1999	1	11.7	0.71	0.02	0.46
20702	1	0	L201	201	SqCC	1	2	3	2	2	M	0	28/09/1921	08/05/1997	75.7		19/05/1998	1	12.5	0.40	0.00	1.50

20681	1	1	L197	197	SqCC	1	2	3	2	2	M	0	09/10/1924	28/04/1997	72.6		23/05/1998	1	13.0	1.49	0.00	0.51
20644	0	0	L186	186	AdenoCa	0	3	5	2	1	M	0	19/07/1937	24/02/1997	59.6		11/04/1998	1	13.7	1.27	0.14	0.64
20771	1	1	L238	238	SqCC	1	2	3	3	2	M	0	12/09/1934	15/09/1997	63.0		06/11/1998	1	13.9	0.90	0.25	0.82
20632	1	0	L179	179	SqCC	1	2	3	3	2	M	0	14/05/1940	10/02/1997	56.7		08/05/1998	1	15.1	0.82	0.05	0.52
20734	1	0	L217	217	AdenoCa	0	2	3	2	2	F	1	13/08/1940	30/06/1997	56.9		03/10/1998	1	15.3	1.71	0.06	1.32
91559	0	0		91559	SqCC	1	1	1	2	0	M	0	31/08/1931	17/08/2011	80.0	20/12/2012		0	16.4	0.08	0.00	0.44
20641	1	0	L184	184	SqCC	1	2	3	2	0	M	0	14/02/1935	20/02/1997	62.0		17/08/1998	1	18.1	0.39	0.04	0.71
20599	0	1	L157	157	AdenoCa	0	2	3	2	1	M	0	26/01/1927	18/11/1996	69.8		26/05/1998	1	18.5	0.49	0.00	1.06
20566	0	0	L147	147	SqCC	1	3	5	2	1	M	0	13/05/1928	17/10/1996	68.4		01/05/1998	1	18.7	2.73	0.00	1.16
74	0	0	L260	260	SqCC	1	1.5	2	2	0	M	0	06/02/1939	11/11/1997	58.8		17/06/1999	1	19.4	0.99	0.00	0.45
20438	0	1	L129	129	SqCC	1	1	1	2	1	M	0	20/10/1922	25/07/1996	73.8		17/03/1998	1	20.0	1.04	0.00	0.72
20683	0	1	L199	199	AdenoCa	0	1.5	2	2	1	M	0	07/10/1916	28/04/1997	80.6		27/12/1998	1	20.3	0.64	0.00	0.24
20571	1	0	L152	152	SqCC	1	2.5	4	2	1	M	0	25/10/1940	29/10/1996	56.0		03/01/1999	1	26.5	1.00	0.05	0.80
79606	0	0		79606	SqCC	1			1	1	M	0	14/01/1943	12/10/2010	67.7	20/12/2012		0	26.7	0.69	0.05	1.18
20639	1	1	L182	182	SqCC	1	2	3	3	0	M	0	21/03/1947	17/02/1997	49.9		02/06/1999	1	27.8	1.70	0.03	0.91
20787	1	0	L254	254	AdenoCa	0	2	3	2	0	M	0	16/01/1924	27/10/1997	73.8		19/02/2000	1	28.2	1.45	0.10	
20705	1	1	L204	204	SqCC	1	2	3	2	1	M	0	15/07/1937	15/05/1997	59.8		14/09/1999	1	28.4	1.08	0.48	1.12
20559	1	0	L144	144	SqCC	1	2	3	2	0	F	1	14/10/1935	03/10/1996	61.0		21/03/1999	1	30.0	0.42	0.00	1.04
20625	0	0	L172	172	SqCC	1	2.5	4	2	1	M	0	09/12/1931	27/01/1997	65.2		01/10/1999	1	32.6	0.84		0.82
20774	1	0	L241	241	SqCC	1	2	3	2	1	M	0	17/07/1938	16/09/1997	59.2		03/03/2001	1	42.1	0.64	0.13	1.36
21025	0	0	L290	290	LCCL		1	1	1	0	M	0	14/04/1921	23/03/1998	76.9		14/07/2002	1	52.5	1.78	0.06	
20737	0	1	L220	220	AdenoCa	0	3	5	2	0	F	1	18/06/1926	10/07/1997	71.1		27/01/2002	1	55.4	1.23	0.20	1.03
20570	1	0	L151	151	SqCC	1	1	1	2	1	F	1	28/08/1926	24/10/1996	70.2		10/10/2001	1	60.4	0.46	0.00	0.15
20643	1	1	L185	185	AdenoCa	0	1	1	2	1	M	0	22/11/1930	24/02/1997	66.3		04/12/2002	1	70.3	0.58	0.00	1.40
20784	1	0	L251	251	AdenoCa	0	3	5	2	0	M	0	07/04/1923	20/10/1997	74.5		26/11/2003	1	74.3	1.18	0.00	
20520	1	0	L136	136	SqCC	1	2	3	2	0	M	0	06/04/1925	12/08/1996	71.4		29/11/2002	1	76.7	0.46	0.45	0.00
20402	1	0	L112	112	SqCC	1	2	3	2	0	M	0	18/10/1923	03/06/1996	72.6		06/11/2002	1	78.2	2.11	0.00	1.35
20600	0	1	L159	159	AdenoCa	0	2	3	2	0	M	0	27/05/1948	25/11/1996	48.5		02/06/2003	1	79.3	1.97	0.00	0.65
20795	1	1	L257	257	SqCC	1	2	3	4	1	M	0	11/04/1926	31/10/1997	71.6		14/05/2004	1	79.6	0.91	0.00	0.27

20725	0	1	L221	221	AdenoCa	0	1	1	2	0	F	1	28/08/1929	15/07/1997	67.9		15/02/2004	1	80.2	0.58	0.00	0.66
20778	0	1	L245	245	AdenoCa	0	2	3	3	2	M	0	01/05/1926	25/09/1997	71.4		17/05/2004	1	80.9	1.07	0.12	0.64
20707	1	1	L206	206	SqCC	1	3	5	1	1	M	0	01/03/1922	05/06/1997	75.3		14/12/2004	1	91.6	2.00	0.00	0.35
20595	0	1	L158	158	AdenoCa	0	2	3	2	0	F	1	29/04/1928	19/11/1996	68.6		15/10/2005	1	108.4	0.83	0.05	1.03
20159	0	0	L369	369	AdenoCa	0	2	3	2	0	F	1	12/06/1932	11/01/1999	66.6		10/07/2008	1	115.6	1.13	0.07	0.93
20708	1	0	L207	207	SqCC	1	2	3	1	1	F	1	25/04/1943	09/06/1997	54.1		26/05/2007	1	121.3	0.67	0.04	1.08
39440	1	0		273	SqCC	1			2	0	M	0	11/04/1934	22/12/1997	63.7		26/03/2008	1	124.9	1.53	0.04	
20626	1	1	L173	173	SqCC	1	2	3	2	0	F	1	13/03/1924	27/01/1997	72.9		04/07/2007	1	127.0	1.27	0.00	0.46
21027	1	1	L291	291	SqCC	1	1	1	2	0	M	0	31/12/1937	24/02/1998	60.2		28/02/2009	1	134.1	1.86	0.00	1.99
20579	1	0	L153	153	SqCC	1	2	3	2	0	M	0	31/01/1930	11/11/1996	66.8		06/07/2008	1	141.8	2.18	0.04	0.61
20701	1	0	L200	200	SqCC	1	2	3	2	0	F	1	13/09/1925	08/05/1997	71.6		19/05/2009	1	146.5	1.20	0.11	0.60
20677	1	1	L192	192	AdenoCa	0	2	3	2	0	M	0	25/12/1924	14/04/1997	72.3		15/06/2009	1	148.2	0.55	0.00	0.47
20985	1	1	L283	283	SqCC	1	2	3	2	1	F	1	04/05/1944	29/01/1998	53.7	16/02/2012		0	171.0	0.57	0.00	0.14
20703	1	1	L202	202	SqCC	1	2	3	2	0	F	1	20/09/1929	12/05/1997	67.6	16/02/2012		0	179.8	0.55	0.08	1.26
20627	1	0	L174	174	SqCC	1	2	3	2	0	M	0	18/11/1932	30/01/1997	64.2	20/12/2012		0	193.4	0.58	0.06	0.58
20620	1	1	L167	167	SqCC	1	2	3	2	0	M	0	05/07/1924	09/01/1997	72.5	20/12/2012		0	194.1	1.06	0.13	1.44